Lithogeochemistry and Hydrothermal Alteration of the Halfmile Lake South Deep Zone, a Volcanic Hosted Massive Sulphide Deposit, Bathurst Mining Camp, New Brunswick

by

Lawrence Kwabena Mireku

Thesis

submitted in partial fulfillment of the requirements for

the Degree of Master of Science (Geology)

Acadia University

Fall Convocation 2001

TABLE OF CONTENTS

List of Figures

List of Tables

ACKNOWLEDGEMENTS

First of all I give thanks to God for seeing me through my graduate studies at Acadia and taking me a step forward in my professional career. I owe a lot of gratitude to my parents, especially my mother (Margaret Akosua Mireku), and Mr. Reginald Sackey-Addo for their commitment to my education and entire life. I also wish to extend my sincere gratitude to my wife, Margaret Agyeiwaa Mireku, for standing with me in the most difficult times.

I will be forever grateful to Dr. Clifford R. Stanley, my supervisor, for his motivation and inspiration, and for being a great mentor. To Dr. Rob P. Raeside (Dept. Head, Geology), Dr. Sandra Barr, Dr. Alan MacDonald, Dr. Ian Spooner, and the entire faculty in the geology department, I say many thanks for the diverse ways you contributed to make my studies at Acadia a success. Fellow students and friends at Acadia University have every reason to celebrate with me, for every opportunity they seized to spur me on.

Without the tremendous financial assistance and other supports from the National Science and Engineering Research Council (NSERC, Canada) and Noranda Inc (Exploration), this success story would have been a dream untold. Last but not the least, I express my sincere gratitude to Don Osburn and Bob MacKay for helping me with thin section preparation and electron microprobe analysis, respectively. Cheers to Sheila Potter for exposing me to the rudiments of CorelDraw.

ABSTRACT

The Halfmile Lake South Deep zone (HMLSDZ), Bathurst Mining Camp, New Brunswick, was discovered by Noranda Inc (Exploration) as a result of a 3-D seismic survey. Mineralization consists of Pb-Zn-Cu and hosted by an overturned Lower Tetagouche Group volcano-sedimentary package. Epiclastic rocks are interbedded with subordinate fine-grained felsic pyroclastic rocks that dominate the structural hangingwall. Locally crystal rich felsic tuffs and subordinate epiclastic rocks comprise the immediate structural footwall. This sequence was intruded by quartz-feldspar porphyritic intrusions and cut by intermediate to basaltic dykes. The host rocks to the deposit have suffered sub-greenschist facies metamorphism, polyphase deformation, and are variably hydrothermally altered.

The host rocks can be geochemically discriminated using trace element ratios such as Zr/TiO_2, Nb/TiO_2, *etc*. These ratios indicate that four volcanic compositions existence at the HMLSDZ: rhyolite, dacite, andesite, and basalt. The aphyric and feldspar ± quartz phyric volcanic rocks are rhyolitic and dacitic in composition whereas the epiclastic rocks are predominantly dacitic. Pearce element ratio (PER) diagrams, molar element ratio (MER) diagrams, and petrographic examination demonstrate that hydrothermal activity involved muscovite, chlorite, and minor carbonate formation. A lateral and vertical zone (200 – 300 m) of intense alteration is developed in the immediate structural hangingwall to the HMLSDZ. This alteration halo is characterized by additions of Fe, H and variable K, and losses of Na and minor Ca. due to hydrothermal activity.

Results from this study demonstrate that metamorphism and deformation have not significantly obscured hydrothermal alteration signatures.

1 - INTRODUCTION

1.1 - Background

The Bathurst Mining Camp (BMC), New Brunswick, contains several globally important volcanic-hosted massive sulphide (VHMS) deposits, including the world-class Brunswick No. 12 mine (Figure 1.1). Other past producing mines in the camp include Austin Brook, Brunswick No. 6, Caribou, CNE, Heath Steele, Murray Brook, Restigouche, Stratmat, and Wedge. By the end of 1998, the Bathurst camp had produced approximately 130 million tonnes of ore grading 3.0 % Pb, 7.7 % Zn, 0.5 % Cu, and 89.1 % g/t Ag. In addition to the mineral deposits, another 35 deposits with delineated (but uneconomic) Pb-Zn resources are known (McCutcheon and Walker 2001). One of these is the Halfmile Lake deposit, which is the subject of this study.

Mining activities began in the camp after the discovery of the Austin Brook hematite-magnetite-rich iron formation in 1897. Approximately 164,000 tonnes of iron ore were mined from this deposit between 1911 and 1913. The mine was reopened in 1942 and produced an additional 130,000 tonnes of ore before closing a year later (McCutcheon 1997).

In the summer of 1952, a university thesis by Mr. A. B. Baldwin (supervised by Dr. G. S. Mackenzie, University of New Brunswick, Fredericton) alerted a group of entrepreneurs to the presence of massive sulphide mineralization near Bathurst. Headed by M. J. Boylen, these entrepreneurs organized a diamond drilling program that resulted in the discovery of the Brunswick No. 6 massive sulphide orebody in the footwall to "Zone 3" of the Austin Brook iron deposit (Linderman 1913).

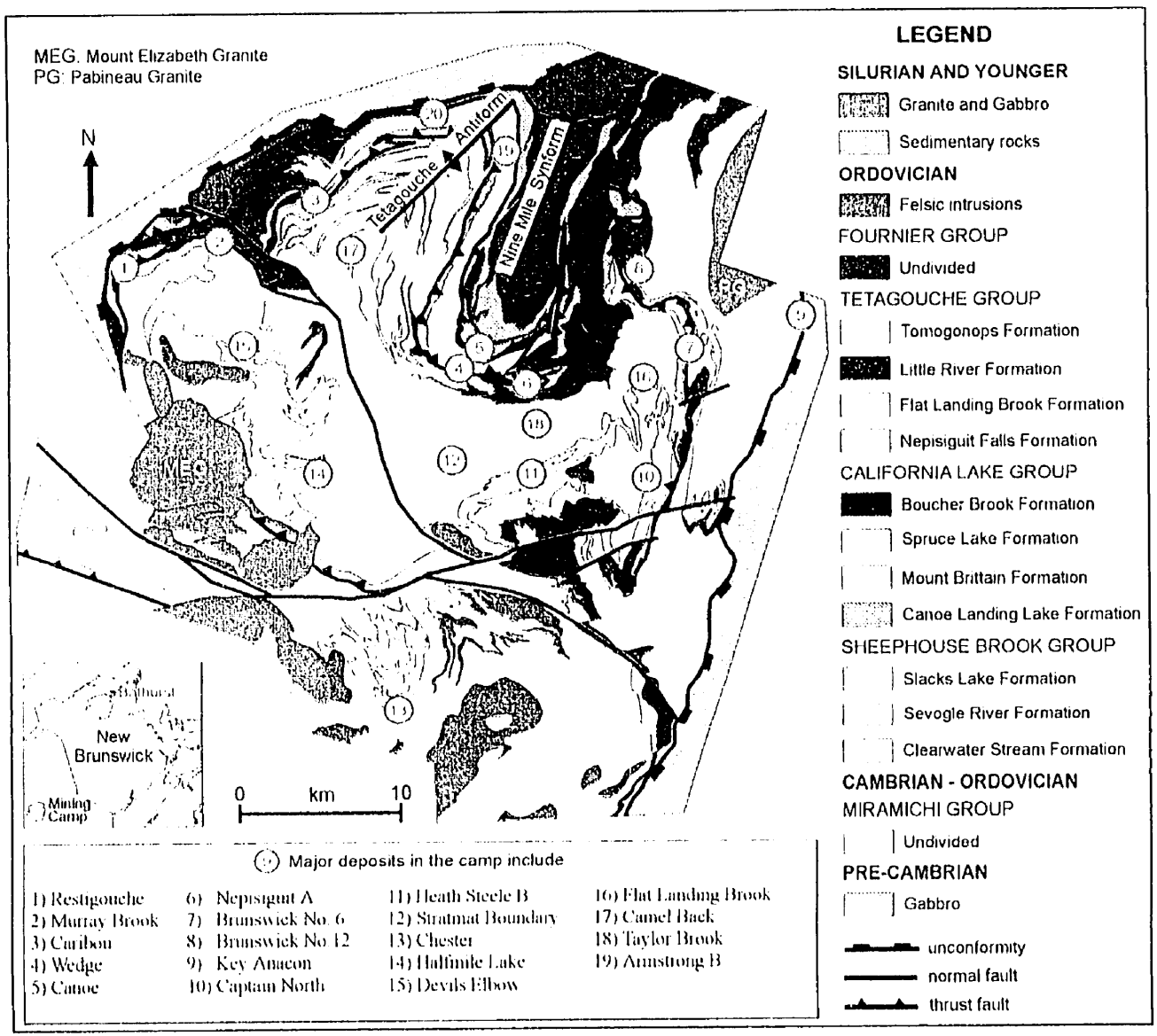

Figure 1.1 Geological map of the Bathurst Mining camp (from Thomas *et al.* 2000)

The M. J. Boylen group discovered an additional deposit in the spring of 1953 on the Anacon-Leadridge group of claims as a result of drilling a strong electromagnetic anomaly (MacKenzie 1958). This second property became known as Brunswick No. 12, as it represented the 12th project of the M. J. Boylen entrepreneurial group. Shortly thereafter, the M. J. Boylen group was incorporated into the Brunswick Mining and Smelting Corporation and they subsequently staked the remaining areas around the Brunswick No. 6 and No. 12 deposits. All other VHMS deposits in the camp were discovered after this initial activity. A detailed description of the past producing mines is presented in McCutcheon and Walker (2001), however, a brief summary of a subset of these deposits provided below.

The Brunswick No. 6 massive sulphide orebody produced 12.125 Mt of ore grading 5.43 % Zn, 2.16 % Pb, 0.39 % Cu, and 67.0 % g/t Ag during its operating life from 1966 to 1983. Between 1964 and 2000, the Brunswick No. 12 deposit produced 95.697 Mt of ore grading 8.81 % Zn, 3.49 % Pb, 0.35 % Cu, and 101.0 g/t Ag (McCutcheon and Walker 2001). Presently the only operating mine in the Bathurst camp, Brunswick No. 12 has less than ten years of mineable reserves.

Cominco discovered the Wedge deposit, located on the north bank of the Nepisiguit River and 40 km southwest of Bathurst in 1957 following the identification of a gossanous outcrop and 6000 meters of drilling of an electromagnetic anomaly. The deposit was brought into production in 1962 and the mine closed in 1968. The total ore produced was 1.503 Mt grading 0.65 % Pb, 1.61 % Zn, 2.88 % Cu, and 20.6 g/t Ag (McCutcheon and Walker 2001).

The Caribou Zn-Pb-Cu deposit, located 50 km west of Bathurst, in the north-central part of the Bathurst mining camp, was discovered by Anaconda Company (Canada) Ltd in December 1955 (Cheriton 1960). Past production from Caribou includes: 337,400 tonnes of 3.66 % Cu from a supergene blanket, mined by open pit methods between 1970 and 1974; 61,500 tonnes of gossan mined in 1970 but heap-leached between 1982 and 1983, which yielded 110,000 oz. of Ag and 8,300 oz. of Au; and 728,400 tonnes of 3.54 % Pb and 7.17 % Zn mined from underground between 1988 and 1990 (McCutcheon and Walker 2001). The known massive sulphide body, including low grade pyrite-pyrrhotite mineralization, is approximately 65 Mt and remains open at depth. The deposit contains a present resource of 4.621 Mt of ore grading 3.22 % Pb, 6.77 % Zn, and 98 g/t Ag, with an additional 216,000 tonnes grading 3.82 % Cu. The Caribou deposit has been developed to a depth of 287 m by ramp and sublevels and a production shaft has been sunk to a depth of 140 m. The property is currently controlled by Breakwater Resources Ltd. and is in a standby/maintenance state.

At the time of discovery in the fall of 1958 the Restigouche deposit, located on the northern limb of the Upsalquitch Lake Anticlinorium, was called the Charlotte prospect. The deposit was discovered by New Jersey Zinc Co. (Canada) Ltd. but presently owned by Breakwater Resources Ltd. Drill-proven reserves are estimated at 1.59 million tonnes grading 6.81 % Zn, 5.38 % Pb, 108 g/t Ag, and 1.1 g/t Au (McCutcheon and Walker 2001).

The Murray Brook deposit, located approximately 65 km west of Bathurst, was discovered by Kennco Explorations (Canada) Ltd., in 1956. The discovered was a result of stream sediment geochemical survey developed to trace the source of a copper-bearing

float. Production at the deposit did not begin until 1989 when NovaGold Resources Inc. commenced open-pit mining of a precious metal-rich gossan (Rennick and Burton 1992). The gossan was exhausted in 1992 and yielded a total production of 1.41 million grams Au and 10.78 million grams Ag (Burton 1993). The total sulphide resource at the Murray Brook deposit is 12.5 million tonnes of ore grading 0.48 % Cu, 0.66 % Pb, 1.95 % Zn, and 31.4 g/t Ag (McCutcheon and Walker 2001).

The discovery of the Little River (later known as Heath Steele) orebodies was a result of the very first airborne electromagnetic survey conducted by American Metal Company in 1954 (McCutcheon and Walker 2001). These deposits were later named after one long-serving employee of American Metal Company, Mr. Heathcliff Steele. Heath Steele is the second largest Zn-Pb-Cu-Ag deposit in the Bathurst mining camp. After 40 years of operation, the Heath Steele mine closed in October 1999 upon depletion of its economic reserves. The total production from the various orebodies at the Heath Steele is presented in Table 1.1.

Table 1.1 – Summary of Heath Steele mining production

Heath Steele	Tonnage	Pb (%)	Zn (%)	Cu (%)	Ag (g/t)
ACD Zones	553,100	4.18	11.26	0.29	111
B Zone	1,439,500	2.38	5.99	1.69	101
B-5 Zone	10,100,000	1.8	10.59	0.51	57
C-North	2,700,000	2.04	6.03	0.39	81
E Zone	917,000	2.39	5.79	1.47	102
H2 Zone	5,600,000	4.74	12.28	0.88	154
HC-4 Zone	8,000,000	3.17	10.15	0.14	88
West Grid	961,500	3.12	7.01	0.14	87

The Halfmile Lake (HML) deposit is one of the largest undeveloped VHMS deposits in the BMC. It contains significant base metal sulphides in four zones; the North, South Upper AB, South Lower AB, and South Deep zones. These occur within an overturned

volcano-sedimentary package and comprise breccia matrix and bedded Zn-Pb-rich massive sulphides, and Cu-rich stockwork sulphides. The HML South (Upper AB zone) deposit was discovered by Texas Gulf Sulphur Co. following airborne electromagnetic and soil geochemistry surveys. In the same year, Great Sweet Grass Oils Co. and Bay Copper Mines intersected the HML North and South Lower AB zones, respectively. Between 1974 and 1977, Mattagami Mines embarked on an extensive drilling of the HML North deposit. Additionally, Kidd Creek Mines and Billiton Canada conducted further exploration on the Upper and Lower AB zones in 1973 and between 1979-1982, respectively (Adair 1992). In 1998, a 3-D seismic survey conducted by Noranda Mining Inc (Exploration) led to the discovery of the HML South Deep zone (HMLSDZ) deposit, down dip from the South Lower AB zone.

As of 1998, the resource of the HML South Upper AB zone was 1.018 Mt at 2.62 % Pb, 7.58 % Zn, 0.42 % Cu, and 48.13 g/t Ag, and the HML South Lower AB zone was estimated at 7.51 Mt grading 2.83 % Pb, 8.95 % Zn. 0.1 % Cu, and 38.8 g/t Ag (Noranda Feasibility report, 1998). A resource evaluation in 1994 indicated that the HML North zone contains 1.179 Mt of Pb-Zn mineralization grading 0.85 % Pb, 4.51 % Zn, 0.47 % Cu, and 9 g/t Ag (McCutcheon and Walker 2001). A resource evaluation has not been completed for the HMLSDZ. Additional reserves are required to make this deposit an economically viable mine.

1.2 - Purpose of Study

Exploration for additional VHMS deposits is presently ongoing in the Bathurst camp. There, Noranda Exploration Inc. holds rights to explore almost 100,000 hectares of ground. Several other mining companies are also actively exploring in the Bathurst

Camp. The objectives of these exploration programs are to discover stand-alone deposits, and to define additional reserves near the Brunswick No. 12 deposit, in order to feed its concentrator complex.

The top of the HMLSDZ is approximately 900 m above surface and has been tested by ten diamond drill holes. The high cost of deep diamond drill programs make it desirable to extract as much geological information as possible from each drill core in order to assist in evaluating the potential economic viability of a deposit.

The purpose of this study was to assist in this regard by:

- recognizing and quantifying hydrothermal alteration mineral modes and zoning of haloes surrounding the HML South Deep massive sulphide zone,
- assessing the extent to which the geological environment of HML controlled the expression of the alteration haloes surrounding the South Deep zone;
- examining how and to what extent deformation-related metasomatism has modified the expression of hydrothermal alteration at the HMLSDZ; and
- identifying exploration parameters that are specific to deposit-related hydrothermal alteration and independent of prior igneous fractionation and subsequent deformation-induced metasomatism.

Pearce element ratio (PER) analysis was used in combination with other geological techniques (*e.g.*, thin section petrology and electron microprobe analysis) to pursue the above objectives.

1.3 - Location, Access, and Physiography

The study area comprises the region around the HML South Deep massive sulphide deposit located within the BMC of northern New Brunswick. It is located approximately 45 km west-southwest of the Brunswick No. 6 and No. 12 deposits, and 60 km southwest of Bathurst. The study area is accessible by dirt roads that branch off New Brunswick highway 430, south of Bathurst (Figure 1.2).

The HML deposit is on Crown land, and located near the boundary of the Northern and Eastern Miramichi Highlands. The Northern Highlands have rugged relief and are underlain by Lower Palaeozoic sedimentary and igneous rocks. Topography is strongly bedrock controlled; high areas are generally angular or peaked where underlain by resistant volcanic rocks, and rounded or flat-topped where underlain by intrusive (mainly granitic) rocks. Elevations generally range between 450 m and 600 m above sea level. The Eastern Highlands has gently rolling and hummocky terrain, and are underlain by Cambro–Ordovician volcanic and epiclastic rocks. Elevations are generally below 450 m above sea level, with local relief commonly 60-120 m above sea level (Rampton *et al.* 1984).

The Miramichi and Nepisiguit Rivers drain the HML area and are located immediately to the south and north, respectively. Watercourses exhibit both U-shaped (glacial origin) and incised V-shaped (fluvial origin) valley geometries.

Black spruce, balsam fir, jack pine, and alders occur in the low-lying areas, and red maple and white birch occur in the higher areas to the north. Wildlife includes species such as moose, black bear, deer, coyote, fox and partridge. Human activities in the HML area include logging, mineral exploration, hunting and fishing.

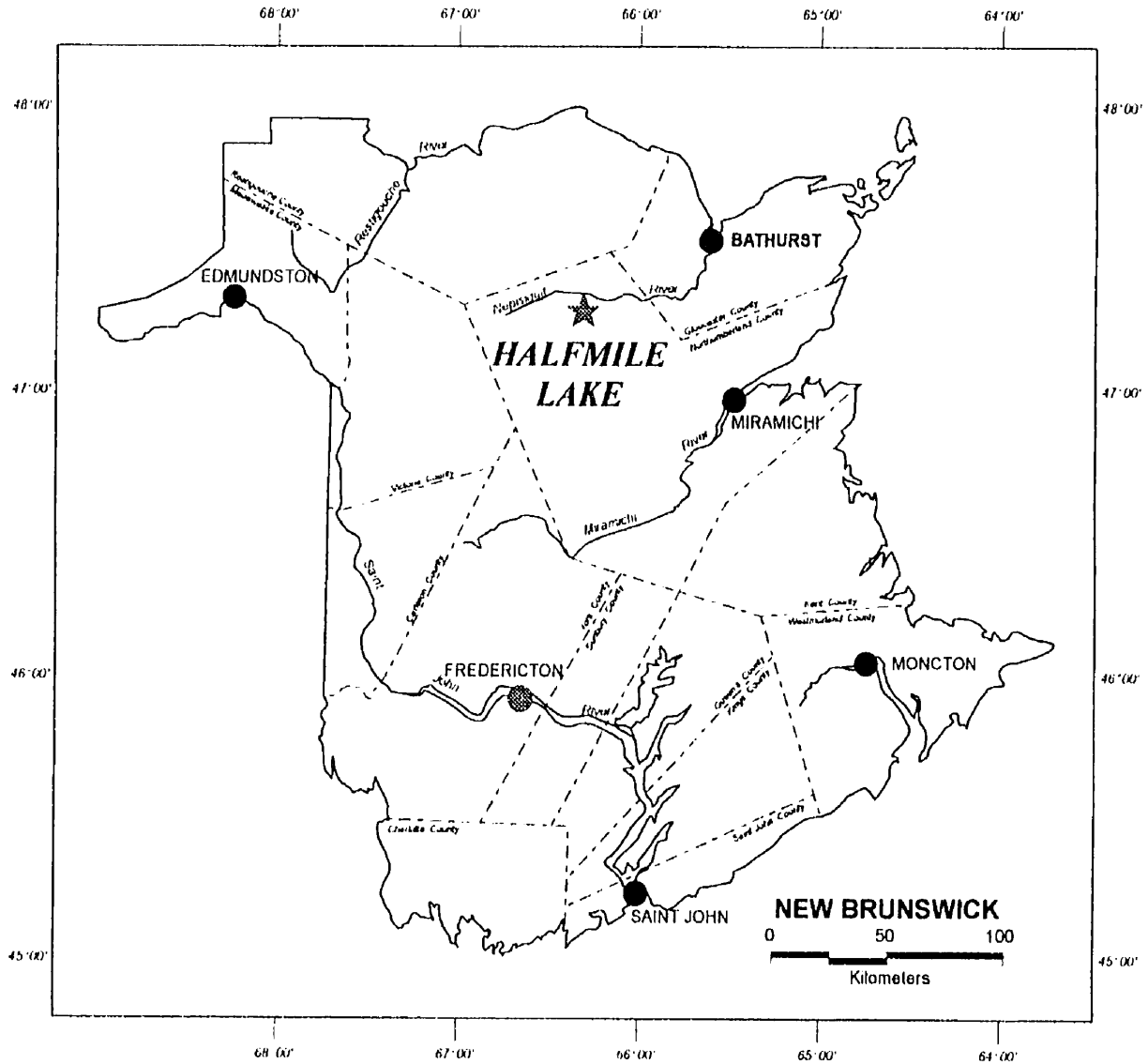

Figure 1.2 - Location map of study area

As is typical in the Bathurst Camp, outcrop comprises less then 5% of the surface area, largely because of variable thicknesses of glacial deposits (mostly till).

1.4 - Regional Geology

The rocks of the BMC belong to the Arenig-Llanvirn (465 – 470 Ma) Sheephouse, Tetagouche and California Lake groups, and the Llandeilo-Caradoc (460 Ma) Fournier Group (Wilson *et al.* 1998; Thomas *et al.* 2000). These groups conformably to disconformably overlie the Cambrian-Early Ordovician Miramichi Group (Figure 1.3) and are separated from one another by D_2 or younger thrust faults (McCutcheon 1997). Additionally, two thrust faults separate the three different stratigraphic sequences within the California Lake Group. A zone of blueschist metamorphism, typically associated with subduction zone environments, occurs along the thrust faults separating the California Lake and Fournier groups, part of the Brunswick subduction complex of van Staal (1994).

Descriptions of the various groups and formations comprising the BMC can be found in Thomas *et al.* (2000), van Staal and Rogers (2000), Fyffe *et al.* (1996), McCutcheon *et al.* (1993), Wilson (1993), and van Staal *et al.* (1992). Only the Tetagouche Group is described here because it hosts the Halfmile Lake deposit.

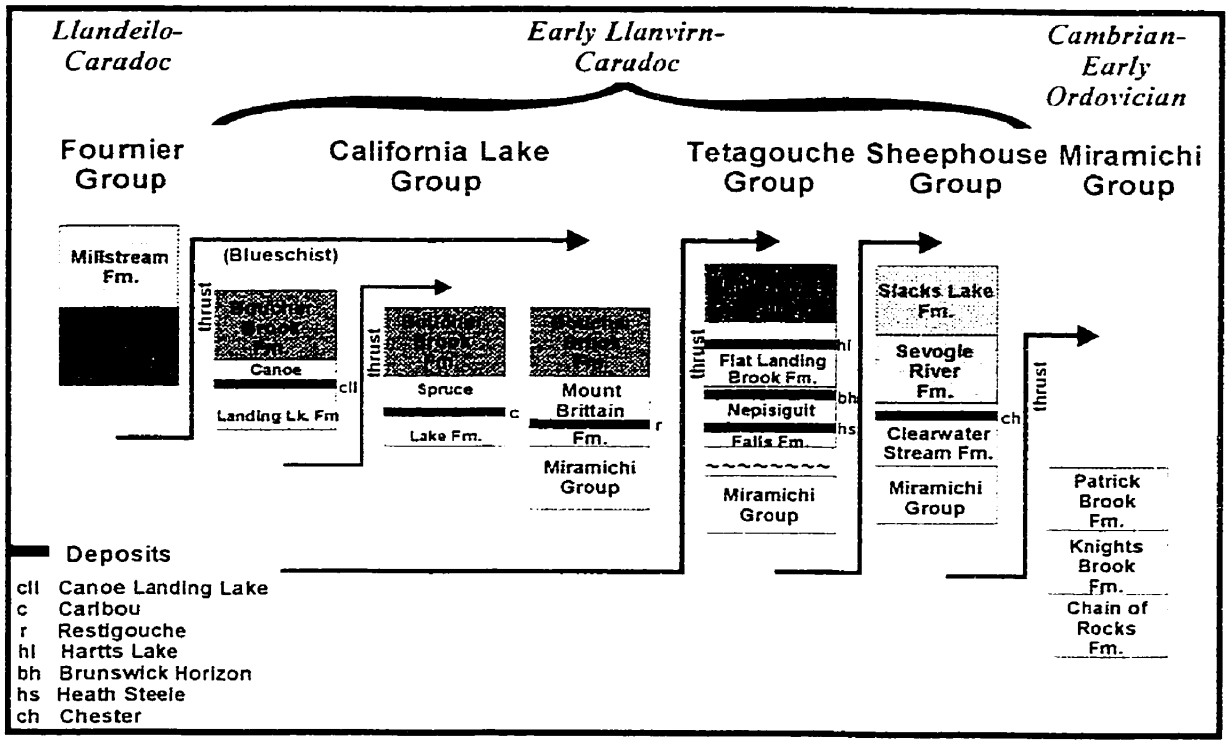

Figure 1.3. Schematic tectono-stratigraphy of the Bathurst Mining Camp showing the relationships among the various groups and the approximate positions of massive sulphide deposits (*used with permission*, from McCutcheon and Walker 2001)

The Tetagouche Group conformably to disconformably overlies the Miramichi Group and is structurally overlain by the California Lake Group. It is interpreted to have formed within an intracrustal (continental) proto-back-arc basin environment above a SE-dipping subduction zone (van Staal 1987; van Staal *et al.* 1991). The group subsequently underwent ductile deformation and was metamorphosed to upper greenschist facies in the Late Ordovician (Caradocian) to Late Silurian (Ludlovian) during closure of the back-arc basin (van Staal and Fyffe 1995a,b).

Felsic volcanic rocks dominate the Tetagouche Group but there are also minor mafic volcanic and sedimentary rocks. Of the 45 known VHMS deposits in the Bathurst mining camp, the Tetagouche Group hosts 31 of them, including the HML deposit. The four constituent formations within the Tetagouche Group, in ascending stratigraphic order, are the Nepisiguit Falls, Flat Landing Brook, Little River, and Tomogonops Formations (McCutcheon and Walker 2001).

The Nepisiguit Falls Formation (host to 23 of the 31 deposits) is characterized by intrusions of quartz-feldspar porphyry, medium to coarse grained quartz-feldspar-rich tuffs and volcaniclastic rocks with minor intercalated aphyric tuff (McCutcheon and Walker 2001). The pyroclastic or epiclastic rocks are commonly intercalated with light to dark greenish grey chloritic mudstone (locally Fe-rich) that constitutes the "*Brunswick Horizon*". The Nepisiguit Falls formation is 469 ± 2 Ma, based on U-Pb zircon dating (McCutcheon and Walker 2001).

Three additional members assigned to the Nepisiguit Falls Formation, include:

(i) Lucky Lake member - felsic ash tuff, lapilli tuff and minor quartz-phyric tuff (Wilson *et al.* 1998),

(ii) Little Falls member - ash tuff and fine to medium grained quartz-feldspar-phyric epiclastic rocks interbedded with black shale (Langton and McCutcheon 1993), and

(iii) Vallee Lourdes member - thin nodular to silciclastic limestone, calcareous sandstone and siltstone, disconformably overlying the Miramichi Group (van Staal *et al.* 1988).

The Flat Landing Brook Formation (host to 8 of 23 deposits) consists of aphyric to feldspar-phyric (± quartz) rhyolitic flows, hyaloclastites, pyroclastic rocks, minor sedimentary rocks, and minor iron formation. The crystal-rich rocks consist of feldspar and/or quartz phenocrysts (1 to 3 mm) supported in a cryptocrystalline matrix. The greater part of these rocks is interpreted to be hyaloclastites (van Staal 1987; Langton and McCutcheon 1990; Wilson 1993). The Flat Landing Brook Formation is reported to be 466 ± 2 Ma based on U-Pb zircon dating (Roger *et al.* 1997).

Mappable members within the Flat Landing Brook Formation include:

(i) Moody Brook member - fragmental rocks containing felsic clasts in a greenish grey to greenish black matrix of intermediate to mafic composition (Wilson 1993),

(ii) Forty Mile Brook member – tholeiitic pillow basalt flows and associated diabase and gabbro (van Staal *et al.* 1991), and

(iii) Roger Brook member – felsic crystal, lithic tuff and minor rhyolitic (Wilson *et al.* 1998)

The Little River Formation of Wilson *et al.* (1998) consists of mafic volcanic and associated epiclastic rocks that conformably overlie the Flat Landing Brook Formation.

Majority of these rocks were previously assigned to the Boucher Brook Formation of van Staal and Fyffe (1991). The Brunswick Mines and Beresford members are part of the Little River Formation (McCutcheon and Walker 2001).

The uppermost unit in the Tetagouche Group is the Tomogonops Formation (Langton 1994). It has been described by McCutcheon and Walker (2001) as a post-volcanic coarsening upwards sequence of light grey, thinly bedded, commonly calcareous siltstone (± limestone) and fine grained sandstone. The Tomogonops Formation apparently conformably overlies the early Caradocian shale and chert that marks the end of the Ordovician volcanism.

1.5 - Previous Work

1.5.1 - Bathurst Camp

The first lithogeochemical study to be published on the BMC was conducted by Whitehead and Goodfellow (1978) who used trace element concentrations to distinguish between tholeiitic and alkalic basalts. Their findings indicated that the large tonnage Brunswick deposits are spatially associated with the most alkalic basalts, which at the time were being interpreted as island arc deposits. Subsequently, van Staal (1987) used compositional and petrogenetic trace element discrimination plots of mafic and felsic volcanic and plutonic rocks to substantiate that the BMC formed in a back-arc rift setting. Additionally van Staal *et al.* (1991) used similar trace element compositional discriminants to map out the various suites of mafic and volcanic rocks in the BMC.

Most recent studies were part of a multi-disciplinary research program (EXTECH-II), sponsored by the federal and provincial governments and supported by the mining industry (Lentz 1996a). Five topics were addressed:

(1) provenance and paleoenvironmental characteristics of epiclastic rocks (Lentz *et al.* 1996);

(2) chemical variations in hydrothermal sedimentary rocks (iron formation) associated with massive sulphide deposits (Goodfellow 1975a,b; Peter and Goodfellow 1996);

(3) petrogenetic and lithotectonic synthesis of mafic to felsic volcanic and epiclastic rocks for chemostratigraphic applications (Lentz *et al.* 1996; Lentz 1995; Barrett and MacLean 1994a; Lentz and Goodfellow 1992, 1993a, 1993b, 1994);

(4) determination of chemical changes associated with hydrothermal alteration zones (Lentz 1996b); and

(5) deformation-induced metasomatism accompanying the development of a tectonic fabrics (Lentz 1999).

Lentz (1996a) documented that fine grained sedimentary rocks of the Miramichi Group have relatively higher Al_2O_3, LREE, HREE, Y, and Th but lower Mn compared with similar rocks in the Boucher Brook (now Little River) Formation. Lentz *et al.* (1996) also indicated that the high Al_2O_3 and high-field strength elements in the Patrick Brook Formation are characteristic of mature epiclastic rocks derived from intense chemical weathering in their source area. In contrast, the preservation of albite in the Boucher Brook epiclastic rocks was interpreted to indicate more immature epiclastic character. These observations were also used to suggest that the Boucher Brook Formation sediments were derived from their associated volcanic rocks (Lentz *et al.* 1996).

compared with those of the Nepisiguit Falls Formation (Lentz 1996b). At the Heath Steele B zone deposit, Lentz (1997) documented similar compositional differences between footwall and hanging wall crystal tuffs that challenge previous structural interpretations that they are part of the same unit. He indicated that the hanging wall tuff has slightly higher Zr, Y, REE, and Th as well as higher Zr/TiO_2 compared to the footwall crystal tuff.

The overprinting effect of deformation-induced material transfer was investigated by Lentz (1999), who analyzed four samples from the footwall to the Brunswick No. 6 massive sulphide deposit. Lentz (1999) documented that fabric development by pressure solution (solution transfer) occurred during the early stages of deformation (D_1) and was progressively enhanced by the continuous supply of aqueous fluid generated during dehydration of epiclastic and volcanic rocks, leading to the development of mica-rich septa and quartz-rich microlithons. He concluded that there was open system, rather than a closed system, redistribution of elements between these two domains.

1.5.2 - Halfmile Lake

The first detailed description of the Halfmile Lake deposit (South upper AB) was presented by Harley (1977), which included half a dozen whole-rock analyses on the felsic volcanic rocks. However, the first published lithogeochemical study on the Halfmile Lake deposit was that of Adair (1992). His study was conducted on 65 samples collected from a 920-metre interval in drillhole HN88-16 that cuts the entire stratigraphic sequence. The suite of elements analyzed included major oxide, rare-earth elements (REE) elements. Subsequently, Lentz (1996a) used data from Adair (1992) to investigate trace element ratios and trends in drill hole HN88-16.

Adair (1992) indicated that compared with rocks mildly altered hydrothermally, those associated with the stringer zone are characterized by sodium depletion, minor potassium enrichment, Co and Cu enrichment, and minor Ba depletion. Strongly chloritized black argillites were found to contain low total alkalis and silica, reflecting their alteration mineralogy. Zn and Mg enrichment and strong Ba depletion within the massive sulphide zone was reported by Adair (1992).

Adair (1992) used Winchester and Floyd trace element discrimination diagrams to determine the compositions of the felsic volcanic rocks, which plotted in the dacite/rhyodacite field. Mafic volcanic rocks mainly plotted in the andesite field. Adair (1992) also indicated that trace element characteristics of the sedimentary rocks at Halfmile Lake suggest that they were derived exclusively from the felsic volcanic rocks.

1.6 - Methodology

A summary of the various techniques adopted in the study of the petrology and lithogeochemistry of the rocks hosting the HMLSDZ follows.

1.6.1 - Drillcore Logging

Prior to sample collection, the ten drill cores through the HMLSDZ were logged from the base (structural footwall) into the structural hanging wall. These logs, with their lithologic descriptions, are presented in Tables A1-A10 (Appendix A). Information collected from each drill hole includes core interval, rock type, a brief description or modifier of the rock type, and the degree and type of hydrothermal alteration. The units identified were siltstone, mudstone, greywacke, cherty tuff, felsic tuff, dyke, basalt, quartz-feldspar porphyry, and quartz-eye tuff. Intervals where sulphide mineralization was encountered in these host rocks were also noted.

Significant differences were observed between these logs and those produced by Noranda during exploration of the HMLSDZ. These differences are attributable to the intense alteration and deformation that these rocks have suffered, the finely interbedded nature of the volcano-sedimentary package, and the difficulty in distinguishing between pyroclastic volcanic rocks and epiclastic rocks derived from them.

1.6.2 - Sampling

Within each logged geological interval, representative samples were collected to investigate the lithogeochemistry and petrology of the different rock types. The downhole depth and survey coordinates for two hundred and twenty two (222) samples collected from ten drill holes are presented in Table B.1 (Appendix B). The samples were collected from the base of these drill holes (at most 50 meters into the structural footwall or stratigraphic hanging wall), through the deposit, up to as much as 400 m into the structural hanging wall (stratigraphic footwall).

The field description of the samples, including rock type, modifier, and alteration characteristics are presented in Table B.2 (Appendix B). The rock types recorded in some cases differed from the names of the logged intervals from which they were collected due to the interbedded, transitional and intensely altered nature of the stratigraphic sequence.

1.6.3 - Laboratory Rock Descriptions

Further description of the drill core samples was conducted in the geology laboratory at Acadia University, prior to submitting the samples to X-Ray Analytical Laboratory (XRAL) in Don Mills, Ontario for geochemical analysis. The parameters identified for each sample included rock type, modifier, mineralogy and degree of alteration, the intensity of quartz veining, and the abundance of sulphide ore minerals. These are

presented in Table B.3.1 (Appendix B). The degree of alteration was estimated on a relative scale of 1 to 5. A value of 1 represented least altered, whereas a value of 5 denoted most altered samples. Similarly, the abundance of sulphide minerals was also scaled from 1 to 5, 1 being trace and 5 being abundant. The presence and intensity of quartz veining was also estimated in percent.

These hand sample descriptions, obtained under optimal conditions (under proper light conditions, on washed samples, using diagnostic mineral tests, *etc.*), varied in some cases from the hand sample descriptions collected in the field. These changes illustrate the difficulty in accurately identifying these rocks reflecting subtle lithological variations, metasomatism and intense deformation. Magnetic susceptibility and density readings were recorded for all the samples and are presented in Table B.3.2 (Appendix B).

1.6.4 - Thin Sections

Due to the difficulty in conclusively identifying the lithologies and the degree of alteration of hand samples, 81 standard thin sections were investigated. The results of the petrographic analysis of these thin sections, representing the various lithologic units encountered at the HMLSDZ, are presented in Appendix C. The data collected for each sample included texture, matrix and phenocryst (if any) size, mineral mode, hydrothermal alteration assemblage, structural features, and any other relevant geological characteristics.

1.6.5 - Electron Microprobe Analysis

Electron microprobe analysis was conducted on 20 polished thin sections to determine the compositions of primary (igneous) and secondary (alteration) minerals. The compositions of the suite of minerals examined (muscovite/phengite, chlorite,

feldspars, carbonate, epidote, titanite, and biotite) are presented in Table D.1 – D.6 (Appendix D). Geological standards were used to crosscheck the accuracy and precision of the analytical technique.

The EMP analyses were carried out on a JEOL 733 electron microprobe equipped with four wavelength diffraction spectrometers (WDS) and an Oxford Link eKL energy dispersive system (EDS). The energy dispersive system was used for all elements. Resolution of the energy dispersive detector was 137 eV at 5.9 keV.

Each spectrum was acquired for 40 seconds with an accelerating voltage of 15 kV and a beam current of 15 nA. The electron microprobe spot size was approximately 1 micron. The raw data were corrected using Link's ZAF matrix correction program. Instrument calibration was performed on cobalt metal. The precision of the instrument on cobalt metal (n = 10) was ± 0.5% at one standard deviation. Accuracy for the major elements was ± 1.5 to 2 %, relative. Geological standards were used as controls. Detection limits for most elements using the energy dispersive system ranged from approximately 0.1 to 0.3 percent.

1.6.6 - Geochemical Analysis

Analytical results for 222 samples are presented in Table E.1 (Appendix E). This geochemical database includes the analytical technique (A.M.), detection limit (D.L.) and analytical unit (A.U.) for each element analyzed. The results include major oxides (SiO_2, Al_2O_3, CaO, MgO, Na_2O, K_2O, Fe_2O_3, MnO, TiO_2, P_2O_5, Cr_2O_3, LOI, total S, total C, and H_2O^+), major elements (Na, Mg, Al, P, K, Sr, Ca, Ti, Fe), lithophile trace elements (Rb, Sr, Y, Zr, Nb, Ba, Be) and transition trace elements (Cu, Pb, Zn, Ag, Co, Ni, As, Mo, Cd, Sc, Sn, Sb, Bi, V, Cr, Mn). The geochemical analyses were conducted by X-ray Analytical Laboratory (XRAL) in Don Mills, Ontario.

The major oxides and lithophile trace elements were analyzed using lithium metaborate ($LiBO_2$) fusion-XRF and pressed pellet-XRF techniques, respectively. The lithophile and transition trace elements in the sulphide-bearing samples were analyzed using an aqua regia digestion with an ICP finish. LECO correlation spectrometry was used to determine total C and total S, and H_2O^+ concentrations in the samples were determined using the Penfield technique.

1.6.7 - Geochemical Data Evaluation

VHMS deposits exhibit variations in lithogeochemical composition as a result numerous effects. Some of these variations are related to mineral deposit formation processes, *e.g.*, hydrothermal metasomatism, whereas others result from geological processes *e.g.*, sediment deposition, diagenesis, igneous fractionation, seafloor metamorphism, regional or contact metamorphism, weathering, *etc.* Still other variations are mathematical figments of the nature of compositional data and reflect variations that, although possibly of interest to the mathematician, are generally of no interest to

geologists (*e.g.*, closure). Finally, other variations are unavoidable and a result of sampling and analytical error (Stanley and Madeisky 1996).

Geochemical investigation of the rocks hosting the HMLSDZ was pursued using Pearce element ratio (PER) analysis. PER analysis is one of several techniques for studying compositional variation in rocks, and can be tailored to investigate specific material transfer processes (igneous fractionation, sediment deposition, diagenesis, hydrothermal metasomatism, *etc.*). The advantage of the PER methodology over other material transfer techniques (Akella 1966; Gresens 1967) is that the PER's are expressed in molar, rather than mass, terms. As a consequence, primary and secondary material transfer processes can be investigated using the stoichiometry of the various minerals and chemical reactions involved in these processes as templates for comparison and hypothesis testing.

Theoretically, PER analysis, and all other material transfer techniques, are based on a fundamental material transfer equation:

$$X_{ip} + dX_i = X_{id}, \tag{1.1}$$

where X_{ip} is the amount (moles, mass or volume) of the element i in the parent rock, X_{id} is the amount of the element i in the daughter rock, and dX_i is the amount of the element i added or removed from the parent by the material transfer process. The concentration (x) of the element i in the parent or daughter rock is defined by the relation:

$$x = \frac{X}{S}, \tag{1.2}$$

where X is the amount (moles, mass or volume) and S is the system rock size. By substitution of Equation 1.2 into Equation 1.1, we obtain:

$$S_p x_{ip} + dX_i = S_d x_{id}, \tag{1.3}$$

where S_p is the size of the parent rock, S_d is the size of the daughter rock, and x_{ip} and x_{id} are the concentrations of element X in the parent and the daughter rock, respectively. An equation of this form exists for every element ($i = 1 \ldots n$, where n is the number of elements) in a set of parent and daughter rocks.

In order to solve the set of equations for any n elements in a suite of rocks, at most n unknowns must exist. However, each material transfer equation (Equation 1.3) has five variables and only two of which are common to each equation. This means that there are initially $3n+2$ unknowns, which are too many to allow simultaneous solution of the n equations. The concentration terms (x_{ip} and x_{id}) in each equation can be determined by geochemical analysis of the parent and daughter rocks. This reduces the number of unknowns to $n+2$; still too many for simultaneous solution of the n equations. We can further reduce the number of unknowns to $n+1$ by invoking the Scaling Law (which states that, fixing the size of one extensive variable in a system will cause all other extensive variables in the system to be scaled accordingly without loss of generality). Thus, we can assign a parent rock size of 100 (for example). The last unknown can only be eliminated by imposing a geologically reasonable assumption.

Three fundamentally different approaches (Pearce 1968; Akella 1966; Gresens 1967) have been utilized to this purpose, and each uses an additional geological or geochemical constraint to formulate an additional equation such that the number of equations equals the number of unknowns. The approach used in this study, Pearce (1968), is discussed below. The alternative techniques, *i.e.*, Akella (1966) and Gresens (1967), are discussed and contrasted in Stanley and Madeisky (1996).

Consider two elements (X and Z) in a rock that have been affected by a material transfer process (*e.g.*, igneous fractionation, hydrothermal metasomatism, diagenesis, clastic fractionation, metamorphic metasomatism, *etc.*). Hence:

$$S_p x_p + dX = S_d x_d, \quad \text{and} \quad S_p z_p + dZ = S_d z_d. \tag{1.4}$$

If we assume a parent rock size (S_p), and measure the parent and daughter rock compositions, there are two material transfer equations in three unknowns (dX, dZ, S_d). A third equation, or an assumption (constraint) is thus required to allow simultaneous solution of the unknowns. One equation-providing constraint employed by the Pearce (1968) and Akella (1966) methods is that one element (say Z) did not participate in the material transfer (*i.e.* - it was conserved). The equation:

$$dZ = 0, \tag{1.5}$$

is thus the third equation necessary to solve the system of equations. As a consequence, if Z is conserved, the amount of material transfer of X or any other element (Y), can be determined.

Although the Pearce element ratio approach utilizes the above approach, it is best understood by considering how a concentration ratio changes. For the two elements (X and Z), the ratio of their concentrations can be expressed as:

$$\frac{x}{z} = \frac{X/S}{Z/S} = \frac{X}{Z}, \tag{1.6}$$

from Equation 1.2.

This intensive variable ratio (x/y) is thus equal to its corresponding extensive variable ratio (X/Z). The reason for change in intensive variable ratio can be determined by differentiating the above equation (from first principles calculus):

$$d(\frac{x}{z}) = \frac{dX}{Z} - \frac{X}{Z^2}dZ \tag{1.7}$$

If the denominator element is conserved ($dZ = 0$), this reduces to:

$$d(\frac{x}{z}) = \frac{dX}{Z} \tag{1.8}$$

Thus, the change in an element concentration ratio with a conserved denominator is exactly proportional to the amount of material transfer of the numerator element.

Let us now consider the diagram with axes of two different PER's presented on Figure 1.4, where Z is a conserved element. If a material transfer process changes the composition of a parent rock into a daughter rock, the slope of a line on this diagram between where the parent and daughter rocks plot is:

$$m = \frac{d(y/z)}{d(x/z)} = \frac{ydZ - zdY}{xdZ - zdX} = \frac{dY}{dX}; \tag{1.9}$$

because $dZ = 0$ (Figure 1.4).

Thus, on a PER diagram, the trend describing the effects of material transfer in rocks are linear and the slopes of the lines are solely a function of the material transfer stoichiometry (dX, dY). As a consequence, regardless of the composition of the parent rock, material transfer will cause the daughter rock compositions to be displaced along a line with a fixed slope of dY/dX.

For example, if the material transfer process involved the sorting of albite in a magma, for every mole of albite lost from the melt, one mole of Na and one mole of Al would be lost. Consequently, on an Al/Z versus Na/Z (where Z is a conserved element) PER diagram, the melt composition would be displaced one proportional unit downward

along each axis. As a result, all daughter compositions would plot along a line with unit slope, and this slope is a fingerprint of the material transfer process (albite loss).

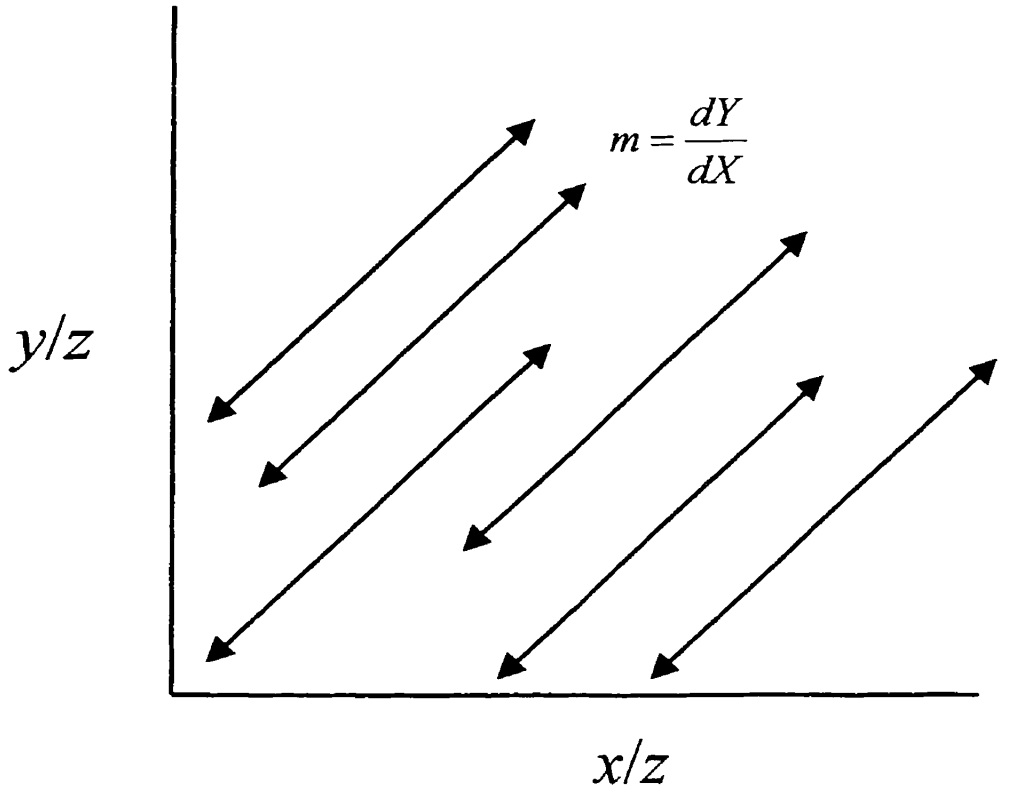

Figure 1.4 - The effect of material transfer on a rock composition is dependent on only the material transfer process stoichiometry ($m = dY/dX$) on a PER diagram where the denominator is conserved ($dZ = 0$). Material transfer will cause rock compositions to be displaced up and down these parallel lines, depending on the signs of dX and dY.

1.6.7.1 - Conserved Elements

The first step in any PER data evaluation involves plotting potentially conserved elements against each other on scatterplots. In hydrothermally altered volcano-sedimentary rocks, these are typically elements that are both incompatible in igneous melts and immobile in hydrothermal fluids (*e.*g., Ti, Zr, Y, Nb, *etc*). Data trends that can be approximated by a single line that passes through the origin are then interpreted to be composed of samples that are related (cogenetic) to a single parent rock composition that was at one time homogeneous. When observed, this also indicates that the elements on both axes are conserved (Figure 1.5). Examination of all possible scatterplots of potentially conserved elements allows identification of elements that are conserved in a suite of rocks, and thus are most suitable as the denominator in any subsequent PER analysis.

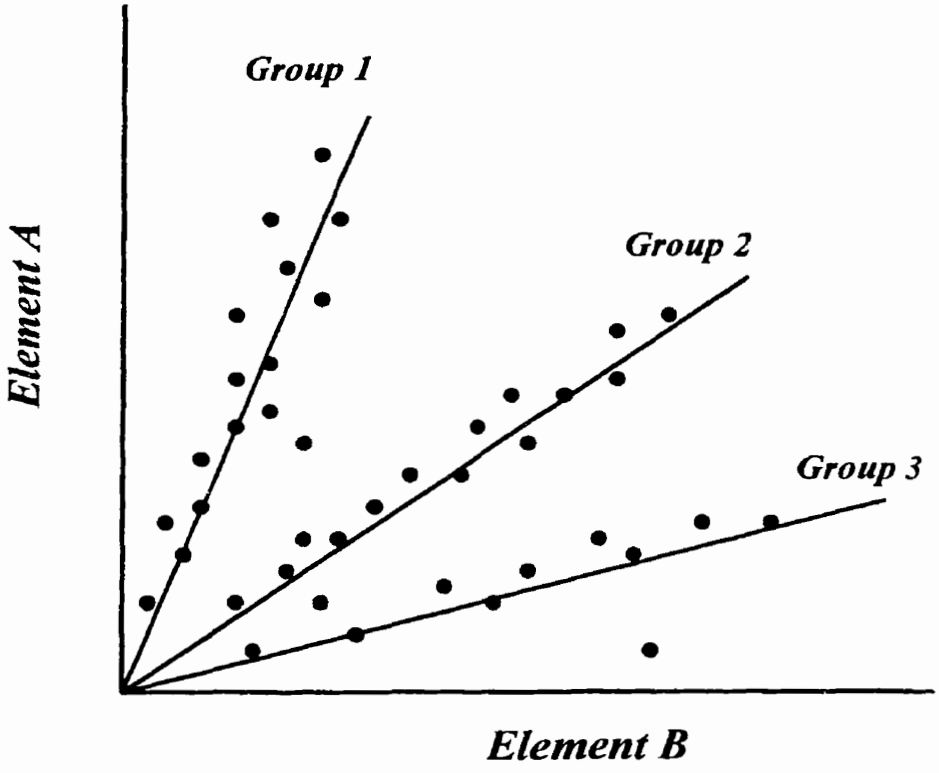

Figure 1.5 - Conserved element scatterplot designed to test the cogenetic hypothesis. The existence of a conserved element in a dataset is critical to any PER lithogeochemical study because it is used in the denominator of all PER's. On this diagram, rock compositions that plot along a single line passing through the origin indicate that the rocks are related to a common parent that was at one time homogeneous, and that the two elements making up the axes of the diagram are conserved. In this example, three distinct rock compositions can be discriminated by the two elements (*A* & *B*). As a consequence, either of these two conserved elements may be selected for use in subsequent PER analysis, but these three rock types must be evaluated independently.

1.6.7.2 - Calculating PER's

Pearce element ratios can be determined directly from mass concentrations by the formula:

$$PER_{i/j} = \frac{x_i / g_i}{x_j / g_j} \tag{1.10}$$

where, x = element/oxide mass concentration, and g = gram formula weight. In this scenario, element j is a conserved element, and if i is a major oxide, the gram formula weight used is the weight of the oxide containing only one cation (*e.g.* – the gram formula weight of $AlO_{3/2}$ instead of Al_2O_3). Table 1.2 and Equation (1.11) illustrate the steps for calculating PER's.

Table 1.2 - Data required to calculate a Pearce element ratio of Al/Ti using Equation 1.10 (Stanley and Madeisky1996)

	Al_2O_3	TiO_2
x (wt. %)	11.00	0.50
g (grams)	101.93/2	79.90

Thus, the Pearce element ratio of Al/Ti is:

$$PER_{Al/Ti} = \frac{11.00 / \left(\frac{101.93}{2}\right)}{0.50/79.9} = 34.49 \tag{1.11}$$

Pearce element ratios were calculated for all major oxides, plus C, S, and OH. These ratios were used to design PER fractionation and metasomatic control diagrams that

assisted in the interpretation of the controls on the composition of the host rocks to the HMLSDZ.

1.6.7.3 - Compositional Variation Controls

Having established that the suite of rocks under investigation is cogenetic and that at least one element is conserved, investigation of the sources of lithogeochemical variation can be pursued. Because host rocks to the HMLSDZ are volcanic and/or epiclastic, a primary lithogeochemical variation in these rocks was probably caused by feldspar fractionation/sorting.

A PER diagram that plots $(2Ca+Na+K)/Z$ versus Al/Z, where Z is a conserved element, can be used to test the hypothesis of feldspar fractionation as a primary control on the composition of feldspar-bearing rocks (Figure 1.6; filled circles). On this diagram, fresh (or least altered) samples will plot along a line with unit slope if they have been affected by feldspar fractionation. However, samples that are displaced from the line with unit slope will have been affected by another or a different material transfer process (open circles). For example, if the feldspar in the rocks was hydrothermally altered to muscovite, the rocks should plot along the line with a slope of 1/3, corresponding to the K/Al ratio in muscovite.

In contrast, if these rocks were chlorite-altered, the samples would plot along the line with zero slope, because chlorite contains no Ca, *Na* or *K*. PER diagrams can thus be used to investigate and model compositional variation controls in rocks, and allow recognition of overprinting or alternative material transfer processes that have affected rocks. In fact, the direction and extent of disparity between rocks affected by another material transfer process and the primary compositional control model can be used to

determine the nature and intensity of that process. For example, in Figure 1.6, the vertical residual from the fresh sample fractionation line to a hydrothermally muscovite or chlorite-altered sample is a measure of the amount of metasomatism (alkali loss) that has affected these rocks.

This PER diagram allows one to quantify the extent of metasomatism (via the vertical residual from the fractionation line) and allows metasomatism to be understood in terms of the resulting hydrothermal alteration mineralogy because specific alteration minerals have material transfer effects with specific behaviour on this diagram. For example, sericitization of any feldspar composition will cause displacement of fresh samples from a line with unit slope to a line with slope of 1/3, reflecting the stoichiometric ratio of (2Ca+Na+K)/Al in muscovite (= 1/3). Similarly, chloritization will displace these rocks to the abscissa (and a zero slope), because of the stoichiometric ratio of (Ca+Na+K)/Al (= 0) in chlorite.

In some cases, multiple material transfer processes can interfere with one's ability to investigate specific compositional variation controls. In these cases, modification of the PER diagram may be necessary to project from a mineral or material transfer. For example, the addition of calcite in the rocks investigated on Figure 1.6 would displace rock compositions straight up across the diagram, obstructing any ability to recognize feldspar sorting control. However, by subtracting CO_2/Z from the ordinate axis, the effects of any Ca addition will be negated because calcite contains 1 mole each of Ca and CO_2. This approach allows one to systematically identify, isolate, and quantify the effects of individual material transfer processes, and allows a thorough investigation of the controls on rock composition.

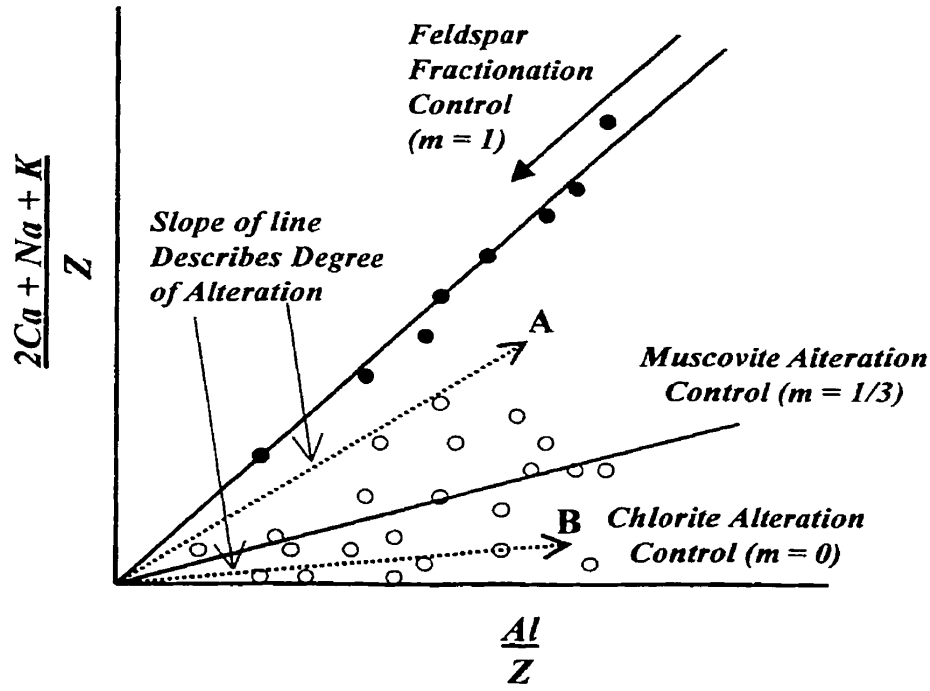

Figure 1.6 - PER diagram to test the hypothesis of feldspar (anorthite, albite, and potassium feldspar) fractionation. On this diagram, feldspar fractionation will displace rock compositions along a line with slope of unity, irrespective of the feldspar composition. Samples that plot below the fractionation line may be interpreted to have undergone an overprinting metasomatic material transfer, (alkali loss). In this example, the solid circles would be fresh or relatively unaltered rocks and the open circles would be moderate to intensely hydrothermally altered.

Molar element ratio diagrams (Figure 1.7) were used to investigate the behaviour of characteristically mobile elements (Si, Mg, Fe, Ca, Na, K, OH, *etc.*) in the HML hydrothermal system. A hybrid element ratio diagram was constructed by plotting the slope, $(2Ca+Na+K-2CO_2)/Al$ (where calcite, the predominant carbonate composition, is projected from), of a line from a data point to the origin on the modified version of Figure 1.6 on the abscissa, and the simple PER of each of the various elements listed above, on the ordinate axis (Figure 1.7). This produces a diagram that allows determination of how hydrothermally altered a rock is (the extent of hydrolysis on the abscissa; 1 = unaltered; 1/3 = muscovite-altered, 0 = chlorite-altered) and how much material transfer of a specific element took place during this hydrothermal alteration.

On this diagram, one can determine which elements participated in the hydrothermal reactions that produced muscovite from feldspar, and chlorite from muscovite.

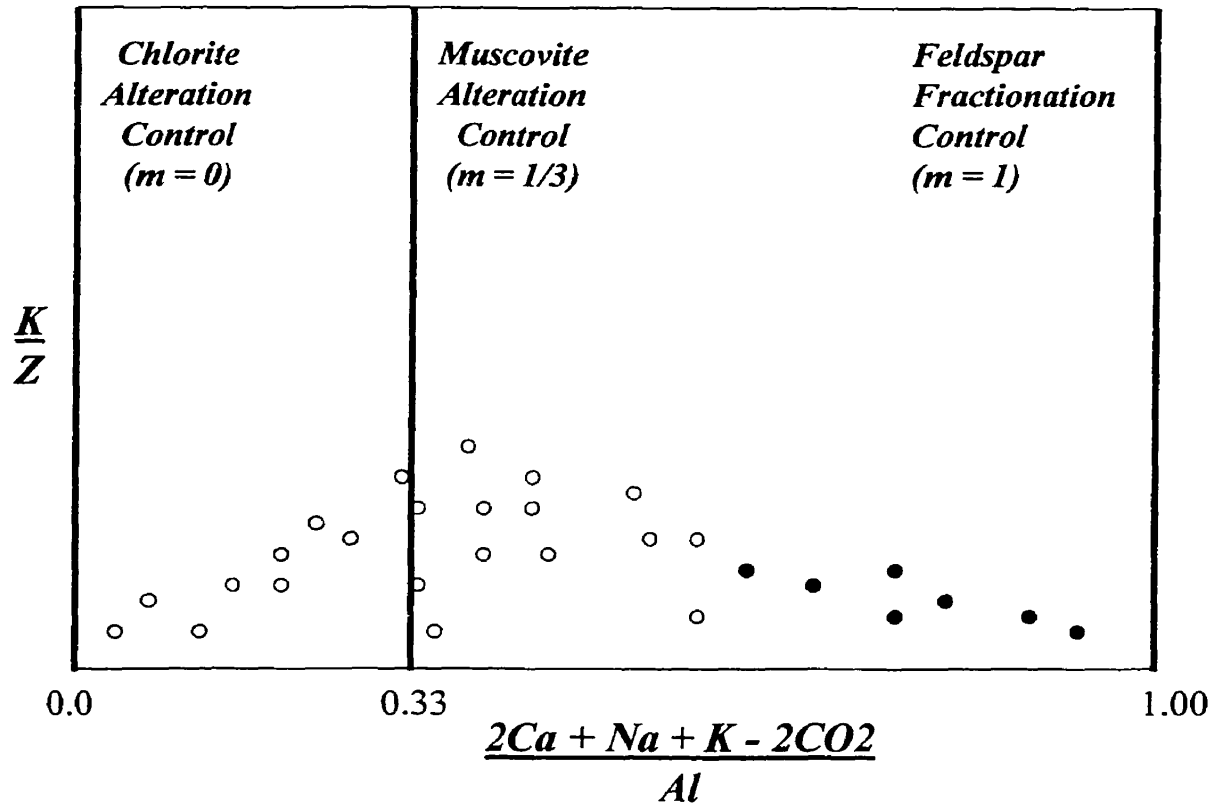

Figure 1.7 – Molar element ratio diagram specifically designed to investigate the material transfer of various elements during hydrothermal alteration. This diagram plots the ratio $(2Ca+Na+K-2CO_2)/Al$ versus K/Z, where Z is any conserved element in the dataset. Note that the material transfer of calcite has no effect on this diagram because subtraction of CO_2 from the numerator causes this diagram to be projected from calcite. The abscissa (also known as *hydrolysis metric*) represents the slope of a line from any point on Figure 1.6 to the origin, and is an optimal estimate of the degree of alteration that has affected the samples. The ordinate gives an actual measure of the amount of K added or removed during the hydrothermal alteration. Samples plotting close to an abscissa value of 1 are fresh or least altered. Muscovite-altered rocks will plot on the abscissa at 1/3 and chlorite-altered rocks will plot at zero on the abscissa axis. The pattern observed in the synthetic data on this diagram indicates that K was added during muscovite alteration of feldspar, but lost during subsequent chloritization.

1.6.7.4 - General Element Ratio Diagrams

General element ratio (GER) diagrams have also been used in evaluation of the lithogeochemical concentrations (Stanley and Madeisky 1996). These diagrams are similar to PER diagrams, in that they have axes composed of molar ratios with a common denominator; however, the denominator is not conserved and may, as in PER diagrams, be a linear combination of elements. GER diagrams use a different petrological constraint than that of denominator conservation to produce the extra equation required to solve the system of material transfer equations (Equation 1.3). The GER approach establishes a stoichiometric relationship between the two diagram numerators *and* the common denominator, instead of just between the two numerators, as in PER diagrams, so that the effects of material transfer can be deduced.

On a GER diagram, the slope of a line between the parent and daughter rocks is:

$$m = \frac{d(\frac{y}{z})}{d(\frac{x}{z})} = \frac{\frac{y}{z} - \frac{dY}{dZ}}{\frac{x}{z} - \frac{dX}{dZ}} \tag{1.11}$$

and this is a function of both initial parent (rock) composition (x, y, z) and material transfer stoichiometry (dX, dY, dZ). As a result, on a GER diagram, material transfer will displace rock compositions along lines with a common intercept (through the point dX/dY, dY/dZ)) instead of along lines with a constant slope, as in the case of PER diagrams (Figure 1.5).

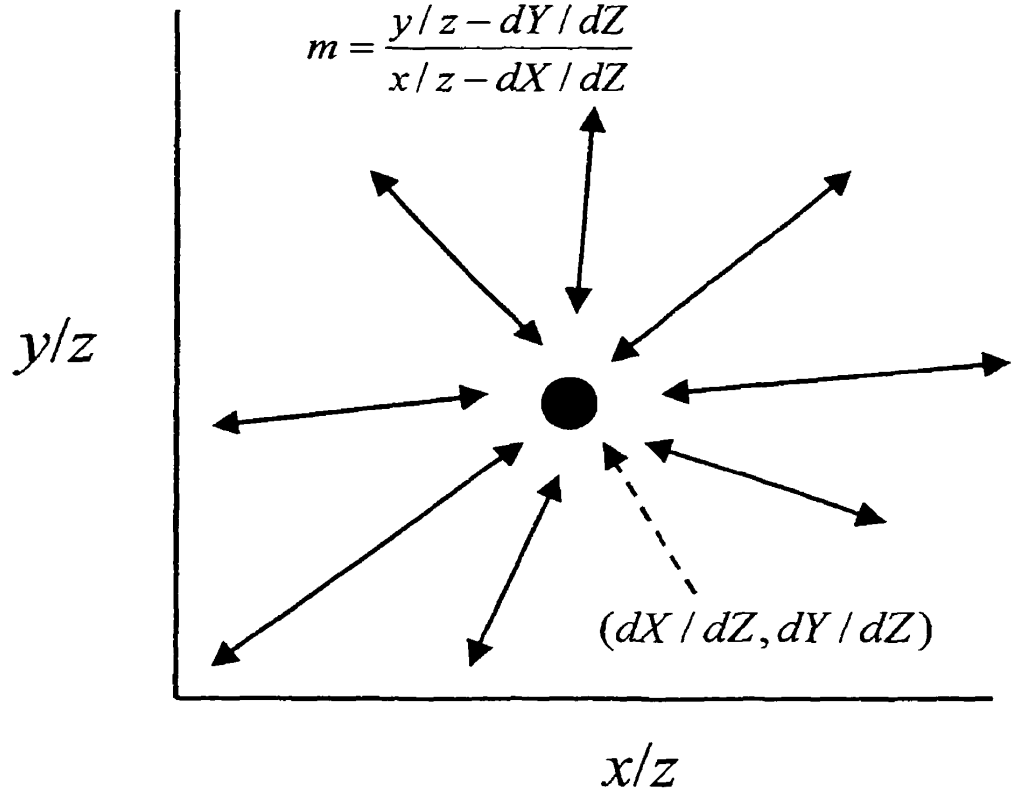

Figure 1.8 - The effect of material transfer on a rock composition is dependent on both the initial rock composition and the material transfer process stoichiometry on a GER diagram. Material transfer will cause rock compositions to be displaced toward or away from the point (*dX*/*dZ*, *dY*/*dZ*), where the material transfer phase plots, depending on the signs of *dX*, *dY*, and *dZ*.

1.6.8 - Spatial Data Presentation

Table B.1 (Appendix B) contains the spatial coordinates (easting, northing, and elevation) for the samples collected. These coordinates were determined with the aid of a MATLAB computer program (Navigator) available on Dr Stanley's web page (*ace.acadiau.ca/~cstanley/index.htm*). This program utilizes drill hole collar coordinates, and down-hole survey information (downhole depth, azimuth and plunge; as derived from Noranda's drill logs) to determine the actual coordinates of samples on the mine grid.

To provide a better perspective of any spatial lithogeochemical patterns that might exist in the dataset, these sample location coordinates were manipulated using a Microsoft-Excel spreadsheet that translates, rotates and tilts the mine grid into an orientation that will provide the best longitudinal perspective of the geochemical data in space. The origin of the mine grid was translated to the point (2000 m, 4000 m, 0 m) and then subsequently rotated 60° counter-clockwise. Finally, the mine grid was tilted 20° westward. This produced a rotated and tilted set of sample location coordinates (RTSL) that allowed production of an oblique longitudinal section that is approximately parallel to the drill holes from which the samples were collected.

The resulting RTSL data was then used to produce longitudinal sections illustrating the degree of hydrothermal alteration observed using molar element ratios specific to this task.

2 – GEOLOGICAL SETTING OF HALFMILE LAKE

2.1 - Stratigraphy

The stratigraphic succession at HML North, South Lower AB, and South Deep Zones is illustrated on Figure 2.1. The "Lower" and "Upper" Tetagouche divisions of Adair (1992) correlate with the Nepisiguit Falls and Flat Landing Brook formations, respectively. The Lower division includes quartz-feldspar porphyry, layered felsic tuff, quartz-eye tuff, felsic lapilli tuff, volcanic-derived sedimentary rocks. These exhibit a transition from a volcanic-dominated stratigraphy in the northeastern part of the deposit to a sediment-dominated stratigraphy in the southwest (Figure 2.2). The Upper division consists of mafic flows and tuff, and mafic volcanic rocks with felsic fragments. These rocks are locally interbedded with the Lower Tetagouche rocks (Adair 1992). Wilson *et al.* 1998 have assigned the mafic rocks at the top of the HML South AB zone stratigraphy to the Moody Brook member of the Flat Landing Brook formation.

Structurally, the entire sequence is overturned, and drill sections exhibit an inverted stratigraphy. The stratigraphic footwall (structural hanging wall) to the massive sulphide zone is dominated by quartz-feldspar porphyritic intrusions, aphyric to phyric pyroclastic rocks and fine to coarse grained epiclastic rocks. The stratigraphic hanging wall (structural footwall) consists of predominantly felsic volcanic rocks that include felsic tuff, crystal tuff, and minor epiclastic rocks. Dykes and flows with compositions ranging from basalt to rhyolitic occur in the footwall and hangingwall.

The rocks at HMLSDZ correlate with the Lower Tetagouche division of Adair (1992). However, the mafic rocks at HMLSDZ are basalt dykes that are commonly

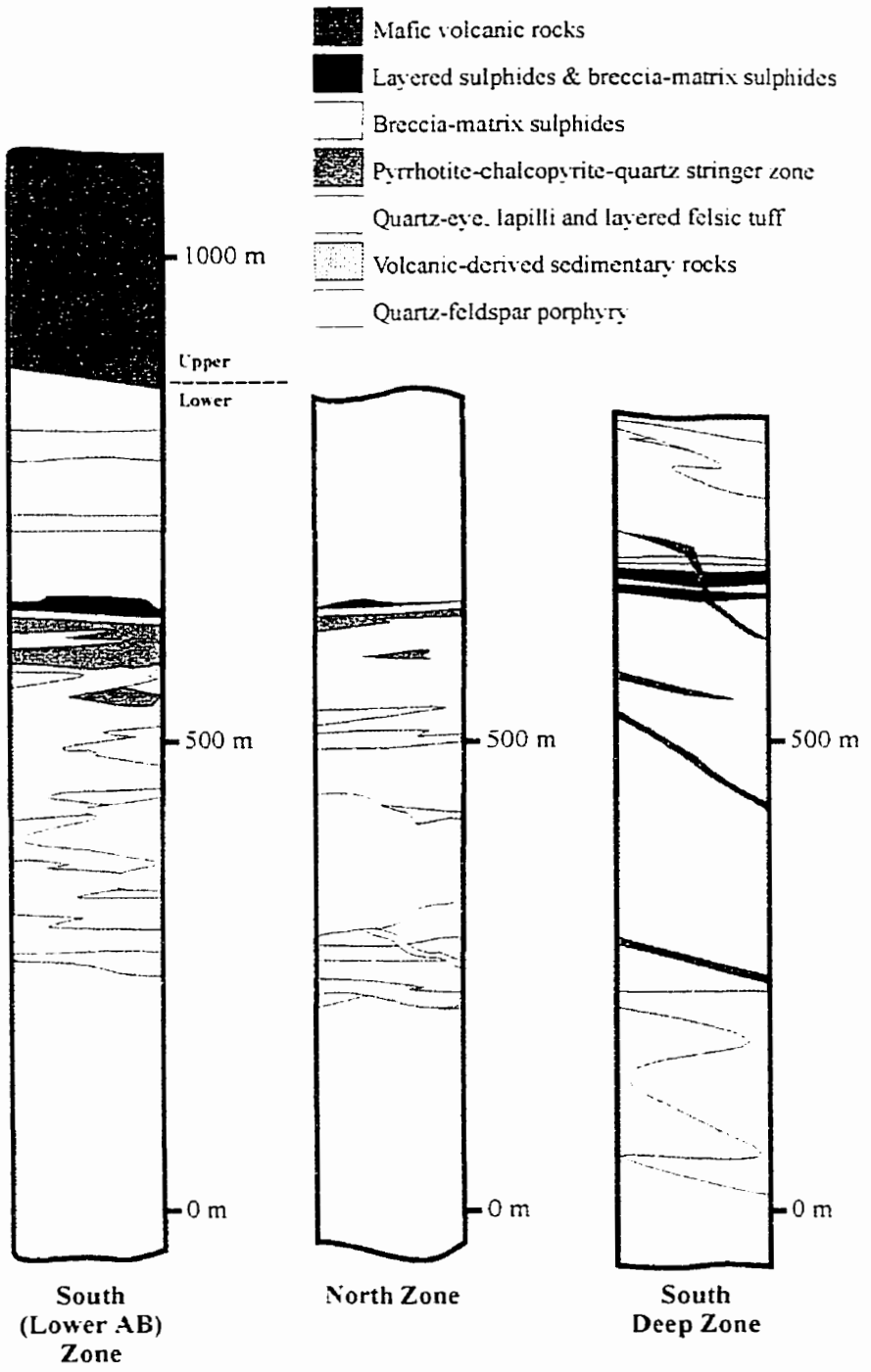

Figure 2.1 - Stratigraphic column of the Halfmile Lake South AB, North, and Deep Zones (modified and augmented from Adair 1992)

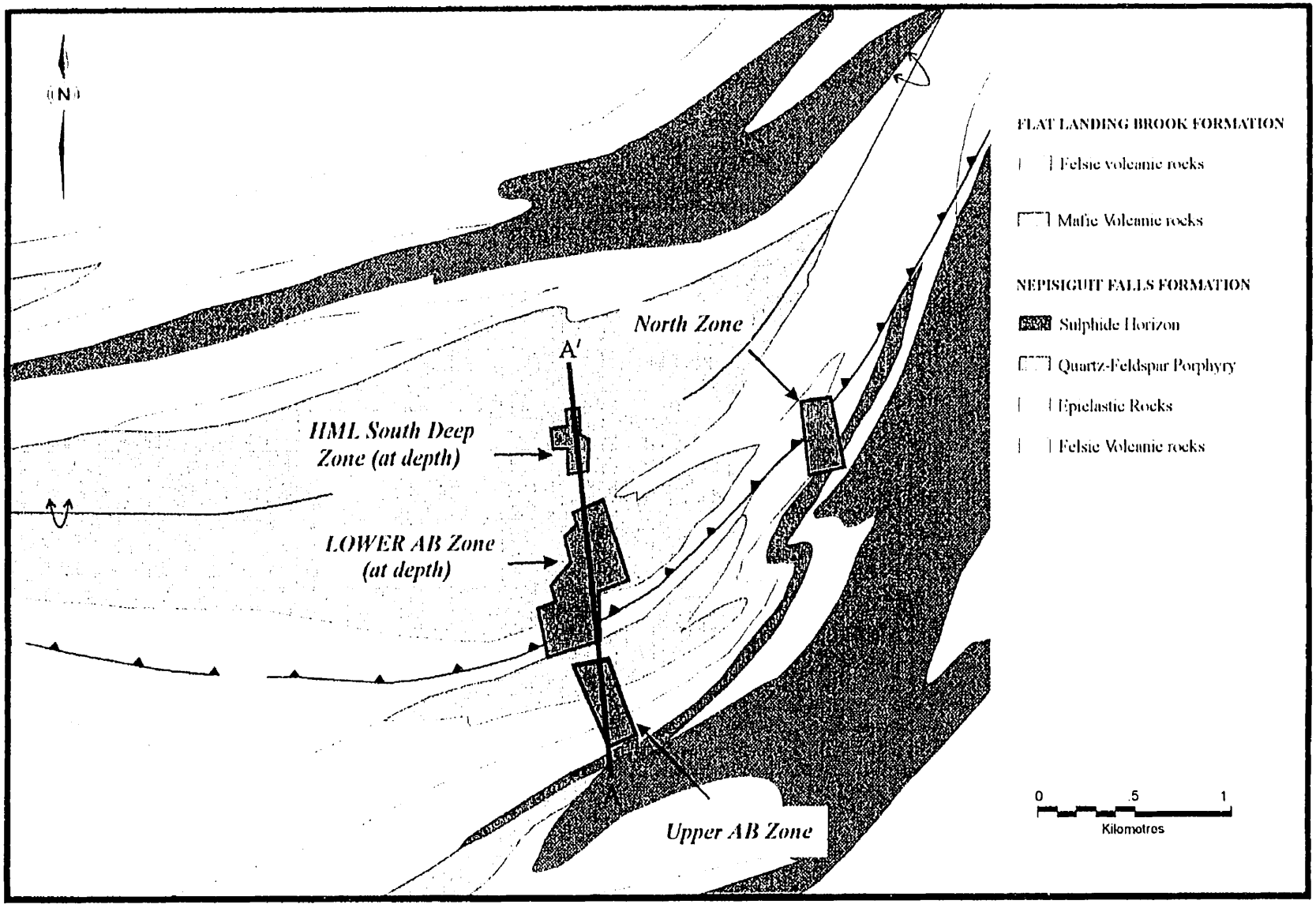

Figure 2.2 - Simplified geological map of Halfmile Lake with surface projections of the Lower AB and Deep zones

intercalated with massive sulphides and restricted in the stratigraphic. Intermediate rocks of andesite composition have been intersected beneath the mineralized zone.

2.2 – Rock Types (Nepisiguit Falls formation)

The rocks hosting the HMSDZ consist of quartz-feldspar porphyry, felsic volcanic rocks, epiclastic, and intermediate to mafic volcanic rocks (Figure 2.2).

2.2.1 - Quartz-Feldspar Porphyry

Quartz-feldspar porphyrtic rocks at HMLSDZ, like other parts of the Bathurst camp, are characterized by quartz and feldspar phenocrysts embedded in a cryptocrystalline matrix (Figure 2.3). These rocks are interpreted to be endogenous volcanic domes and subvolcanic intrusions (Adair 1992). Albite and potassium feldspar are generally the dominant phenocrysts. Quartz phenocrysts are generally less abundant compared to feldspar. The contact between these sub-volcanic intrusions is commonly characterized by chilled margins (Table A1; Appendix A), increased quartz phenocrysts with a decrease in phenocryst size. Quartz flooding and strong sericitization are not uncommon in these rocks. Strong fabric development is occasionally manifested by crenulated bands sericite.

2.2.2 - Felsic Volcanic Rocks

Felsic volcanic rocks at HMLSDZ include quartz-feldspar phyric tuff, quartz- and feldspar phyric tuff, cherty tuff, and aphyric felsic tuff. In contrast to the subvolcanic intrusions, these pyroclastic rocks exhibit medium- to coarse-grained matrix different from the quartz-feldspar porphyries (Figure 2.4 and 2.5). The crystal-rich varieties are predominantly quartz-phyric although minor feldspar-phyric tuffs also exist.

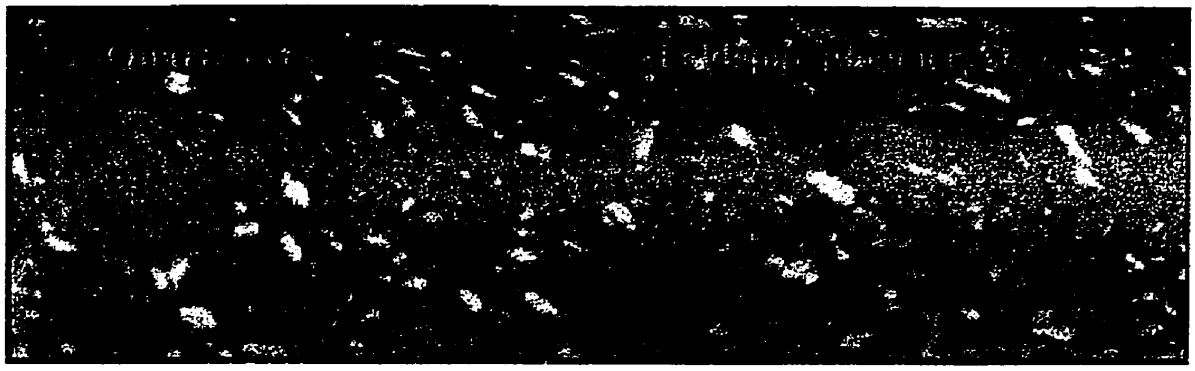

Figure 2. 3 - Quartz-feldspar porphyry at 1354.73m in HN99-124 (NQ core)

Figure 2.4 - Quartz-eye tuff at 1286.41m HN99-119 (NQ core)

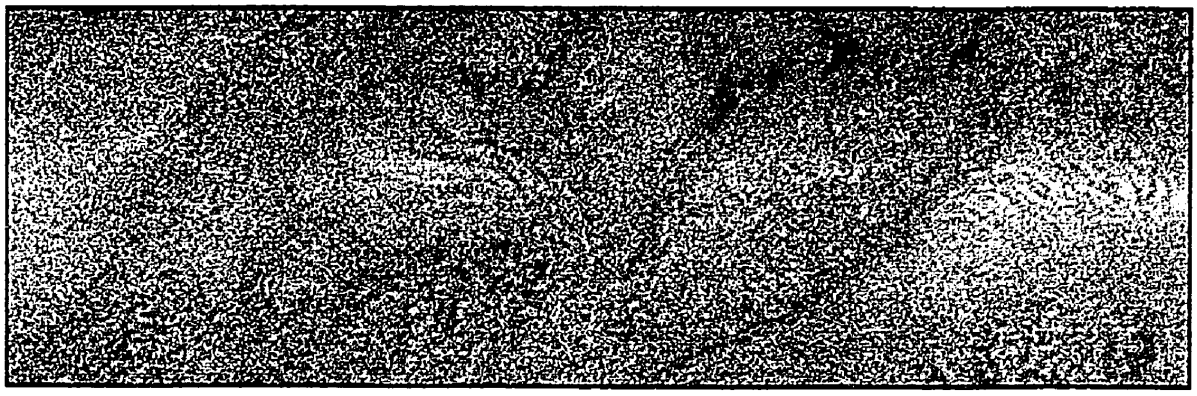

Figure 2.5 - Cherty tuff at 862.21m in DDH HN99-120 (NQ core)

2.2.3 - Epiclastic Rocks

Epiclastic rocks consist of claystone, mudstone, siltstone, and greywacke. They dominate the immediate structural hangingwall to the HMLSDZ and exhibit textural features that suggest they were partly derived from the volcanic rocks. In certain instances, it is not easy to visually distinguish between the coarser grained epiclastic rocks and their felsic pyroclastic counterparts. The epiclastic rocks exhibit fine laminations and bedding and commonly intercalated with felsic tuffs. Muscovite and chlorite alteration are quite pervasive in these rocks. Figures 2.6 to 2.9 are hand samples of meta-claystone, meta-mudstone, meta-siltstone, and meta-greywacke from the HMLSDZ. Strong quartz flooding and sericitization in the epiclastic rocks may be due to peperitic alteration.

2.2.4 - Intermediate and Mafic Volcanic Rocks

Intermediate and mafic volcanic rocks at the HMLSDZ include andesite and basalt dykes (Figure 2.10) and flows. The stratigraphic position and mode of occurrence of these mafic rocks suggest that they may be feeders to the Moody Brook member of the Flat Landing Brook Formation (Wilson *et al.* 1998). It is important to mention that two samples from an interval initially described as basalt in drill hole HN-99-119 (HML-158792 and HML-158793), rather indicated that these are dacitic flow and tuff, respectively. HML-158792 contains amygdules of calcite, epidote, and chlorite.

Figure 2.6 – Chlorite-altered claystone (with carbonate blebs) at 1240.09 in DDH HN99-126 (NQ core)

Figure 2.7 - Complex Folding in muscovite-altered mudstone at 1232m in DDH HN99-123 (NQ core)

Figure 2.8 - Siltstone with deformed Quartz Veins at 1182m in DDH HN99-127 (NQ core)

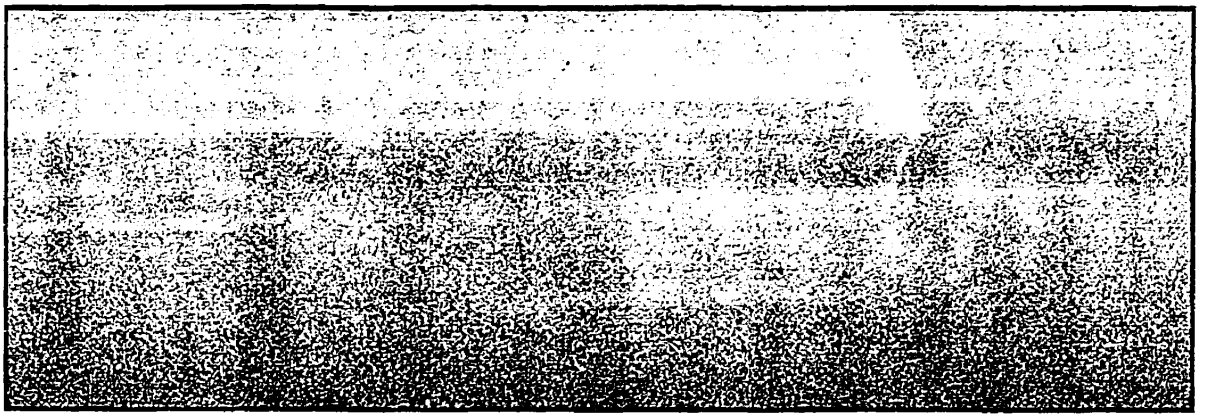

Figure 2.9 - Greywacke at 1060m in DDH HN99-126A (NQ core)

Figure 2.10 - Basalt Dyke at 1386.95m in DDH HN99-119 (NQ core)

2.3 - Tectonic Setting

A detailed discussion of the tectonic setting of the study area can be found in Pajari *et al.* (1977), van Staal (1987), van Staal *et al.* (1991), and van Staal 1994. In summary, the BMC is interpreted to have formed in a back-arc basin that opened during the rifting of a continental crust in the Early Ordovician and closed by a NW-directed subduction event in the Late Ordovician to Early Silurian period. The chronology of events related to the development of this back-arc basin are presented below:

A) "initial stage of rifting in the development of a back-arc basin behind an ensialic arc on the Avalon margin of the Iapetus sea (*ca.* 480 Ma)";

B) "slab roll-back causing mantle upwelling and the generation of widespread felsic volcanism (*ca.* 470 Ma; *e.g.*, Spruce Lake, Clearwater Stream and Nepisiguit Falls Formations", including the HML and other Brunswick VHMS camp deposits)

C) "further crustal melting and thinning, producing a second stage of felsic volcanism and widespread mafic volcanism (*ca.* 465 Ma; *e.g.,* Flat Landing Brook, Sevogle River, and upper Boucher Brook Formations)";

D) "crustal separation resulting in the formation of oceanic crust and pelagic sedimentation (*ca.* 460 Ma; *e.g.,* Fournier Group, and post-volcanic slates and cherts of the Tetagouche Group)";

E) "subduction (D_1) producing an intraoceanic accretionary wedge containing underplated blueschist";

F) "obduction (D_2) of the deformed accretionary wedge and trailing ophiolite onto the continental margin (*ca.* 430 Ma)";

G) "continental collision causing uplift, gravity sliding and refolding of earlier fabrics (420-390 Ma)" (McCutcheon and Walker 2001).

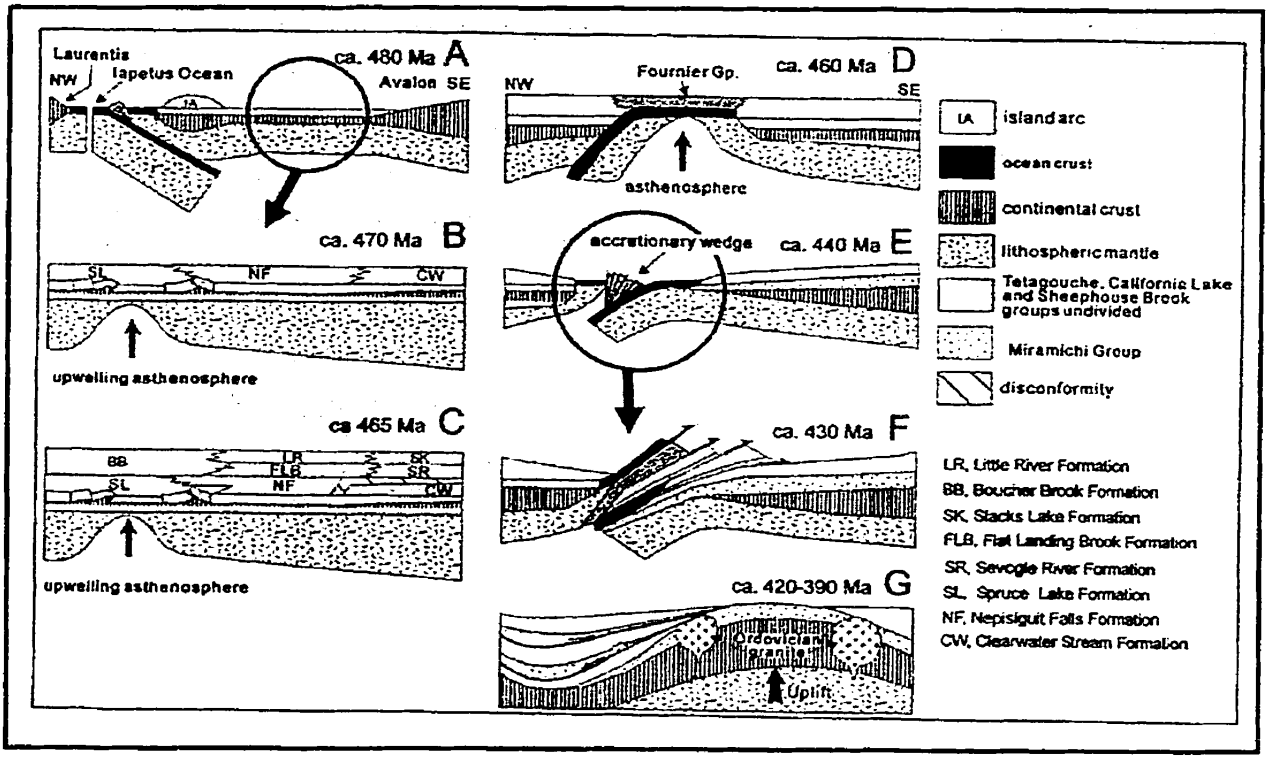

Figure 2.11 – Schematic tectonic model of the Bathurst Camp (*used with permission*, from McCutcheon and Walker 2001)

2.4 - Structure

The structural geology of the Halfmile Lake area has been described in detail by Wilson (1993), de Roo and van Staal (1991), and Adair (1992). For the scope of this study, a brief description is presented and includes the environs of the HMLSDZ. At least three periods of folding (F_1-F_3), and two phases of faulting have been reported by Adair (1992).

D_1 was accompanied by regional-scale folding that resulted in the overturning of the entire stratigraphic sequenced at HML. This produced a pronounced foliation, S_1, which is near parallel to primary layering S_0. In crystal-rich or lithic tuffs, phenocrysts and clasts are significantly stretched parallel to S_1; however, fractures are perpendicular to S_1. This observations suggested to Adair (1992) that S_1 is axial planar to large-amplitude macroscopic F_1 fold. A second stage of schistosity, S_2, associated with the D_2 event is steeply inclined to the S_2.

Movement along D_1 brittle dip-slip faults has created a sheath-like fold in the massive sulphide unit. Adair (1992) suggested that the sheath-like folds may be responsible for the localized thickening of sulphides.

Figure 2.12 – Folding in siltstone at 585.12m in DDH HN99-127 (NQ core)

2.5 - Metamorphism

Regional metamorphism in the HML area is lower greenschist facies and is characterized by the formation of phengitic muscovite in most rocks and chlorite-epidote assemblage in intermediate to mafic rocks. Biotite is present but subordinate to muscovite and chlorite.

2.6 – Massive Sulphide Mineralization

Mineralization at HML is hosted by a sequence of felsic pyroclastic and volcanic-derived, fine grained epiclastic rocks assigned to the Lower Tetagouche Group (Adair 1992). The proportion of volcanic to epiclastic rocks indicates increasing vent proximity from southwest to northeast across the deposit area. Significant concentrations of base metals have been reported in four zones: the North zone, South Upper and Lower AB zones, and the South Deep zone. The mineralization comprises a chalcopyrite-pyrrhotite stringer zone stratigraphically underlain by Pb-Zn massive sulphide zone (Figure 2.13).

2.6.1 - Stringer Zone

The stringer zone at HML consists of patches, blebs, and stringers of pyrrhotite-chalcopyrite that constitute up to 60% of the total rock volume. The relative abundances of pyrrhotite and chalcopyrite range between 5:1 and 1:1 (Adair 1992). The host rocks are predominantly mudstone and siltstone, with subordinate felsic volcanic rocks. Alteration is most intense in the epiclastic host rocks and consist of selvedges of muscovite and (Adair 1992). Because of the deformation events at HML, the stringer zone is locally transposed to form a lateral facies with the massive sulphide. Adair (1992) indicated that the transition zone between the stringer zone and massive sulphides is marked sharp increase in total sulphides

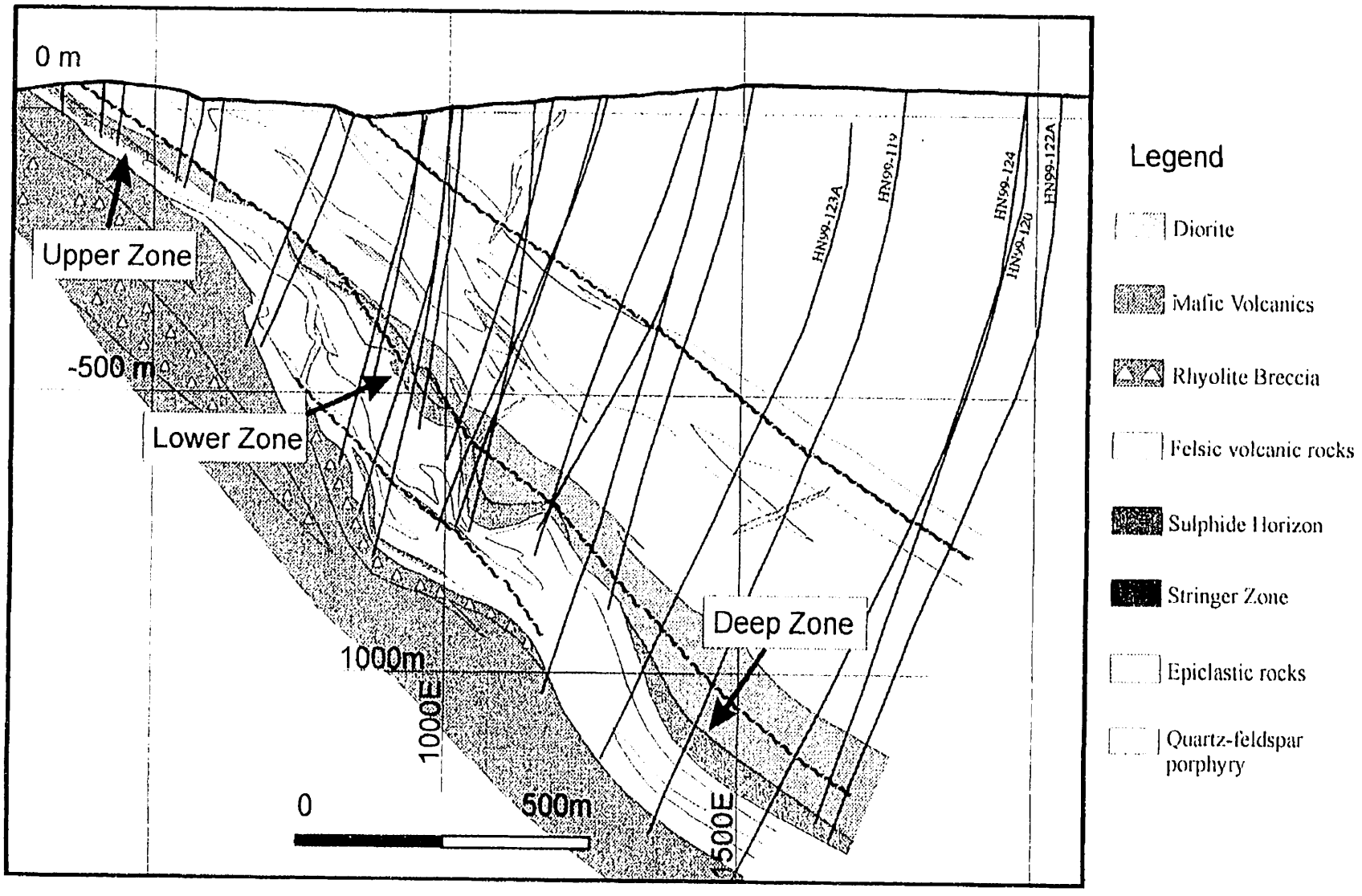

Figure 2.13 - SSW-NNE Halfmile Lake Composite Section (Section A-A'; Figure 2.2)

2.6.2 - Massive Sulphide Zone

The massive sulphide zone consist of breccia-matrix and layered sulphide zone The breccia-matrix sulphides, which represents the bulk of the sulphide mineralization, consist of black chloritic schist fragments of variable size, supported by a matrix of sulphides that constitute 50% to 90% of the rock.

Pyrrhotite and subordinate chalcopyrite, pyrite, sphalerite, and galena constitute the breccia-matrix zone. The transition between the breccia zone and layered sulphide zone is marked by a decrease in pyrrhotite concentration (Adair 1992). Breccia-matrix sulphides average 4% to 10% Zn + Pb.

The layered sulphide zone consists of strongly chlorite-altered fine-grained rocks, usually described as "black argillite". Mineralization is dominated by pyrite, and subordinate concentrations of pyrrhotite, sphalerite, and galena. Layered sulphides range from 5% to 20% Zn + Pb.

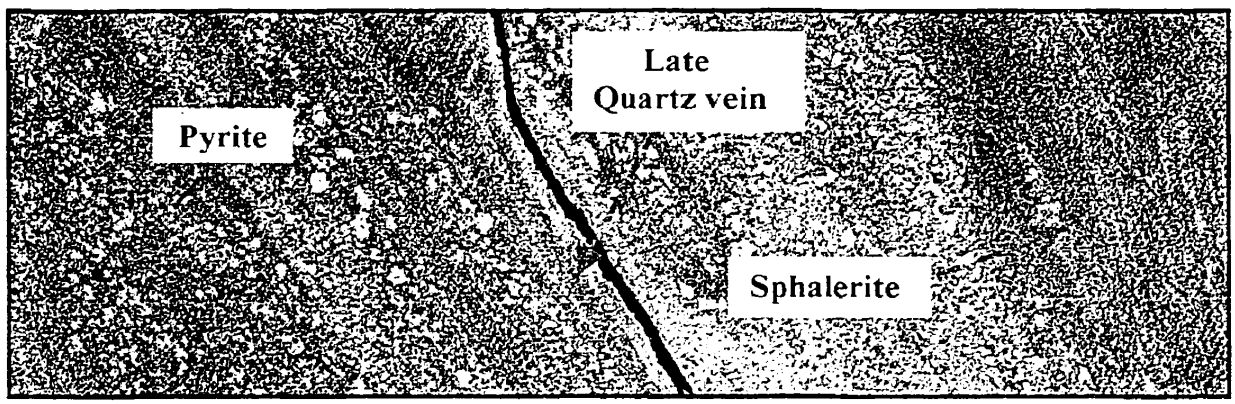

Figure 2.14 - Massive sulphide mineralization at 1372m in DDH HN99-128 (NQ core)

2.7 - Hydrothermal Alteration

Hydrothermal alteration associated with the deposition of massive sulphides is strongly developed in the stratigraphic footwall (structural hangingwall). The alteration assemblage consists of quartz-muscovite-chlorite-carbonate ± epidote. The felsic volcanic rocks are predominantly muscovite ± chlorite altered, whereas the mafic rocks are altered to a chlorite ± carbonate ± epidote assemblage. Epiclastic rocks are the most strongly and pervasively chlorite ± muscovite altered. Carbonate alteration in the epiclastic rocks is negligible.

Figure 2.15 - Variably muscovite-altered siltstone at 1336.8m in DDH HN99-124A (NQ core)

2.8 - Mineral Deposit Model

Classification of the massive sulphide deposits in the Bathurst mining camp can be undertaken in two ways:

(1) with respect to the distance the mineralization occurs from its feeder conduit (proximal – close to hydrothermal vent *versus* distal – displaced from hydrothermal vent), and

(2) with respect to the location of initial sulphide crystallization (autochthonous – *in situ* versus allochthonous – transported and redeposited).

These classification criteria have been discussed by Jambor (1979). His study investigated the alteration, sulphide and gangue mineralogy of the Bathurst camp VHMS deposits with the aim of establishing whether these might provide insights into where these VHMS deposits formed, relative to their hydrothermal fluid conduits. He noted that even with the identification of such a center, a simple classification (distal-proximal) of these deposits is difficult because they generally exhibit well-developed thin bedding and locally deposited sulphide clasts. Nonetheless, Jambor (1979) has presented a tentative classification of the Bathurst camp massive sulphide deposits with reference to their established or assumed distance (proximal *versus* distal) from feeder conduits.

In the following discussion, the HML deposit is compared with the Kuroko deposits, which shares compelling similarities and differences with the former. The Kuroko deposits of Japan occur in less deformed Miocene felsic volcanic rocks that are coeval with the deposition of sulphide mineralization near hydrothermal vents (Tatsumi and Watanabe 1971). These deposits possess a distinct chalcopyrite-rich stockwork zone overlain by a zone of massive sulphides containing pyrite, sphalerite, galena, and

chalcopyrite. The massive sulphides of the Kuroko deposits occur as concordant lenses in topographic depressions to the side of, or overlying the stockwork zones. The presence of cherty beds and massive sulphides are interpreted to represent a hiatus in deposition of volcanic and clastic epiclastic rocks during which chemical precipitation of chert and sulphides occurred.

Mineralization at HML consists of a stratiform massive sulphide zone containing pyrite, sphalerite, galena and chalcopyrite stratigraphically underlain by a pyrite-chalcopyrite stringer zone. The sulphide lens is lenticular and elongate, a feature that is in contrast with the Kuroko deposits and possibly a consequence of deformation. The fine banding in the massive sulphide zone at HML is similar to that of the Kuroko deposits and considered to be primary bedding because it is parallel with the enclosing rocks. In contrast to the pipe-like stockwork zone of the Kuroko deposits, the stringer zone at HML laterally extensive. However, the extent of ore grade Cu-rich stringers within the HML deposit is restricted and similar to the Kuroko deposits. The sheet-like form and wide lateral extent of the massive sulphide zone at HML is different from the thick, lenticular and discontinuous massive sulphide bodies of the Kuroko deposits. Due to differences in metamorphic grade at the Kuroko and HML deposits, it is difficult to compare alteration patterns; however, these two deposits exhibit distinct quartz-sericite and quartz-muscovite-chlorite alteration assemblages that are related to hydrothermal activity.

Jambor (1979) characterized the HML deposit in proximal category of Large (1977) based on the following:

1) the deposit is rich in Cu, as well as Pb and Zn;

2) distinct footwall alteration is present, although not in a pipe;

3) sulphides are predominantly pyrrhotite and pyrite, but the stringer and massive zones are mainly blanket-shaped; and

4) the presence of good metal and mineral zoning but deposit occurs in a mixed epiclastic-volcanic environment.

Characteristic features of the HML deposit, including sulphide mineralogy, alteration assemblage, and relative abundance of volcanic and epiclastic rocks were used by Adair (1992) to classify of the deposit as a proximal VHMS type. These findings substantiate earlier observations made by Jambor (1979), Stanton (1972) and Large (1977). In spite of these differences, the HML deposit can be described as a proximal Kuroko-type VHMS deposit.

3 – HALFMILE LAKE SOUTH DEEP ZONE (HMLSDZ)

3.1 - Rock Units

A thin section petrographic study of a subset of the samples from the rocks hosting the HMLSDZ was conducted to resolve difficulties encountered during field and laboratory hand sample descriptions of lithology and degree of alteration. The samples were chosen to represent the various rock units (felsic pyroclastic and epiclastic rocks, lava flows, and sub-volcanic intrusions) and alteration assemblages (muscovite, chlorite, carbonate, silica, *etc.*) identified in the field. Other parameters determined included texture, size and abundance of phenocrysts, primary and alteration minerals, and any geologically important feature. A summary of the results is discussed below and a detailed description of each sample is presented in table form in Appendix C.

3.1.1 - Epiclastic Rocks

Petrographic studies reveal that epiclastic rock types at the HMLSDZ include claystone, mudstone, siltstone, and greywacke (Figure 3.1 to 3.4), respectively. These units are characterized by fine to coarse grained, isogranular or heterogranular recrystallized quartz matrix, which varies from 20 microns in meta-claystone to about 400 microns in meta-greywacke. Alteration minerals include muscovite and chlorite; carbonate minerals were not observed in thin sections. Chlorite is subordinate to muscovite and only very intense in a few samples. The chlorite grains are disseminated or fibrous and display a pronounced pleochroism with distinct brownish-purple to Prussian blue (Fe-rich end-member) interference colours under crossed polars (Figure 3.5; HML-158932).

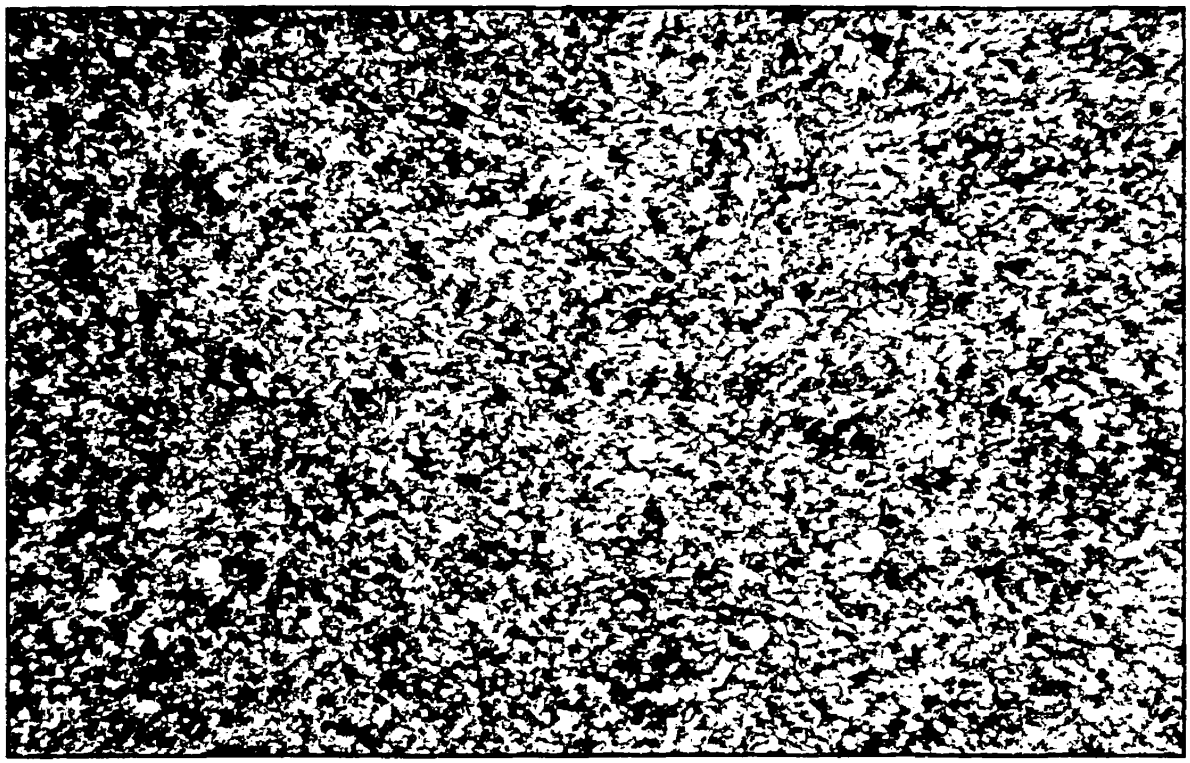

Figure 3.1 – Photomicrograph of claystone (HML-158934) taken under crossed polars (horizontal field of view = 3 mm)

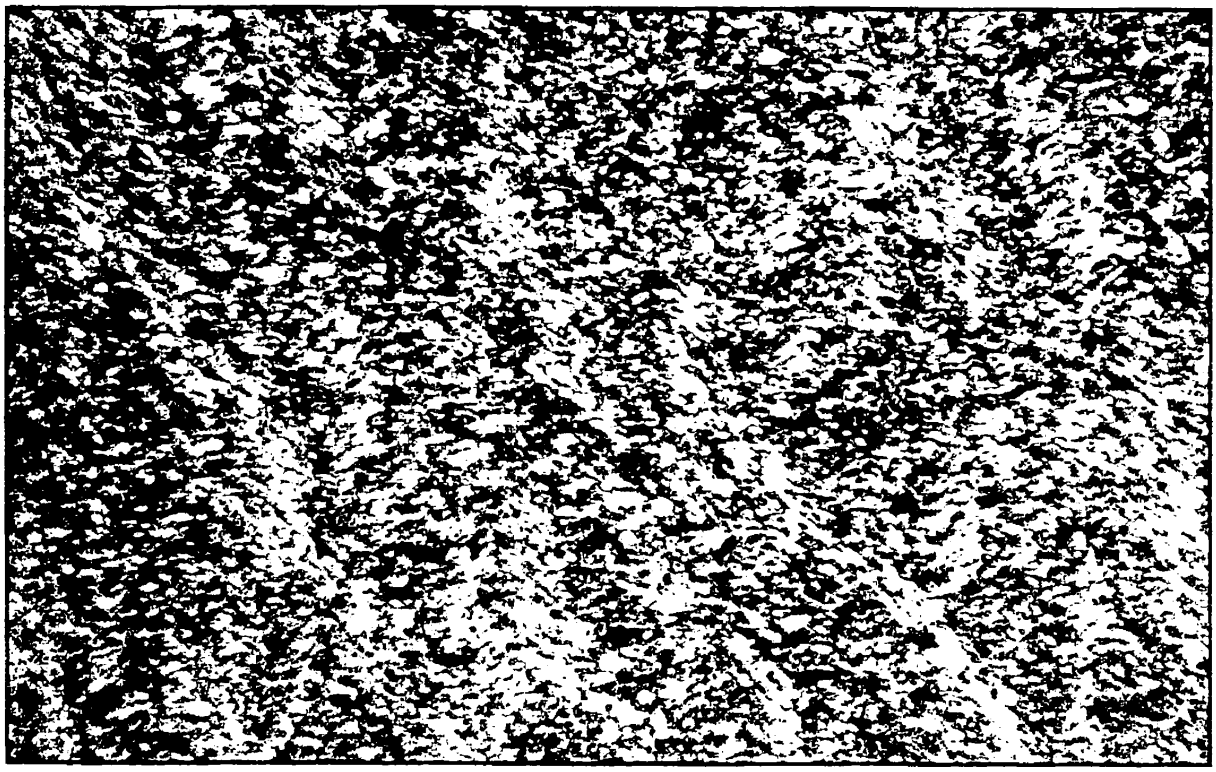

Figure 3.2 – Photomicrograph of mudstone (HML-158976) taken under crossed polars (horizontal field of view = 3 mm)

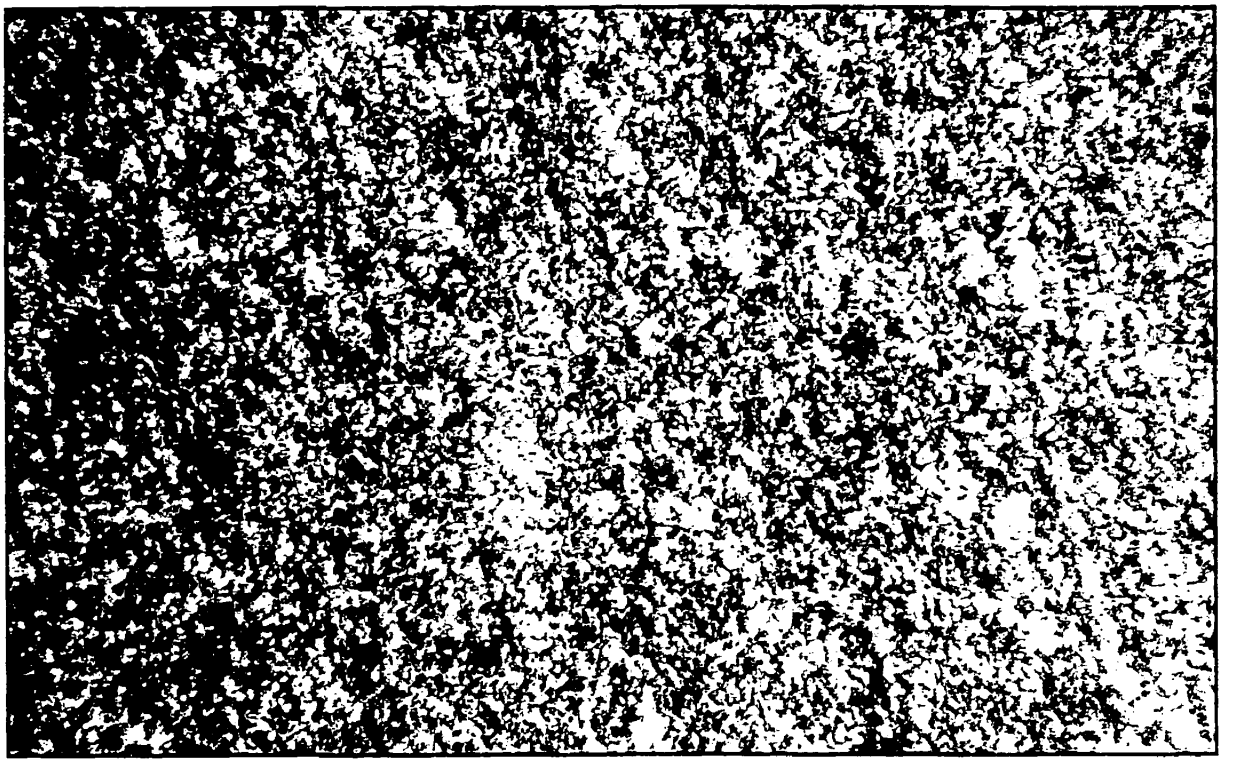

Figure 3.3 – Photomicrograph of siltstone (HML-158960) taken under crossed polars (horizontal field of view = 3 mm)

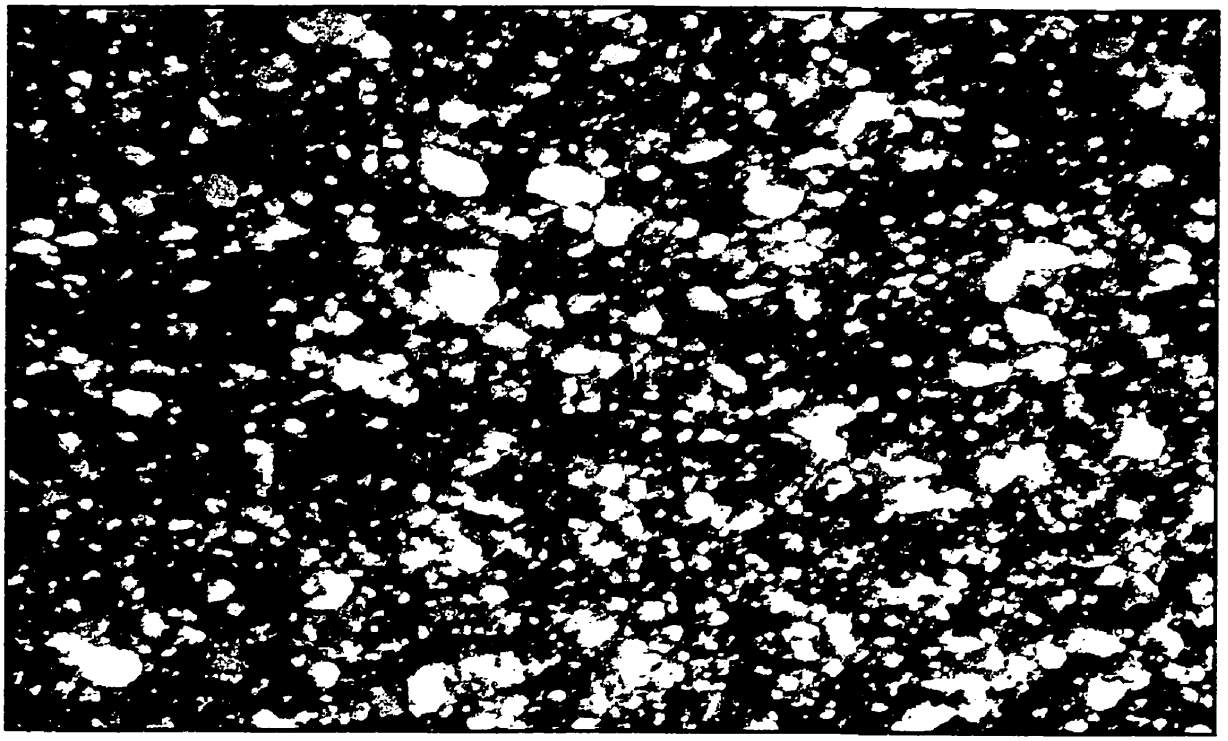

Figure 3.4 – Photomicrograph of greywacke (HML-158931) taken under crossed polars (horizontal field of view = 3.5 mm).

Muscovite grains are flaky or acicular or occur as crenulated fibrous bands with strong interference colours. On a thin section scale, the abundance of fine grained muscovite (sericite) ranges from about 2 % in least altered rocks to about 40 % in most altered samples. Chlorite abundance is between 2 % in least altered samples to approximately 50 % in very altered samples. Mineral associations observed include, quartz plus chlorite and quartz plus opaque sulphide mineral assemblages. Frequently, fine grained disseminated sulphides are concentrated along foliation planes in muscovite-altered samples that exhibit strong fabric development. Euhedral to subhedral pyrite and other opaque (sulphide) minerals are also present. There was rarely any feldspar phenocryst in the thin section samples of epiclastic rocks.

Intense deformation is manifested by a discrete S_2 spaced crenulation cleavage superimposed on pervasive S_1 foliation (Figure 3.6; HML-158834). Diffused S_2 crenulation cleavage development is also present, but subordinate to discrete cleavage development. Distinct mica-rich (septum) and quartz-rich (microlithon) domain parallel to S_1 are present and indicative of pressure solution.

3.1.2 - Pyroclastic (tuffaceous) Volcanic Rocks

Pyroclastic rocks in the vicinity of the HMLSDZ include felsic tuffs, cherty tuff, quartz- and/or feldspar-phyric tuffs. The matrix (~ 15 – 40 microns) of these tuffaceous rocks is fine grained and isogranular to polygonal mosaic. Quartz and feldspar phenocrysts range in size (long dimension) from 50 – 350 and 50 – 1800 microns, respectively (Figure 3.7; HML-158890). In the quartz- and feldspar-phyric samples, feldspar is mostly the predominant phenocryst. The chlorite grains are disseminated or fibrous and display a pronounced pleochroism with distinct brownish-purple to Prussian

blue (Fe-rich end-member) and olive-greenish-brown interference colours under crossed polars.

Figure 3.5 – Photomicrograph of pervasive Prussian-blue chlorite in chloritic iron formation (HML-158932) taken under crossed polars (horizontal field of view = 3 mm).

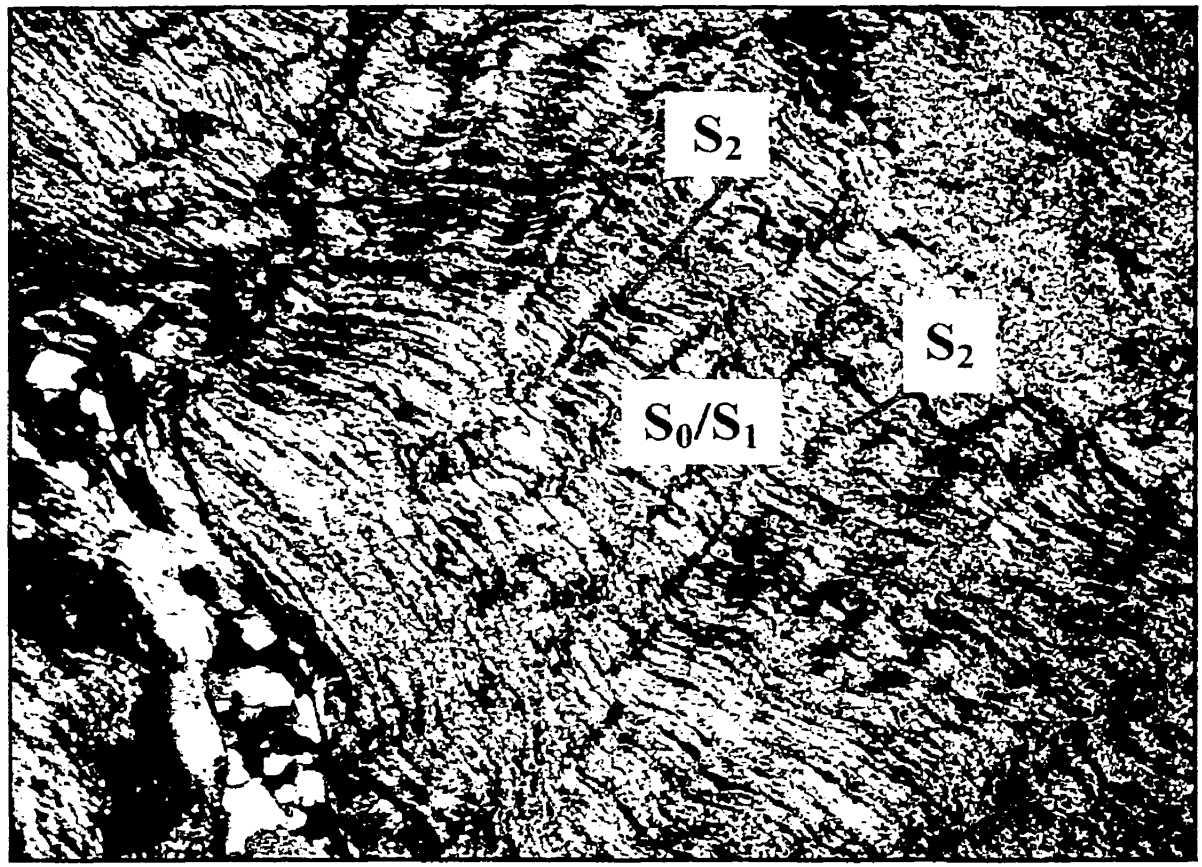

Figure 3.6 – Photomicrograph of S_1/S_2 spaced crenulation (HML-158834) in very altered meta-sediment taken under crosses polars (horizontal field of view = 3 mm).

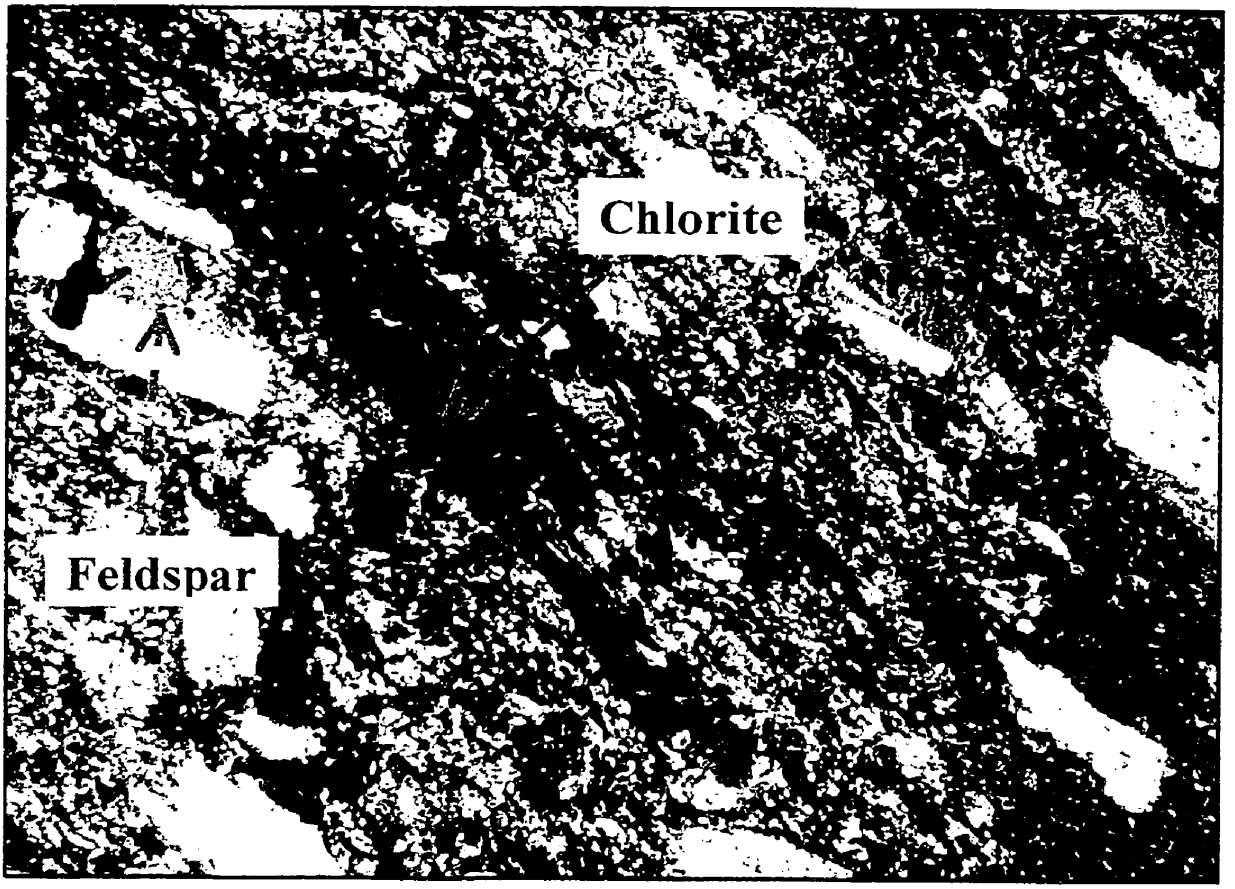

Figure 3.7 – Photomicrograph of a feldspar-phyric tuff (HML-158890) taken under crossed polars (horizontal field of view = 3 mm).

Muscovite grains are flaky or acicular or occur as fibrous bands with strong interference colours. Muscovite and chlorite abundance is approximately 15 and 20 % in most altered samples, respectively. Sample HML-158826 (Figure 3.8) contain approximately 5 % carbonate minerals. Minor opaque sulphide grains were observed. The most predominant mineral association is chlorite plus feldspar.

S_2 spaced cleavage with well defined mica-rich and quartz-rich domains was observed in sample number HML-158937 (Figure 3.9).

Effusive Volcanic Rocks

The felsic volcanic rocks identified from petrographic studies are lava flows and dykes. Samples of flow origin are fine to medium grained (~ 25 microns) and predominantly aphyric, although one of these samples is feldspar-phyric. Muscovite and chlorite abundance is approximately 15 and 20 %, respectively, in most altered samples. Sample HML-158792 (Figure 3.10) also contains clinopyroxene, which has been altered to an epidote plus carbonate assemblage. Only one sample was found to contain biotite HML-158794 (Figure 3.11). Crenulation cleavage is also present but observed in only sample HML 158837.

The dykes (two basalts and one dacite) are fine to very fine grained with 12 % fine grained muscovite and 8 % green to Prussian blue chlorite. Carbonate blebs up to 20 % are common in dykes (HML-158909; Figure 3.12).

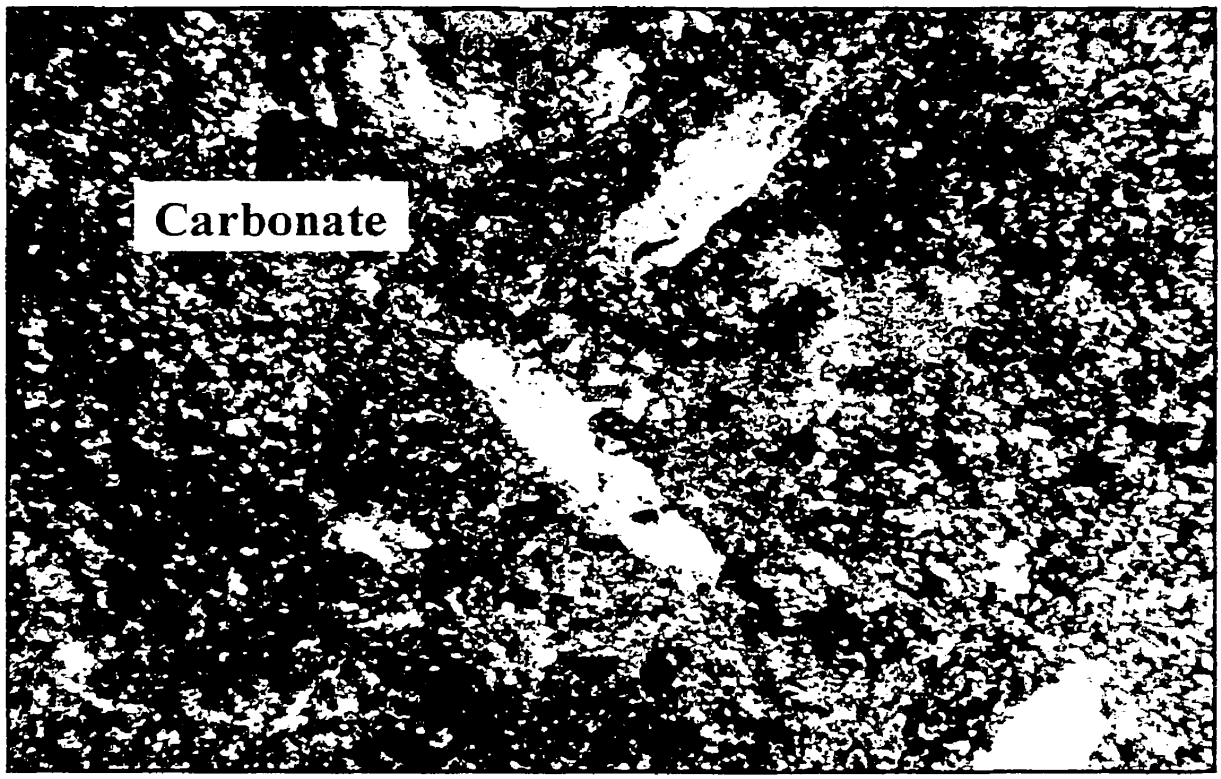

Figure 3.8 – Photomicrograph of carbonate in a feldspar phyric tuff (HML-158890) taken under crossed polars (horizontal field of view = 3 mm).

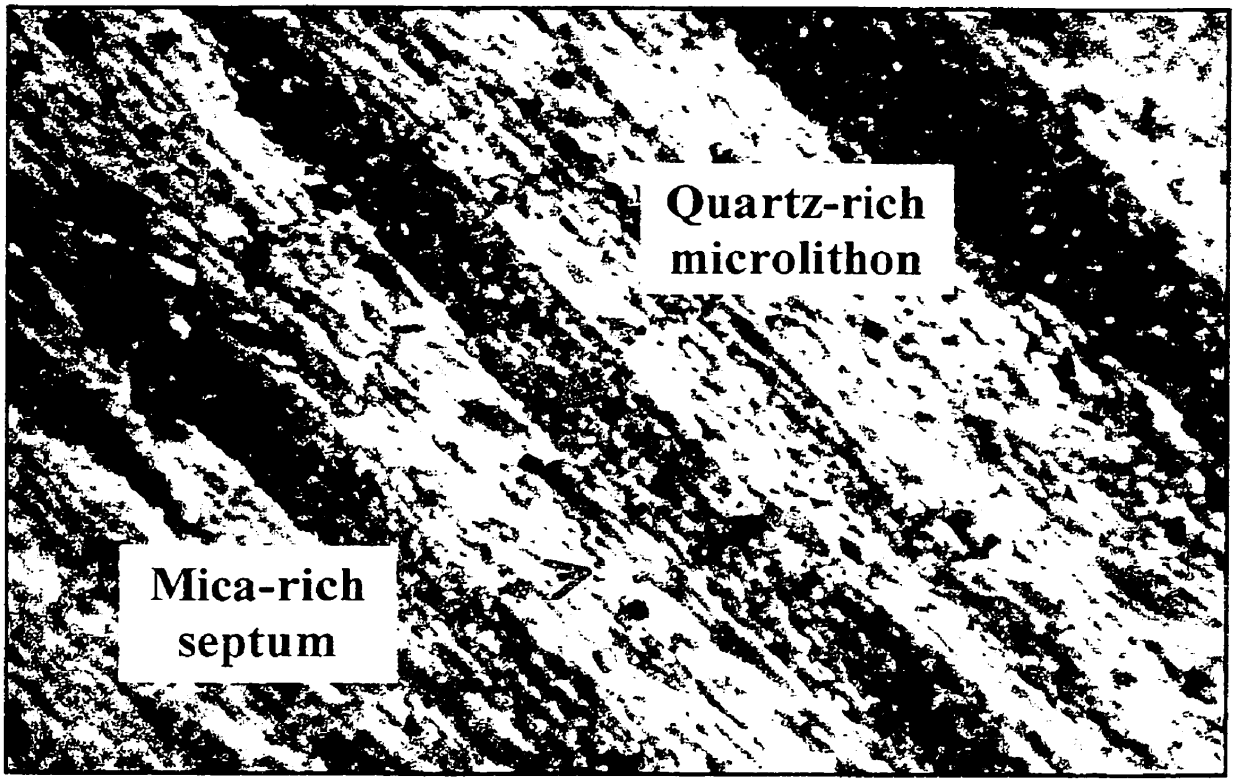

Figure 3.9 – Photomicrograph of S_2 spaced cleavage indicating quartz-rich (microlithon) and mica-rich (septum) in s felsic tuff (HML-158937) taken under crossed polars (horizontal field of view = 3 mm)

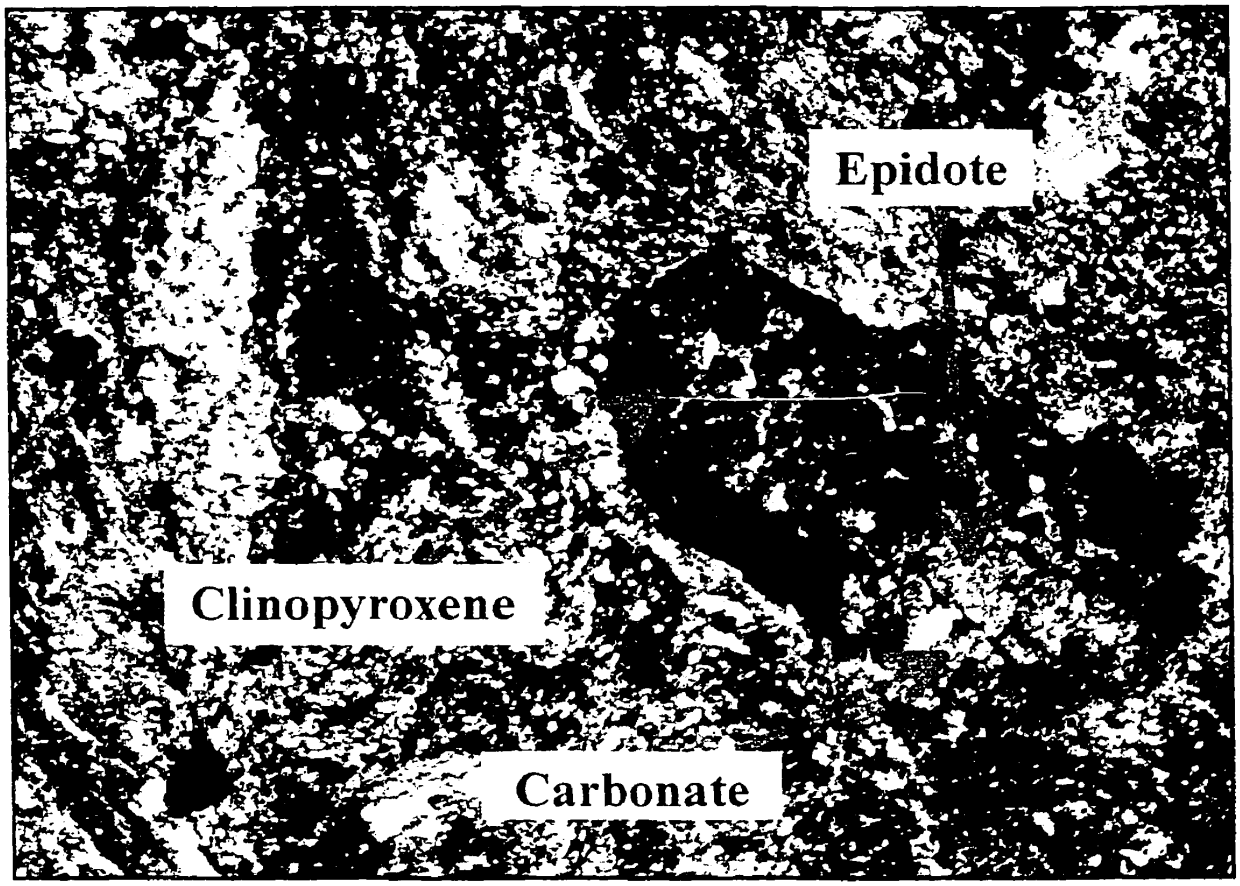

Figure 3.10 – Photomicrograph of clinopyroxene altered (HML-158972) to epidote plus carbonate assemblage (horizontal field of view = 3 mm) in a dacite flow

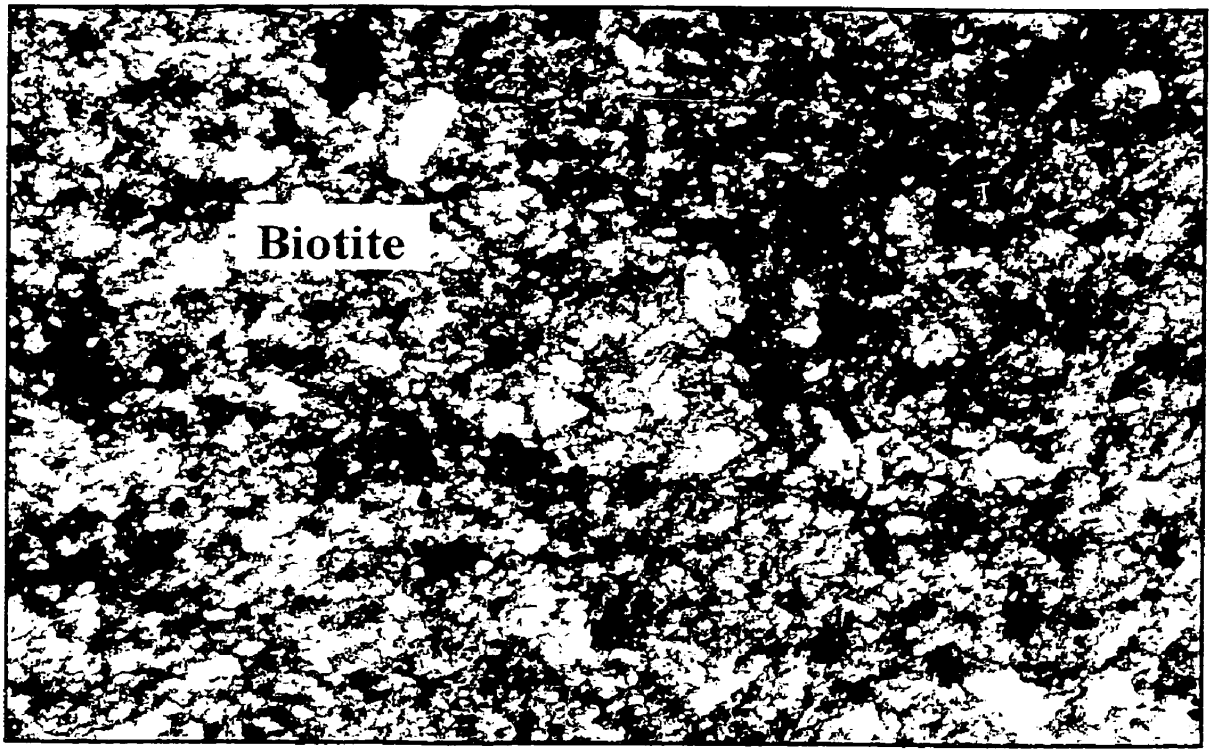

Figure 3.11 – Photomicrograph of biotite (HML-158974) in andesite flow taken under crossed under crossed polars (horizontal field of view = 1.5 mm)

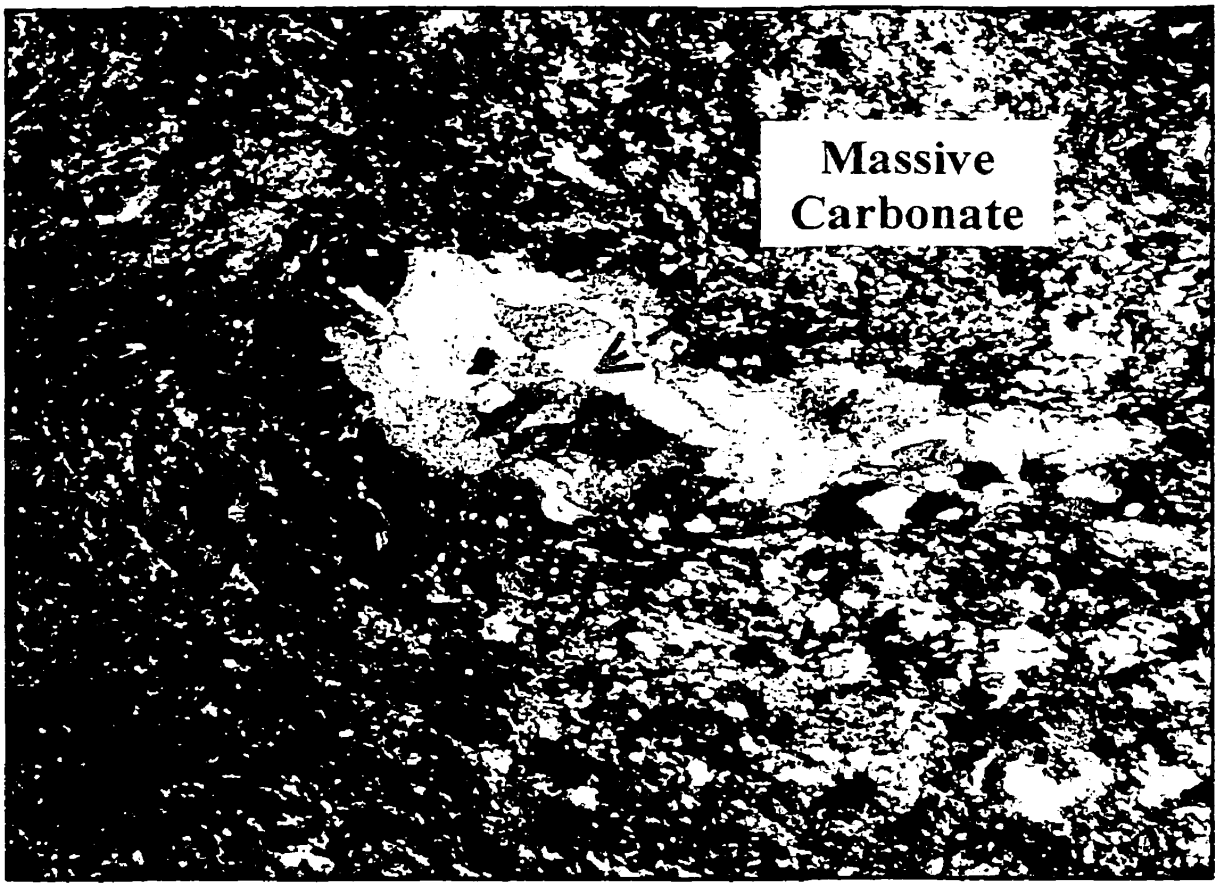

Figure 3.12 – Photomicrograph of carbonate in felsic dyke (HML-158909) taken under crossed polars (horizontal field of view = 3 mm)

3.1.4 - Quartz-Feldspar Porphyry

Quartz-feldspar porphyries at HML contain visible quartz and feldspar phenocrysts in a very fine grained cryptocrystalline matrix (Figure 3.13; HML-158850). Quartz and feldspar phenocrysts vary from 100 -1200 and 40 - 2400 microns, respectively. In thin section, the matrix is isogranular, heterogranular, or polygonal mosaic. The feldspar grains are 'dusty' in appearance, exhibit variable degrees of alteration and commonly are associated with blebs of chlorite and/or bands of fibrous muscovite. Prussian-blue chlorite grains also occur as inclusions in feldspar grains probably due to differential alteration. The quartz-feldspar porphyry samples are predominantly muscovite-altered with subordinate chlorite alteration. S_1/S_2 crenulation cleavage is present and observed in only one instance (Figure 3.14; HML-158798).

3.2 - Fabric Development

S_2 cleavage development commonly displaying features associated with pressure solution is present in all rock types at the HMLSDZ, although it is predominant in the epiclastic rocks. Pressure solution is a material transfer process known to be associated with sub-greenscist and greenschist facies metamorphism (De Roo 1989; McCaig and Knipe 1990; Gratier 1987). This mechanism, which involves dissolution and re-precipitation in a fluid medium, was recognized by Lentz (1999) as the dominant process responsible for solution transfer associated with cleavage development in the felsic volcanic rocks at Brunswick No. 6. The dissolution is enhanced on surfaces normal to the maximum principal stress with deposition occurring preferentially on surfaces normal to the minimum principal stress (Kearey 1996).

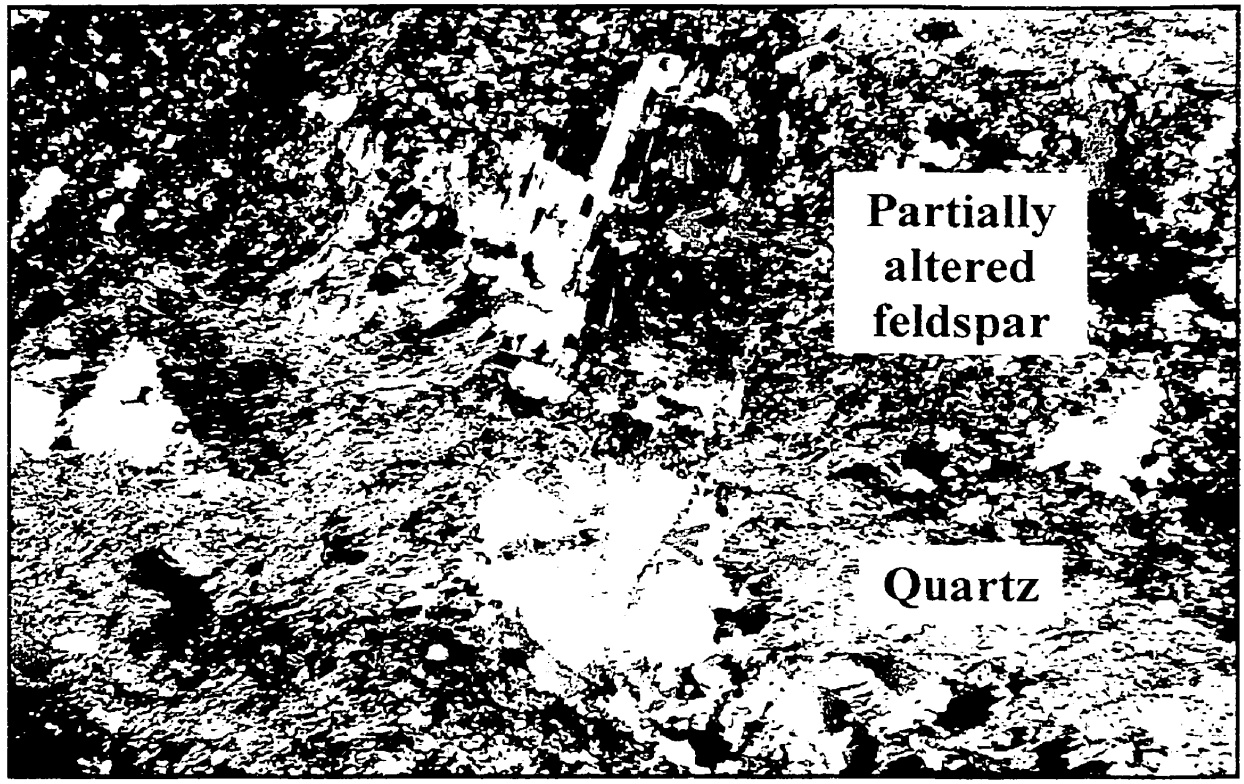

Figure 3.13 – Photomicrograph of quartz-feldspar porphyry (HML-158850) taken under crossed polars (horizontal field of view = 3.5 mm)

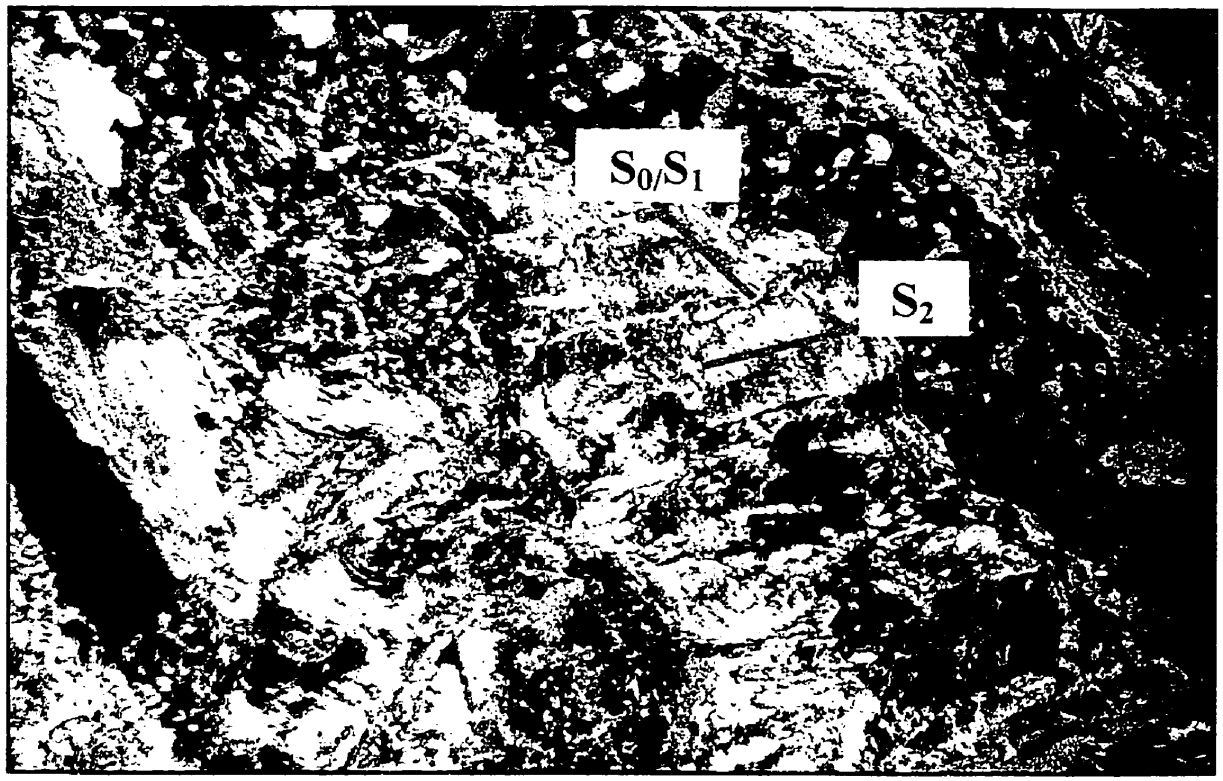

Figure 3.14 – Photomicrograph of crenulation cleavage in quartz-feldspar porphyry (HML-158798) taken under crossed polars (horizontal field of view = 3 mm)

Gray and Durney (1979) described the significance of strain and the mechanisms of formation of pressure solution. They indicated that the development of pressure solution involves a physico-chemical redistribution of minerals, and is a function of relative solubilities and chemical mobilities. They emphasized that cleavage domains are sites of the removal, by pressure solution, of substantial amounts of host rock, leaving behind insoluble residues of clayey and carbonaceous material. According to Gray and Durney (1979), pressure solution occurs on grain and/or layer boundary discontinuities oriented at right angles to the direction of minimum stress.

Movement of dissolved material follows paths controlled by chemical potential gradients that are related in magnitude and direction to the local stress environment. Cleavage domains emerge along the limbs, or former positions of limbs, of microfolds in the continuous cleavage of the host rock. The cleavage spacing observed in rocks undergoing this kind of deformation is related to the dominant wavelength of the microfolds and the amount of solution-induced shortening across the limbs of the microfolds (Gray 1979).

Observations from petrographic study of samples from the rocks hosting the HMLSDZ suggests that fabric development probably accompanied D_1 and D_2 events associated with the tectonic development of the BMC. In sample HML-158910 (Figure 3.15), the consistent parallel trends of inclusion trails in titanite grains suggest that titanite grew after S_1 but before crenulation and development of S_2.

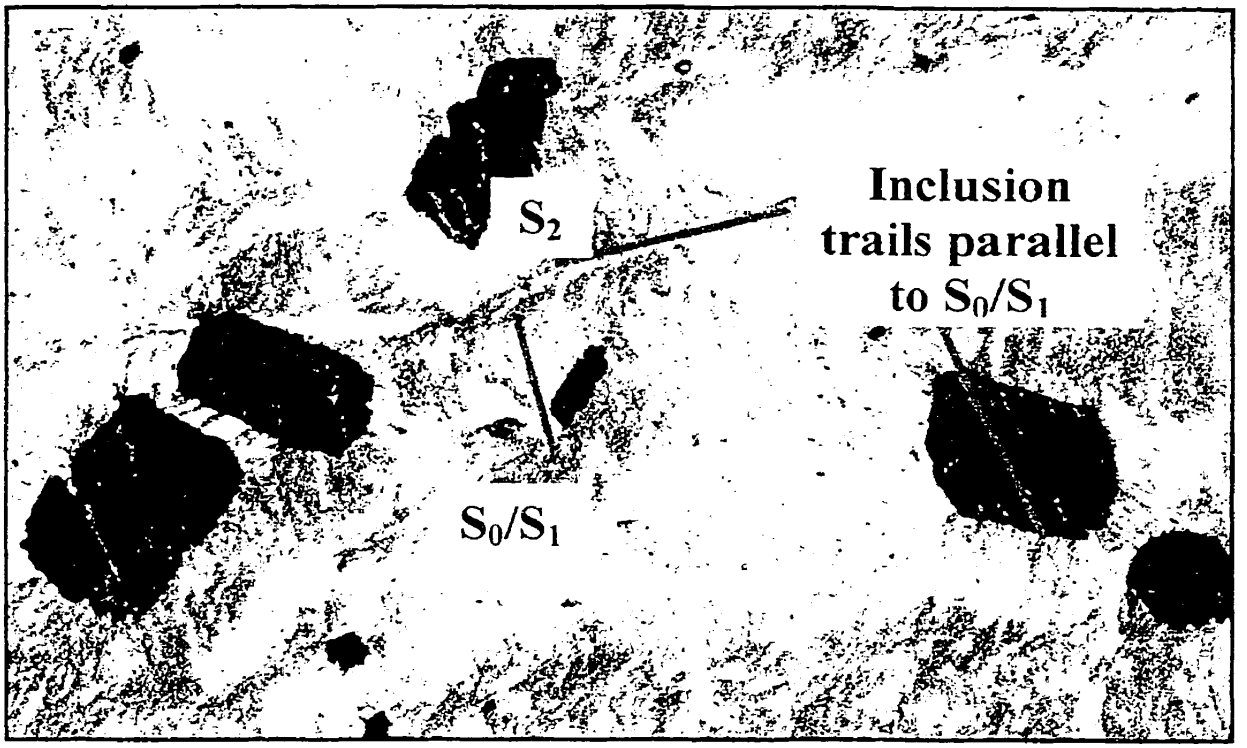

Figure 3.15 – Photomicrograph of inclusion trails in titanite grains in a mudstone (HML-158910) taken under crossed polars (horizontal field of view = 3.5 mm)

F_2 microfolds identified in sample HML-158867 (Figure 3.16) are probably responsible for crenulation of micaceous layers, without significantly affecting the quartz-rich layers. Spaced S_2 cleavage cuts across both the micaceous- and quartz-rich layers. Microfolding (F_2), crenulation and crenulation cleavage developments are coeval with D_2 deformation. The absence of documentary or field evidence for S-C fabric development at Halfmile Lake probably indicates that this area is distal to the major shear zone associated with the D_2 event. In general, the observed D_2 fabric, which appears to characterize the rocks at the HMLSDZ varies between the diffused and discrete spaced crenulation domains of Davies and Reynolds (1996). Such cleavage is more indicative of shortening than shearing.

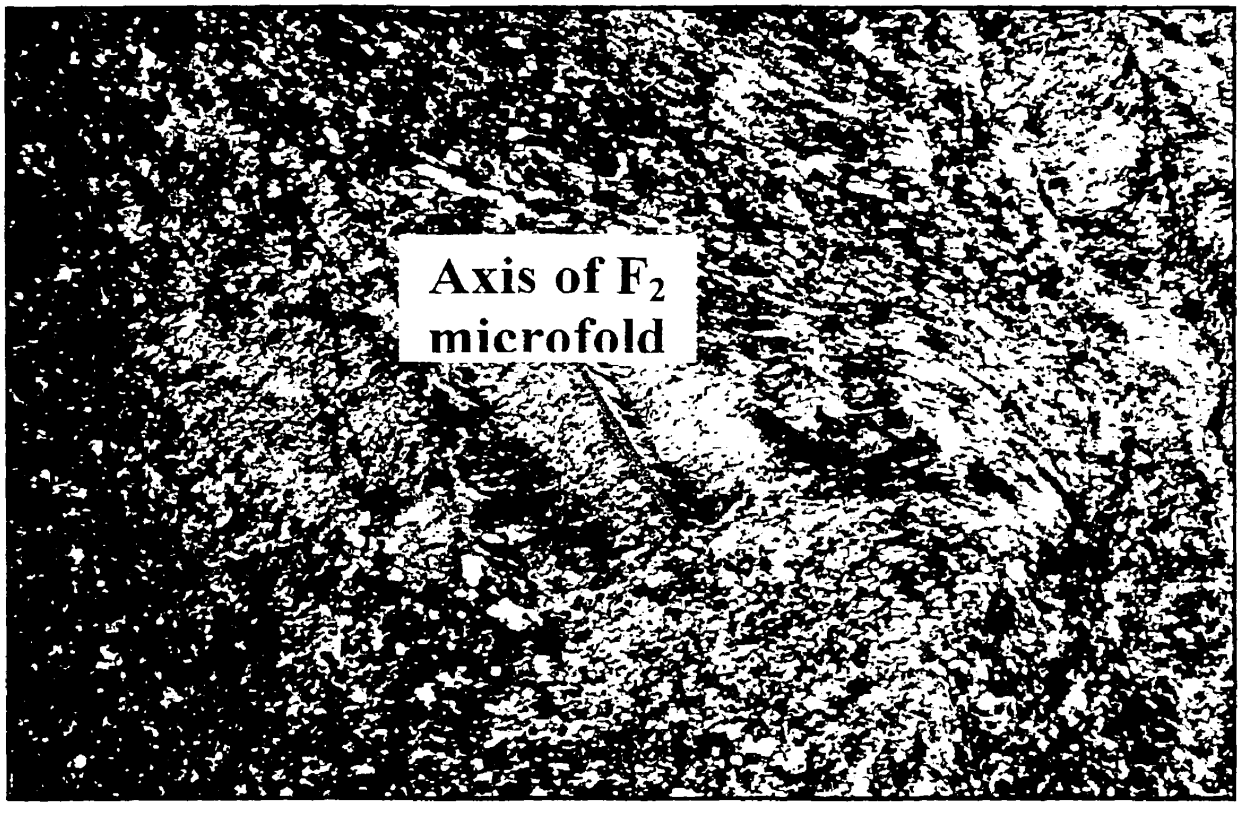

Figure 3.16 – Photomicrograph of F_2 microfolds in meta-sediment (HML-158867) taken under crossed polars (horizontal field of view = 3 mm)

3.3 - Mineral Compositions

The compositions of primary and secondary (alteration) minerals identified from petrographic study of samples from the rocks hosting the HMLSDZ were determined using electron microprobe analysis. The suite of minerals evaluated includes feldspar, pyroxene, epidote, muscovite/phengite, chlorite, biotite, carbonate, and titanite. The molar compositions of these minerals have been calculated from the probe results and are presented in Tables D.1 through D.6 (Appendix D).

Feldspars

The composition of feldspar in the rocks hosting the HMLSDZ was determined from the analysis of three (dacitic and rhyolitic) aphyric to feldspar phyric volcanic rocks. The mineral grains were probed on the core and rim to determine any incidence of replacement. The raw data from the probe results (wt. %) were utilized to calculate the elemental constitution of the feldspar minerals based on eight atoms of oxygen in the silicate structure of feldspars. One of the feldspar grains in sample number HML-158844 displays an albite-rich core and potassium feldspar-rich rim. All other grains were albite. The results indicate that albite is predominant over potassium feldspar in these rocks (Figure 3.17).

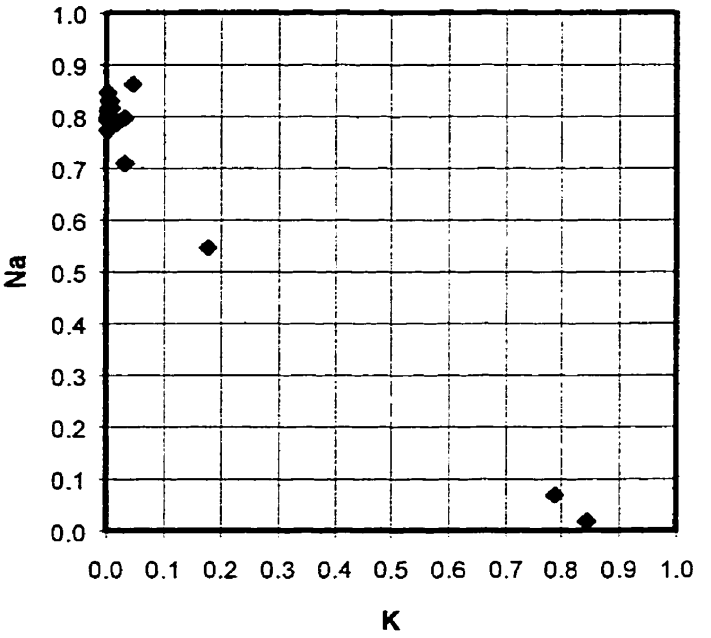

Figure 3.17 – Plot of the elemental amounts of K versus Na to examine the alkali feldspar composition in three samples (Table D.2.1) from HMLSDZ. The data indicate that albite is predominant over potassium feldspar in feldspar-phyric rocks. The low total Na+K is probably a result of Na volatilization during analysis.

Figure 3.18 indicates that the initial amount of anorthite in the HMLSDZ was minimal, and was either destroyed during hydrothermal activity or not present initially.

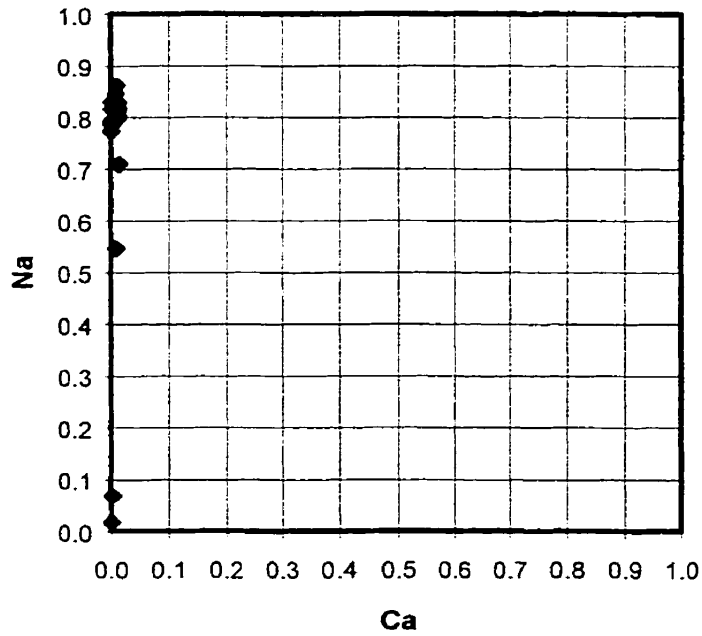

Figure 3.18 – Plot of the elemental amounts of Ca versus Na to examine the plagioclase composition in three samples (Table D.2.1) from HMLSDZ. The data suggest that plagioclase is predominantly albite and the low Ca+Na is probably the result of volatilization during analysis.

Calcite

Observation from thin section petrography, combined with valid mineral compositions determined from microprobe analysis indicates that calcite is the predominant carbonate mineral in the alteration halo surrounding the HMLSDZ. The concentrations of individual elements in the carbonates minerals were deduced from the concentration of their oxides balanced on three atom of oxygen. The data plot just below the calcite composition (Figure 3.19).

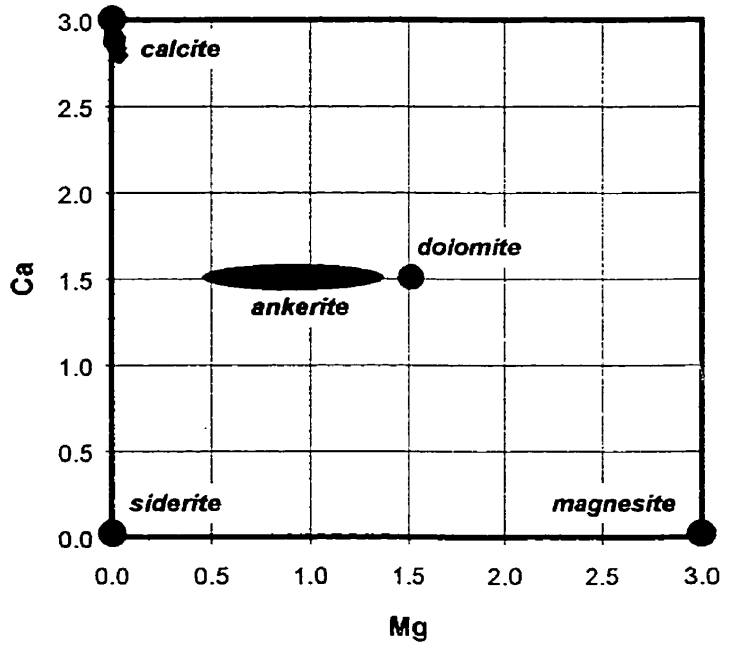

Figure 3.19 – Plot of the elemental amounts of *Mg* versus *Ca* to examine the composition of carbonates in five samples (Table D.4.1) from HMLSDZ. The data cluster around the calcite node, demonstrating that calcite is the predominant carbonate in these rocks.

Muscovite/Phengite

The results of electron microprobe analysis on samples containing muscovite minerals demonstrate the presence of significant concentrations of Fe and Mg in muscovite. The amounts of the constituent elements in the muscovite grains were determined based on twenty two oxygen atoms in the ideal muscovite structure ($K_2Al_6Si_6O_{20}(OH)_4$). The data on Figure 3.20 indicate that the composition of muscovite varies from an ideal muscovite composition to a phengitic composition ($K_2(Fe,Mg)Al_4Si_7O_{20}(OH)_4$). Because phengitic muscovite is typical of high pressure-low temperature regional metamorphism and not hydrothermal alteration, the Fe and Mg in the muscovite was probably initially present in chlorite (as a result of hydrothermal activity), and was remobilized during metamorphism to produce the observed phengitic muscovite composition.

Figure 3.20 also demonstrates that a significant number of samples from the epiclastic and strongly altered (unknown protolith) rocks contain an illitic muscovite composition corresponding to the formula, $(Na,K)_{3/2}(Fe,Mg)_{1/2}Al_{9/2}Si_7O_{20}(OH)_4$. The average molar abundance of Na in the K site in illitic muscovite is 3 %.

A chi-square contingency test (Spiegel 1975) was performed on the muscovite analysis presented in Figure 3.20. The contingency test results (Table 3.1) indicate that the epiclastic rocks at the HMLSDZ contain predominantly illite, whereas the volcanic rocks contain predominantly muscovite/phengite.

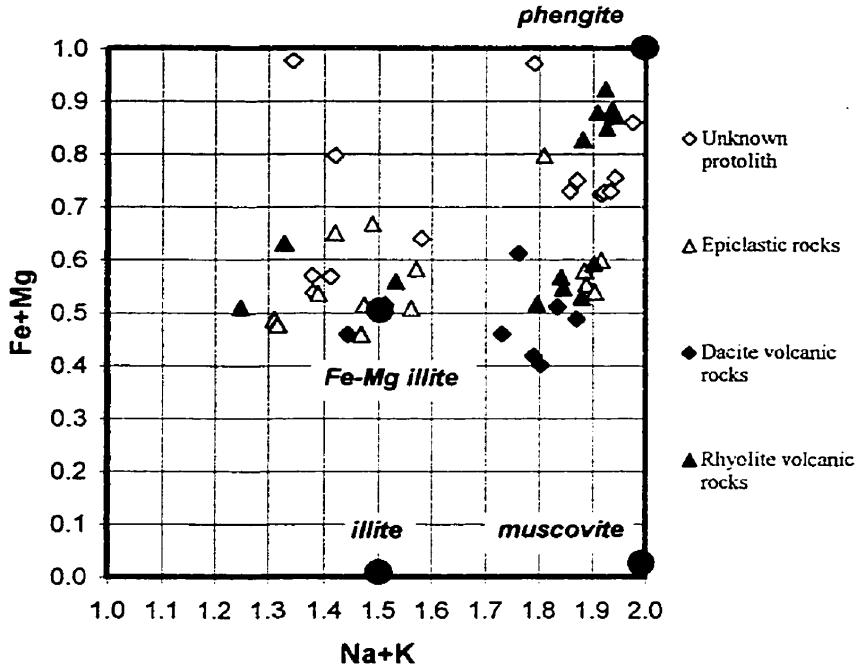

Figure 3.20 – Plot of the elemental amounts of (Na+K) versus (Fe+Mg) to examine the composition of muscovite in seven samples (Table D.1.1) from HMLSDZ. The data indicate that these muscovite-altered samples contain significant concentrations of Fe and Mg, and thus have a phengitic composition typical of high pressure-low temperature metamorphism. A subset of these samples has approximately 1.5 atoms of (Na+K) in their interlayer site, indicating that they have illitic affinities. As the majority of these illitic muscovite compositions occur in epiclastic rocks, this evidence may merely be products of likely Anchizone burial metamorphism rather than a result of hydrothermal alteration.

The test determines whether the results observed could likely be obtained at random. Table 3.1 also indicates that the test statistic ($X^2 = 9.41$) exceeds the X^2 critical value (3.84) at $\alpha = 0.05$ and 1 degree of freedom, suggesting that this is likely not a random result. Thus, the illitic muscovite composition occurs preferentially in the epiclastic rocks whereas the muscovite/phengite composition occurs in the volcanic rocks. The presence of this illitic muscovite composition in the dacitic epiclastic rocks is probably consequence of diagenesis (from montmorillonite) or burial metamorphism, whereas the muscovite composition in the volcanic rocks is probably a consequence of hydrothermal alteration.

Table 3.1 – Chi-square contingency test results for muscovite/phengite altered samples

	Sediments	**Volcanics**		Test	Results
Illite	9	3	**12**	X^2 =	9.41
Muscovite/ Phengite	4	16	**20**	degree of freedom	1
Total	**13**	**19**	**32**	Critical value	3.84

Chlorite

The compositional diversity of chlorite in the rocks hosting HMLSDZ indicates a bimodal distribution (Figure 3.21). The data indicates that chlorite in this rocks is bimodal with an Fe-rich daphnite ($Fe_7Mg_2Al_6Si_5O_{20}(OH)_{16}$) and a Mg-rich daphnite ($Fe_5Mg_4Al_6Si_5O_{20}(OH)_{16}$). The data trend on Figure 3.22 also suggests that a range of chlorite composition exists from chlinochlore to Mg-rich daphnite.

$Fe_7Mg_2Al_6Si_5O_{20}(OH)_{16} \rightarrow Fe_7Mg_3Al_4Si_6O_{20}(OH)_{16}$,

and

$Fe_5Mg_4Al_6Si_5O_{20}(OH)_{16} \rightarrow Fe_5Mg_5Al_4Si_6O_{20}(OH)_{16}$.

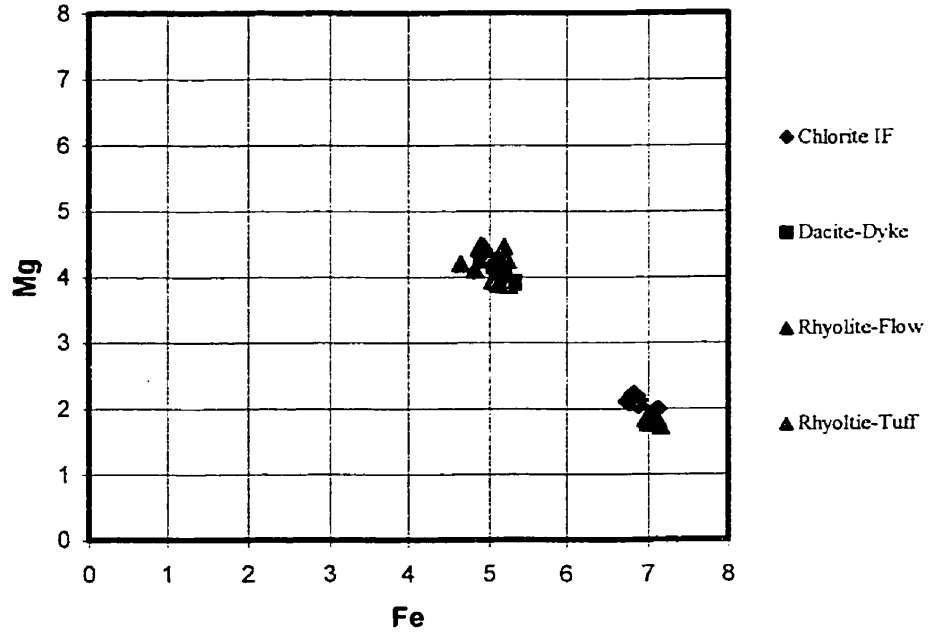

Figure 3.21 – Plot of the elemental amounts of *Fe* versus *Mg* to examine the composition of chlorite in five samples (Table D.3.1) from HMLSDZ. The data indicate that the chlorite compositions in these samples vary from a *Fe*-rich daphnite ($Fe_7Mg_2Al_6Si_5O_{20}(OH)_{16}$) to *Mg*-rich daphnite ($Fe_5Mg_4Al_6Si_5O_{20}(OH)_{16}$).

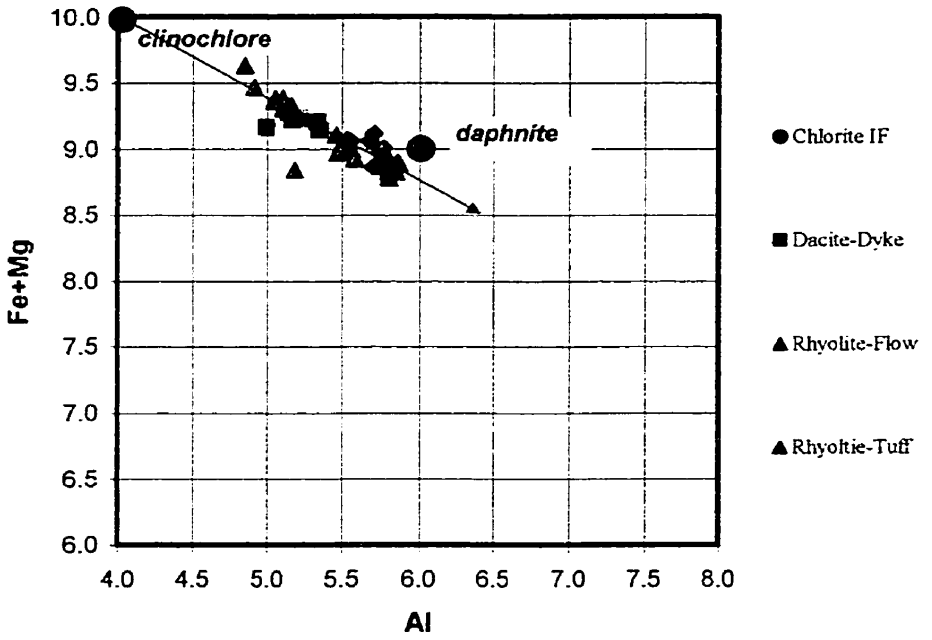

Figure 3.22 – Plot of the elemental amounts of *Al* versus *Fe+Mg* to examine the composition of chlorite in five samples (Table D.2.1) from HMLSDZ. The data indicate that the chlorite compositions in these samples vary from a clinochlore to Mg-rich daphnite.

Biotite

The only sample containing biotite, HML-158794, was an andesite dyke, and its composition is presented in Figure 3.23. This biotite composition has an average *(Fe+Mg)/K* ratio of approximately 2.56, which is less than the ratio for end member biotite (= 3). The composition of biotite ranges between that observed in meta-aluminous igneous rocks (Al < 2.4) and that observed in pelitic rocks containing excess aluminum (Al > 3.0). This suggests that the biotite is probably a result of a mildly hydrothermally altered (muscovite) dyke.

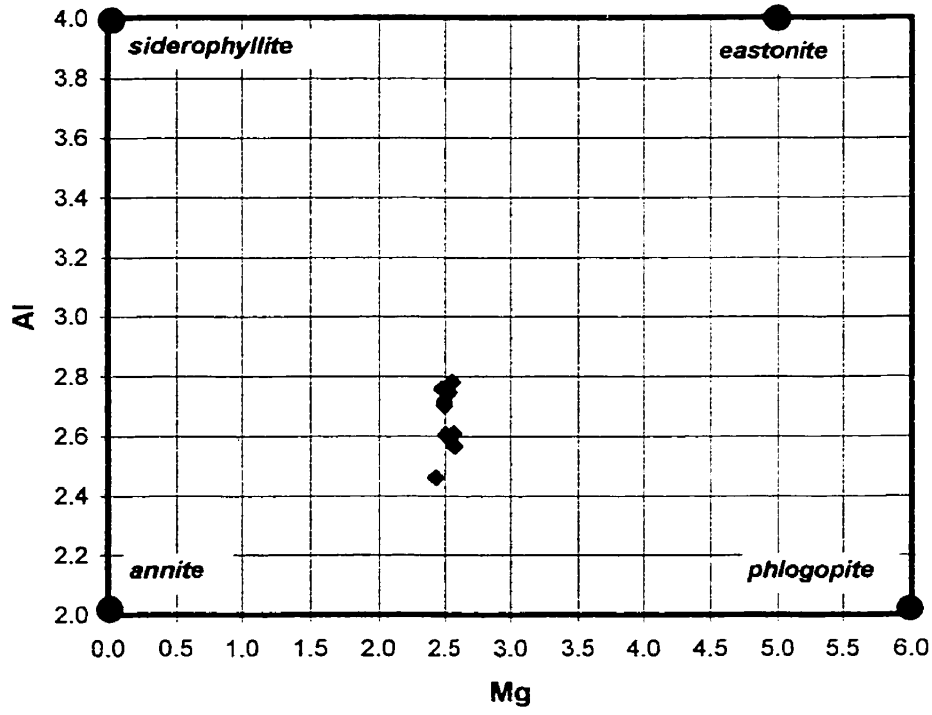

Figure 3.23 – Plot of the elemental amounts of *Al* versus *Fe+Mg* to examine the composition of biotite in one sample (Table D.5.1) from HMLSDZ.

4 - LITHOGEOCHEMISTRY

4.1 – Classification and Composition

Prior to designing PER diagrams to investigate the primary and secondary material transfer processes that have affected the rocks hosting the HMLSDZ, the existence of a conserved element in the rock suite was established. The search for a conserved element was conducted by plotting potentially conserved elements previously identified in the Bathurst camp (Zr, Y, Nb, Ti, *etc.*; Lentz 1996a) against each other.

Figures 4.1, 4.2 and 4.3 are scatterplots designed to test the cogenetic hypothesis and assist in identifying conserved element(s) in the rocks hosting the HMLSDZ. Data trends on Figure 4.1 confirm that four volcanic compositions exist in the HMLSDZ host rocks. These volcanic compositions define unique trends that can be approximated by single lines that pass through the origin. This feature is an indication that the samples along each line are related to rocks derived from parent compositions that were at one time homogeneous, and that the axes elements in each suite are conserved. Thus, we fail to reject the cogenetic hypothesis (Stanley and Madeisky 1996) and conclude that these rocks were derived from four parent compositions each of which were at one time homogeneous. TiO_2 and Nb are thus conserved elements in each suite.

Samples plotting along the line with steepest slope on Figure 4.1 (average Nb/TiO_2 = 38 ppm/wt. % and Nb/TiO_2 >24 ppm/wt. %; Table 4.1) and on Figure 4.2 (average Zr/TiO_2 = 571 ppm/wt. % and Zr/TiO_2 > 470 ppm/wt. %; Table 4.1) have high average SiO_2 concentrations (72.58 wt. %; Table 4.2).

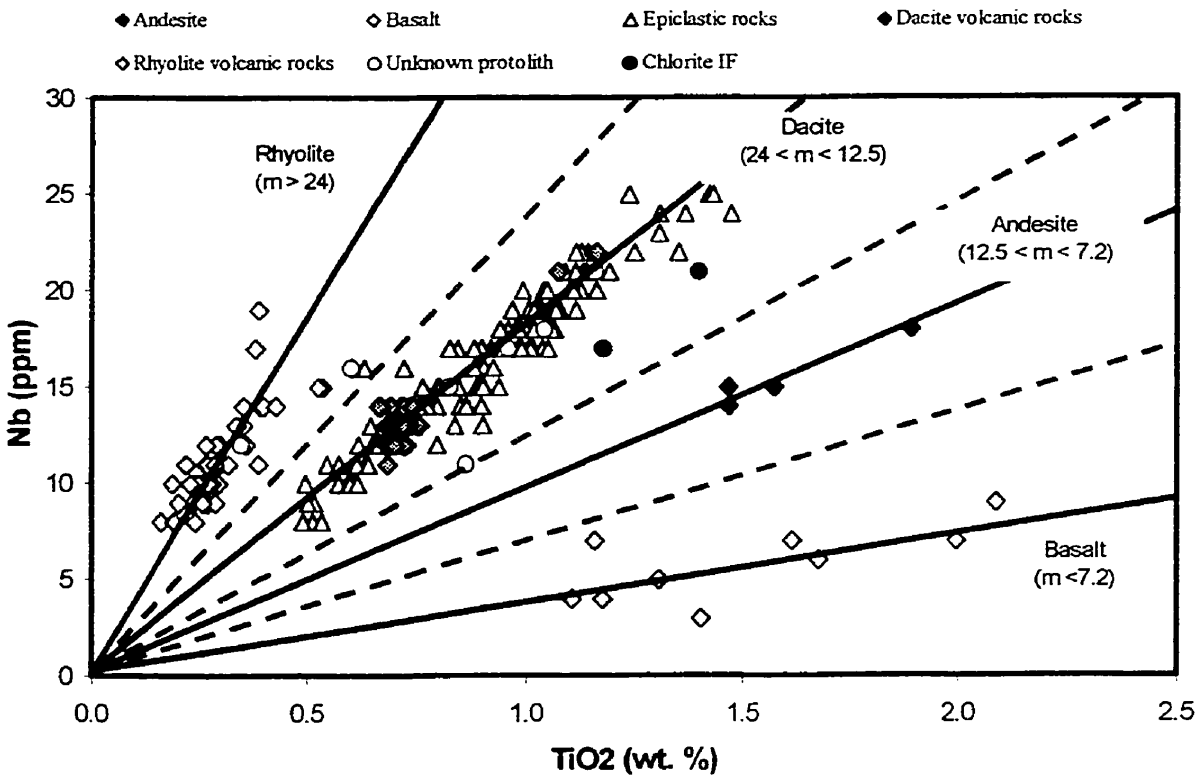

Figure 4.1 - Conserved element scatterplot designed to test the hypothesis that the rocks hosting the HMLSDZ are cogenetic. Data trends on this diagram indicate that the host rocks to the HMLSDZ can be divided into four volcanic compositions.

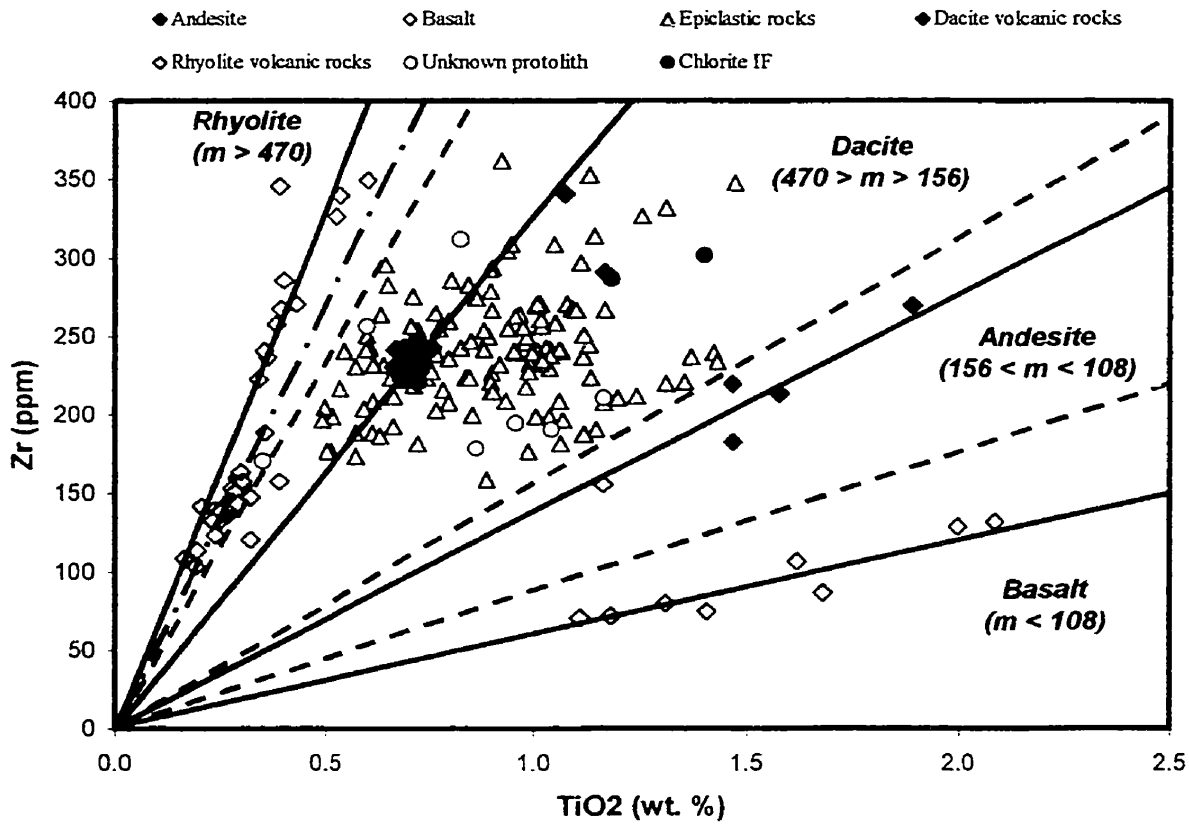

Figure 4.2 - Conserved element scatterplot designed to test the cogenetic hypothesis that the rocks hosting the HMLSDZ are cogenetic. Although significant scatter exists among the epiclastic rocks on this plot, the four volcanic compositions identified on Figure 4.1 can be discriminated using this TiO_2 *versus* Zr plot. With the exception of Zr in the sediments, Ti and Zr are conserved elements in these rocks, and can be used as denominators in PER's.

These are thus considered to be rhyolitic in composition. Samples plotting on the line with shallower slope ($Nb/TiO_2 < 12.5$ and < 24 ppm/wt. % and $Zr/TiO_2 > 108$ and < 470 ppm/wt. % on Figure 4.2; Table 4.1) have SiO_2 concentrations averaging 65.26 wt. % (Table 4.2), consistent with a dacitic composition. Finally, samples plotting below these data trends are interpreted to be of andesitic and basaltic composition based on their Nb/TiO_2 and Zr/TiO_2 ratios (Table 4.1) and their average SiO_2 wt. % concentrations (Table 4.2). In contrast, the four volcanic compositions postulated from Figures 4.1 and 4.2 cannot be discriminated using P_2O_5/TiO_2 ratios (Figure 4.3).

Because the lines through these data on Figures 4.1 and 4.2 pass through the origin, TiO_2, Zr, and Nb are interpreted to be conserved elements in these volcanic and volcanic-derived rocks (with the possible exception of Zr in the epiclastic rocks, which appear to have undergone differential sorting relative to TiO_2). Consequently, any of these elements could be used as a conserved element denominator in the PER diagrams used to investigate the sources of compositional variation in these rocks. In the subsequent PER analysis, Ti, being the most conserved element (due to its relatively low detection limit, and high analytical accuracy and precision) was used as the conserved element denominator.

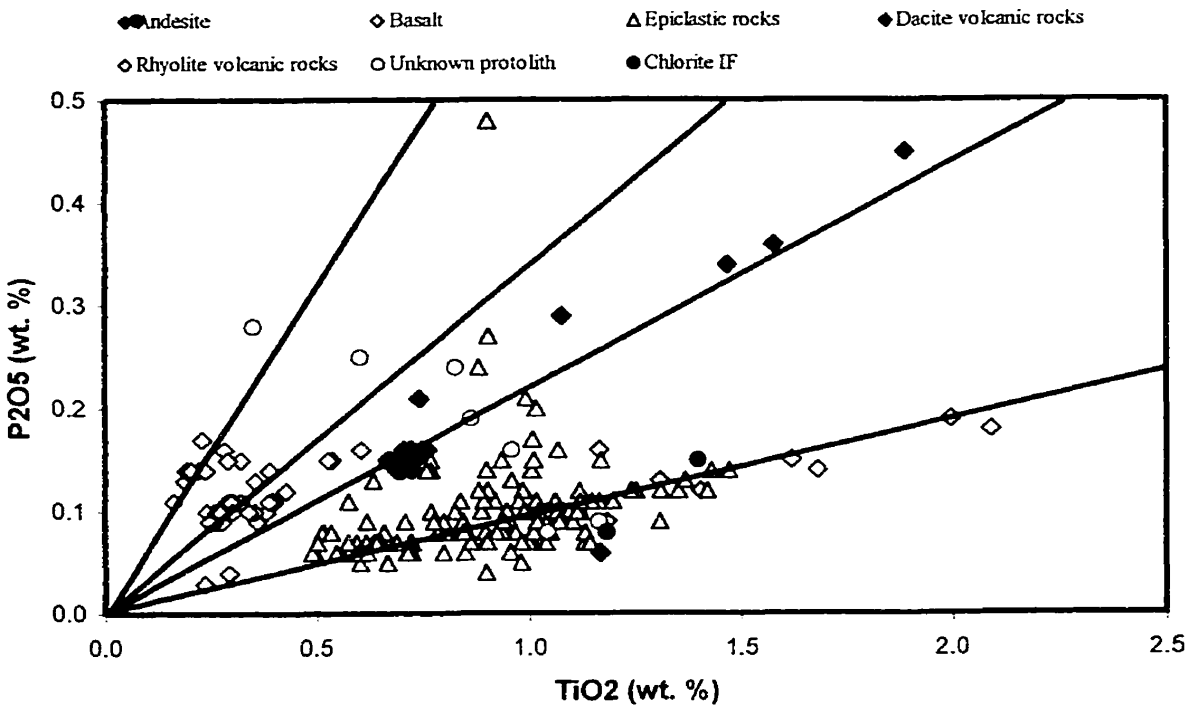

Figure 4.3 - Conserved element scatterplot designed to test the hypothesis that the suite of rocks hosting the HMLSDZ are cogenetic. The four volcanic compositions identified in Figures 4.1 and 4.2 cannot be discriminated using this TiO_2 *versus* P_2O_5 plot. Because Ti has been previously identified as a conserved element in the dataset, the significant scatter on this plot is probably a result of P_2O_5 mobility during hydrothermal activity (and/or metamorphism).

The HMLSDZ host rocks were classified using a combination of the distinct data trends on Figures 4.1 and 4.2 and the thresholds separating these trends. Samples below the line with slope corresponding to a Nb/TiO_2 ratio of 7.2 ppm/wt. % on Figure 4.1 were classified as basalt. Similarly, samples with Nb/TiO_2 ratios corresponding to andesite, dacitic and rhyolitic compositions were classified accordingly (Table 4.1). Similar thresholds for Zr/TiO_2 on Figure 4.2, although displaying a few outliers, were also used in an independent classification of the samples.

Table 4.1 – Classification based on conserved element ratios.

Volcanic Composition		***Average (ppm/wt. %)***	***Range (ppm/wt. %)***
	Nb/TiO_2		
Basalt		4	< 7.2
Andesite		10	7.2 – 12.5
Dacitic		18	12.5 - 24
Rhyolitic		38	> 24
	Zr/TiO_2		
Basalt		69	< 108
Andesite		139	108 – 156
Dacitic		286	156 - 470
Rhyolitic		571	> 470

The concentrations of SiO_2 for each group were utilized to assign a compositional name to each classification group: basalt, andesite, dacitic and rhyolitic. Table 4.2 presents a summary of the mean concentrations of selected oxides and lithophile trace elements for each composition. A comparison of the Nb/TiO_2 and Zr/TiO_2 ratios indicate that out of the two hundred and twenty two (222) samples studied, only six were inconsistently classified by these two ratios (Table 4.3). Clearly, both classification

schemes are overwhelmingly consistent; suggesting both or either could be used to confidently determine the group membership of lithogeochemical samples from the HMLSDZ.

Table 4.2 - Mean concentrations of a subset of analyzed elements that were used to assign formal names to each geochemical group.

mean	SiO_2	TiO_2	Al_2O_3	*Y*	*Zr*	*Nb*
Basalt	43.26	1.50	15.81	29.67	101.00	5.78
Andesite	57.58	1.60	15.63	56.50	221.75	15.50
Dacitic	65.26	0.88	14.64	48.48	240.83	15.80
Rhyolitic	72.58	0.31	12.87	47.57	179.65	11.41

Table 4.3 - Comparative classification results for Zr/TiO_2 and Nb/TiO_2 ratios.

averages	*Basalt*	*Andesite*	*Dacitic*	*Rhyolitic*
Basalt	**8**	0	0	0
Andesite	1	**4**	0	0
Dacitic	0	0	**165**	5
Rhyolitic	0	0	0	**42**

4. 2 – Pearce Element Ratio Analysis

The mineralogy of the HMLSDZ host rocks suggests that primary compositional variability in these rocks may be due to feldspar and/or quartz fractionation/sorting. A PER diagram that plots the molar ratios of Al/Ti *versus* (2Ca+Na+K)/Ti (Figure 4.4) was used to investigate the control of feldspar fractionation on the composition of these rocks.

On Figure 4.4, fractionation (sorting) of any composition of feldspar will cause the samples to be displaced up or down along the line with unit slope. The upper edge of the data is roughly parallel to the feldspar control line (m = 1), but slightly displaced from it. This is an indication of both igneous fractionation (involving feldspar sorting) and a secondary material transfer process (*e.g.*, hydrothermal metasomatism). Thus, the samples plotting proximal to the feldspar control line are considered to be least altered (*i.e.*, fresh), and the downward vertical displacement of other samples plotting below this line is a result of metasomatism. Samples plotting along the line with a slope of 1/3 are interpreted to be samples that are muscovite-altered, with a *K/Al* ratio = 1/3. Samples affected by chlorite alteration are displaced farther downwards towards the line with zero slope, because *K*, *Na*, and *Ca* are absent in the mineral formula of chlorite.

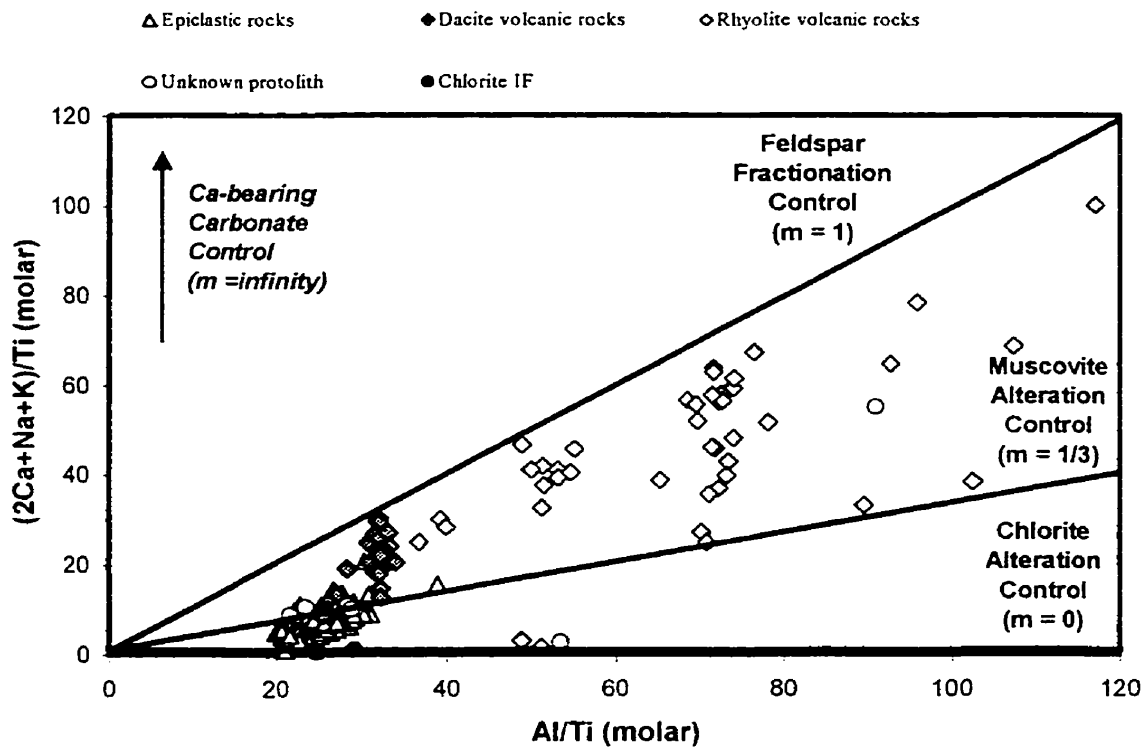

Figure 4.4 - PER diagram of Al/Ti plotted against (2Ca+Na+K)/Ti for samples from the HMLSDZ. On this diagram, fractionation of any composition of feldspar displaces rock compositions along the line with unit slope. Data plotting along this line with unit slope represent least altered (or fresh) samples. Muscovite-altered samples plot along a line with slope of 1/3, and chlorite-altered samples plot along the abscissa.

Geological information (Appendix B.2, B.3.1, and B.3.2) collected from the field and supported by electron microprobe and thin section petrographic studies indicate that significant carbonate, probably introduced during either hydrothermal activity or metamorphism, exists in the HMLSDZ host rocks. Consequently, the amount and predominant type of carbonate mineral present was verified using a PER diagram that plots Ca/Ti versus CO_2/Ti (Figure 4.5). On this diagram, the presence of calcite displaces rock composition upwards along a line with unit slope. Samples containing dolomite or ankerite are displaced upwards along a line with slope of two, and samples containing siderite will be displaced upwards along the ordinate axis. Samples containing only anorthite will plot along the abscissa.

Most samples plot along or just below the calcite control line, indicating that calcite is probably the predominant carbonate composition in these rocks. This evidence is consistent with acid effervescence tests on hand samples, as well as electron microprobe analyses, which indicate the presence of calcite. Samples plotting above the dolomite/ankerite control line indicate the presence of siderite in some rhyolitic volcanic rocks: however, the amount of siderite is subordinate to calcite in most samples (Appendix D). Consequently, in the following PER diagrams, wherever *Ca* occurs in an axis ratio numerator, a corresponding amount of CO_2 has been subtracted from that numerator. This causes these diagrams to be projections from calcite, and ensures that the addition or loss of calcite has no effect on where samples plot on these diagrams.

Having established that calcite is the predominant carbonate composition in these rocks, a modified PER feldspar fractionation diagram with axes of Al/Zr *versus* $(2Ca+Na+K-2CO_2)/Ti$ that is insensitive to the effect of calcite alteration was plotted

(Figure 4.6). This diagram has identical attributes to that of Figure 4.4, except that calcite alteration has no effect. The influence of calcite alteration in these samples can be observed on this diagram because samples that plotted close to the feldspar fractionation control line on Figure 4.4 are displaced slightly downwards from it.

Rhyolitic volcanic rocks exhibit significant variation along the Al/Ti axis, and thus exhibit the most feldspar fractionation. These samples also define discrete downward vertical trends that indicate alkali loss during metasomatism. These rhyolitic samples also appear to be subdivided into groups on Figure 4.6, and thus may be related to intermittent eruptive products tapping a single magma chamber at depth, although these are geochemically similar. With the exception of three chlorite-altered samples, all rhyolitic samples are least altered to muscovite-altered.

Dacitic volcanic rocks at the HMLSDZ do not exhibit significant feldspar fractionation, but do perhaps exhibit a weak downward vertical displacement that could be interpreted as a result of metasomatism. As indicated on Figure 4.6, these rocks are moderately altered, with only four samples that appear to be completely muscovite-altered. In contrast, the epiclastic rocks do not exhibit significant evidence for feldspar fractionation, but are the only rock type exhibiting significant chlorite alteration.

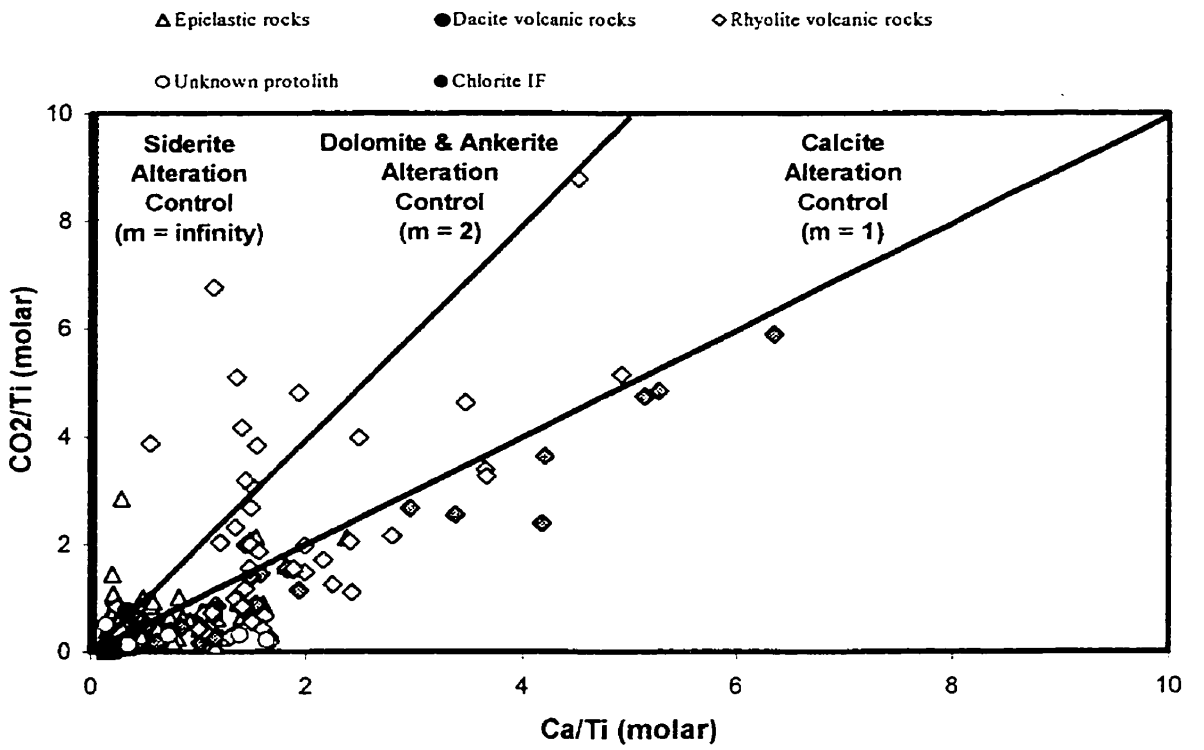

Figure 4.5 - PER diagram of Ca/Ti plotted against CO_2/Ti for samples from the HMLSDZ. Observations from this plot, coupled with microprobe data indicate that calcite is the predominant carbonate mineral in these rocks.

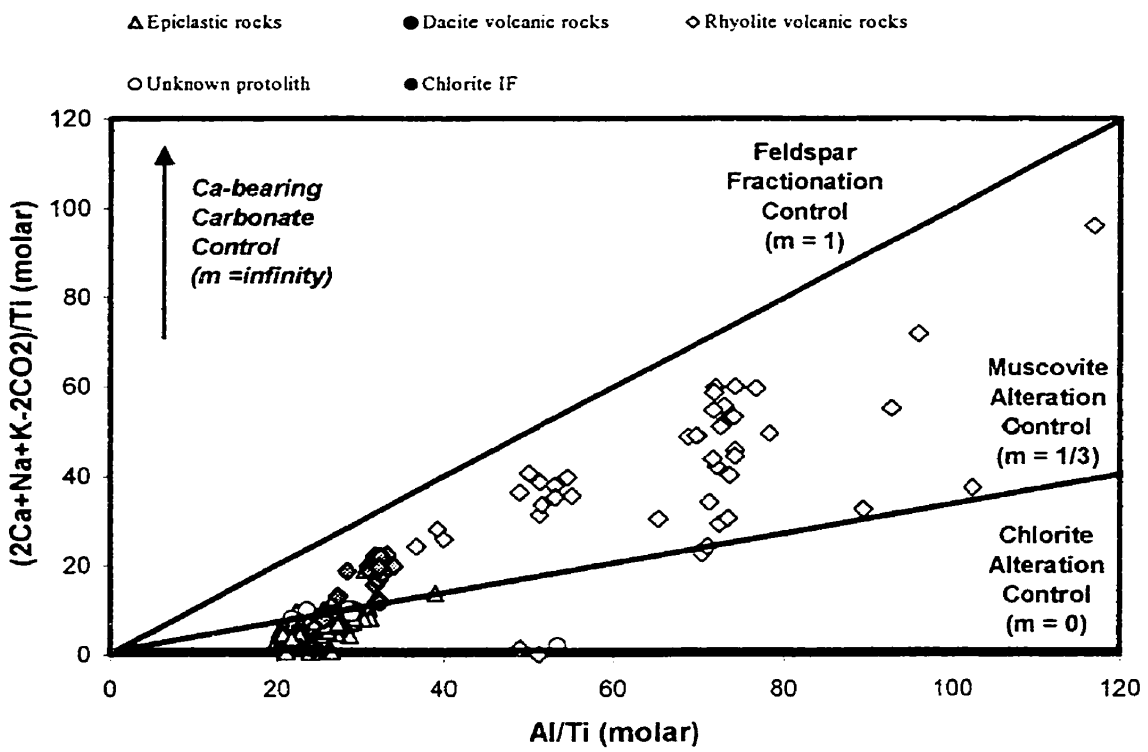

Figure 4.6 - PER diagram of Al/Ti plotted against $(2Ca+Na+K-2CO_2)/Ti$ for samples from the HMLSDZ. On this diagram, fractionation of any composition of feldspar will displace rock compositions along a line with unit slope. Addition of calcite will have no impact on this diagram. Data plotting along a line with unit slope represent least altered (or fresh) samples. Muscovite-altered samples plot along a line with slope of 1/3, whereas chlorite-altered samples plot along the line parallel to the abscissa. Rhyolitic samples exhibit significant feldspar fractionation.

Figure 4.7 presents a PER diagram that plots (Si+Al)/Ti on the abscissa and (Al-Ca+CO_2)/Ti on the ordinate. On this diagram, which is a projection from calcite, fractionation of quartz, or the metasomatic addition - *silicification,* or loss - *de-silicification,* of silica, will displace rock compositions horizontally across the diagram along the abscissa. In contrast, fractionation of feldspar of any composition will displace rock compositions along a line with a slope of 1/4. Thus, this diagram was used to determine the proportional involvement of quartz and feldspar fractionation.

If the slope of a data trend on this diagram is ***m***, then the quartz/feldspar fractionation ratio corresponding to that trend equals:

$$\frac{X_{QTZ}}{X_{FS}} = \frac{4m-1}{-m} \qquad (4.1)$$

(derived from equations presented in Stanley and Madeisky 1996).

The rhyolitic samples on this diagram exhibit a trend corresponding to a line with slope of approximately 7/50, whereas the epiclastic rocks exhibit a predominantly horizontal trend either due to silicification/desilicification or more likely quartz fractionation. The dacitic volcanic rocks exhibit no variation, suggesting neither significant quartz nor feldspar fractionation. Using equation 4.1, the quartz/feldspar fractionation molar ratio in the rhyolitic samples is estimated to be 3:1. The molar volumes of quartz (22.67 mole/cm^3) and albite (99.71 mole/cm^3), the predominant minerals undergoing fractionation in these rhyolitic volcanic rocks, were used to estimate the quartz/feldspar fractionation ratio, which turns out to be 2:3 by volume. This ratio suggests that feldspar fractionation is slightly more important than quartz fractionation in the rhyolitic samples.

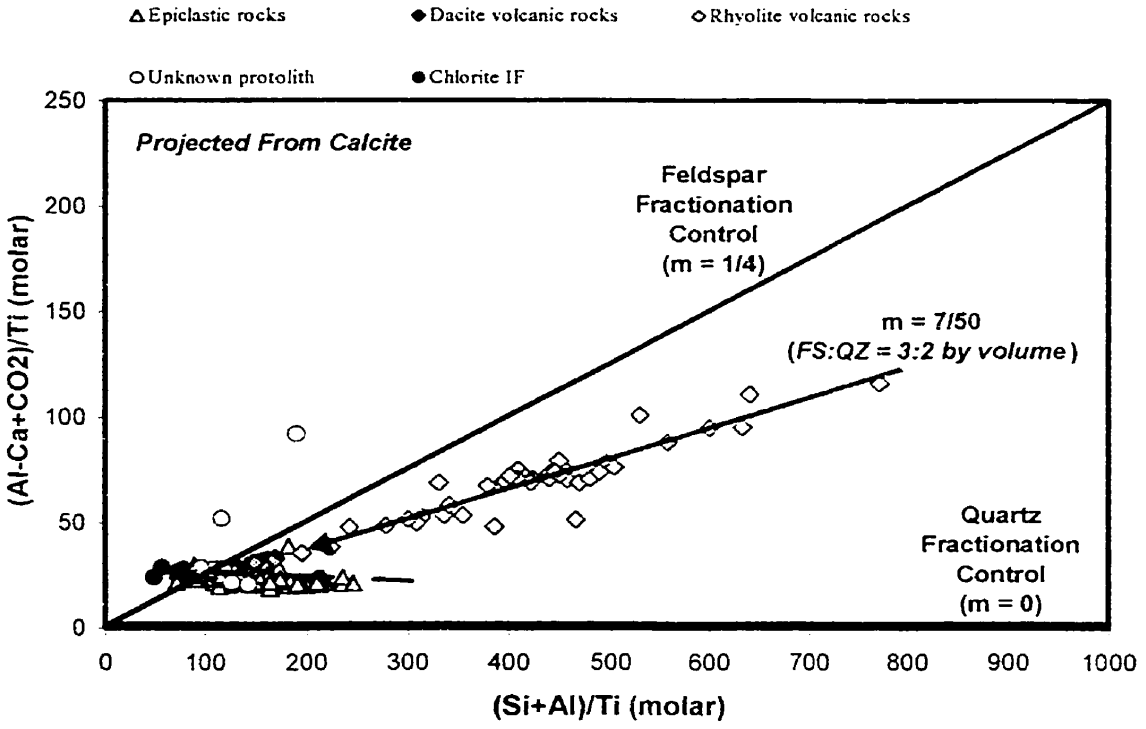

Figure 4.7 - PER diagram of (Si+Al)/Ti plotted against (Al-Ca+CO_2)/Ti for samples from the HMLSDZ. On this plot, epiclastic rocks exhibit a horizontal trend suggesting either quartz fractionation or silicification/desilicification or both. Rhyolitic samples plot along a line with slope of 7/50. This ratio suggests a quartz/feldspar ratio of 2:3 by volume for the rhyolitic volcanics, suggesting that feldspar fractionation predominates over quartz fractionation in the rhyolitic volcanic rocks. The dacitic volcanic rocks exhibit no variation, suggesting neither quartz or feldspar fractionation.

Figures 4.8 through 4.10 describe specific fractionation models relating to anorthite, albite and potassium feldspar, respectively. As indicated on Figure 4.8, there is little evidence in any rock type to support significant fractionation of end-member anorthite in the HML South Deep host rocks.

The data trend on Figure 4.9 defined by samples of rhyolitic composition indicates that they have undergone significant albite fractionation. Dacitic volcanic and epiclastic rocks exhibit little evidence for albite fractionation and the former are relatively less altered than the latter. As in Figure 4.9, fractionation of potassium feldspar is evident in only the rhyolitic samples (Figure 4.10). The dacitic volcanic and epiclastic rocks have compositions that do not suggest the presence of potassium feldspar fractionation. Rather, their compositions suggest they have been altered to muscovite and/or chlorite.

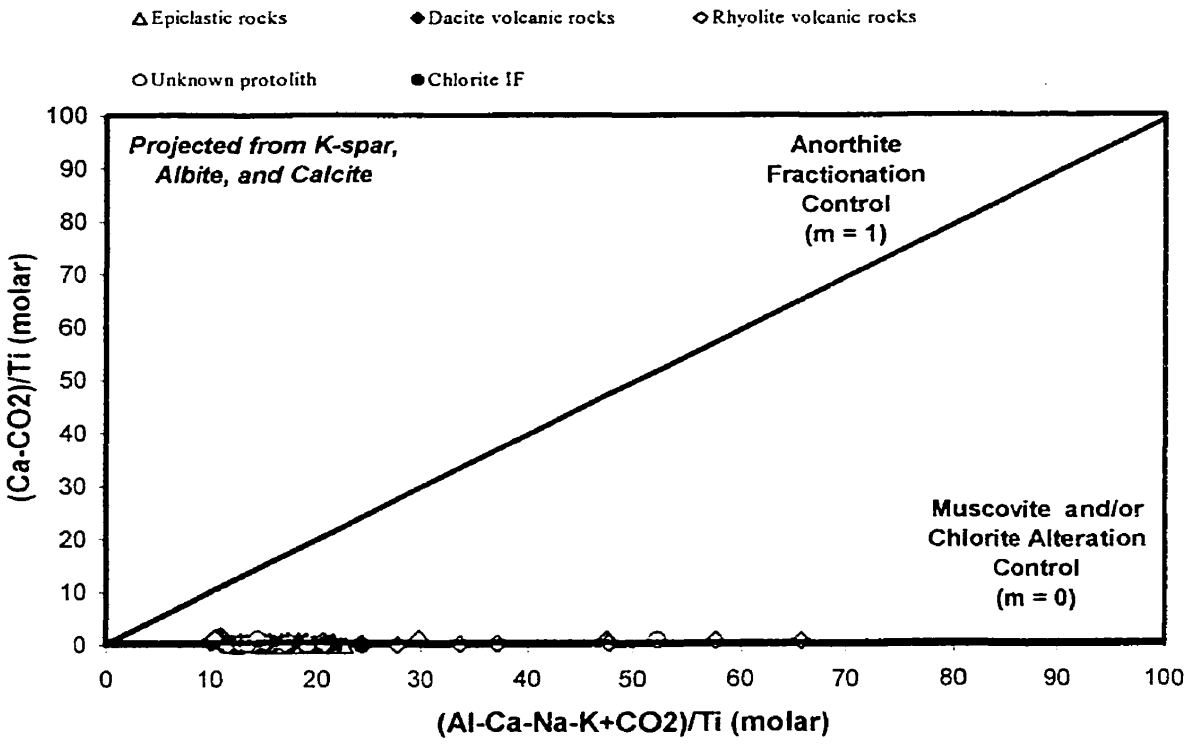

Figure 4.8 - PER diagram of (Al-Ca-Na-K+CO2)/Ti plotted against (Ca-CO_2)/Ti for samples from the HMLSDZ. This diagram is sensitive to anorthite fractionation only, and is unaffected by fractionation of other feldspars or calcite alteration. Fractionation of anorthite displaces rock compositions along a line with unit slope. Similarly, muscovite and/or chlorite alteration causes displacement of rock compositions along the abscissa (zero slope). The numerator on the ordinate axis represents silicate-bearing calcium, most likely, anorthite. Clearly, anorthite fractionation was insignificant in these rocks.

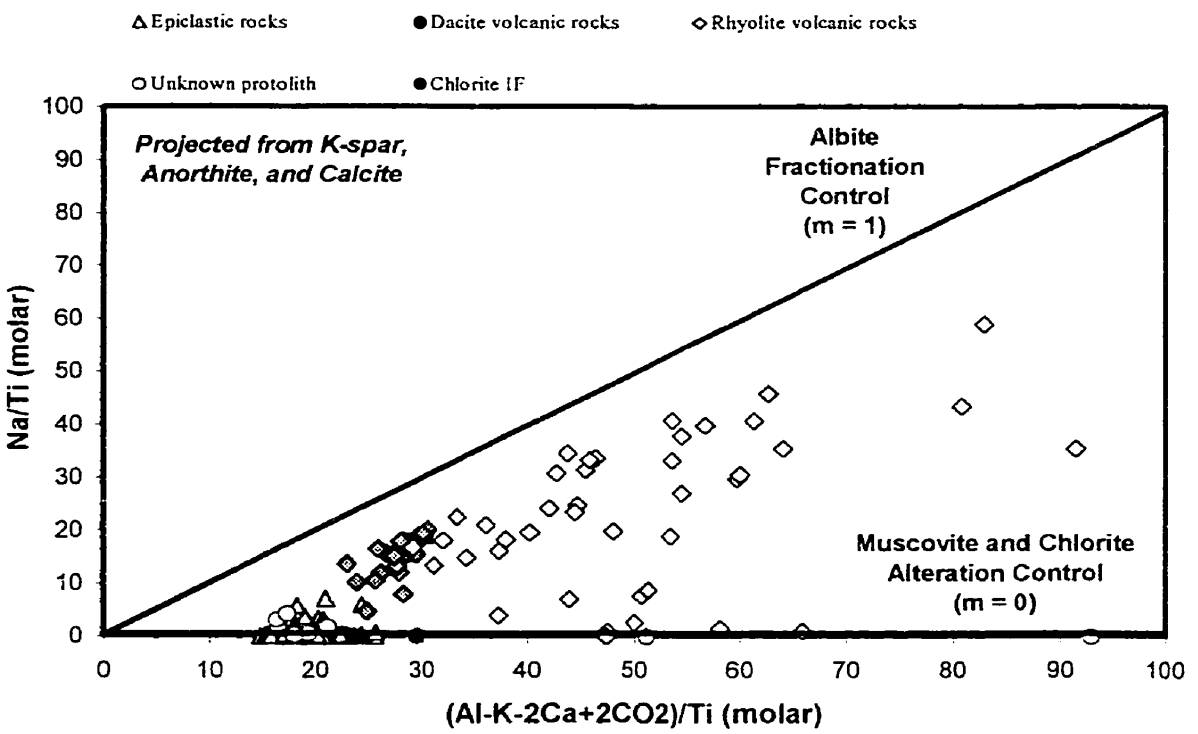

Figure 4.9 - PER diagram of (Al-K-2Ca+2CO2)/Ti plotted against Na/Ti for samples from the HMLSDZ. This diagram is sensitive to only albite fractionation, and is unaffected by fractionation of other feldspars. It is also a projection from calcite. Fractionation of albite displaces rock compositions along a line with unit slope; muscovite alteration causes displacement of samples along the abscissa (zero slope). The rhyolitic samples exhibit significant fractionation of Na-rich feldspar. Dacitic volcanic rocks exhibit minor albite fractionation and are relatively less altered compared with epiclastic rocks. We can infer from this plot that albite is the predominant feldspar controlling the composition of these rocks.

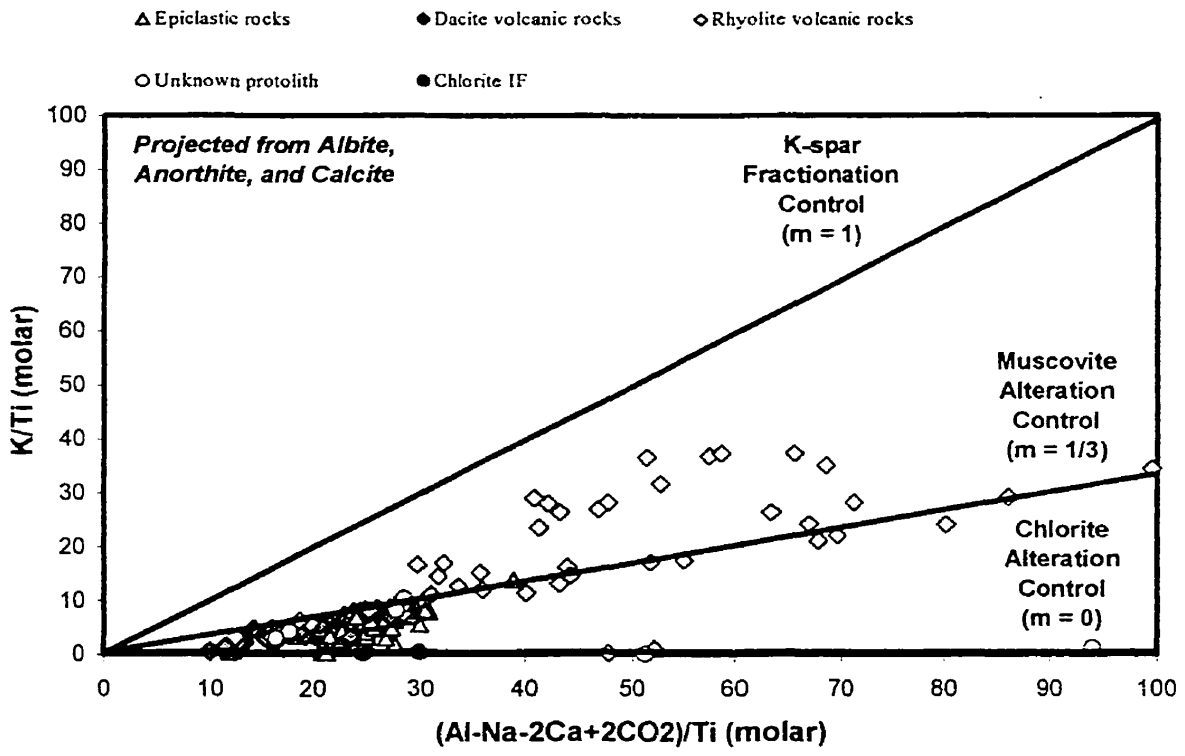

Figure 4.10 - PER diagram of (Al-Na-2Ca+2CO_2)/Ti plotted against K/Ti for samples from the HMLSDZ. This diagram is sensitive to only potassium feldspar fractionation. Data plotting along a line with unit slope are considered to be fresh; muscovite-altered samples plot along a line with slope of 1/3, and completely chlorite-altered samples plot along the abscissa. The significant number of rhyolitic samples plotting between the potassium feldspar and muscovite control lines indicate that potassium feldspar fractionation occurred in the rhyolitic rocks. No conclusive evidence of potassium feldspar fractionation is observed in any other rock type.

4. 3 – Molar Element Ratio Analysis

Hydrothermal activity associated with the formation of VHMS deposits such as the HMLSDZ, is typically accompanied by chemical reactions between the hydrothermal fluid and the host rocks. These reactions involve the addition or removal of various chemical species such as Na, K, OH, CO_2, *etc*. The consequence of these reactions is the development of vertical and lateral alteration haloes that are targets used in exploring for these mineral deposits. Because of the overprinting of hydrothermal alteration signatures by other secondary material transfer processes (*e.g.*, metamorphism), it is sometimes difficult to recognise and quantify deposit-related hydrothermal alteration signatures.

A molar element ratio (MER) diagram that is a special projection of multivariate geochemical space and insensitive to the effects of igneous fractionation was designed to investigate the control of metasomatism on the rocks hosting the HMLSDZ. This diagram consists of the slope [$(2Ca+Na+K-2CO_2)/Al$] of a line from a data point to the origin on Figure 4.6, also known as *hydrolytic alteration index*, plotted against the PER's of each component that was mobile in the hydrothermal system. Figures 4.11 through 4.20 present these special MER diagrams for elements that are mobile in the HML hydrothermal system.

The hydrolytic alteration index is unaffected by quartz sorting and carbonate alteration processes. The hydrolysis index reports a value of unity for rocks that have not been subjected to any hydrolysis (*i.e.* - are fresh), a value of 1/3 for rocks that are completely muscovite-altered, and a value of zero for rocks that are completely chlorite-altered.

Figure 4.11 plots $(2Ca+Na+K-2CO_2)/Al$ *versus* Si/Ti. The data trends for both rhyolitic and dacitic volcanic rocks do not indicate that net addition or removal of silica accompanied hydrothermal alteration. However, the observed variation in the rhyolitic volcanic rocks is probably a result of quartz phenocryst sorting rather than metasomatic addition or removal of SiO_2.

The above observation is contrary to the observed siliceous nature of some drill core from the HMLSDZ. An explanation for this apparent contradiction is that the siliceous nature of these rocks may be a consequence of the formation of quartz (and muscovite) during the hydrothermal alteration of feldspar and not due to the metasomatic addition of SiO_2. In the breakdown of feldspar to muscovite, SiO_2 is produced, and may have precipitated as quartz. This could suggest that "quartzification", rather than "silicification", may have accompanied hydrolytic alteration. The possible chemical reactions responsible for muscovite formation by the breakdown of feldspar must be balanced on Al, because the hydrothermally altered samples on Figure 4.6 plot below those that are relatively fresh, indicating that Al was immobile during hydrothermal alteration. The relevant chemical reactions constrained in this way are:

$$\underset{\text{(Albite)}}{3\ NaAlSi_3O_8} + K^+ + 2\ H^+ \Rightarrow \underset{\text{(Muscovite)}}{KAlSi_3O_{10}(OH)_2} + \underset{\text{(Quartz)}}{\mathbf{6\ SiO_2}} + 3\ Na^+ \qquad \text{(i)}$$

and

$$\underset{\text{(K-spar)}}{3\ KAlSi_3O_8} + 2\ H^+ \Rightarrow \underset{\text{(Muscovite)}}{KAlSi_3O_{10}(OH)_2} + \underset{\text{(Quartz)}}{\mathbf{6\ SiO_2}} + 2\ K^+ \qquad \text{(ii)}$$

In contrast, the epiclastic rocks exhibit a crude increase in SiO_2 with hydrolytic alteration on Figure 4.11, indicating that SiO_2 addition occurred with chloritization. Constraining the chemical reaction producing chlorite from muscovite by balancing on Al (as above) results in the following chloritization reaction:

$$\begin{array}{c} 3 \text{ Muscovite} + 6\ SiO_2 + 30\ (Fe,Mg)^{+2} + 48\ H_2O \\ \Rightarrow \\ 3 \text{ Chl} + 3\ K^{+} + 56\ H^{+} \end{array} \qquad \text{(iii)}$$

This reaction suggests that SiO_2 could have been added to the rocks during chloritization, and this could explain the observed minor increase in SiO_2 in chlorite-altered epiclastic rocks. Thus, observations from Figure 4.7 suggesting that quartz fractionation or silicification/desilicification or both, occurred in epiclastic rocks can be further constrained. The trend exhibited by epiclastic rocks on Figure 4.11 indicates a possible consequence of silicification or quartz sorting.

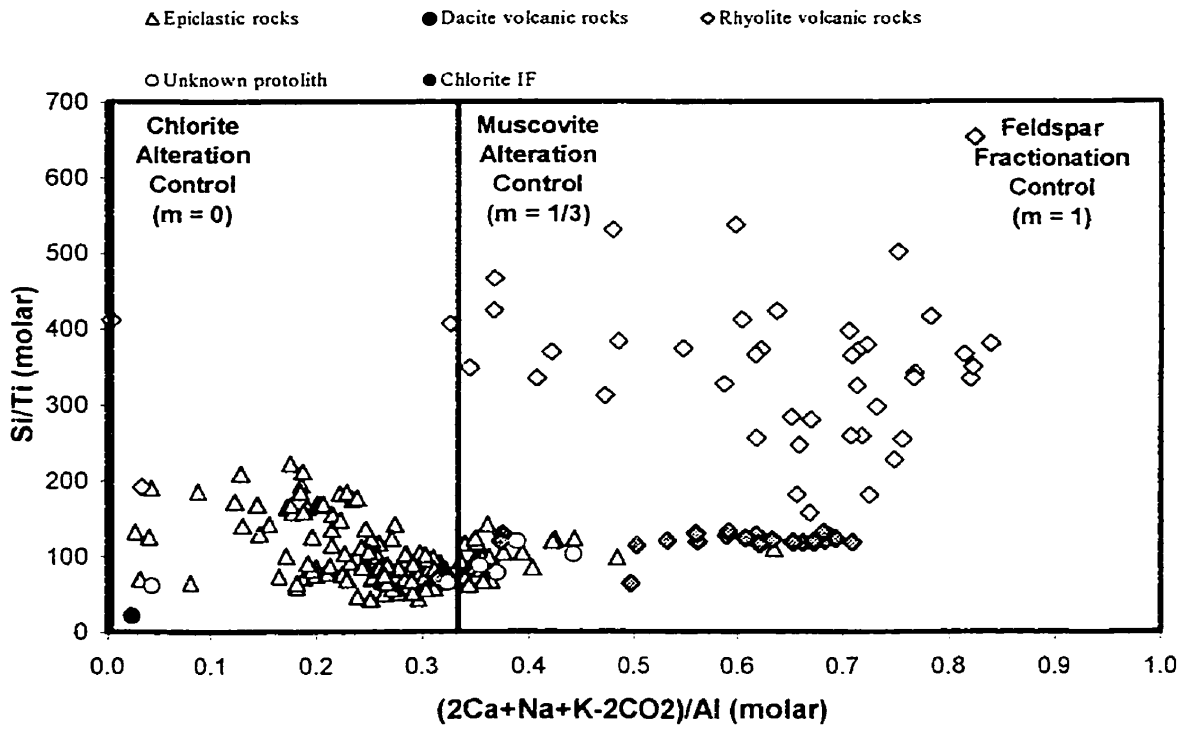

Figure 4.11 - MER diagram plotting $(2Ca+Na+K-2CO_2)/Al$ *versus* Si/Ti for samples from the HMLSDZ. The abscissa is essentially the slope of a line from a data point to the origin on Figure 4.6. It is thus a measure of the extent of hydrolysis that each sample has undergone (1 = no hydrolysis; 0 = complete hydrolysis, probably to chlorite; 1/3 corresponds with hydrolysis to muscovite). This diagram is also a projection from calcite, hence, addition or loss of calcite will not displace samples on this diagram. Samples of variably muscovite-altered rhyolitic and dacitic volcanic rocks exhibit no change in Si with extent of hydrolysis. In contrast, possible addition of SiO_2 may have occurred in chlorite-altered epiclastic rocks.

Figure 4.12 plots $(2Ca+Na+K-2CO_2)/Al$ *versus* Fe/Ti. On this diagram, increasing hydrolysis is unaccompanied by significant Fe addition in rhyolitic and dacitic volcanic rocks. However, addition of Fe occurred in epiclastic rocks during chloritization and this is consistent with the proposed chloritization reaction (iii). Addition of Fe has accompanied hydrolysis in hydrothermal systems associated with other VHMS deposits in the Bathurst camp (Lentz 1996a), and these Fe additions have also been associated with chloritization.

Figure 4.13 plots $(2Ca+Na+K-2CO_2)/Al$ *versus* Mg/Ti. As with Fe, Mg addition occurred in chloritic epiclastic rocks. In contrast, there is no Mg addition but same variation in the amount of Mg in muscovite-altered rhyolitic and dacitic volcanic rocks. The cause of this Mg variation is unknown, but the Mg probably resides within the phengitic muscovite observed in some samples.

Figure 4.14 plots $(2Ca+Na+K-2CO_2)/Al$ versus Mn (ppm). On this diagram, increasing hydrolysis does appear to correlate with Mn abundance, suggesting Mn addition in samples, particularly the chlorite-altered epiclastic rocks. The addition of Fe, Mg, and Mn in the epiclastic rocks likely resulted from the alteration of muscovite to chlorite. However, a notable feature on this plot is the abrupt increase in the amount of Mn in epiclastic rocks near the muscovite control line, coincident with phengite and muscovite compositions.

Figure 4.15 plots $2Ca+Na+K-2CO_2)/Al$ versus Na/Ti. This plot indicates that hydrolytic alteration proceeded with Na loss in all rocks during muscovite alteration. This metasomatic loss is consistent with the albite to muscovite alteration reaction (i), above, where Na is lost to the hydrothermal fluid.

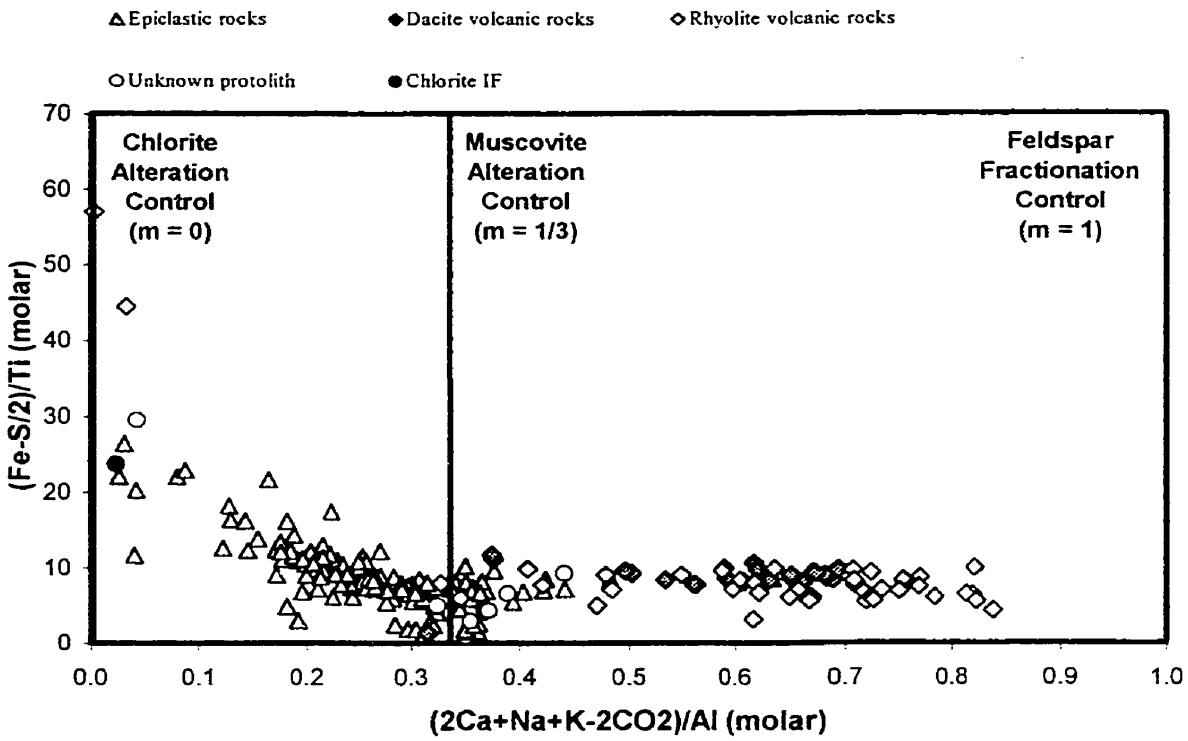

Figure 4.12 - Molar ratio diagram plotting $(2Ca+Na+K-2CO_2)/Al$ *versus* Fe/Ti for samples from the HMLSDZ. Samples of both rhyolitic and dacitic volcanic rocks exhibit no significant change in Fe with extent of hydrolysis. However, chlorite-altered epiclastic rocks exhibit Fe addition during formation of chlorite from muscovite.

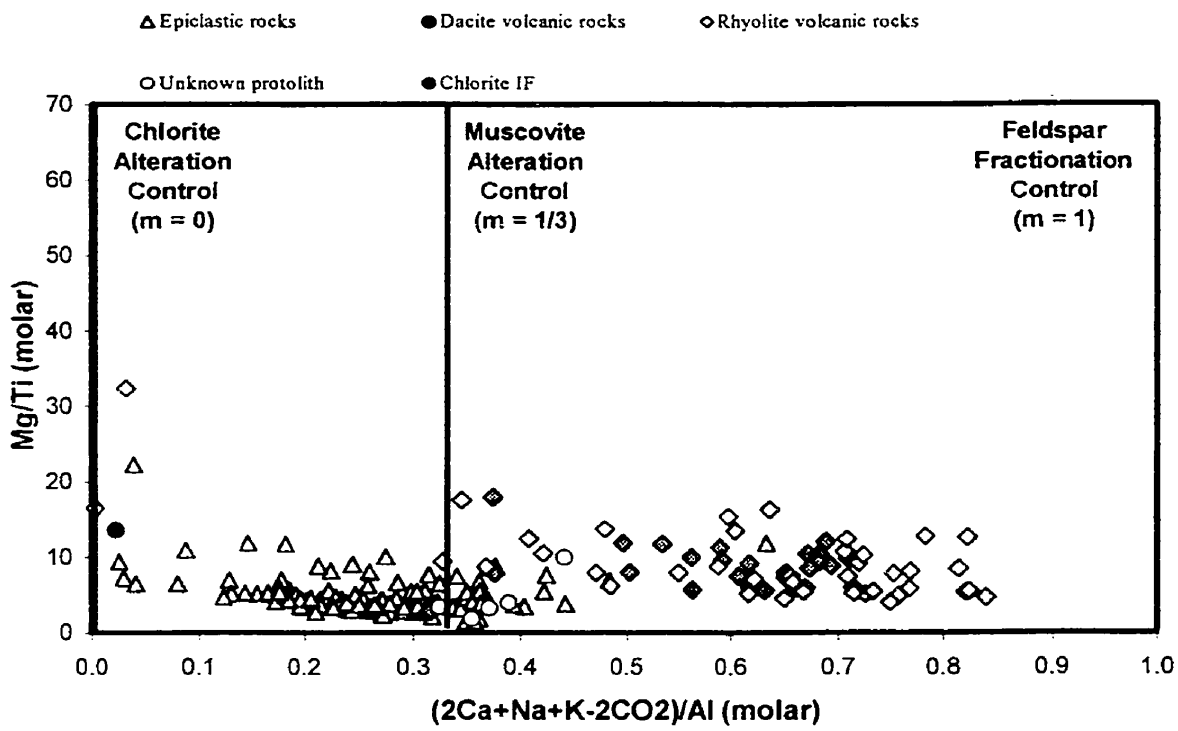

Figure 4.13 - This molar ratio diagram plots $(2Ca+Na+K-2CO_2)/Al$ *versus* Mg/Ti for samples from the HMLSDZ. Minor Mg addition accompanied chlorite alteration in the epiclastic rocks.

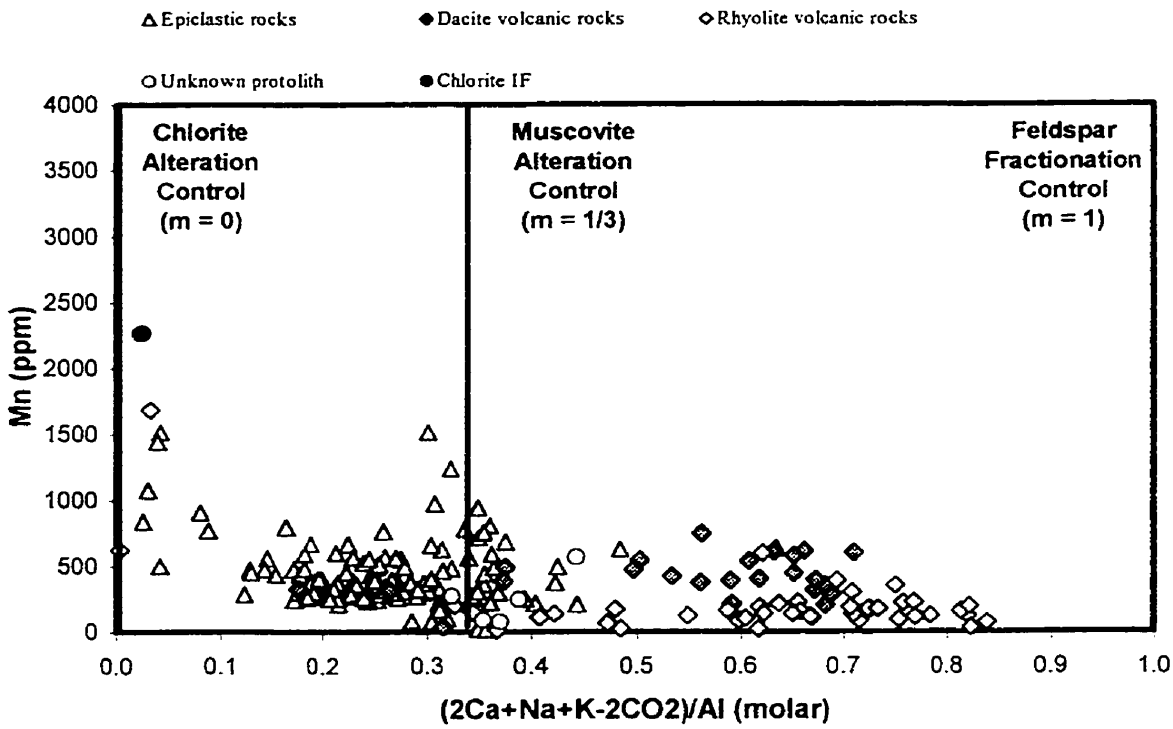

Figure 4.14 - This molar ratio diagram plots $(2Ca+Na+K-2CO_2)/Al$ against Mn for samples from the HMLSDZ. Significant Mn addition is evident in a few muscovite- and chlorite-altered epiclastic rocks.

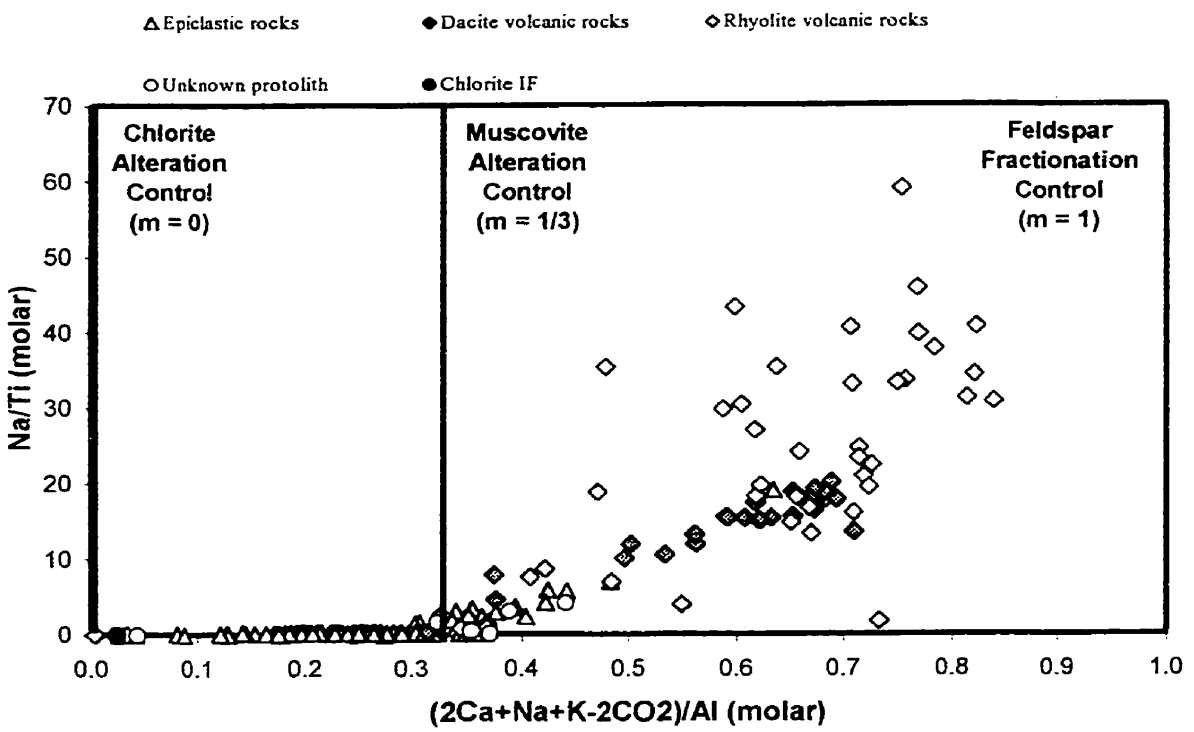

Figure 4.15 - This molar ratio diagram plots $(2Ca+Na+K-2CO_2)/Al$ against Na/Ti for samples from the HMLSDZ. This diagram is also a projection from calcite, so addition or loss of calcite will not displace samples on this diagram. Na loss accompanied muscovite alteration in the rhyolitic and dacitic volcanic rocks.

Figure 4.16 plots $(2Ca+Na+K-2CO_2)/Al$ *versus* K/Ti. On this diagram, increasing hydrolysis involves the addition of K during muscovite alteration in dacitic volcanic rocks, because they had little or no potassium to start with. Rhyolitic samples do not exhibit any loss or gain in potassium because it was possibly contributed by the breakdown of contained potassium feldspar during hydrolysis. Potassium was lost during chlorite alteration of epiclastic rocks.

The addition of K during muscovite alteration in the dacitic volcanic rocks, and the loss of K during chloritization in the epiclastic rocks are consistent with the proposed chemical reactions (above) for each of these alteration styles.

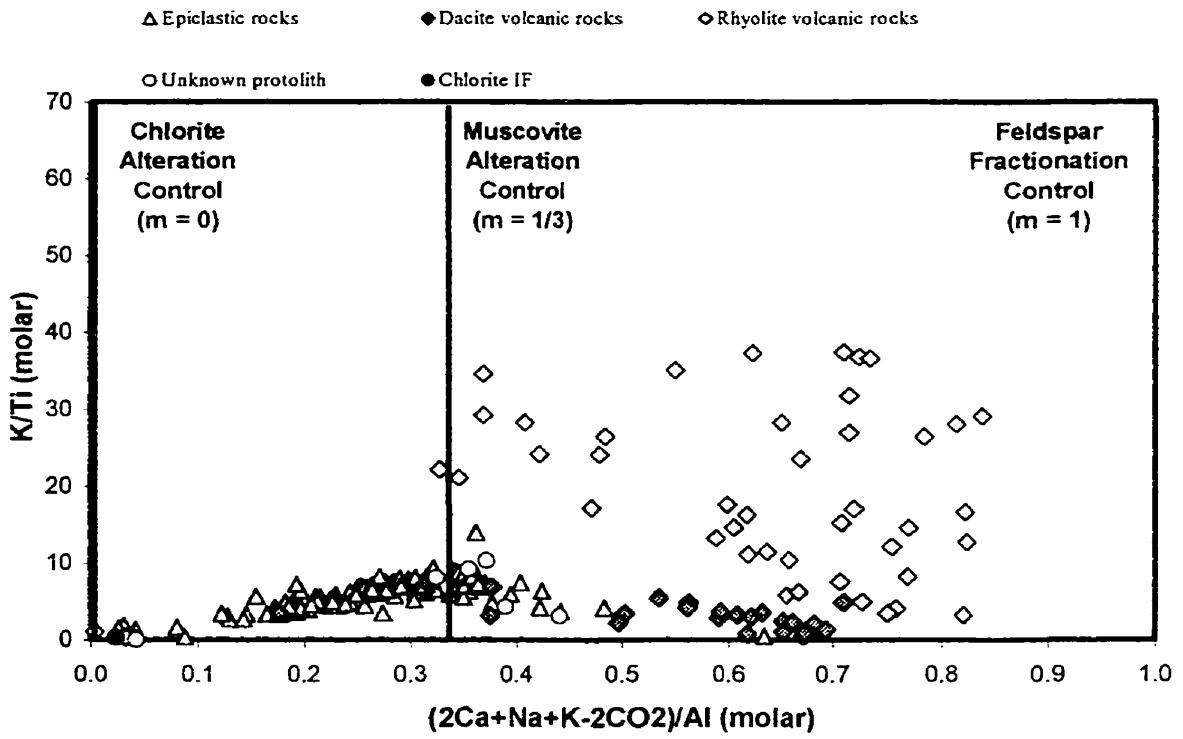

Figure 4.16 - Molar ratio diagram plotting $(2Ca+Na+K-2CO_2)/Al$ *versus* K/Ti for samples from the HMLSDZ. Addition of potassium occurred in dacitic volcanic rocks during muscovite alteration but was lost in the epiclastic rocks and a few rhyolitic rocks during chlorite alteration. The bulk of the rhyolitic rocks are partially to completely muscovite-altered and do not indicate any significant addition or loss of K because they initially contained potassium feldspar provided K for the hydrolysis reaction.

Figure 4.17 plots (2Ca+Na+K-2CO_2)/Al (molar) *versus* Ca/Ti (molar). On this diagram, increasing hydrolysis does not involve significant addition or removal of calcium. This observation can be explained using the reaction below, which is balanced on Al:

$$\underset{\text{(Anorthite)}}{3\ CaAl_2Si_2O_8} + 3\ CO_2 + 2\ KAlSi_3O_8 + 3\ H_2O \qquad \text{(i)}$$

$$\Rightarrow$$

$$2\ KAlSi_3O_{10}(OH)_2 + 3\ CaCO_3 + 2\ SiO_2$$
$$\text{(Muscovite)} \qquad\qquad \text{(Quartz)}$$

In this case, any Ca liberated by the breakdown of anorthite is reprecipitated as calcite, and not lost from the rocks. The low amount of Ca in these rocks reflects the absence of Ca-rich plagioclase. Comparing Figures 4.17 and 4.15, reveals that there is far more Na in the fresh rhyolitic and dacitic volcanic rocks, suggesting that the composition of the plagioclase in these rocks was largely albitic.

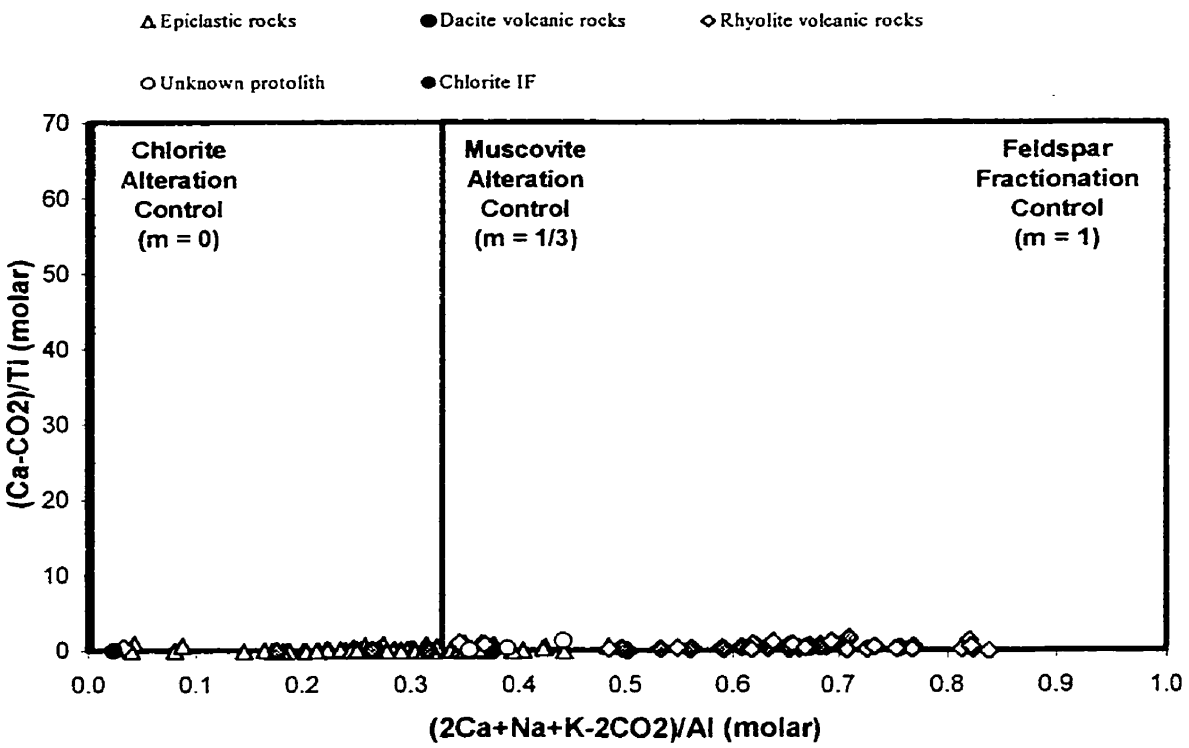

Figure 4.17 - Molar ratio diagram plotting $(2Ca+Na+K-2CO_2)/Al$ *versus* Ca/Ti for samples from the HMLSDZ. No significant Ca addition or loss occurred during muscovite or chlorite alteration.

Figure 4.18 plots (2Ca+Na+K-2CO_2)/Al (molar) *versus* CO_2/Ti (molar). On this diagram, increasing hydrolysis involved minor addition of CO_2 in rhyolitic and probably dacitic volcanic rocks. This observation is consistent with the reaction (iv) involving he breakdown of plagioclase to form muscovite and calcite.

Figure 4.19 plots (2Ca+Na+K-2CO_2)/Al (molar) *versus* S/Ti (molar). The S/Ti ratio is an appropriate measure of the amount of sulphide minerals (largely pyrite) present. Addition of sulphur is evident in epiclastic rocks and occurred only in completely muscovite-altered samples and samples altering to chlorite.

Figure 4.20 plots (2Ca+Na+K-2CO_2)/Al (molar) *versus* OH/Ti. It demonstrates that epiclastic rocks underwent water addition as muscovite-altered to chlorite, and that water addition also accompanied alteration of feldspar to muscovite in the rhyolitic and dacitic volcanic rocks. The OH additions are consistent with hydrolysis reactions involving the breakdown of feldspar to form muscovite and of muscovite to form chlorite.

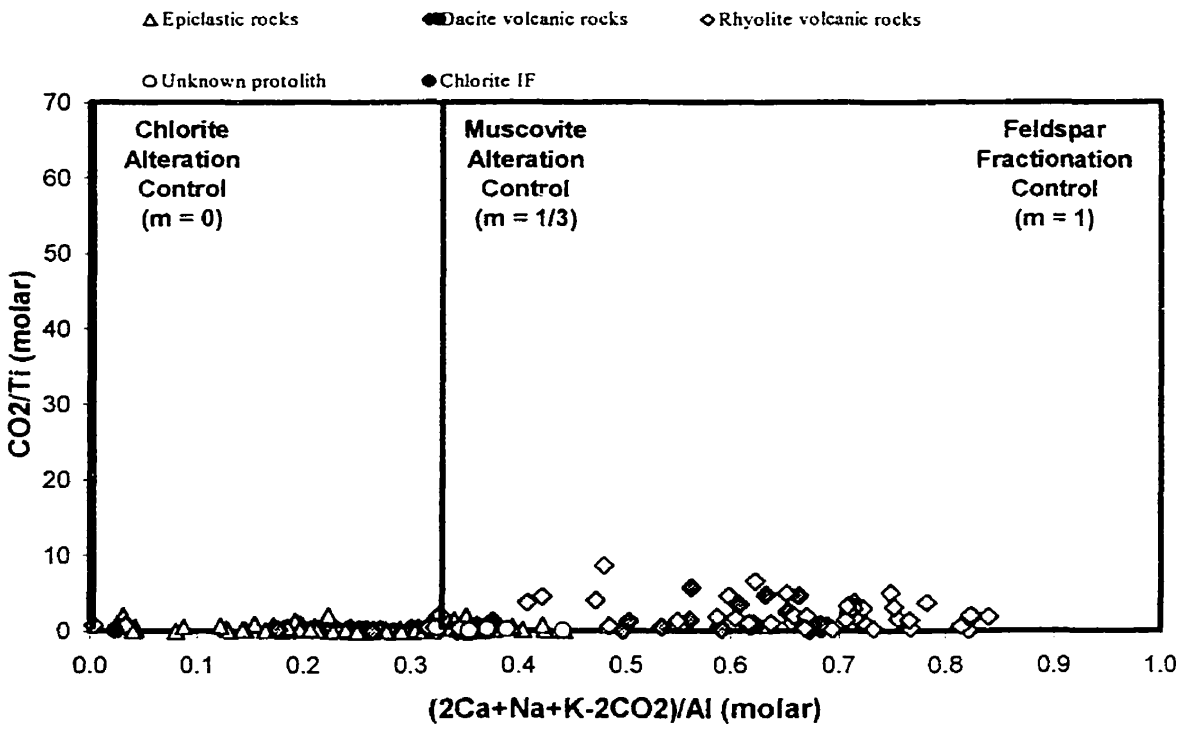

Figure 4.18 - Molar ratio diagram plotting $(2Ca+Na+K-2CO_2)/Al$ *versus* CO_2/Ti for samples from the HMLSDZ. Refer to Figure 4.11 for the characteristic features of this diagram. Slight CO_2 addition occurred during muscovite alteration of rhyolitic and dacitic volcanic rocks.

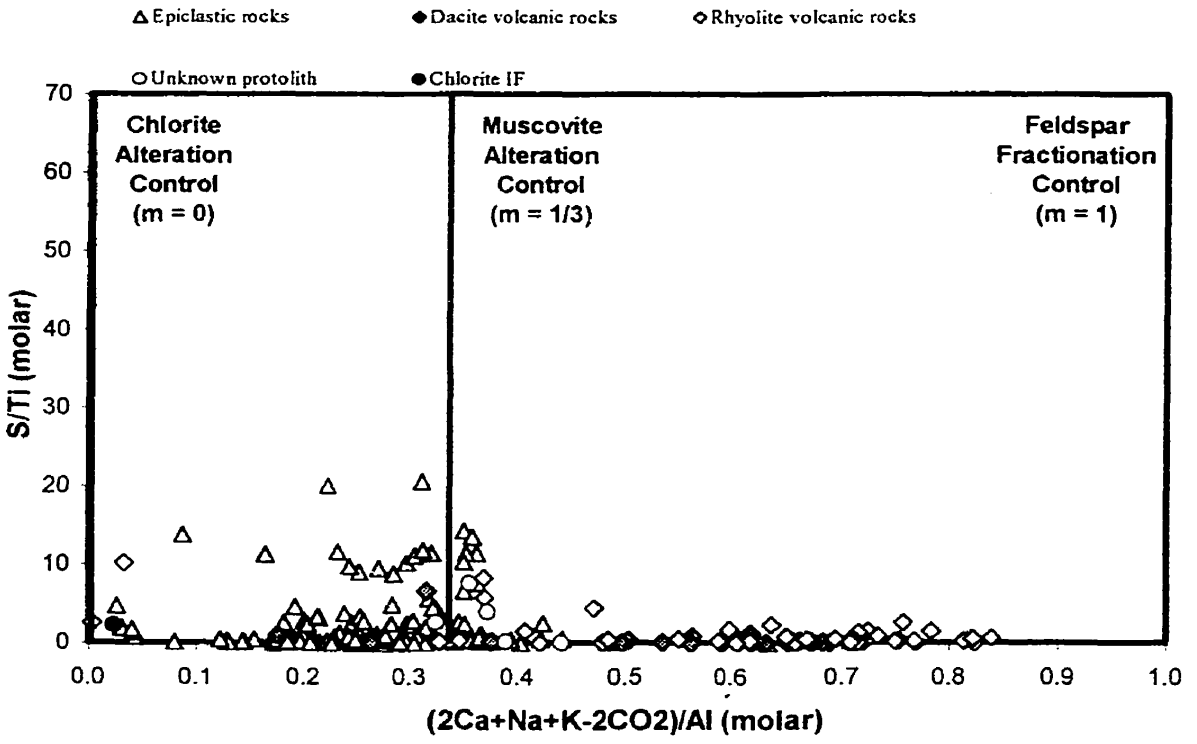

Figure 4.19 - Molar ratio diagram plotting $(2Ca+Na+K-2CO_2)/Al$ *versus* S/Ti for samples from the HMLSDZ. Significant sulphur addition is evident in epiclastic rocks and occurs only in volcanic rocks that were completely muscovite-altered.

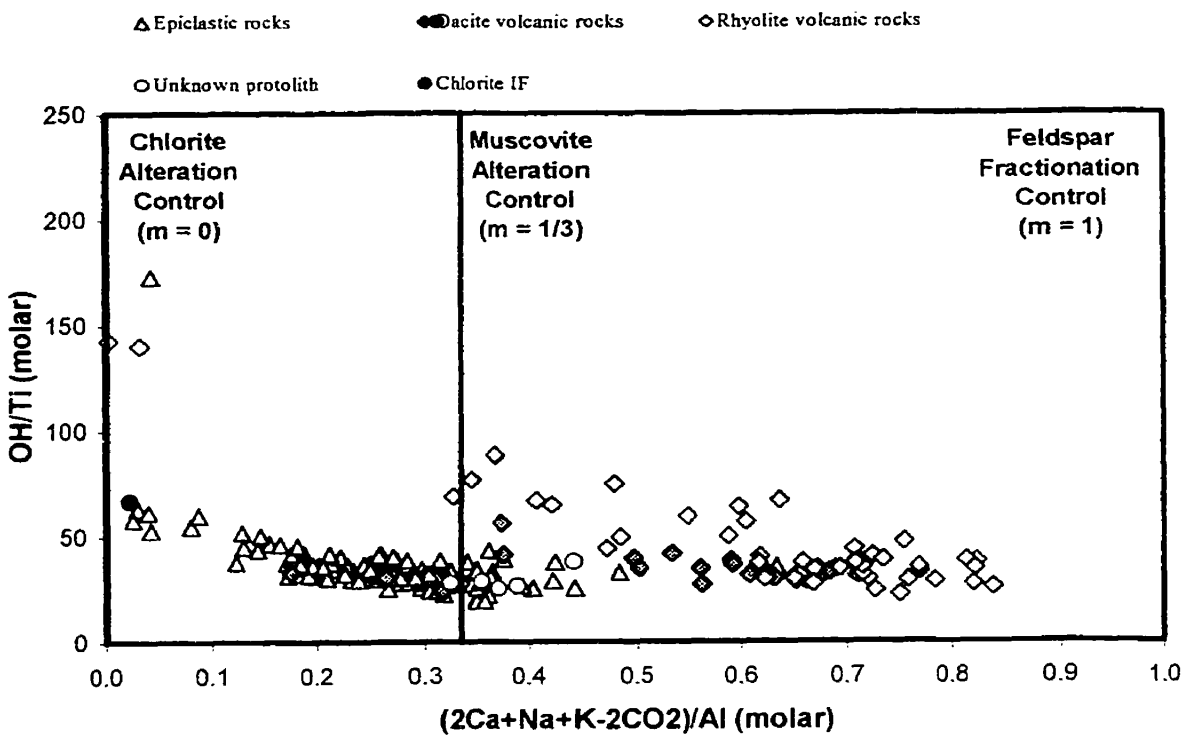

Figure 4.20 - Molar ratio diagram plotting $(2Ca+Na+K-2CO_2)/Al$ *versus* OH/Ti for samples from the HMLSDZ. Addition of structural water accompanied both muscovite and chlorite alteration and occurred in all rock types.

Finally, the hydrolysis metric ($2Ca+Na+K-2CO_2$)/Al) was plotted against the concentrations (ppm) of the three economic base metals found in the HMLSDZ (Cu, Pb, and Zn). The trends on these plots (Figures 4.21 through 4.23) indicate that addition of these elements, especially Pb and Zn, occurred mostly in the epiclastic rocks. A significant increase in these elements is evident in muscovite-altered samples, and consistent with that of S (Figure 4.19), suggesting that Cu, Pb, and Zn in these rocks reside largely in sulphide minerals (chalcopyrite, galena and sphalerite).

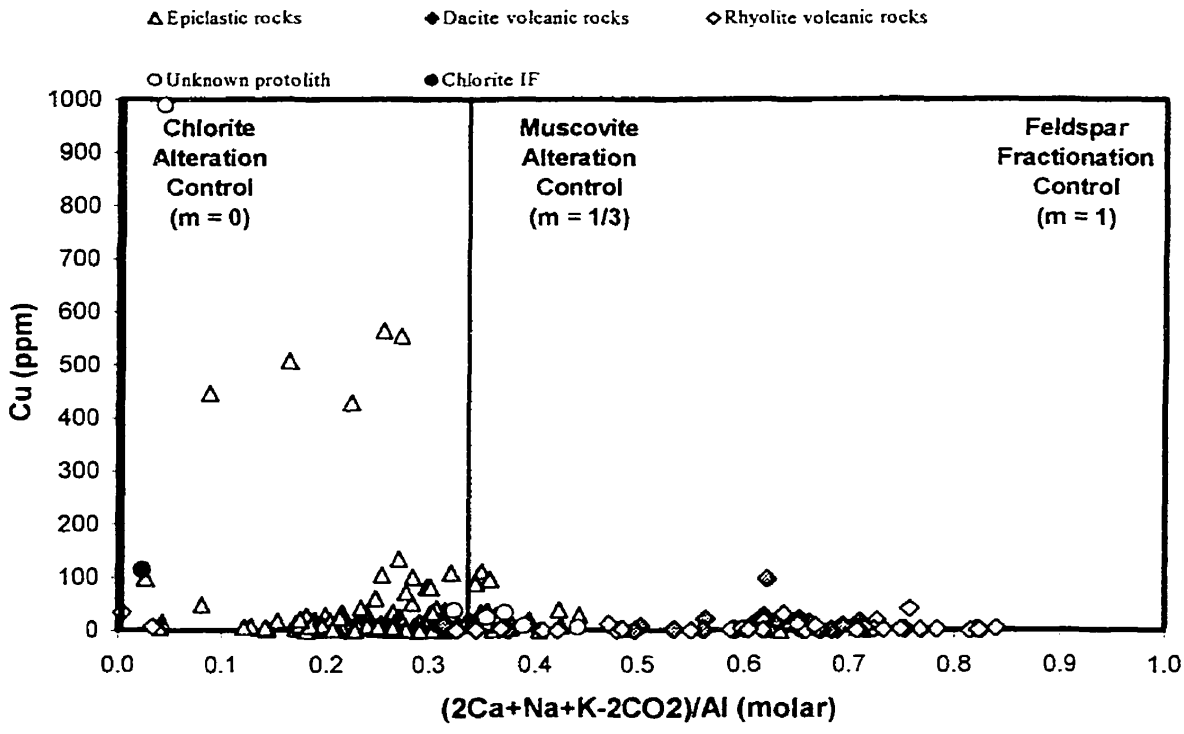

Figure 4.21 - Molar ratio diagram plotting $(2Ca+Na+K-2CO_2)/Al$ *versus* Cu for samples from the HMLSDZ. Minor Cu addition is coincident with chloritization of epiclastic rocks.

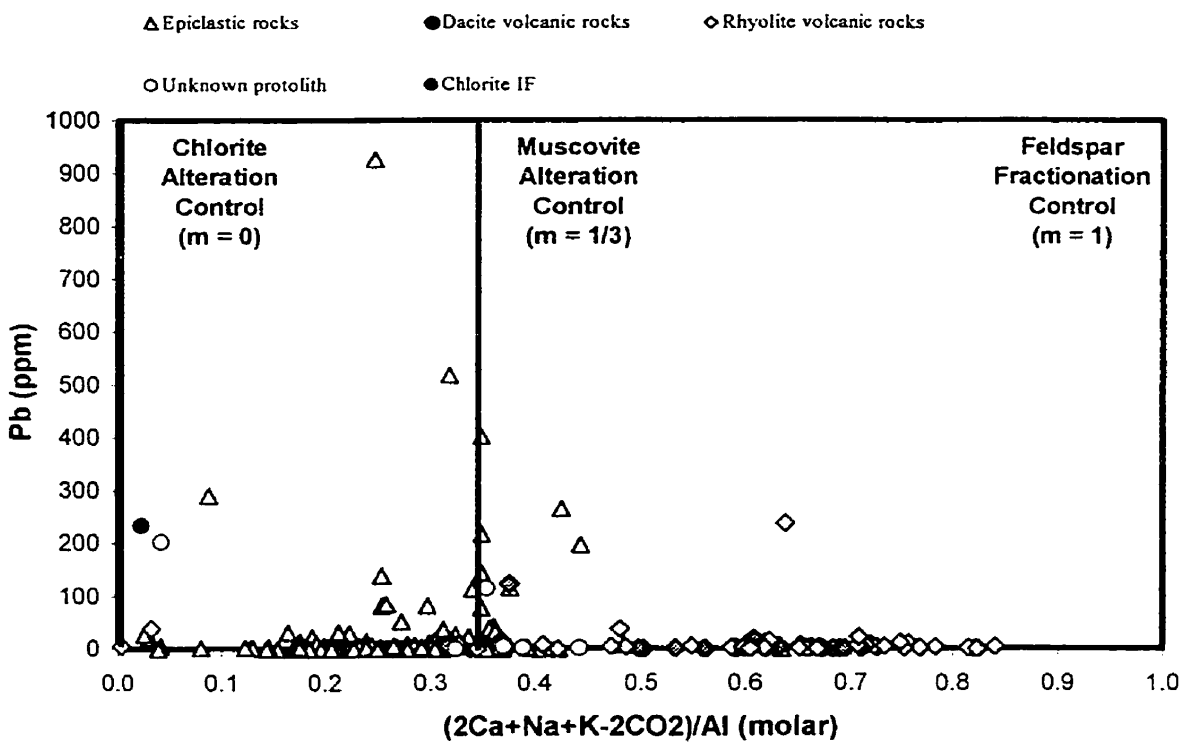

Figure 4.22 - Molar ratio diagram plotting $(2Ca+Na+K-2CO_2)/Al$ *versus* Pb for samples from the HMLSDZ. Significant Pb addition is coincident with most muscovite-altered epiclastic rocks.

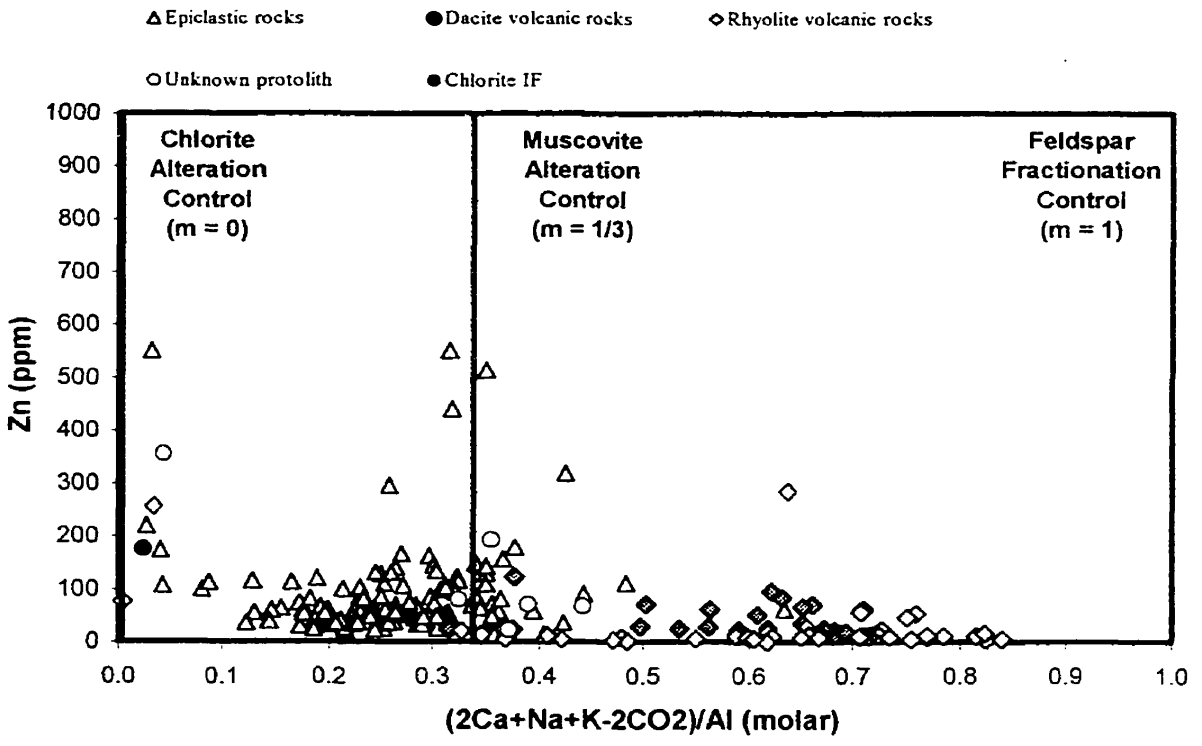

Figure 4.23 - Molar ratio diagram plotting $(2Ca+Na+K-2CO_2)/Al$ *versus* Zn for samples from the HMLSDZ. Addition of Zn is coincident with muscovite and/or chlorite alteration of epiclastic rocks.

4.4 - General Element Ratio Analysis

In addition to the MER and PER diagrams, general element ratio (GER) diagrams (Stanley and Madeisky 1996) were also used to investigate primary compositional variability in the host rocks to the HMLSDZ (Figures 4.24 and 4.25). GER diagrams are unique in the sense that their design does not require the presence of a conserved element in the dataset. Additionally, material transfer phases plot at specific nodes, which means that addition or removal of a phase will cause rock compositions to be displaced toward or away from its node.

Figure 4.24 plots molar (Na+K)/Al on the abscissa and (Fe+Mg-S/2)/Al on the ordinate. This diagram is thus a projection from pyrite. On this diagram, plagioclase plots at the origin (0, 0), muscovite plots at (1/3, 0), chlorite plots at (0, 5/2), potassium feldspar plots at (1, 0) and biotite plots at (1, 3), as indicated. The location of data points on this plot suggests biotite is not an important phase in the rocks hosting the HMLSDZ. Furthermore, the data plot crudely along two lines; one between feldspar and muscovite (muscovite-altered samples) and one between muscovite and chlorite (chlorite-altered samples). Note that the samples do not plot along a trend between feldspar and chlorite, indicating that only two separate and distinct alteration reactions (feldspar $\rightarrow$ muscovite and muscovite $\rightarrow$ chlorite) have affected these rocks. Additionally, the rock compositions observed are not consistent with ideal end-member clinochlore.

Numerous epiclastic rocks plot on a mixing line between chlorite and muscovite. This mixing line constrains the compositions of these minerals to be other than ideal. The left end of this mixing line defines a chlorite composition with an (Fe+Mg)/Al ratio of approximately 3/2, whereas the right end

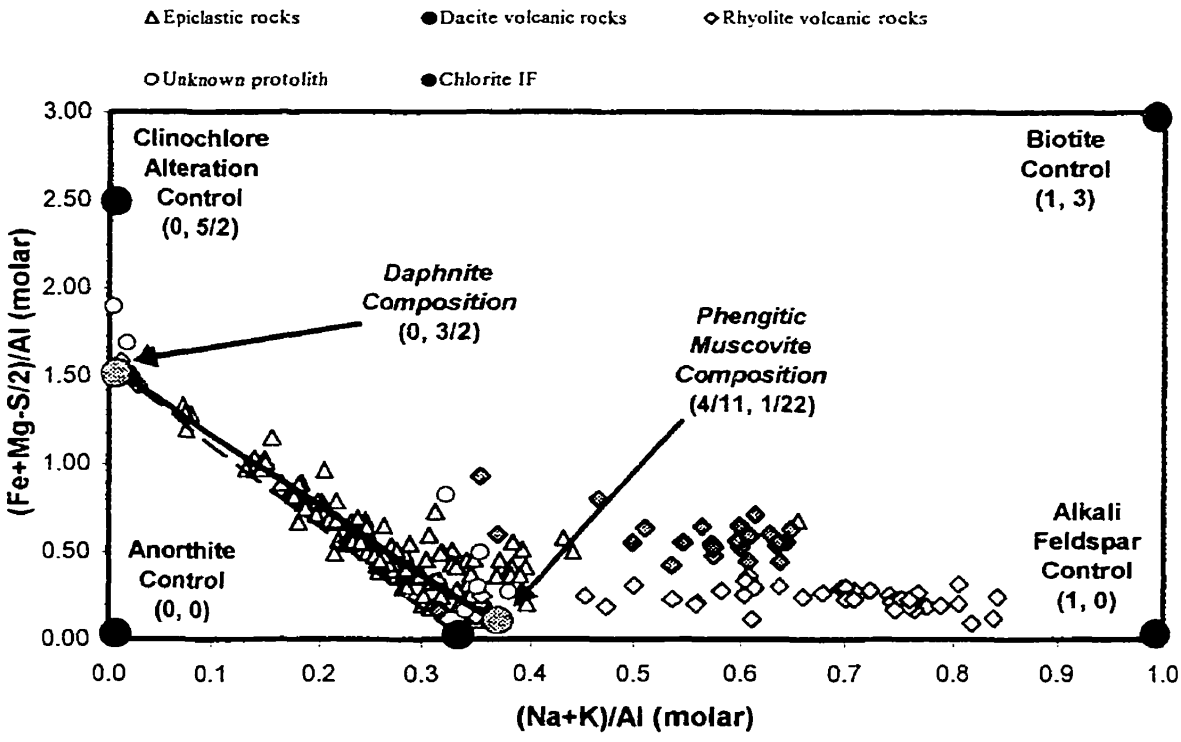

Figure 4.24 - GER diagram of (Na+K)/Al *versus* (Fe+Mg-S/2)/Al for samples from the HMLSDZ. The S/2 subtraction on the ordinate makes this diagram a projection from pyrite (FeS_2). The trend defined by epiclastic rocks coincides with (Na+K)/Al (on the right) and (Fe+Mg-S/2)/Al (on the left) ratios of 4/11 and 3/2, respectively, corresponding to phengite and daphnite compositions, respectively. Also, compared to the rhyolitic rocks, dacitic volcanic rocks have a higher initial iron budget.

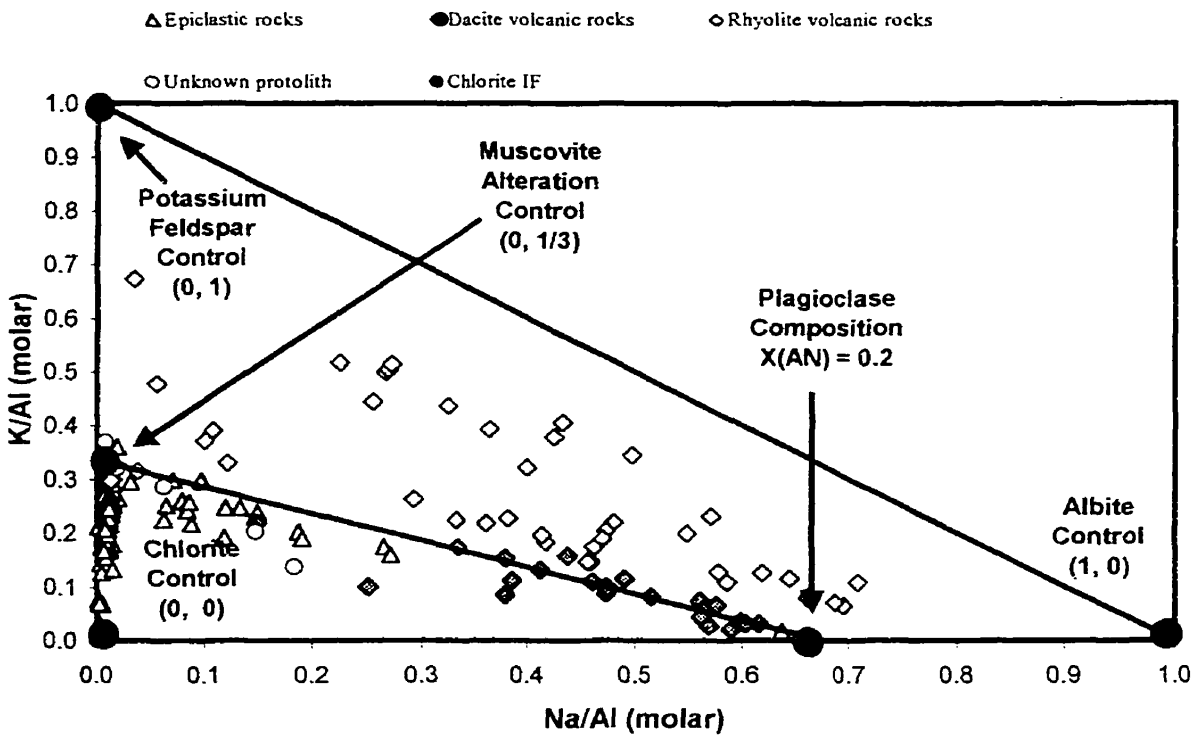

Figure 4.25 - GER diagram of *Na/Al* (molar) *versus K/Al* (molar) for samples from the HMLSDZ. The Na/Al ratio of 2/3 in fresh dacitic volcanic rocks corresponds to a plagioclase composition of An_{20}. This diagram also verifies the importance of albitic plagioclase (oligoclase) and potassium feldspar in the rhyolitic samples and illustrates the muscovite and chlorite alteration in the epiclastic rocks.

defines a muscovite composition with a K/Al ratio of 4/11 and an (Fe+Mg)/Al ratio of 1/22. Thus, because the primary solid solutions in chlorite are $FeMg_{-1}$ (ferromagnesian exchange) and $MgSiAl_{-2}$ (tschermak exchange), the chlorite composition is a daphnite with a formula of approximately $(Fe,Mg)_9Al_6Si_5O_{20}(OH)_{16}$. Similarly, because the major solid solution in muscovite is also tschermak exchange, the composition of the muscovite is phengitic muscovite, with a formula of approximately $K_2(Fe,Mg)_{1/4}Al_{11/2}Si_{25/2}O_{20}(OH)_4$. These compositions are consistent with the electron microprobe compositions measured and described in Chapter 3.

The plagioclase composition in the feldspar phyric rocks at the HMLSDZ was deduced using the GER diagram on Figure 4.25. On this diagram (*Na/Al* versus *K/Al*), chlorite plots at the origin (0, 0), muscovite plots at (1/3, 0), potassium feldspar plots at (1, 0) and albite plots at (0, 1). The trend exhibited by the rhyolitic and dacitic volcanic rocks suggest that the former contains a mixture of albite and potassium feldspar (as observed in the electron microprobe samples), whereas the dacitic volcanic rocks contain only plagioclase with a (Na+K)/Al ratio of 2/3 (oligoclase). Thus, dacitic volcanic rocks initially contained plagioclase with a composition of $Na_{4/5}Ca_{1/5}Al_{6/5}Si_{14/5}O_8$ (An_{20}) prior to muscovite alteration.

4.5 - Spatial Geochemical Trends

A two-dimensional model of the geochemical signatures observed on PER, MER and GER plots was developed to understand the spatial variation of secondary material transfer indices within the structural footwall and hangingwall to the HMLSDZ. The model consists of a north-south longitudinal section that was constructed by rotating and tilting the plane containing the drill holes 60° (60°/70° by right hand rule) counter-clockwise and 20° westwards, respectively, to produce a new set of grid coordinates. The *x*-, *y*- and *z*-axes of this new grid are the northing, elevation, and the various lithogeochemical parameters specific to different styles of hydrothermal alteration on each of the subsequent plots.

Figure 4.26 is a 60°/70° longitudinal section that illustrates the extent of hydrolytic alteration each sample has been subjected to and the relative intensity of this alteration parameter relative to its location in the structural hangingwall (above) and footwall (below) to the deposit. The diagram indicates that volcanic rocks proximal and distal to the deposit are less intensely altered compared with the epiclastic rocks in the section. The presence of dykes in the structural hangingwall (stratigraphic footwall) that display little hydrolytic alteration suggests that they post-date hydrothermal alteration and mineralization.

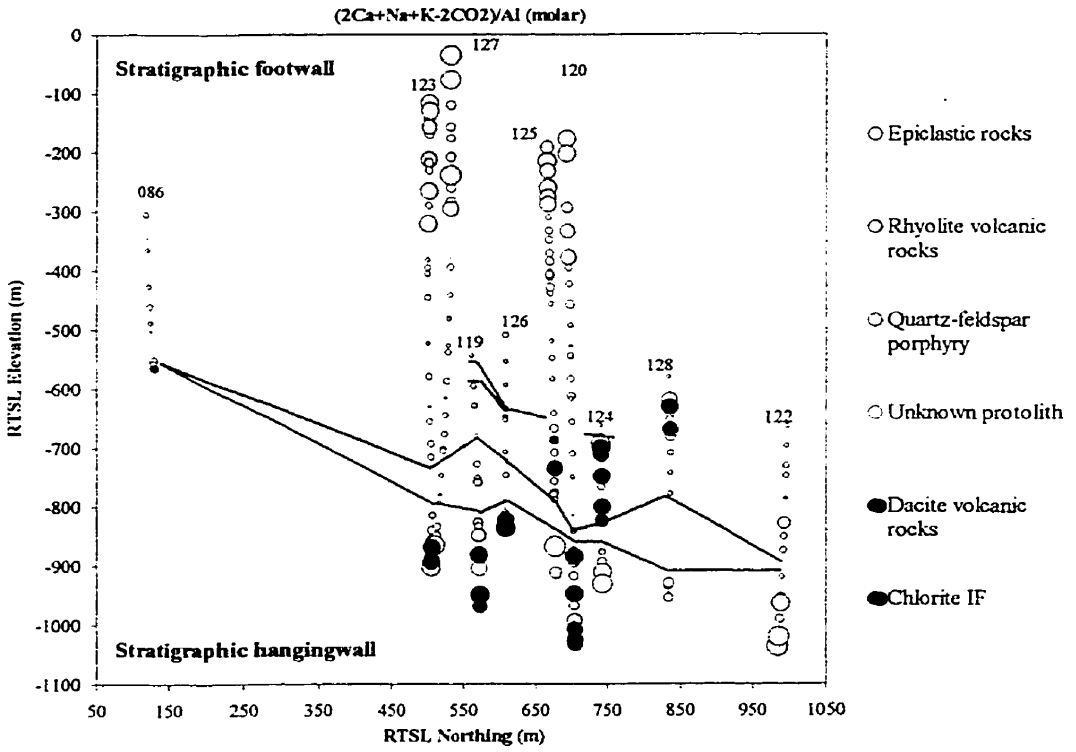

Figure 4.26 – A longitudinal section (see text for explanation) that plots the northing, elevation, and alteration index, $2Ca+Na+K-2CO_2)/Al$, of each sample from the HMLSDZ. This geochemical parameter is a measure of the extent of hydrolytic alteration each sample has been subjected. The red lines show an outline of the mineralized zone. The smaller bubble sizes represent samples that are significantly altered, whereas the larger bubbles represent least altered samples. Alteration is most intense in the structural hangingwall (stratigraphic footwall) immediately above the deposit.

Figure 4.27 plots Na/Al, and illustrates the amount of albite present in each sample. It is thus a measure of how fresh or altered (muscovite or chlorite) altered each sample is. The epiclastic rocks have very low Na/Al ratio probably reflecting samples that have lost significant amounts of Na, either through hydrolysis or because they did not initially contain significant amounts of Na-bearing minerals. The volcanic rocks on the other hand, have relatively high Na/Al ratios. This observation is consistent with thin section petrographic studies where albite phenocrysts were identified to be predominant in feldspar porphyritic volcanic rocks.

Figure 4.28 plots K/(Al-Na) and illustrates the extent of potassium feldspar hydrolysis in the rocks hosting the HMLSDZ. The diagram indicates that all rock types immediately above the deposit (in the structural hanging wall) have either lost significant amounts of potassium or did not initially contain significant amounts. Overall, the quartz-feldspar porphyritic intrusive rocks and rhyolitic volcanic rocks have relatively higher amounts of K even in the structural footwall, a feature that is consistent with the potassium feldspar they have been observed to contain.

Figure 4.29 plots (Fe+Mg-S/2)/Al and illustrates the extent of chlorite alteration in the samples representing the rocks hosting the HMLSDZ. The diagram indicates that most epiclastic rocks and a few volcanic rocks contain significant amounts of chlorite. The horizontal trend of highly chloritized epiclastic rocks immediately above the main massive sulphide zone coincides with a subordinate mineralized zone in the structural hangingwall to the HMLSDZ.

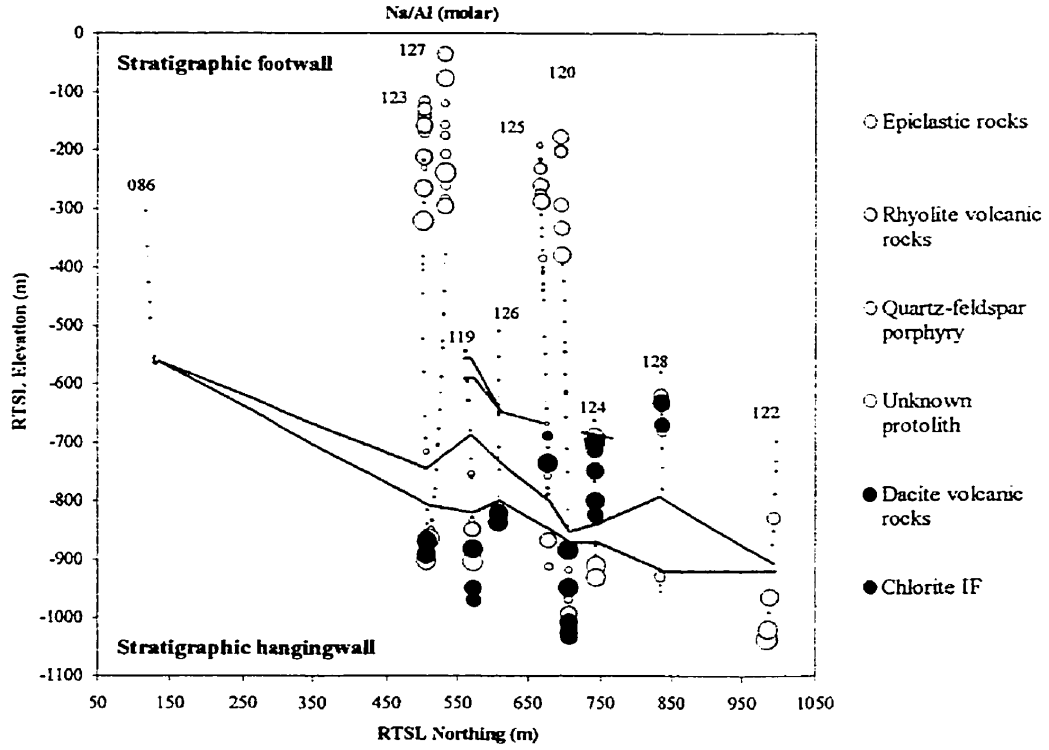

Figure 4.27 – A longitudinal section (see Figure 4.26) that plots Na/Al molar ratio of each sample from the drill holes through the HMLSDZ. This diagram demonstrates that the epiclastic rocks do not contain significant albite or other Na-bearing minerals, or because the Na was completely lost during muscovite alteration.

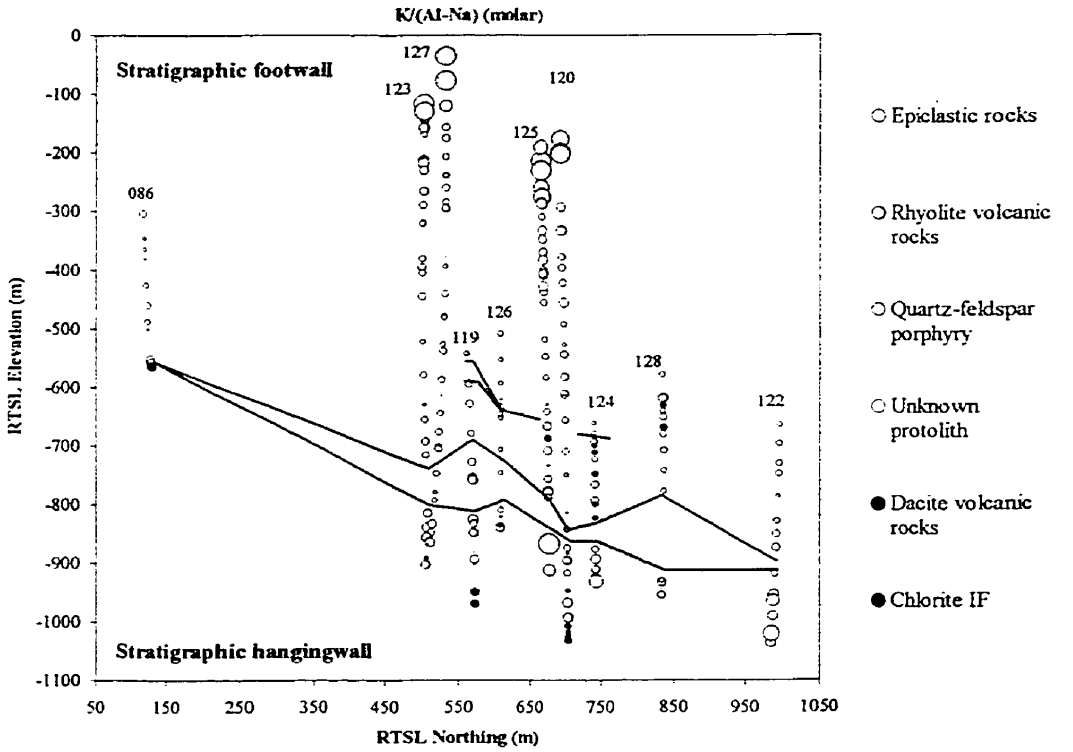

Figure 4.28 – A longitudinal section (see Figure 4.26) that plots the K/(Al-Na) molar ratio of each sample from the HMLSDZ. This geochemical parameter is specific to the extent of muscovite alteration in each sample, and also a projection from albite. The bubble sizes indicate the degree of muscovite alteration in these samples. The smaller bubble sizes represent samples that are significantly muscovite-altered (low *K/Al*) and the larger bubbles are partially muscovite-altered or almost fresh. Consistently, the epiclastic rocks in the immediate footwall and hangingwall to the deposit exhibit the most intense alteration.

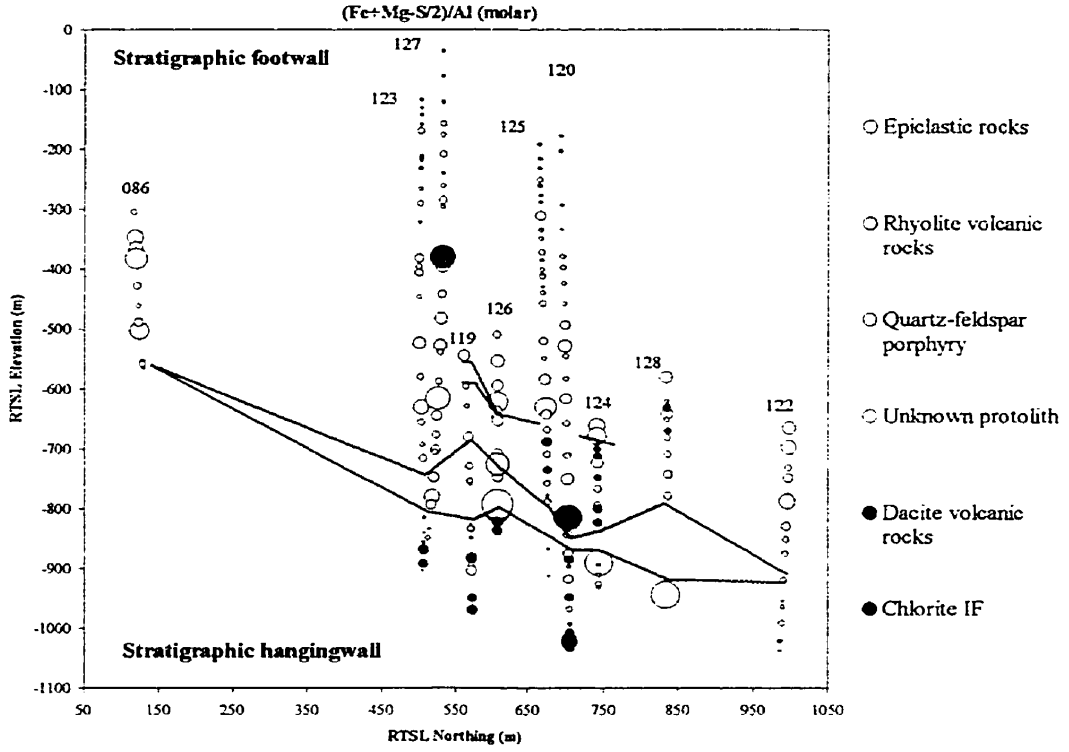

Figure 4.29 – A longitudinal section (see Figure 4.26) that plots *(Fe+Mg-S/2)/Al* molar ratio of each sample from the HMLSDZ. This geochemical parameter is a measure of the extent of chlorite alteration in each sample. The section describes the intensity of chlorite alteration in these samples. The smaller bubble sizes represent samples that are less chloritized and the larger bubbles represent most intensely chloritized samples.

Figure 4.30 plots S/Ti and illustrates the amount of sulphur (sulphide minerals) present in each sample. Rocks immediately adjacent to mineralization have high amounts of sulphide. The horizontal sulphide-rich zone above the main mineralized envelope on this plot is at the same stratigraphic horizon as the high chlorite-rich zone in the epiclastic rocks on Figure 4.29. This probably indicates that sulphide minerals and chlorite alteration accompanied the minor mineralization at this stratigraphic level.

Figure 4.31 plots (Fe-S/2)/Mg and describes the variation of Fe/Mg ratio of chlorite sample in the structural hangingwall and footwall to the HMLSDZ. The diagram indicates that within the zone immediately above the mineralized envelope (structural hangingwall), epiclastic rocks contain predominantly Fe-rich chlorite. In contrast, higher up in the structural hangingwall and immediately below the deposit, all rock types (predominantly volcanic rocks) exhibit relatively low Fe/Mg ratios.

Figure 4.32 presents CO_2/Ti and compares the amount of carbonate minerals present in each rock type in the structural footwall and hangingwall to the HMLSDZ. The diagram indicates that intrusive and pyroclastic volcanic rocks are higher in carbonate minerals compared with epiclastic rocks. This observation is consistent with the Figure 4.5, which indicated that the significant carbonate alteration did not occur in the epiclastic rocks.

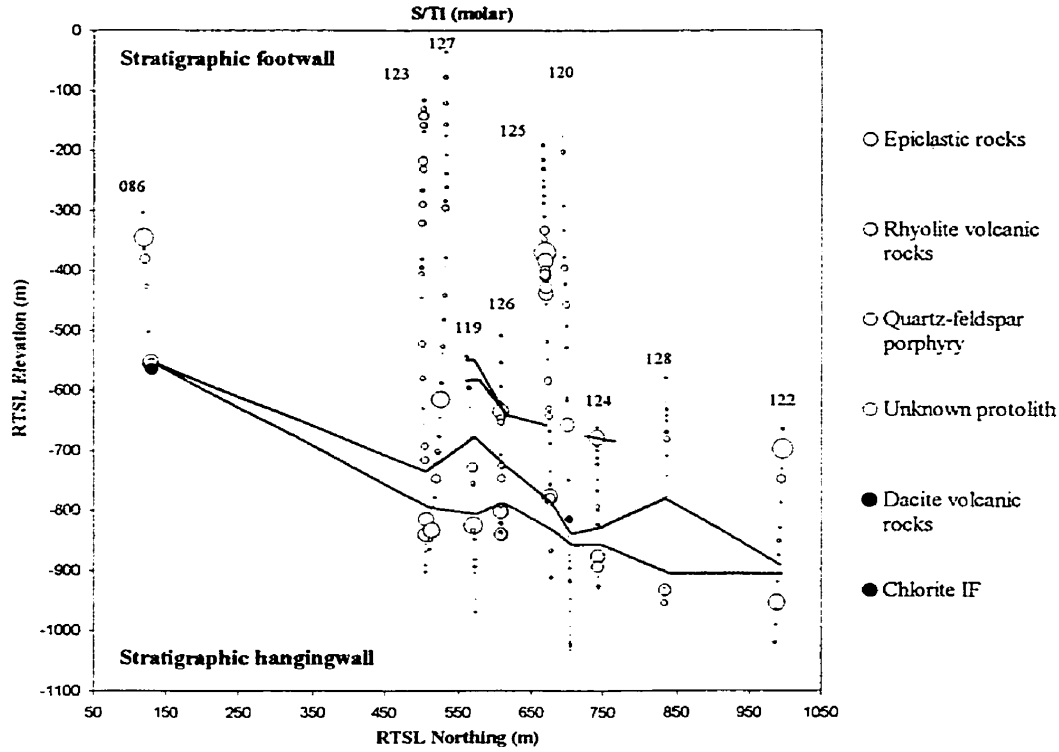

Figure 4.30 – A longitudinal section (see Figure 4.26) that plots the S/Ti (molar) of each sample from the HMLSDZ. The smaller bubble sizes represent samples with low concentration; the larger bubbles represent samples with higher concentration of sulphur. This diagram indicates that there are two sulphide-rich zones above and just below the main mineralized envelope.

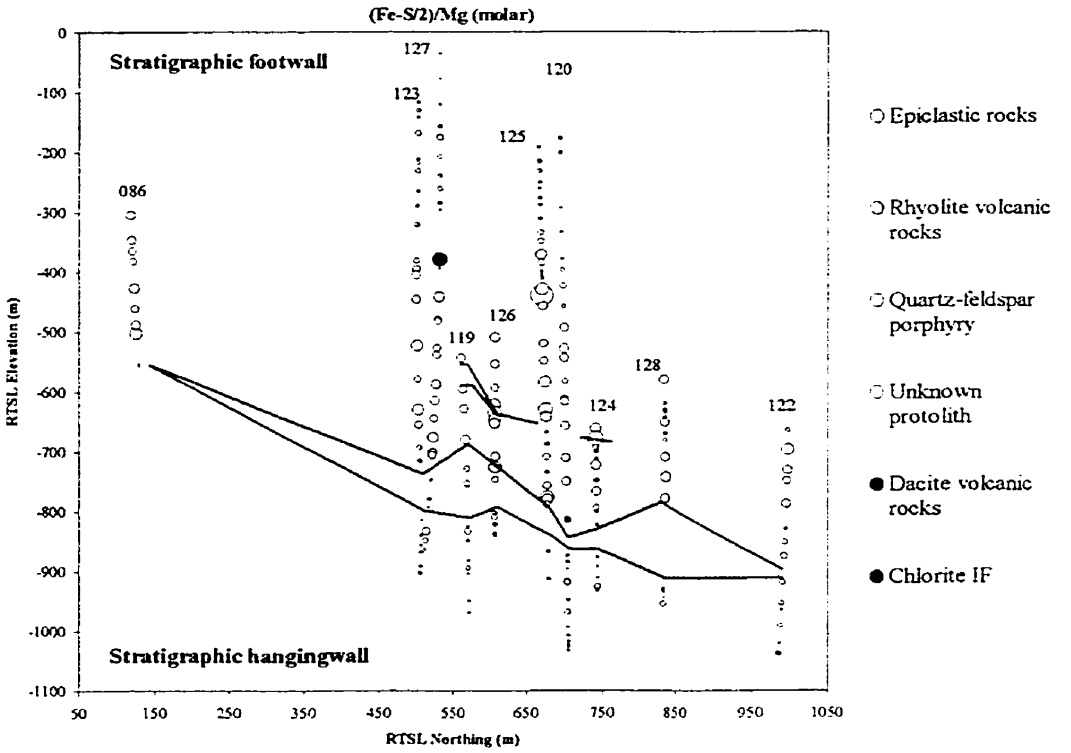

Figure 4.31 — A longitudinal section (see Figure 4.26) that plots the (Fe-S/2)/Mg ratio of each sample from the HMLSDZ. This geochemical parameter is a measure of the Fe/Mg ratio (corrected for the presence of pyrite) in each sample. The bubble sizes describe the relative abundance of Fe-rich and Mg-rich silicate minerals in these rocks. The bigger the bubble sizes, the higher the Fe/Mg ratio. This diagram indicates that the epiclastic rocks contain significantly higher Fe/Mg ratios (probably reflecting Fe-rich chlorite).

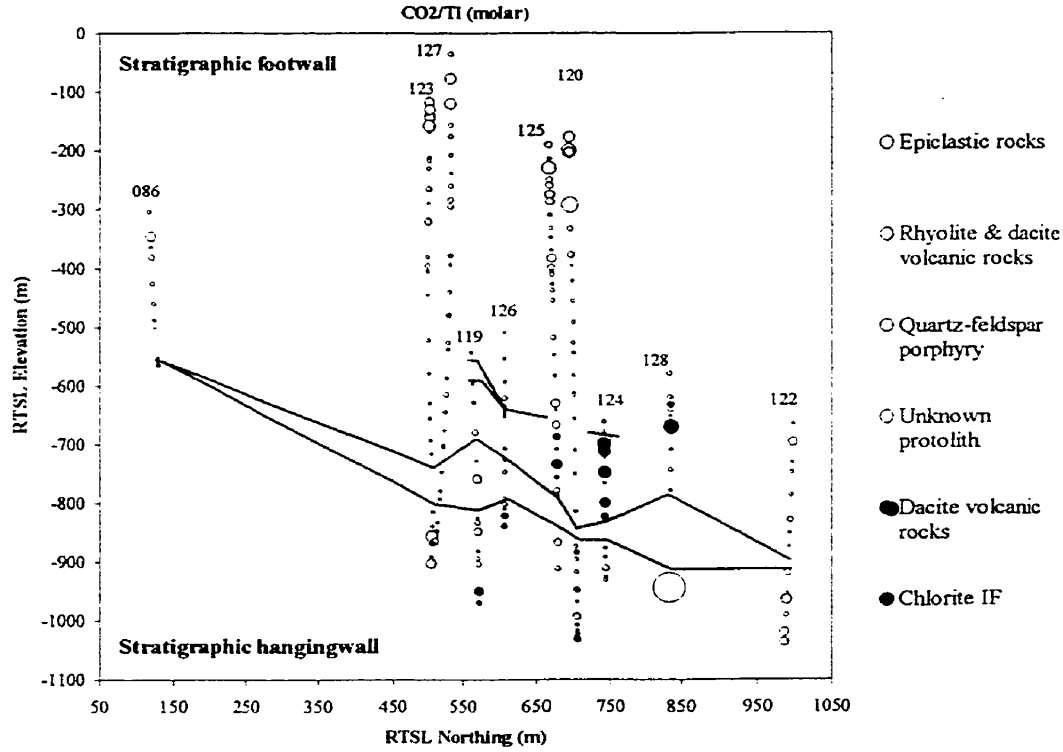

Figure 4.32 – A longitudinal section (see Figure 4.26) that plots the CO_2/Ti ratio of each sample from the HMLSDZ. The bubble sizes indicate the degree of carbonate alteration in these samples. The smaller bubble sizes represent samples with minor carbonate and the larger bubbles indicate samples with significantly higher carbonate concentrations. This diagram indicates that the volcanic rocks have higher concentrations of carbonate minerals, compared with their epiclastic counterparts.

Figure 4.33 plots CO_2/Ca and identifies samples with siderite. The data indicates that with the exception of a few, majority of the samples containing siderite (quartz-feldspar porphyry and epiclastic rocks) occur just above the stratigraphic horizon where mineralization was formed.

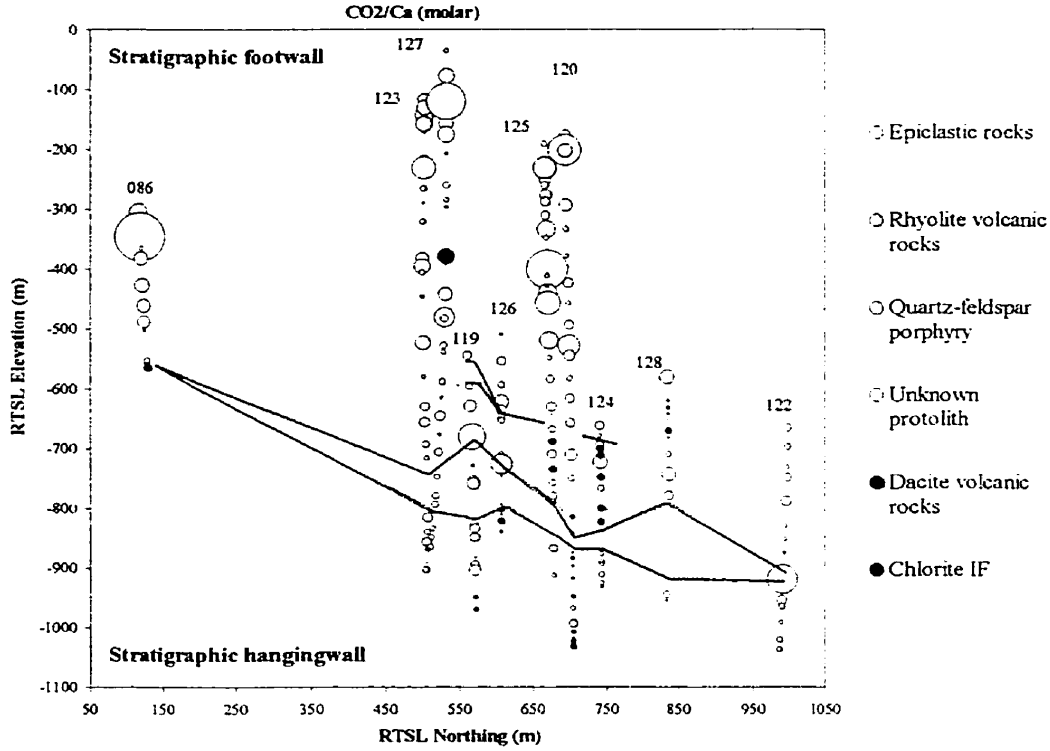

Figure 4.33 – A longitudinal section that plots the CO_2/Ca (molar) of each sample from the HMLSDZ. The smaller bubble sizes represent samples with calcite and/or dolomite/ankerite and the larger bubbles represent samples with siderite. It appears that the epiclastic rocks and volcanic rocks (predominantly quartz-feldspar porphyritic rocks) contain significant siderite but these are distal to the deposit.

5 – DISCUSSION & CONCLUSIONS

The rocks hosting the HMLSDZ can be divided into four volcanic compositions based on their trace element compositions: rhyodacite, dacite, andesite and basalt (Figure 4.1, 4.2). These compositional descriptions are consistent with data trends on a Winchester and Floyd (1977) diagram in Figure 5.1. Intrusive rocks (quartz-feldspar porphyry) are rhyolitic in composition whereas aphyric to phyric pyroclastic rocks span the rhyodacite to dacite fields (Figure 4.1 and 5.1). Andesite and basalts in the study area do not exhibit features characteristic of the Moody Brook member in the Flat Landing Brook Formation, although this assertion is limited due to the restricted scope of this study. These more mafic rocks appear to be dykes cutting the sequence and thus may be feeders to the Moody Brook member (Figure 5.2).

An attempt was made to investigate the different populations that appear to exist in the rhyolitic samples (Figure 4.6). These populations are separated by Al/Ti (molar) thresholds of 40, 60 and 80 (R1 < R2 < R3 < R4: Figure 5.3). R1 has the lowest Al/Ti ratio and is spatially restricted to the structural hangingwall of the HMLSDZ. R2, R3, and R4 occur in the structural hangingwall and immediate footwall. Geochemistry and petrology of these samples do not reveal differences among these rhyolitic populations.

Intrusive rocks (quartz-feldspar porphyry) in the structural hangingwall and footwall to the mineralized zone are geochemically and visually similar. Fabric development is stronger in the latter but this may be a consequence of the smaller thicknesses of this lithology in the structural footwall. As a result, rocks of Flat Landing Brook affinity do not appear to be present in the drill core examined.

The geochemical characteristics of the epiclastic rocks indicate that they are similar to the volcanic rocks that are interbedded with them. However, the epiclastic rocks display no evidence of feldspar sorting, and thus appear distinctly different from the volcanic rocks.

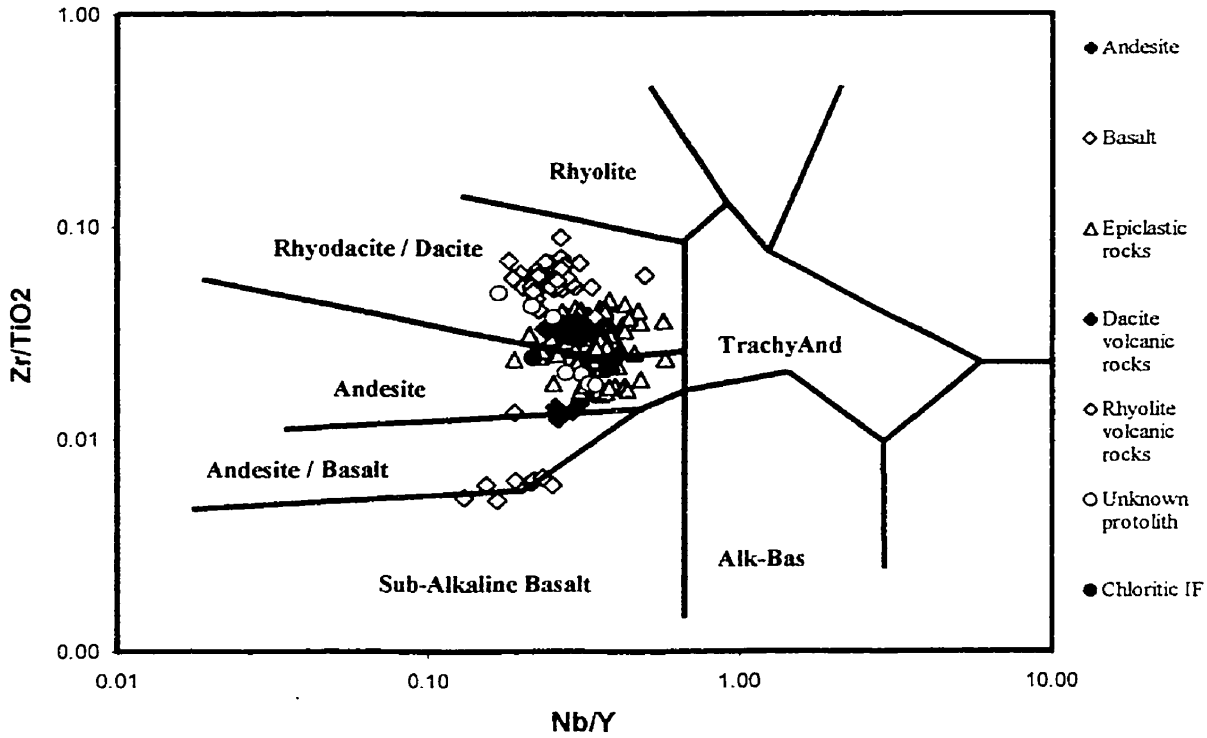

Figure 5.1 – Winchester and Floyd (1977) trace element discrimination diagram. Felsic volcanic rocks plot in the rhyodacite to dacite fields, mafic rocks plot in the andesite to basalt fields, and the epiclastic rocks in the dacite to andesite fields.

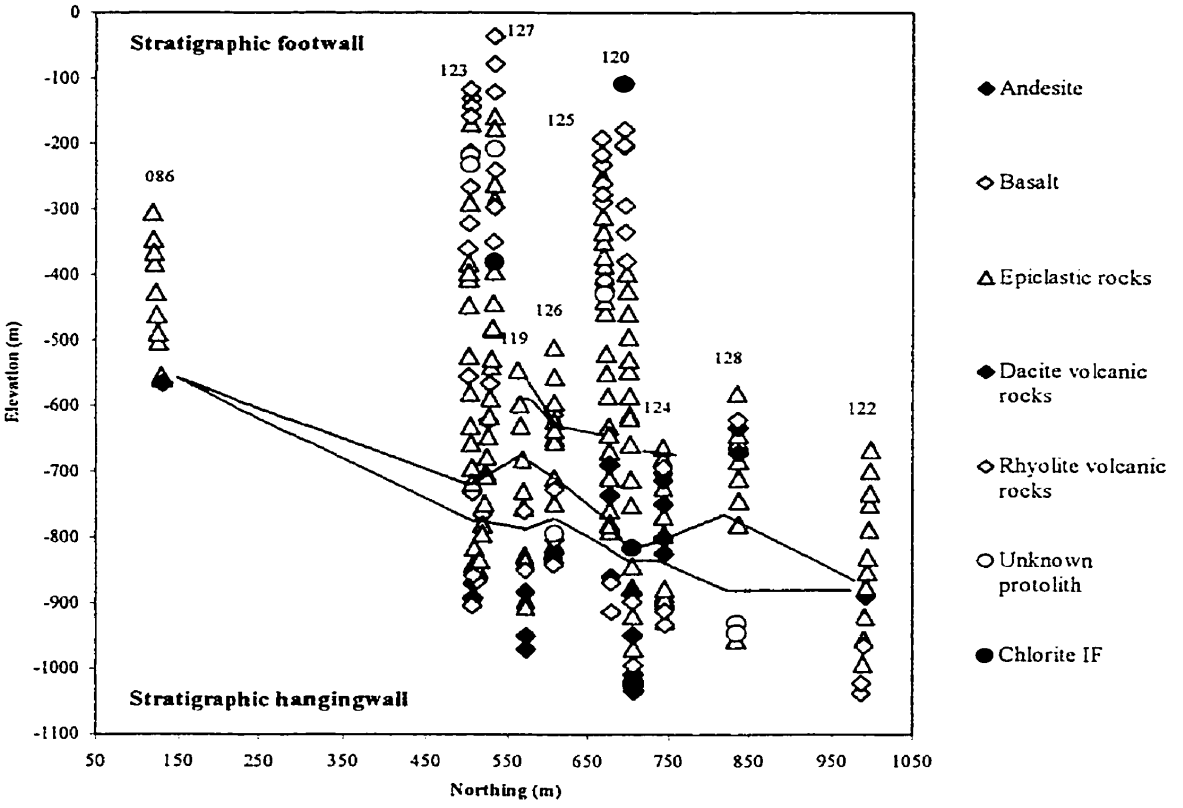

Figure 5.2 – Longitudinal section (similar to Figure 4.26) illustrating the spatial location of each sample collected from the HLSDZ.

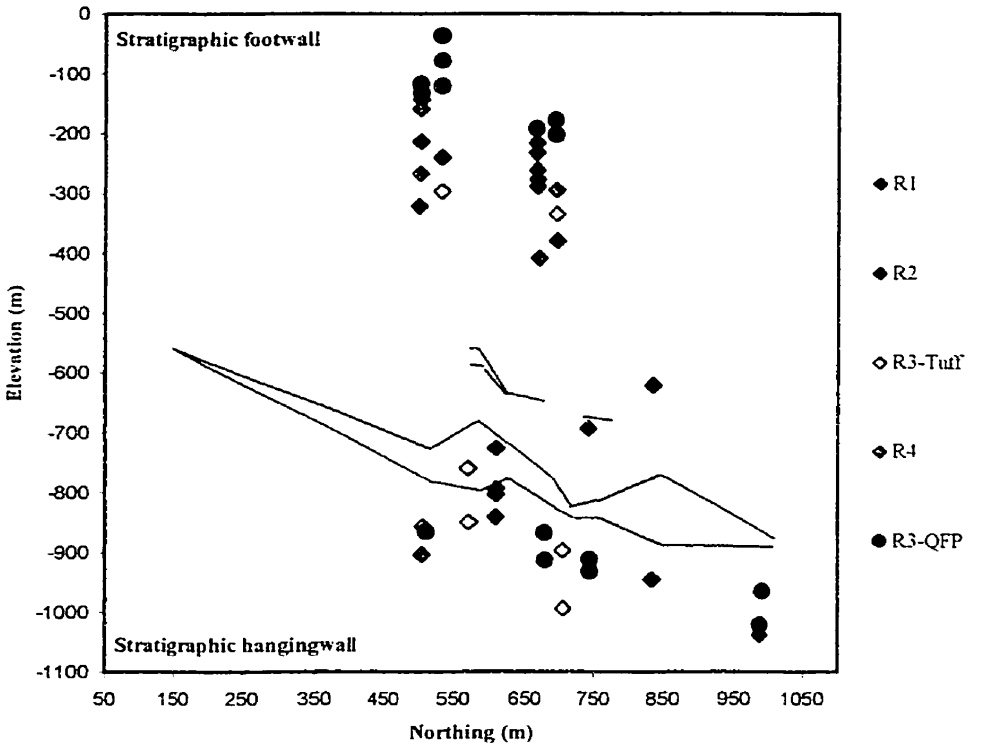

Figure 5.3 - Longitudinal section (similar to Figure 4.26) showing the spatial location of the samples from the rhyolite populations in Figure 4.6. With the exception of group R2, the rhyolites plot in both the structural hangingwall and footwall.

Pearce element ratio analysis of the rocks hosting the HMLSDZ indicates that the felsic volcanic rocks have been affected by igneous fractionation and hydrothermal metasomatism. The interaction of hydrothermal fluids that formed the HMLSDZ and its host rocks resulted in the formation of alteration minerals such as muscovite, chlorite, and calcite. Because felsic volcanic rocks do not contain significant primary ferromagnesian minerals, the formation of alteration minerals such as chlorite, requires a hydrothermal metasomatic process to introduce the requisite Fe and Mg. The hydrothermal mineral modes and compositions observed in especially epiclastic rocks at the HMLSDZ appear to be at least partially a function of their original composition before the onset of hydrothermal activity.

The rhyolite volcanic rocks (quartz-feldspar porphyries, quartz-feldspar-phyric tuff, and aphyric tuff) were primarily affected by quartz, albite, and potassium feldspar fractionation and were subsequently altered to muscovite and subordinate chlorite. The absence of evidence for Fe addition during muscovite alteration (Figure 4.13) and the presence of Fe-rich chlorite (although less abundant in these rocks) support the hypothesis that overprinting of muscovite alteration by chlorite alteration is minimal. Minor but significant carbonate alteration in the rhyolitic volcanic rocks is present and associated with muscovite alteration, although evidence of siderite alteration also exists in some samples (Figure 4.5).

The dacitic volcanic rocks are predominantly feldspar- and/or quartz-phyric tuffs that exhibit only minor feldspar fractionation. These rocks probably contained only plagioclase with a composition of An_{20}, as demonstrated by the data trend of these samples on Figure 4.25. Because these rocks did not initially contain significant

potassium feldspar, the observed addition of potassium is consistent with the proposed hydrolytic reaction responsible for the formation of muscovite during hydrothermal alteration (Figure 4.17). These dacitic volcanic rocks do not plot above the calcite control line of Figure 4.5, indicating that the carbonate composition in these samples is controlled exclusively by calcite.

The epiclastic rocks do not exhibit significant feldspar fractionation and were affected by metasomatic Si addition and/or possibly quartz sorting (Figure 4.7). These rocks are relatively 'more altered' than the rest of the lithologic units in the vicinity of the HMLSDZ, ranging from almost completely muscovite- or chlorite-altered, although this may be solely due to initial lithological controls. The lack of evidence for feldspar sorting and the presence of illitic muscovite compositions in the epiclastic rocks suggest that these epiclastic rocks probably initially contained montmorillonite that was converted to illite during diagenesis. The variation in Zr and TiO_2 concentrations in the epiclastic rocks compared with other rock types (Figure 4.2), is probably a consequence of sedimentary sorting of zircon, and this may have occurred at the same time as quartz sorting. Potassium addition and removal occurred in these rocks during muscovite and chlorite alteration, respectively. Significant Fe, Mg, and Mn addition also occurred during chlorite alteration, because they contain Prussian-blue chlorite, a typical hydrothermal alteration product.

Figures 4.29 and 4.31 demonstrate that chlorite alteration in the rocks hosting the HMLSDZ forms a footwall alteration zone that is a vector to mineralization. These plots define a zone of pervasive chlorite alteration in the structural hangingwall (stratigraphic footwall) of the deposit up to approximately 250 m above massive sulphides. In addition,

Figures 4.29 and 4.30 indicate that strong chlorite and sulphide haloes exist in the narrow mineralized zone located approximately 100 m above the main HMLSDZ.

Previous work at Halfmile Lake suggested that silicification (*i.e.*, hydrothermal addition of silica) occurred in the alteration halos surrounding the deposits (Adair 1992). However, this study demonstrates that quartz fractionation or silicification or both processes probably occurred. Furthermore, the 'siliceous' character of the HMLSDZ host rocks may be a consequence of muscovite alteration, which produced quartz by the reactions:

$$3\ NaAlSi_3O_8 + K^+ + 2\ H^+ \Rightarrow KAlSi_3O_{10}(OH)_2 + 6\ SiO_2 + 3\ Na^+$$
(Albite) (Muscovite) (Quartz)

and :

$$3\ KAlSi_3O_8 + 2\ H^+ \Rightarrow KAlSi_3O_{10}(OH)_2 + 6\ SiO_2 + 2\ K^+$$
(K-Spar) (Muscovite) (Quartz)

Silica was recognized as the only element that has been extensively mobilized during deformation-induced metasomatism via pressure solution in the Bathurst mining camp (Lentz 1999). However, the alteration indices used to investigate material transfers in the current study do not involve silica, hence the effect of deformation-induced metasomatism does not interfere with the MER analysis. Consequently, the patterns observed on diagrams in this analysis, except for SiO_2, can either be attributed to be solely due to hydrothermal metasomatism or igneous fractionation.

Similarly, metamorphic metasomatism has also had little effect on these rocks. This can be demonstrated because high pressure-low temperature metamorphism typically involves the loss of H_2O, CO_2 and S. Because chemographic and spatial patterns

involving these volatile elements are consistent with a more comprehensive hydrothermal alteration model for the HML host rocks, metamorphic metasomatism has not significantly impacted the compositions of these rocks. Additionally, the felsic volcanic rocks, which represent the largest part of the rocks at the HMLSDZ, do not originally contain significant ferromagnesian minerals to form chlorite during greenschist facies metamorphism.

Due to the fundamentally variable composition of chlorite, it is difficult to assess the extent of metamorphic control on the chlorite composition in the rocks hosting the HMLSDZ. Nevertheless, variation in (Fe-S/2)/Mg ratios around the HMLSDZ suggests that metamorphism has not completely homogenized any original (hydrothermal) chlorite compositional zoning.

Furthermore, the formation of phengite (from muscovite or illite) during metamorphism only involves minor Al loss, K, (Fe,Mg) addition, and Si addition and loss, but non of these occurred on a scale large enough to obliterate hydrothermal alteration signatures, as ample K, Fe, Mg, Al, and Si existed in these rocks to allow phengite formation without significant metasomatism, and these elements still exhibit chemographic and geographic variations consistent with metasomatic and igneous processes. Finally, the presence of illite in the dacitic epiclastic rocks suggests that metamorphism is relatively weak and low grade, and has not converted illite to muscovite.

In summary, the observed geochemical patterns, both between elements and in space, can be exclusively recognized as the result of simple igneous and hydrothermal processes, and if deformation-induced or metamorphism-related metasomatism

overprinted these rocks, the extent of these processes are minor, because the rock's igneous and hydrothermal signatures are still evident.

REFERENCES

Adair, R.N. 1992. Stratigraphy, structure, and geochemistry of the Halfmile Lake massive-sulphide deposit, New Brunswick. Explor. Mining Geol., Vol. 1, No. 2, pp. 151-166.

Akella, J. 1966. Calculation of Material Transport in Some Metasomatic Processes. Neues Jahrbuch für Mineralogische Abhandlungen, vol. 104, p. 316-329.

Barrett, T.J. and MacLean, W.H. 1994. Chemostratigraphy and hydrothermal alteration in exploration for VHMS deposits in greenstones and younger volcanic rocks. *In* Alteration and Alteration processes Associated with Ore-Forming Systems (D.R. Lentz, ed.). Geol. Assoc. Can., Short Course Notes, vol 11, pp. 433-467.

Burton, D.M. 1993. The Murray Brook (Cu-rich) massive sulphide deposit, Bathurst Camp, New Brunswick: *In* Guidebook to the metallogeny of the Bathurst Camp. *Edited by* S.R. McCutcheon and D.R. Lentz, Trip #4 of Bathurst '93: 3rd Annual Field Conference, Geological Society of CIM, pp. 135-143.

Cheriton, C.G. 1960. Anaconda exploration in the Bathurst District of New Brunswick, Canada: AIME Transactions, 217, pp. 278-284.

Davies, G.H. and Reynolds, S.J. 1996. Structural Geology. 2nd Ed., Wiley & Sons, pp 70-71 and 442-443.

de Roo, J.A. 1989. Mass transfer and preferred orientation development during extensional microcracking in the slate-belt folds, Elura Mine, Australia. *J. Metamorphic Geol.*, Vol. 7, pp. 311-322.

de Roo, J.A., and van Staal, C.R. 1991. The structure of the Halfmile Lake region, Bathurst Camp, New Brunswick. Geological Survey of Canada, Paper 91-1D, pp. 179-186.

Fyffe, L.R., van Staal, C.R., and Sangster, D.F. 1990. Late Precambrian-Early Paleozoic volcanic regimes and associated massive sulphide deposits in the northeastern mainland Appalachians. CIM Bulletin, 83, No. 938, pp. 70-78.

Fyffe, L.R., McCutcheon, S.R., and Wilson, R.A. 1996. The Miramich-Tetagouche boundary and its relationship to the Patrick Brook Formation. Atlantic Geology, vol. 32: p. 70.

Goodfellow, W.D. 1975a. Major and minor element halos in the volcanic rocks at Brunswick No.12 sulphide deposit, New Brunswick, Canada. *In* development in Economic geology 1, Geochemical exploration 1974 *Edited by* I.L. Elliot & W.K. Fletcher, eds.), Elsevier, Amsterdam, the Netherlands (279-295).

Goodfellow, W.D. 1975b. Rock Geochemical Exploration and Ore Genesis at the Brunswick No. 12 deposit. Ph.D. thesis. University of New Brunswick, Fredericton, New Brunswick.

Gratier, J.P. 1987. Pressure solution-deposition creep and associated tectonic differentiation in sedimentary rocks. Geological Society Special Publication, No. 29, pp. 25-38.

Gray, D.R. 1979. Microstructure of crenulation cleavages" an indication of cleavage origin. American Journal of Science, vol 279, pp. 97-128.

Gray, D.R., and Durney, D.W. 1979. Investigations on the mechanical significance of crenulation cleavage. Tectonophysics, vol. 58, pp. 35-79.

Gresens, R.L. 1967. Composition-volume relationships in metasomatism. Chemical Geology, vol. 2, p. 47-55.

Harley, D.N. 1977. Geology of the Halfmile Lake Zn-Pb-Cu Deposit, New Brunswick. unpub. M.Sc. thesis, University of Western Ontario, London, Ontario, 208 p.

Jambor, J.L. 1979. Mineralogical evaluation of proximal-distal features in New Brunswick massive sulphide deposits. Canadian Mineralogist, vol. 17, pp. 649-664.

Kearey, P. 1996. Dictionary of Geology. Penguin Books, London, England, 245 p.

Langton, J.P. 1994. Tomogonops project, NTS 21 P/4 west, Gloucester County, New Brunswick. *In* Current Research 1993. *Edited by* S.A.A. Merlini, New Brunswick Department of Natural Resources and Energy, Minerals Resources Division, Miscellaneous Report 12, pp. 87-93.

Langton, J.P. and McCutcheon, S.R. 1993. Brunswick Project, NTS 21 P/5 west, 21 P/4 west, Gloucester County, New Brunswick. *In* Current Research. *Edited by* S.A. Abbot, New Brunswick Department of Natural Resources and Energy, Minerals Resources Division, Miscellaneous Report 12, pp. 87-93.

Large, R.R. 1977. Chemical evolution and zonation of massive sulphide deposits in volcanic terrains. Economic Geology, vol 72, pp. 549-572.

Lentz, D.R. 1995. Stratigraphy and structure of the Key Anacon massive sulphide deposit compared with the Brunswick Deposits, Bathurst Mining Camp, New Brunswick: *In* Geoscience Research 1994. *Edited by* J.P. Langton, New Brunswick Department of Natural Resources and Energy, Minerals Resources Division, Miscellaneous Report 15, pp. 23-44.

_____1996a. Recent advances in lithogeochemical exploration for massive sulphide deposits in volcano-sedimentary environments: petrogenetic, chemostratigraphic, and alteration aspects with examples from the Bathurst camp, New Brunswick. *In* Current Research 1995. *Edited by* B.M.W. Carroll, New Brunswick Department of Natural Resources and Energy, Minerals and Energy Division, Mineral Resource Report 96-1, pp. 73-119.

_____1996b. Trace element systematics of felsic volcanic rocks associated with massive sulphide deposits in the Bathurst Mining Camp: petrogenetic, tectonic and chemostratigraphic implications for VMS deposits. *In* Trace Element Geochemisry of Volcanic Rocks: Applications for Massive Sulphide Exploration (D.A. Wyman, ed.). Geological Association of Canada Short Course Notes 12, pp 359-402.

_____1997. The phosphorous-enriched, S-type Middle River rhyolite, Tetagouche Group, northeastern New Brunswick: Canadian Mineralogist, vol. 35, pp 673-690.

_____1999. Deformation-induced mass transfer in felsic volcanic rocks hosting the Brunswick No. 6 massive-sulphide deposit, New Brunswick: Geochemical effects and petrogenetic implications. The Canadian Mineralogist, Vol. 37, pp. 489-512.

_____ and Goodfellow, W.D. 1992a. Re-evaluation of the petrology and depositional environment of felsic volcanic and related rocks in the vicinity of the Brunswick No. 12 massive sulphide deposit, Bathurst Mining Camp, New Brunswick. Geol. Surv. Can., Pap. 92-1E. 333-342.

_____ and _____ 1993a. Petrology and mass-balance constraints on the origin of quartz augen schist associated with the Brunswick massive sulphide deposits, Bathurst, New Brunswick. Can. Mineral. 31, p. 877-903.

_____ and _____ 1993b. Mineralogy and petrology of the stringer sulphide zone in the discovery hole at the Brunswick No. 12 massive sulphide deposit, Bathurst, New Brunswick: Geological Survey of Canada Paper 93-1E, p. 249-258.

_____ and _____ 1994. Petrology and geochemistry of altered volcanic and sedimentary rocks associated with the FAB stringer sulphide zone, Bathurst, New Brunswick. Geol. Surv. Can., Paper 94-D, 123-133.

_____ and _____ 1996. Intense silicification of footwall sedimentary rocks in the stockwork alteration zone beneath the Brunswick No. 12 massive sulphide deposit, Bathurst, New Brunswick. Can. J. Earth Sci. 33, 284-302.

_____, Goodfellow, W.D., Brooks, E. 1996. Chemostratigraphy and depositional environment of an Ordovician sedimentary section across the Miramichi Group – Tetagouche Group contact, northeastern New Brunswick, Atlantic Geology, vol. 32 pp.101-122.

Linderman, E. 1913. Austin-Brook iron-bearing district, New Brunswick. Canadian Department of Mines, Mines Branch Publication No. 105.

MacKenzie, G.S. 1958. History of mining exploration; Bathurst-Newcastle District, New Brunswick. CIM Bulletin, 51, No. 551, pp. 156-161.

McCaig, A.M., and Knipe, R.J. 1990. Mass-transport mechanisms in deforming rocks: Recognition using microstructural and microchemical criteria. GEOLOGY, v. 18, p. 824-827.

McCutcheon, S.R. 1990. Base Metal Deposits of the Bathurst-Newcastle District. *In* Field Guide to Massive Sulphides in Northern New Brunswick. *Edited by* L.R. Fyffe. New Brunswick Department of Natural Resources and Energy, Minerals and Energy Division, p. 42-71.

_____1997. Geology and massive sulphide deposits of the Bathurst Camp, New Brunswick. Field Trip B7 Guidebook, Geological Association of Canada Annual Meeting, Ottawa, Canada. pp. 40-63.

_____and Walker J.A. 2001. Volcanogenic massive sulphide deposits of the Bathurst Camp, New Brunswick. Field Trip B7 Guidebook, Geological Association of Canada,

Mineralogical Association of Canada, Joint Annual Meeting, St. Johns, Newfoundland, Canada. pp. 1-89.

_____, Langton J.P, van Staal, C.R., and Lentz D.R. 1993. Stratigraphy, tectonic setting and massive sulphide deposits of the Bathurst Mining Camp, northern New Brunswick. *In* Guide book to the metallogeny of the Bathurst camp. *Edited by* S.R. McCutcheon and D.R. Lentz, Trip # 4, Bathurst '93, 3rd Annual Field conference, Geological Society, Canadian Institute of Mining and Metallurgy, pp. 1-39.

Pajari, G.E. Jr, Rast, N., and Stringer, P. 1977. Paleozoic volcanicity along the Bathurst-Dalhousie geotraverse, New Brunswick, and its relations to structure. *In* Volcanic regimes in Canada. *Edited by* W.R.A. Baragar, L.C. Coleman, and J.M. Hall. Geological Association of Canada, Special Paper 16, pp. 111-124.

Pearce, T.H. 1968. A contribution to the theory of variation diagrams. Contributions to Mineralogy and Petrology, vol. 19, pp. 142-157.

Peter, J.M. and Goodfellow, W.D. 1996. Bulk and rare earth element geochemistry of massive sulphide-associated hydrothermal sediments of the Brunswick horizon, Bathurst Mining Camp, northern New Brunswick. Canadian Journal of Earth Sciences, vol 33, pp. 252-283.

Rampton, V.N., Gauthier, R.C., Thibault, J., and Seaman, A.A., 1984. Quaternary geology of New Brunswick: Geological Survey of Canada, Memoir 416, 77 p.

Rennick, M.P. and Burton, D.M. 1992. The Murray Brook deposit, Bathurst Camp, New Brunswick: geologic setting and recent developments. Exploration and Mining Geology, 1: 137-142.

Rogers, N., Wodicka, N., McNicoll, V., and van Staal, C.R. 1997. U-Pb ages of Tetagouche Group felsic volcanic rocks, northern New Brunswick: Geological Survey of Canada Current Research 97-F, p. 113-119.

Spiegel, M.R. 1975. Schaum's Outline of Theory and problems of Probability and Statistics. pp 372. McGraw-Hill Book Company, NY.

_____ and Madeisky, H.E. (1996): Lithogeochemical Exploration for Metasomatic Zones Associated with Hydrothermal Mineral Deposits Using Pearce Element Ratio Analysis. Mineral Deposit Research Unit, Short Course Notes, 195 p.

Stanton, R.L. 1972. Ore Petrology. McGraw-Hill, New York.

Sullivan, R.W. and van Staal, C.R. 1996, Preliminary chronostratigraphy of the Tetagouche and Fournier Groups, Bathurst, New Brunswick: Geological Survey of Canada, Paper 95-F, p. 43-56.

_____ and Halls, C. 1969. The distribution of divalent trace elements between sulphides, oxides, silicates, and hydrothermal solutions. I. Thermodynamic basis. Geochem. Cosmochin. Acta 49, 853-864.

Tatsumi, T., and Watanabe, T. 1971. Geological environment of the Kuroko deposits. Society of Mining Geologists Japan Spec. Issue 3, pp. 216-220.

Thomas M.D., Walker, J.A., Keating, P., Shives, R., Kiss, F. and Goodfellow, W.D. 2000. Geophysical atlas of massive sulphide signatures, Bathurst Camp, New Brunswick. Geological Survey of Canada Open File 3887, and New Brunswick Department of Natural Resources and Energy, Minerals and Energy Division Open File 2000-9.

van Staal, C.R. 1987. Tectonic setting of the Tetagouche Group in Northern New Brunswick: implications for plate tectonic models of the Northern Appalachians. Canadian Journal of Earth Sciences, 24, p. 1669-1692.

_____1994. Brunswick subduction complex in the Canadian Appalachians: Record of the Late Ordovician to Late Silurian collision between Laurentian and the Gander margin of Avalon: Tectonics, v. 13, p. 946-962.

_____ and Fyffe, L.R. 1991. Dunnage and Gander zones, New Brunswick: Canadian Appalachian Region. New Brunswick Department of Natural Resources and Energy, Mineral Resources, Geoscience Report 91-2, 39 p.

_____ and Fyffe, L.R. 1995a. Gander zone - New Brunswick: Geological Survey of Canada, Geology of North America, vol. F-1, pp. 216-223.

_____ and Fyffe, L.R. 1995b. Dunnage zone - New Brunswick: Geological Survey of Canada, Geology of North America, vol. F-1, pp.166-178.

_____, and Williams, P.F. 1984. Structure, origin, and concentration of the Brunswick 6 and 12 orebodies. Econ. Geol. 79, 1669-1692.

_____, Fyffe, L.R., Langton, J.P., and McCutcheon, S.R. 1992. The Ordovician Tetagouche Group, Bathurst Camp, northern New Brunswick: history, tectonic setting, and distribution of massive sulphide deposits. Exploration and Mining Geology 1, 93-103.

_____, Winchester, J.A, and Cullen, R., 1988. Evidence for D1-related thrusting and folding in the Bathurst-Millstream River area, New Brunswick. *In* Current Research, Part B, Geological Survey of Canada, Paper 88-1B, pp.1669-1692.

_____, Ravenhurst, C.E., Winchester, J.A., Roddick, J.C., and Langton, J.P. 1990. Post-Taconic blueschist suturein the northern Appalacians of northern New Brunswick, Canada, Geology, vol 24, pp. 1073-1077.

_____Winchester, J.A, and Bedard, J.A., 1991. Geochemical variations in Middle Ordovician volcanic rocks of the northern Miramichi highlands and their tectonic significance: Canadian Journal of Earth Sciences, 28, p. 1031-1049.

Whitehead, R.E.S. and Goodfellow, W.D. 1978. Geochemistry of volcanic rocks from the Tetagouche Group, Bathurst, New Brunswick, Canada. Canadian Journal of Earth Sciences, 15, p. 207-219.

Wilson, R.A. 1993. Geology of the Heath Steele-Halfmile Lake area, Northumberland County, New Brunswick. New Brunswick Department of Natural Resources and Energy, Mineral Resources, Report of Investigation 25, 98 p.

Wilson, R.A., van Staal, C.R., McCutcheon S.R., and Fyffe L.R. 1998a. Revised stratigraphic nomenclature for the Bathurst Mining Camp, Northern New Brunswick.

In Abstracts, 1998: 23rd Annual Review of Activities. *Edited by* B.M.W. Carroll. New Brunswick Department of Natural Resources and Energy, Minerals and Energy Division, Information Circular, 98-3, pp.

Winchester, J.A., and Floyd, P.A. 1977. Geochemical discrimination of different magma series and their differentiation products using immobile elements. Chemical Geology, 20, p. 235-343.

Cover Page for Appendices

Table A.1-A.10

QFP = quartz-feldspar porphyry

QZ = quartz

FS = feldspar

GW = greywacke

MUSC = muscovite

Py = pyrite

STK_Wk = stockwork

Po = pyrrhotite

Cpy = chalcopyrite

Table B.1

RTSL = coordinates after translating grid origin to (2000, 4000, 0), rotating grid *-60°* and tilting grid *20°* (see text for explanation).

Table B.2

QFP = quartz-feldspar porphyry

QTZ = quartz

Table B.3.1

GP = group

CB = carbonate

CL = chlorite

MU = muscovite

SL = silica;

PO = pyrrhotite

PY = pyrite

GN = galena

SP = sphalerite

CP = chalcopyrite

QV = quartz veining

1 = least altered or abundant

5 = most altered or abundant

Table C

Abund = abundance,

QTZ = quartz

FS = feldspar

Phen = phenocryst

Matx = matrix

v.f.g. = very fine-grained

IF = iron formation

Table D

Samp. ID = sample identity

MG = mineral grain
O = oxygen

Table E

A.U. = analytical unit
A.M. = analytical method
D.L. = detection limit

XRF = x-ray fluorescence spectrometry;
ICP = inductively-coupled plasma spectrometry

INF* = interference

Table A.1 - DDH HN95-086 Summary Drill Log

From (m)	To (m)	Rock Type	Modifier	Alteration
707.65	724.80	Siltstone	minor interbedded with greywacke & argillite layers; also sulphide stockwork	
724.80	760.88	Siltstone	with argillite & greywacke beds	
760.88	815.60	Siltstone	with argillite & greywacke beds	weakly muscovite-altered
815.60	840.20	Siltstone	with argillite & greywacke beds	moderately chlorite-altered
840.20	869.90	Sandy Siltstone		weakly muscovite-altered
869.90	900.20	Siltstone	with argillite & greywacke beds;	weakly muscovite-altered
900.20	909.30	Siltstone	chloritic	
909.30	961.00	Siltstone	with interlayers of muscovite- & chlorite-alteration	
961.00	974.14	?		intense muscovite-alteration
HN95-86A				
883.20	907.96	Siltstone	with argillite;	weakly muscovite-altered in patches
907.96	950.74	Massive Sulphide		
950.74	966.90	Felsic Tuff		muscovite-alteration increasing towards base
966.90	974.75	Fault		

Table A.2 - DDH HN99-119 Summary Drill Log

From (m)	To (m)	Rock Type	Modifier	Alteration
973.50	1012.05	Greywacke	interbedded with siltstone; sulphide stockwork	
1012.05	1020.85	Massive Sulphide		
1020.85	1053.00	Greywacke	interbedded with siltstone & argillite; disseminated & bedded sulphide stockwork	
1053.00	1074.60	Siltstone		weakly chloritic
1074.60	1079.40	Siltstone	argillaceous	
1079.40	1080.20	Fault		
1080.20	1166.91	Siltstone	with minor greywacke	weakly chloritic
1166.91	1175.71	Massive Sulphide		
1175.71	1178.40	Siltstone	disseminated sulphide	chloritic
1178.40	1182.20	Quartz-eye Tuff		
1182.20	1194.90	Siltstone	disseminated sulphide	chloritic
1194.90	1201.61	Quartz-eye Tuff		
1201.61	1249.67	Massive Sulphide		
1249.67	1269.50	Cherty Tuff		
1269.50	1279.75	Argillite		chloritic
1279.75	1317.00	Quartz-eye Tuff		
1317.00	1337.40	Siltstone	with minor greywacke	
1337.40	1380.40	Quartz-eye Tuff		
1380.40	1409.70	Basalt		

Table A.3 - DDH HN99-120 Summary Drill Log

From (m)	To (m)	Rock Type	Modifier	Alteration
633.94	637.60	Black Dyke	possibly chilled margin to QFP	
637.60	808.00	QFP		
808.00	831.00	Cherty Tuff		muscovite-altered & ankeritic
831.00	849.00	Siltstone		
849.00	857.00	Cherty Tuff		sericitized
857.00	868.87	Cherty Tuff		
868.87	878.00	Felsic Tuff		less altered
878.00	904.65	Siltstone		variably sericitized
904.65	913.00	Greywacke		
913.00	929.63	Siltstone		sericitized
929.63	942.62	Siltstone		
942.62	952.50	Siltstone		sericitized
952.50	964.14	Siltstone		chloritic
964.14	999.60	Argillite	variably bleached	
999.60	1004.00	Greywacke		
1004.00	1032.66	Siltstone	interbedded with argillite	variably sericitized
1032.66	1045.46	Greywacke	interbedded with siltstone	
1045.46	1082.69	Siltstone	interbedded with greywacke	
1082.69	1087.53	Greywacke		
1087.53	1108.86	Siltstone	interbedded with greywacke	
1108.86	1121.05	Siltstone	interbedded with greywacke	
1121.05	1145.14	Greywacke	interbedded with siltstone	

Table A.3 - DDH HN99-120 Summary Drill Log (continued)

From (m)	To (m)	Rock Type	Modifier	Alteration
1145.14	1331.24	Sandy Siltstone		minor STK-WK PY-PO-CPY
1331.24	1335.43	Massive Sulphide	stockwork	
1335.43	1344.50	Argillite		less chloritic with abundant STK-WK sulphide
1344.50	1359.65	Argillite		minor STK-WK sulphide
1359.65	1387.15	Silty Argillite		disseminated PY
1387.15	1399.21	Massive Sulphide	stockwork	
1399.21	1409.40	Argillite		less chloritic with abundant STK-WK sulphide
1409.40	1417.44	Felsic Dyke		Calcite in fractures
1417.44	1427.75	Argillite	with chert bands	
1427.75	1439.36	Massive Sulphide		
1439.36	1443.67	Felsic Tuff	flow banded? devitrified? banded	
1443.67	1454.82	Silty Argillite		
1454.82	1492.38	Felsic Tuff	locally Quartz phyric	
1492.38	1506.35	Silty Argillite	at top	
1506.35	1542.70	Felsic Tuff	QZ-phyric, crystal-rich bottom & crystal-poor top; contact @ 1526.52	
1542.70	1547.28	Argillite		Chloritic
1547.28	1551.35	Felsic Tuff	flow banded? devitrified? crenulated	
1551.35	1558.90	Quartz-eye Tuff	QZ-FS phyric; crystal-rich bottom, crystal-poor top	
1558.90	1561.70	Silty Argillite		
1561.70	1571.13	Quartz-eye Tuff		
1571.13	1572.77	Fault		

Table A.4 - DDH HN99-122 Summary Drill Log

From (m)	To (m)	Rock Type	Modifier	Alteration
1092.10	1138.95	Siltstone	interbedded with argillite	
1138.95	1157.78	Greywacke	interbedded with argillite	
1157.78	1200.00	Siltstone	interbedded with argillite	
1200.00	1209.11	Sandy Siltstone		
1209.11	1246.00	Siltstone	interbedded with argillite	
1246.00	1249.30	Greywacke		
1249.30	1264.10	Siltstone	interbedded with argillite	
1264.10	1294.40	Sandy Siltstone		
1294.40	1331.25	Siltstone	interbedded with argillite	
1331.25	1335.51	Silty Argillite		chloritic
1335.51	1382.33	Siltstone	interbedded with argillite	chloritic from base to 1374.56
1382.33	1412.37	Massive Sulphide		
1412.37	1413.88	Siltstone		muscovite altered
1413.88	1432.56	QZ-FS Porphyry		
1432.56	1433.68	Argillite		
1433.68	1449.35	QZ-FS Porphyry		
1449.35	1460.72	Silty Argillite		
1460.72	1495.10	QZ-FS Porphyry		
1495.10	1496.57	Cherty Tuff		

Table A.5 - DDH HN99-123 Summary Drill Log

From (m)	To (m)	Rock Type	Modifier	Alteration
516.04	543.08	QFP		
543.08	577.60	Cherty Tuff	greywacke occurs between 569.65-571.5	
577.60	611.20	Siltstone		chloritic
611.20	656.95	Cherty Tuff	variably muscovite altered	intense @ 623.42-635.41
656.95	660.50	Siltstone		
660.50	669.70	Cherty Tuff	unaltered	
669.70	700.05	Siltstone	interbedded with chlorite-argillite & greywacke	variably sericitized
700.05	714.76	Cherty Tuff		
714.76	723.90	Siltstone		
723.90	725.90	Felsic Dyke	feldspar-phyric	
725.90	757.93	Siltstone		variably muscovite-chlorite altered
757.93	763.52	Dyke	intermediate	
763.52	812.29	Siltstone	interbedded with argillite, minor sulphide stockwork	
812.29	836.07	Siltstone	interbedded with greywacke, minor sulphide stockwork	
836.07	845.00	Argillite	interbedded with siltstone, chloritic	
845.00	862.00	Argillite	with greywacke	variably muscovite-altered
862.00	867.00	Greywacke		
867.00	879.00	Siltstone		variably muscovite altered
879.00	882.44	Siltstone	interbedded with siltstone	variably muscovite altered
HN99-123A				
731.45	732.74	Siltstone		
732.74	737.30	Dyke		
737.30	757.43	Siltstone	variably muscovite altered	

Table A.5 - DDH HN99-123 Summary Drill Log (continued)

From (m)	To (m)	Rock Type	Modifier	Alteration
757.43	767.57	Dyke		
767.57	787.94	Cherty Tuff	with minor greywacke,	moderately sericitized
787.94	804.15	Cherty Tuff	with minor greywacke	moderately sericitized
804.15	847.50	Greywacke	with minor siltstone; moderate sulphide stockwork	
847.50	894.00	Siltstone	interbedded with argillite	moderately chlorite-altered
894.00	909.83	Greywacke		
909.83	928.12	Siltstone	with minor sulphide stockwork	
928.12	954.35	Greywacke		
954.35	959.20	Dyke		
959.20	992.62	Siltstone	with bedded sulphide; moderate sulphide stockwork	
992.62	1031.75	Siltstone	interbedded with argillite	
1031.75	1050.10	Greywacke	interbedded with siltstone	
1050.10	1065.56	Greywacke	mildly sericitized	
1065.56	1129.68	Siltstone	with bedded sulphide; moderate sulphide stockwork	
1129.68	1135.10	Greywacke	with disseminated sulphide	
1135.10	1137.92	Dyke		
1137.92	1214.63	Massive Sulphide		
1214.63	1254.20	Greywacke		moderately variably sericitized
1254.20	1263.00	QFP		
1263.00	1269.90	Siltstone		
1269.90	1292.33	Quartz-eye Tuff		
1292.33	1299.77	Cherty Tuff		
1299.77	1322.22	Siltstone	variably bleached	moderately sericitized

Table A.6 - DDH HN99-124 Summary Drill Log

From (m)	To (m)	Rock Type	Modifier	Alteration
944.00	1134.30	Siltstone	with interbedded argillite	Chloritic
1134.30	1138.80	Cherty Tuff		
1138.80	1151.00	Felsic Dyke		calcite blebs and fractures
1151.00	1158.00	Cherty Tuff		
1158.00	1181.60	Siltstone	with interbedded argillite	chloritic with pyrite-pyrrhotite
1181.60	1203.40	Felsic Dyke		calcite plus euhedral coarse grained pyrite
1203.40	1243.30	Argillite	with interbedded siltstone	chloritic
1243.30	1255.90	Felsic Dyke		calcite plus euhedral coarse grained pyrite
1255.90	1257.90	Fault		
1257.90	1266.49	Siltstone	with interbedded argillite	
1266.49	1271.56	Felsic Dyke	minor quartz phenocrysts	calcite plus euhedral coarse grained pyrite
1271.56	1318.43	Massive Sulphide		
1318.43	1335.80	Siltstone	with interbedded argillite	minor disseminated pyrite along bedding planes
1335.80	1349.20	Sericite Schist		zones of disseminated pyrite plus ankerite
1349.20	1365.88	QFP	with interbedded argillite	
1365.88	1371.60	Siltstone	with interbedded argillite	chlorite cleavage selvedges
1371.60	1377.09	QFP	with 20 % interbedded argillite	

Table A.7 - DDH HN99-125 Summary Drill Log

From (m)	To (m)	Rock Type	Modifier	Alteration
581.20	598.00	QFP		
598.00	650.78	Rhyolite Flow		chloritic
650.78	661.25	Siltstone		
661.25	666.78	Rhyolite Flow/Dyke?		
666.78	667.25	Felsic Tuff		chloritic
667.25	673.25	Siltstone	banded	sericitized
673.25	676.20	Cherty Tuff		
676.20	679.29	Cherty Tuff	deformed	chloritic
679.29	689.84	Siltstone		
689.84	696.95	Cherty Tuff		
696.95	714.96	Siltstone	interbedded with greywacke; disseminated stockwork sulphide	
714.96	738.14	Argillite	interbedded with siltstone;	sericitized and sulphidic
738.14	745.22	Cherty Tuff		
745.22	795.45	Siltstone	MUSC altered siltstone interbedded with MUSC-altered argillite (subordinate) & GW	
795.45	801.60	Greywacke	slightly MUSC-altered along margins	
801.60	813.20	Siltstone/Cherty Tuff?	MUSC-altered; interbedded with argillite; some stockwork sulphide	
813.20	829.58	Greywacke		
829.58	833.16	Cherty Tuff	sericitized	
833.16	843.08	Cherty Tuff	variably sericitized	
843.08	854.74	Greywacke	interbedded with sericitized argillite	
854.74	980.24	Siltstone	interbedded with greywacke; 854.74-877 & 883.5-892.84 are CHL-altered; 943.36-950 and 964.6-968.04 are MUSC-altered with relatively strong chlorite alteration between MUSC-alteration; 968.04-980.24 is more GW with interbedded argillite and is variably sericitized	

Table A.7 - DDH HN99-125 Summary Drill Log (continued)

From (m)	To (m)	Rock Type	Modifier	Alteration
980.24	1007.69	Siltstone	interbedded with argillite; minor sulphide stockwork	less chloritic
1007.69	1025.33	Siltstone	with sulphide stockwork	mod chloritic
1025.33	1050.34	Greywacke	interbedded with argillite, also sulphide stockwork; chloritic up to 1041.2	
1050.34	1068.53	Siltstone	interbedded with argillite, also sulphide stockwork;	chloritic
1068.53	1084.00	Felsic Tuff		
1084.00	1107.17	Dyke		
1107.17	1116.54	Siltstone	chloritic with sulphide stockwork	
1116.54	1135.70	Siltstone		less chloritic
1135.70	1138.18	Dyke		
1138.18	1147.90	Siltstone	interbedded with argillite; chloritic	
1147.90	1175.80	Greywacke	with interbedded chloritic argillite	
1175.80	1193.00	Siltstone	with sulphide stockwork	variably MUSC-altered
1193.00	1260.70	Massive Sulphide		
1260.70	1262.80	Felsic Tuff	quartz-phyric	
1262.80	1292.46	QFP		
1292.46	1294.97	Argillaceous Siltstone		
1294.97	1318.56	QFP		

Table A.8 - DDH HN99-126 Summary Drill Log

From (m)	To (m)	Rock Type	Modifier	Alteration
973.80	993.65	Siltstone	interbedded with argillite	
993.65	1013.60	Siltstone		
1013.60	1024.69	Siltstone	interbedded with argillite	
1024.69	1045.46	Siltstone		
1045.46	1056.20	Argillite	interbedded with siltstone	
1056.20	1069.85	Greywacke		
1069.85	1077.00	Argillite	interbedded with siltstone	
1077.00	1083.09	Greywacke		strongly muscovite altered
1083.09	1102.44	Siltstone	interbedded with argillite; chloritic	
1102.44	1114.48	Siltstone	interbedded with argillite; bands of semi-massive sulphide, 10 & 15cm thick in section	chloritic
1114.48	1118.41	Greywacke		
1118.41	1146.00	Siltstone	interbedded with argillite and stockwork sulphide mineralization	
1146.00	1193.69	Siltstone	interbedded with argillite and meta-greywacke	chloritic
1193.69	1197.86	Meta-Mudstone		muscovite altered
1197.86	1202.61	Meta-Mudstone	stockwork sulphide	
1202.61	1215.91	Massive Sulphide		
1215.91	1228.39	Siltstone	interbedded with argillite and stockwork sulphide mineralization;	moderately sericitized
1228.39	1262.61	Massive Sulphide		
1262.61	1263.43	Argillite		chloritic
1263.43	1267.38	Felsic Dyke		
1267.38	1283.20	Greywacke	with interbedded argillite; abundant massive- semi-massive sulphide beds and stringers	
1283.20	1289.76	Felsic Tuff		
1289.76	1297.93	Felsic Dyke	quartz-phyric	

Table A.8 - DDH HN99-126 Summary Drill Log (continued)

From (m)	To (m)	Rock Type	Modifier	Alteration
1297.93	1300.68	Felsic Tuff		chloritic
1300.68	1304.63	Felsic Tuff		
1304.63	1306.38	Felsic Dyke		
1306.38	1311.25	Sericite Schist		

Table A.9 - DDH HN99-127 Summary Drill Log

From (m)	To (m)	Rock Type	Modifier	Alteration
411.16	570.18	Quartz-feldspar porphyry		
570.18	588.10	Cherty Tuff		
588.10	594.25	Siltstone		
594.25	596.65	Quartz-feldspar porphyry		
596.65	631.00	Siltstone		
631.00	680.00	Cherty Tuff		
680.00	685.20	Siltstone		chloritic
685.20	711.90	Cherty Tuff		
711.90	714.67	Greywacke		
714.67	727.90	Cherty Tuff		
727.90	740.00	Silty Argillite	sulphidic	
740.00	781.30	mafic dyke	with beds of argillite; have late brittle fractures filled with quartz	
781.30	811.50	Argillaceous Siltstone		chloritic
811.50	844.00	Greywacke	interbedded with siltstone	
844.00	932.08	Greywacke	interbedded with argillite; patchy bands of chlorite	
932.08	962.56	Siltstone	interbedded with argillite	
962.56	968.65	Argillite		
968.65	987.25	Siltstone	interbedded with greywacke	
987.25	999.50	Siltstone	chloritic with abundant stockwork sulphide	
999.50	1023.53	Siltstone	interbedded with greywacke	
1023.53	1047.20	Siltstone	interbedded with argillite & stockwork sulphide	
1047.20	1050.95	Purple Siltstone		
1050.95	1078.38	Argillaceous Siltstone		chloritic

Table A.9 - DDH HN99-127 Summary Drill Log (continued)

From (m)	To (m)	Rock Type	Modifier	Alteration
1078.38	1094.67	Silty Argillite		chloritic
1094.67	1121.05	Siltstone	interbedded with argillite	
1121.05	1133.25	Siltstone		
1133.25	1146.08	Argillite	chloritic; with stockwork sulphide	
1146.08	1171.66	Silty Argillite		
1171.66	1191.85	Siltstone	interbedded with argillite	
1191.85	1193.46	Felsic dyke	feldspar-phyric & carbonate rich	
1193.46	1216.40	Siltstone	interbedded with argillite	
1216.40	1216.85	Fault		
1216.85	1224.69	Argillite	bleached	
1224.69	1251.00	Argillaceous Siltstone		
1251.00	1252.80	Argillite		chloritic
1252.80	1269.10	Felsic Tuff		MUSC-altered
1269.10	1289.40	Felsic Tuff		ankerite blebs
1289.40	1300.89	Quartz-feldspar porphyry		

Table A.10 - DDH HN99-128 Summary Drill Log

From (m)	To (m)	Rock Type	Modifier	Alteration
1016.36	1070.00	Siltstone	with interbedded argillite & minor greywacke;	variably chloritic
1070.00	1090.09	Quartz-eye Tuff	with large disseminated Py; bleached from top to 1079m	
1090.09	1116.20	Argillite	with minor interbedded siltstone	
1116.20	1125.46	Felsic Dyke		
1125.46	1135.38	Sandy Siltstone	with bedded sulphide	
1135.38	1230.98	Siltstone	interbedded with argillite	
1230.98	1380.80	Massive Sulphide		
1380.80	1382.40	Quartz-eye Tuff		chloritic
1382.40	1394.00	Felsic Tuff	muscovite altered with disseminated semi-massive sulphide	
1394.00	1397.40	Argillite		chloritic with carbonate
1397.40	1407.71	Felsic Tuff		muscovite altered

Table B.1 - Sample Location Data

Sample Number	DDH Name	From (m)	To (m)	Midpoint Easting (m)	Mid-point Northing (m)	Mid-point Elevation (m)	RTSL Easting (m)	RTSL Northing (m)	RTSL Elevation (m)
158779	HN99-119	981.63	981.90	2746.37	3829.34	-389.80	356.2	561	-544.5
158780	HN99-119	1033.45	1033.71	2757.77	3814.68	-438.16	357	563.6	-596.2
158781	HN99-119	1066.40	1066.63	2764.71	3805.23	-468.94	357.4	564.9	-629.1
158782	HN99-119	1117.59	1117.89	2775.92	3790.42	-516.67	358.4	567.2	-680.3
158783	HN99-119	1165.86	1166.22	2785.89	3776.08	-561.71	359.4	568.6	-728.6
158784	HN99-119	1191.29	1191.50	2791.06	3768.39	-585.31	360	569.3	-753.9
158785	HN99-119	1196.56	1196.76	2792.13	3766.78	-590.20	360.1	569.4	-759.1
158786	HN99-119	1263.57	1263.83	2805.53	3745.87	-652.48	362.1	570.5	-826.2
158787	HN99-119	1271.06	1271.32	2807.00	3743.49	-659.42	362.4	570.6	-833.6
158788	HN99-119	1286.26	1286.56	2809.99	3738.64	-673.54	362.9	570.8	-848.9
158789	HN99-119	1319.52	1319.84	2816.57	3728.06	-704.38	364.1	571.2	-882.1
158790	HN99-119	1332.04	1332.40	2819.08	3724.08	-716.01	364.5	571.4	-894.6
158791	HN99-119	1341.54	1341.77	2820.97	3721.10	-724.76	364.8	571.5	-904.1
158792	HN99-119	1386.81	1387.09	2829.77	3706.90	-766.86	366.1	572.1	-949.3
158793	HN99-119	1407.16	1407.36	2833.51	3700.61	-785.81	366.5	572.1	-969.6
158794	HN99-120	635.00	635.29	2663.69	4235.19	-67.12	97.5	692.4	-106.9
158795	HN99-120	705.49	705.70	2677.55	4212.43	-132.33	100.2	693	-177.3
158796	HN99-120	730.91	731.14	2682.75	4203.93	-155.73	101.6	693.2	-202.7
158797	HN99-120	729.43	729.69	2682.44	4204.44	-154.38	101.5	693.2	-201.2
158798	HN99-120	821.90	822.10	2701.77	4172.47	-238.94	107.6	694	-293.5
158799	HN99-120	862.09	862.33	2710.38	4158.56	-275.67	110.4	694.5	-333.6
158800	HN99-120	907.14	907.40	2720.31	4143.17	-316.83	113.6	695.4	-378.5
158801	HN99-127	910.29	910.54	2702.43	3843.17	-336.20	342.7	529.9	-482.5
158802	HN99-127	907.93	908.17	2702.09	3843.91	-333.98	342.7	530.0	-480.1
158803	HN99-127	869.83	870.08	2696.66	3855.27	-298.03	343.2	531.0	-442.1
158804	HN99-127	822.07	822.36	2689.78	3868.54	-252.69	344.6	531.6	-394.3
158805	HN99-127	806.83	807.04	2687.51	3872.82	-238.20	345.1	531.8	-379.1
158806	HN99-127	777.33	777.46	2682.99	3881.20	-210.29	345.7	532.1	-349.6

Table B.1 - Sample Location Data (continued)

Sample Number	DDH Name	From (m)	To (m)	Midpoint Easting (m)	Mid-point Northing (m)	Mid-point Elevation (m)	RTSL Easting (m)	RTSL Northing (m)	RTSL Elevation (m)
158807	HN99-127	723.60	723.87	2674.26	3896.91	-159.67	346.1	532.4	-295.9
158808	HN99-127	712.20	712.47	2672.36	3900.26	-148.94	346.1	532.4	-284.5
158809	HN99-127	688.54	688.72	2668.47	3907.08	-126.57	346.4	532.5	-260.8
158810	HN99-127	666.68	666.90	2664.96	3913.17	-105.89	346.9	532.5	-238.9
158811	HN99-127	635.33	635.53	2659.87	3921.95	-76.22	347.5	532.4	-207.6
158812	HN99-127	603.50	603.78	2654.46	3931.17	-46.28	347.7	532.4	-175.8
158813	HN99-127	585.00	585.23	2651.26	3936.63	-28.88	347.7	532.3	-157.3
158814	HN99-127	548.34	548.62	2644.96	3947.47	5.55	347.7	532.3	-120.6
158815	HN99-127	505.31	505.52	2637.79	3959.87	46.15	348.1	532.3	-77.6
158816	HN99-127	463.60	463.88	2631.01	3971.50	85.60	348.9	532.2	-35.9
158817	HN99-125	858.94	859.20	2849.24	3869.32	-290.09	406.1	670.1	-456.5
158818	HN99-125	921.92	922.15	2860.57	3852.24	-349.63	405.0	671.4	-519.5
158819	HN99-125	951.30	951.62	2865.93	3844.30	-377.45	404.5	672.1	-548.9
158820	HN99-125	986.33	986.58	2872.36	3834.90	-410.54	403.8	672.9	-583.9
158821	HN99-125	1032.87	1033.13	2881.07	3822.50	-454.55	403.0	674.3	-630.4
158822	HN99-125	1044.85	1045.06	2883.31	3819.33	-465.86	402.7	674.6	-642.3
158823	HN99-125	1070.38	1070.63	2887.92	3812.56	-490.06	402.1	675.2	-667.9
158824	HN99-125	1090.51	1090.80	2891.38	3807.23	-509.18	401.5	675.6	-688.0
158825	HN99-125	1111.30	1111.61	2894.79	3801.75	-528.96	400.8	675.8	-708.8
158826	HN99-125	1137.26	1137.50	2898.94	3794.90	-553.61	399.9	676.0	-734.7
158827	HN99-125	1159.69	1160.00	2902.50	3788.94	-574.98	399.1	676.1	-757.2
158828	HN99-125	1179.68	1179.97	2905.65	3783.63	-593.98	398.4	676.1	-777.1
158829	HN99-125	1182.15	1182.47	2906.04	3782.97	-596.34	398.4	676.1	-779.6
158830	HN99-125	1191.38	1191.65	2907.52	3780.54	-605.10	398.0	676.2	-788.8
158831	HN99-125	1261.42	1261.63	2919.26	3762.37	-671.68	395.6	677.3	-858.8
158832	HN99-125	1269.91	1270.13	2920.74	3760.20	-679.76	395.3	677.5	-867.2
158833	HN99-125	1315.03	1315.33	2928.03	3748.53	-722.77	393.5	678.0	-912.4
158834	HN99-125	841.22	841.44	2846.05	3874.14	-273.32	406.5	669.8	-438.8

Table B.1 - Sample Location Data (continued)

Sample Number	DDH Name	From (m)	To (m)	Midpoint Easting (m)	Mid-point Northing (m)	Mid-point Elevation (m)	RTSL Easting (m)	RTSL Northing (m)	RTSL Elevation (m)
158835	HN99-125	831.09	831.37	2844.23	3876.88	-263.77	406.6	669.6	-428.7
158836	HN99-125	813.47	813.85	2841.08	3881.65	-247.15	407.0	669.2	-411.1
158837	HN99-125	809.55	809.92	2840.38	3882.70	-243.44	407.0	669.1	-407.2
158838	HN99-125	802.68	802.92	2839.15	3884.56	-236.87	407.2	669.0	-400.3
158839	HN99-125	786.85	787.06	2836.36	3888.77	-221.86	407.6	668.7	-384.5
158840	HN99-125	773.17	773.50	2833.92	3892.38	-208.95	407.9	668.4	-370.8
158841	HN99-125	750.82	751.06	2829.75	3898.31	-187.76	408.4	667.7	-348.5
158842	HN99-125	736.09	736.40	2827.13	3902.18	-173.83	408.8	667.4	-333.8
158843	HN99-125	712.50	712.79	2823.13	3908.42	-151.43	409.5	667.1	-310.2
158844	HN99-125	690.21	690.43	2819.12	3914.71	-130.38	409.7	666.7	-287.9
158845	HN99-125	678.48	678.73	2816.97	3918.06	-119.37	409.7	666.5	-276.2
158846	HN99-125	662.81	663.04	2814.11	3922.50	-104.60	409.8	666.3	-260.5
158847	HN99-125	652.72	653.00	2812.29	3925.32	-95.11	409.9	666.1	-250.4
158848	HN99-125	633.69	633.93	2808.85	3930.59	-77.13	410.1	665.8	-231.4
158849	HN99-125	617.73	617.99	2805.99	3934.93	-62.05	410.4	665.5	-215.4
158850	HN99-125	593.55	593.83	2801.84	3941.20	-39.08	411.2	665.0	-191.3
158851	HN95-086	707.65	707.93	2369.53	3593.73	-128.60	460.3	116.9	-304.4
158852	HN95-086	749.34	749.70	2376.21	3585.18	-168.89	456.6	118.4	-345.9
158853	HN95-086	768.43	768.72	2379.21	3581.41	-187.34	454.7	119.1	-364.9
158854	HN95-086	785.35	785.73	2381.79	3578.14	-203.77	453.0	119.7	-381.7
158855	HN95-086	830.61	830.84	2388.52	3569.64	-247.65	448.1	121.3	-426.6
158856	HN95-086	865.00	865.31	2393.67	3563.54	-281.14	444.0	122.7	-460.8
158857	HN95-086	906.84	907.00	2399.82	3556.36	-321.81	438.8	124.4	-502.2
158858	HN95-086	961.41	961.69	2409.66	3547.72	-374.84	432.3	128.6	-556.3
158859	HN95-086	970.05	970.33	2411.33	3546.34	-383.21	431.4	129.4	-564.8
158860	HN95-086	892.56	892.78	2397.67	3558.74	-307.93	440.6	123.8	-488.1
158861	HN95-086	963.35	963.62	2409.99	3547.45	-376.48	432.2	128.8	-557.9
158862	HN95-086	957.91	958.27	2408.99	3548.27	-371.49	432.7	128.3	-552.8

Table B.1 - Sample Location Data (continued)

Sample Number	DDH Name	From (m)	To (m)	Midpoint Easting (m)	Mid-point Northing (m)	Mid-point Elevation (m)	RTSL Easting (m)	RTSL Northing (m)	RTSL Elevation (m)
158863	HN99-123	533.37	533.66	2659.00	3864.31	23.94	428.2	502.9	-130.4
158864	HN99-123	545.26	545.51	2660.89	3860.94	12.72	428.0	502.8	-142.3
158865	HN99-123	519.68	520.00	2656.74	3867.70	37.00	428.9	502.6	-116.7
158866	HN99-123	560.72	560.91	2663.27	3856.24	-1.78	428.0	502.5	-157.7
158867	HN99-123	571.67	571.79	2665.01	3852.93	-12.04	428.0	502.4	-168.6
158868	HN99-123	615.25	615.45	2672.21	3839.87	-53.03	428.0	502.1	-212.2
158869	HN99-123	620.72	620.91	2673.12	3838.25	-58.17	428.0	502.1	-217.7
158870	HN99-123	634.15	634.37	2675.32	3834.28	-70.82	427.9	502.0	-231.1
158871	HN99-123	668.87	669.04	2680.74	3824.15	-103.56	427.5	501.6	-265.8
158872	HN99-123	693.08	693.34	2684.42	3817.04	-126.45	427.2	501.2	-290.1
158873	HN99-123	724.23	724.46	2689.27	3807.50	-155.69	427.3	500.7	-321.2
158874	HN99-123	762.78	762.97	2696.26	3794.48	-191.26	429.0	500.2	-359.7
158875	HN99-123	784.86	785.16	2701.33	3785.21	-210.70	432.2	500.0	-381.5
158876	HN99-123	799.24	799.44	2704.49	3779.54	-223.47	434.0	499.9	-395.8
158877	HN99-123	809.04	809.25	2706.48	3776.04	-232.42	434.7	499.8	-405.6
158878	HN99-123	849.52	849.78	2713.78	3763.76	-270.31	435.2	500.0	-446.0
158879	HN99-123	926.76	927.01	2727.40	3741.57	-343.03	434.8	500.7	-523.3
158880	HN99-123	957.49	957.70	2732.89	3733.09	-372.03	434.3	501.2	-554.0
158881	HN99-123	983.41	983.68	2737.55	3726.05	-396.56	433.8	501.8	-579.9
158882	HN99-123	1033.92	1034.13	2746.43	3712.49	-444.37	432.7	502.7	-630.4
158883	HN99-123	1059.47	1059.72	2750.94	3705.74	-468.62	432.0	503.2	-655.9
158884	HN99-123	1096.83	1097.14	2757.75	3696.24	-504.13	430.8	504.4	-693.3
158885	HN99-123	1119.87	1120.14	2761.95	3690.69	-526.07	429.8	505.2	-716.3
158886	HN99-123	1135.47	1135.82	2764.95	3686.94	-540.96	429.2	505.9	-731.9
158887	HN99-123	1218.87	1219.18	2778.61	3665.88	-620.45	425.5	507.2	-815.1
158888	HN99-123	1243.75	1244.00	2781.66	3659.32	-644.23	424.2	506.6	-840.0
158889	HN99-123	1260.44	1260.74	2783.66	3655.02	-660.25	423.1	506.2	-856.6
158890	HN99-123	1272.66	1272.91	2785.12	3651.95	-671.97	422.3	505.9	-868.8

Table B.1 - Sample Location Data (continued)

Sample Number	DDH Name	From (m)	To (m)	Midpoint Easting (m)	Mid-point Northing (m)	Mid-point Elevation (m)	RTSL Easting (m)	RTSL Northing (m)	RTSL Elevation (m)
158891	HN99-123	1306.86	1307.06	2788.93	3643.45	-704.84	419.8	505.0	-902.9
158892	HN99-123	1295.78	1296.02	2787.75	3646.20	-694.19	420.6	505.3	-891.8
158893	HN99-120	1141.86	1142.05	2770.91	4064.62	-532.10	127.6	699.9	-612.7
158894	HN99-120	1112.43	1112.65	2765.06	4074.11	-504.87	126.5	699.6	-583.3
158895	HN99-120	1073.71	1073.88	2756.90	4087.09	-469.40	124.2	699.0	-544.7
158896	HN99-120	1057.52	1057.72	2753.51	4092.63	-454.47	123.2	698.9	-528.5
158897	HN99-120	1022.08	1022.27	2746.18	4104.71	-421.97	121.1	698.6	-493.1
158898	HN99-120	986.15	986.46	2738.67	4116.92	-389.09	118.8	698.2	-457.3
158899	HN99-120	951.95	952.23	2730.88	4128.32	-357.78	116.6	697.1	-423.2
158900	HN99-120	925.24	925.51	2724.51	4137.11	-333.38	114.8	696.0	-396.6
158901	HN99-124	1374.93	1375.13	2925.93	3883.45	-785.71	261.2	743.6	-931.2
158902	HN99-124	1369.77	1370.04	2925.17	3884.74	-780.81	261.4	743.6	-926.1
158903	HN99-124	1354.61	1354.85	2922.85	3888.57	-766.31	262.2	743.5	-910.9
158904	HN99-124	1339.69	1339.93	2920.50	3892.35	-752.07	262.9	743.4	-896.0
158905	HN99-124	1337.64	1337.82	2920.16	3892.88	-750.08	263.0	743.3	-893.9
158906	HN99-124	1334.86	1335.11	2919.72	3893.57	-747.47	263.1	743.3	-891.2
158907	HN99-124	1320.49	1320.69	2917.40	3897.23	-733.73	263.7	743.1	-876.8
158908	HN99-124	1267.00	1267.22	2908.86	3910.85	-682.73	266.1	742.5	-823.4
158909	HN99-124	1243.60	1243.84	2905.16	3916.84	-660.42	267.1	742.3	-800.0
158910	HN99-124	1237.20	1237.54	2904.16	3918.46	-654.37	267.4	742.3	-793.7
158911	HN99-124	1210.33	1210.60	2899.89	3925.38	-628.73	268.5	742.0	-766.8
158912	HN99-124	1191.78	1191.92	2896.86	3930.20	-611.00	269.2	741.8	-748.2
158913	HN99-124	1166.34	1166.59	2892.67	3936.83	-586.86	270.1	741.5	-722.8
158914	HN99-124	1155.47	1155.70	2890.85	3939.73	-576.53	270.4	741.4	-712.0
158915	HN99-124	1143.88	1144.08	2888.90	3942.89	-565.53	270.7	741.3	-700.4
158916	HN99-124	1122.00	1122.26	2885.22	3949.00	-544.88	271.1	741.1	-678.5
158917	HN99-124	1105.10	1105.31	2882.36	3953.85	-528.92	271.2	741.1	-661.6
158918	HN99-124	1136.36	1136.55	2887.64	3944.97	-558.41	270.9	741.2	-692.8

Table B.1 - Sample Location Data (continued)

Sample Number	DDH Name	From (m)	To (m)	Midpoint Easting (m)	Mid-point Northing (m)	Mid-point Elevation (m)	RTSL Easting (m)	RTSL Northing (m)	RTSL Elevation (m)
158919	HN99-120	1562.23	1562.42	2856.42	3926.47	-919.73	147.7	704.9	-1032.5
158920	HN99-120	1556.15	1556.42	2855.27	3928.35	-914.11	147.5	704.9	-1026.5
158921	HN99-120	1551.62	1551.82	2854.39	3929.78	-909.86	147.4	704.8	-1021.9
158922	HN99-120	1546.80	1547.07	2853.48	3931.27	-905.41	147.3	704.8	-1017.1
158923	HN99-120	1537.12	1537.34	2851.62	3934.31	-896.38	147.0	704.7	-1007.4
158924	HN99-120	1523.05	1523.27	2848.92	3938.71	-883.29	146.6	704.5	-993.3
158925	HN99-120	1497.72	1497.91	2844.07	3946.62	-859.71	146.0	704.3	-968.0
158926	HN99-120	1477.47	1477.67	2840.19	3952.95	-840.87	145.5	704.1	-947.8
158927	HN99-120	1447.63	1447.87	2834.44	3962.33	-813.15	144.6	703.8	-918.0
158928	HN99-120	1426.10	1426.37	2830.23	3969.21	-793.21	143.8	703.6	-896.5
158929	HN99-120	1414.00	1414.30	2827.84	3973.11	-782.02	143.4	703.5	-884.4
158930	HN99-120	1404.26	1404.52	2825.90	3976.27	-772.99	143.0	703.4	-874.6
158931	HN99-120	1372.56	1372.76	2819.51	3986.70	-743.71	141.5	703.1	-842.9
158932	HN99-120	1344.27	1344.48	2813.72	3996.15	-717.70	140.0	702.8	-814.7
158933	HN99-120	1279.61	1279.86	2800.14	4018.29	-658.51	135.8	702.1	-750.2
158934	HN99-120	1239.94	1240.23	2791.51	4031.91	-622.29	133.1	701.4	-710.7
158935	HN99-120	1186.29	1186.56	2779.84	4050.04	-573.15	129.7	700.4	-657.1
158936	HN99-120	1146.04	1146.26	2771.74	4063.27	-535.97	127.8	700.0	-616.9
158937	HN99-126	1310.00	1310.27	2777.47	3867.70	-710.82	229.8	607.2	-840.1
158938	HN99-126	1306.35	1306.61	2776.98	3868.68	-707.33	230.0	607.2	-836.4
158939	HN99-126	1300.29	1300.56	2776.17	3870.31	-701.56	230.3	607.3	-830.4
158940	HN99-126	1291.58	1291.80	2774.98	3872.64	-693.22	230.7	607.5	-821.7
158941	HN99-126	1279.73	1279.97	2773.36	3875.77	-681.91	231.2	607.6	-809.8
158942	HN99-126	1271.96	1272.20	2772.29	3877.81	-674.49	231.6	607.7	-802.1
158943	HN99-126	1262.80	1263.13	2771.01	3880.17	-665.79	232.1	607.8	-793.0
158944	HN99-126	1216.79	1217.00	2764.35	3891.98	-621.76	234.4	607.9	-747.0
158945	HN99-126	1195.57	1195.77	2761.12	3897.42	-601.49	235.4	607.9	-725.8
158946	HN99-126	1177.67	1177.88	2758.32	3902.01	-584.43	236.2	607.7	-707.9

Table B.1 - Sample Location Data (continued)

Sample Number	DDH Name	From (m)	To (m)	Midpoint Easting (m)	Mid-point Northing (m)	Mid-point Elevation (m)	RTSL Easting (m)	RTSL Northing (m)	RTSL Elevation (m)
158947	HN99-126	1122.80	1123.03	2749.91	3916.20	-532.11	238.5	607.5	-653.1
158948	HN99-126	1117.00	1117.24	2749.04	3917.71	-526.58	238.8	607.5	-647.3
158949	HN99-126	1104.93	1105.16	2747.23	3920.86	-515.07	239.3	607.6	-635.2
158950	HN99-126	1091.41	1091.63	2745.21	3924.39	-502.16	239.9	607.6	-621.7
158951	HN99-126	1081.76	1082.04	2743.78	3926.90	-492.99	240.3	607.6	-612.1
158952	HN99-126	1063.75	1064.02	2741.11	3931.61	-475.81	241.1	607.6	-594.1
158953	HN99-126	1023.65	1023.86	2734.86	3942.16	-437.60	242.7	607.5	-554.0
158954	HN99-126	979.35	979.58	2727.85	3953.91	-395.48	244.2	607.3	-509.8
158955	HN99-128	1406.88	1407.17	2989.98	3951.30	-820.86	224.0	833.0	-955.1
158956	HN99-128	1395.95	1396.25	2988.69	3954.02	-810.35	224.8	833.2	-944.2
158957	HN99-128	1385.45	1385.63	2987.43	3956.65	-800.20	225.5	833.5	-933.6
158958	HN99-128	1381.37	1381.65	2986.95	3957.65	-796.33	225.8	833.5	-929.6
158959	HN99-128	1230.24	1230.43	2967.17	3996.90	-651.69	234.1	836.0	-778.7
158960	HN99-128	1194.84	1195.10	2961.68	4006.65	-618.14	235.0	836.2	-743.3
158961	HN99-128	1160.66	1160.95	2955.97	4016.23	-585.85	235.6	836.0	-709.2
158962	HN99-128	1133.32	1133.53	2951.24	4023.93	-560.01	235.9	835.8	-681.8
158963	HN99-128	1121.51	1121.75	2949.16	4027.25	-548.88	236.1	835.6	-670.0
158964	HN99-128	1103.57	1103.75	2945.94	4032.30	-531.94	236.2	835.4	-652.1
158965	HN99-128	1093.14	1093.42	2944.07	4035.20	-522.14	236.3	835.2	-641.7
158966	HN99-128	1083.30	1083.56	2942.29	4037.93	-512.85	236.5	835.0	-631.8
158967	HN99-128	1071.49	1071.71	2940.13	4041.17	-501.68	236.6	834.8	-620.0
158968	HN99-128	1031.48	1031.75	2932.74	4051.99	-463.91	237.3	833.8	-580.0
158969	HN99-122	1495.37	1495.66	3134.14	4005.77	-898.84	220.8	985.1	-1036.9
158970	HN99-122	1479.13	1479.32	3132.49	4010.62	-883.37	221.3	986.1	-1020.6
158971	HN99-122	1449.81	1450.07	3129.06	4019.57	-855.69	221.9	987.6	-991.4
158972	HN99-122	1423.00	1423.19	3125.47	4027.96	-830.45	222.0	988.7	-964.6
158973	HN99-122	1412.82	1413.05	3124.10	4031.12	-820.90	222.1	989.1	-954.4
158974	HN99-122	1377.84	1378.17	3119.42	4041.90	-788.00	222.3	990.4	-919.5

Table B.1 - Sample Location Data (continued)

Sample Number	DDH Name	From (m)	To (m)	Midpoint Easting (m)	Mid-point Northing (m)	Mid-point Elevation (m)	RTSL Easting (m)	RTSL Northing (m)	RTSL Elevation (m)
158975	HN99-122	1347.22	1347.51	3115.33	4051.31	-759.13	222.6	991.6	-888.9
158976	HN99-122	1333.18	1333.41	3113.44	4055.66	-745.88	222.7	992.1	-874.8
158977	HN99-122	1309.82	1310.04	3110.29	4062.91	-723.89	222.9	993.0	-851.5
158978	HN99-122	1287.80	1288.10	3107.30	4069.76	-703.22	223.0	993.8	-829.5
158979	HN99-122	1246.06	1246.39	3101.30	4083.02	-664.12	222.7	995.3	-787.8
158980	HN99-122	1206.80	1207.07	3095.06	4095.65	-627.44	222.1	996.2	-748.5
158981	HN99-122	1189.90	1190.15	3092.29	4101.03	-611.66	221.8	996.5	-731.6
158982	HN99-122	1155.93	1156.16	3086.55	4112.01	-580.02	221.0	997.0	-697.7
158983	HN99-122	1123.61	1123.84	3080.88	4122.77	-550.07	219.8	997.5	-665.4
158984	HN99-127	1293.86	1294.11	2748.84	3724.53	-697.88	337.3	510.8	-865.4
158985	HN99-127	1277.28	1277.49	2747.62	3729.89	-682.22	337.7	512.4	-848.9
158986	HN99-127	1261.77	1262.06	2746.38	3734.82	-667.60	338.2	513.8	-833.5
158987	HN99-127	1221.72	1221.94	2742.73	3747.35	-629.70	339.2	516.9	-793.6
158988	HN99-127	1207.52	1207.79	2741.32	3751.75	-616.30	339.5	517.9	-779.4
158989	HN99-127	1192.64	1192.89	2739.77	3756.34	-602.22	339.9	518.8	-764.6
158990	HN99-127	1175.42	1175.67	2737.89	3761.62	-585.94	340.3	519.8	-747.4
158991	HN99-127	1133.66	1133.96	2732.93	3774.43	-546.53	341.0	522.0	-705.7
158992	HN99-127	1130.00	1130.20	2732.47	3775.58	-543.03	341.1	522.1	-702.0
158993	HN99-127	1104.80	1105.07	2729.18	3783.42	-519.35	341.2	523.2	-676.9
158994	HN99-127	1073.18	1073.47	2724.84	3793.41	-489.68	341.2	524.4	-645.3
158995	HN99-127	1050.06	1050.30	2721.60	3800.88	-468.01	341.0	525.4	-622.2
158996	HN99-127	1043.49	1043.71	2720.66	3803.03	-461.86	340.9	525.6	-615.6
158997	HN99-127	1015.69	1015.99	2716.74	3811.98	-435.88	340.7	526.7	-587.9
158998	HN99-127	993.33	993.55	2713.67	3818.78	-414.76	340.9	527.4	-565.5
158999	HN99-127	966.56	966.83	2710.13	3826.43	-389.38	341.7	528.2	-538.7
159000	HN99-127	955.19	955.44	2708.62	3829.69	-378.58	342.1	528.5	-527.4

Table B.2 – Field-Based Sample Descriptions

Sample Number	Interval Rock Type	Sample Rock Type	Field Modifier	Alteration
158779	Greywacke	Greywacke	interbedded with siltite; sulphide stockwork	
158780	Greywacke	Argillite		
158781	Siltite	Argillaceous Siltite		
158782	Siltite	Siltite	interbedded with greywacke;	weakly chlorite-altered
158783	Siltite	Siltite	interbedded with greywacke;	weakly chlorite-altered
158784	Siltite	Siltite	with disseminated sulphide	chloritic
158785	QTZ-eye Tuff	QTZ-eye Tuff		
158786	Cherty Tuff	Cherty Tuff		
158787	Argillite	Argillite		chloritic
158788	QTZ-eye Tuff	QTZ-eye Tuff		
158789	Siltite	Siltite	with minor greywacke	
158790	Siltite	Siltite	with minor greywacke	
158791	QTZ-eye Tuff	QTZ-eye Tuff		
158792	Basalt	Basalt		
158793	Basalt	Basalt		
158794	Black Dyke	Black Dyke	probably chilled margin to QFP	
158795	QFP	QFP		
158796	QFP	QFP		
158797	QFP	QFP		
158798	Cherty Tuff	Cherty Tuff		
158799	Cherty Tuff	Cherty Tuff		
158800	Greywacke	Greywacke		
158801	Greywacke	Greywacke	banded	chloritic

Table B.2 - Field-Based Sample Descriptions (continued)

Sample Number	Interval Rock Type	Sample Rock Type	Field Modifier	Alteration
158802	Greywacke	Greywacke	banded	chloritic
158803	Greywacke	Greywacke	interbedded with argillite	patchy bands of chlorite
158804	Greywacke	Siltite		
158805	Argillaceous Siltite	Argillite		chloritic
158806	Mafic Dyke	Dyke		
158807	Cherty Tuff	Siltite	deformed	
158808	Greywacke	Siltite	massive	
158809	Cherty Tuff	Silty argillite		
158810	Cherty Tuff	Cherty Tuff		
158811	Cherty Tuff	Cherty Tuff	Banded	
158812	Siltite	Siltite		
158813	Cherty Tuff	Cherty Tuff		
158814	QFP	QFP		
158815	QFP	QFP		
158816	QFP	QFP		
158817	Siltite	Silty Argillite		
158818	Siltite	Siltite		
158819	Siltite	Silty Argillite		
158820	Siltite	Siltite		
158821	Greywacke	Argillite		chloritic
158822	Greywacke	Silty Argillite		
158823	Felsic Tuff	Felsic Dyke		
158824	Felsic Tuff	Felsic Dyke		

Table B.2 - Field-Based Sample Descriptions (continued)

Sample Number	Interval Rock Type	Sample Rock Type	Field Modifier	Alteration
158825	Siltite	Argillite		chloritic
158826	Dyke	Felsic Dyke		
158827	Greywacke	Silty Argillite		
158828	Siltite	Siltite		weakly muscovite-altered
158829	Siltite	Siltite		muscovite-altered
158830	Siltite	Silty Argillite		
158831	Felsic Tuff	Felsic Tuff	quartz-phyric	
158832	QFP	QFP		
158833	QFP	QFP		
158834	Cherty Tuff	Siltite	with sulphide stockwork	muscovite-altered
158835	Cherty Tuff	Argillite		muscovite-altered
158836	Greywacke	Siltite		mildly muscovite-altered
158837	Siltite/ Cherty Tuff	Siltite		very muscovite-altered
158838	Siltite/ Cherty Tuff	Siltite		muscovite-altered
158839	Siltite	Siltite		muscovite-altered
158840	Siltite	Silty Argillite		muscovite-altered
158841	Siltite	Argillite		muscovite-altered
158842	Argillite	Cherty Tuff		muscovite-altered
158843	Siltite	Argillite	with sulphide stockwork	muscovite-altered
158844	Cherty Tuff	Cherty Tuff		muscovite-altered
158845	Cherty Tuff	Greywacke		
158846	Rhyolite Flow/ Dyke?	Siltite		
158847	Siltite	Siltite		chloritic

Table B.2 - Field-Based Sample Descriptions (continued)

Sample Number	Interval Rock Type	Sample Rock Type	Field Modifier	Alteration
158848	Rhyolite Flow	Rhyolite		
158849	Rhyolite Flow	Rhyolite		
158850	QFP	QFP		
158851	Siltite	Siltite	minor greywacke/argillite layers & sulphide stockwork	strongly chlorite-altered
158852	Siltite	Siltite	with argillite & greywacke beds	
158853	Siltite	Siltite	with argillite & greywacke beds	
158854	Siltite	Siltite	with argillite & greywacke beds	weakly muscovite-altered
158855	Siltite	Siltite	with argillite & greywacke beds	moderately muscovite-altered
158856	Sandy Siltite	Sandy Siltite		mildly muscovite-altered
158857	Siltite	Siltite	with argillite & greywacke beds	moderately muscovite-altered
158858	?	?	unknown protolith	intensely muscovite-alteration
158859	?	?	unknown protolith	intensely muscovite-alteration
158860	Siltite	Siltite-Argillite	interbedded	weakly muscovite-altered in patches
158861	Felsic Tuff	Felsic Tuff		muscovite-altered
158862	Felsic Tuff	Felsic Tuff		muscovite-altered
158863	QFP	QFP		
158864	Cherty Tuff	Cherty Tuff		
158865	QFP	QFP		
158866	Cherty Tuff	Cherty Tuff		
158867	Cherty Tuff	Cherty Tuff		
158868	Cherty Tuff	Cherty Tuff		
158869	Cherty Tuff	Cherty Tuff		
158870	Cherty Tuff	Cherty Tuff		

Table B.2 - Field-Based Sample Descriptions (continued)

Sample Number	Interval Rock Type	Sample Rock Type	Field Modifier	Alteration
158871	Cherty Tuff	Siltite		
158872	Siltite	Siltite	interbedded with chlorite-argillite & greywacke	
158873	Felsic Dyke	Felsic Dyke		
158874	Dyke	Felsic Dyke		
158875	Siltite	Felsic Dyke		
158876	Siltite	Siltite	with minor greywacke	moderately muscovite-altered
158877	Siltite	Greywacke	with minor Siltite; moderately stockwork sulphides	
158878	Argillite	Siltite	with interbedded greywacke	moderately chloritized
158879	Siltite	Siltite	with moderately stockwork sulphides	
158880	Dyke	Dyke		
158881	Siltite	Siltite	with bedded and moderate stockwork sulphides	
158882	Greywacke	Greywacke	interbedded with siltite	
158883	Greywacke	Greywacke		
158884	Siltite	Siltite	with bedded and stockwork sulphides	variably muscovite-altered
158885	Siltite	Siltite	with bedded and stockwork sulphides	variably muscovite-altered
158886	Dyke	Dyke		
158887	Greywacke	Greywacke		moderately & variably muscovite-altered
158888	Greywacke	QFP		
158889	QFP	QFP		
158890	QTZ-eye Tuff	QTZ-eye Tuff		
158891	Siltite	Siltite		very bleached moderately muscovite-altered
158892	Cherty Tuff	Cherty Tuff		
158893	Greywacke	Greywacke	with siltite	

Table B.2 - Field-Based Sample Descriptions (continued)

Sample Number	Interval Rock Type	Sample Rock Type	Field Modifier	Alteration
158894	Siltite	Siltite	with greywacke	
158895	Siltite	Greywacke		
158896	Siltite	Siltite	interbedded with greywacke	
158897	Siltite	Siltite	interbedded with argillite	
158898	Argillite	Argillite	variably bleached	
158899	Siltite	Siltite		chloritic
158900	Siltite	Siltite		muscovite-altered
158901	QFP	QFP		
158902	Siltite	Argillaceous Siltite		
158903	QFP	QFP		
158904	Muscovite Schist	Muscovite Schist	Ankerite+Pyrite	
158905	Muscovite Schist	Muscovite Schist		
158906	Siltite	Siltite		
158907	Siltite	Argillaceous Siltite	Pyrite Interbeds	
158908	Felsic Dyke	Felsic Dyke	Quartz Phyric	
158909	Felsic Dyke	Felsic Dyke		
158910	Argillite	Argillite		
158911	Argillite	Argillite		
158912	Felsic Dyke	Felsic Dyke		
158913	Siltite	Argillite	Quartz Stringers	
158914	Cherty Tuff	Cherty Tuff		
158915	Felsic Dyke	Felsic Dyke		
158916	Siltite	Argillite	Disseminated Pyrite	

Table B.2 - Field-Based Sample Descriptions (continued)

Sample Number	Interval Rock Type	Sample Rock Type	Field Modifier	Alteration
158917	Siltite	Siltite		
158918	Cherty Tuff	Cherty Tuff		
158919	QZ Eye Tuff	QZ Eye Tuff	Deformed quartz eyes	
158920	QZ Eye Tuff	QZ-FS Phyric Tuff	Aphyric top	
158921	QZ Eye Tuff	QZ-FS Phyric Tuff	quartz-feldspar rich base	
158922	Argillite	Felsic Dyke	Banded	
158923	Felsic Tuff	QZ-Phyric Tuff	Aphyric top	
158924	Felsic Tuff	QZ-Phyric Tuff	quartz rich base	
158925	Silty Argillite	Silty Argillite		
158926	Felsic Tuff	Felsic Tuff		
158927	Silty Argillite	Silty Argillite		
158928	Argillite	Argillite	with chert bands	muscovite altered
158929	Felsic Dyke	Felsic Dyke		
158930	Argillite	Argillite		
158931	Silty Argillite	Silty Argillite	Disseminated Pyrite	
158932	Argillite	Argillite	With sulphide stockwork	chloritic
158933	Sandy Siltite	Sandy Siltite		
158934	Argillite	Argillite		chloritic
158935	Silty Argillite	Silty Argillite	Strong SX stockwork	
158936	Siltite	Siltite		
158937	Muscovite Schist	Muscovite Schist	Banded	
158938	Felsic Dyke	Felsic Tuff		
158939	Felsic Tuff	Felsic Tuff		chloritic

Table B.2 - Field-Based Sample Descriptions (continued)

Sample Number	Interval Rock Type	Sample Rock Type	Field Modifier	Alteration
158940	Felsic Dyke	Felsic Dyke	quartz-phyric	
158941	Greywacke	Greywacke		muscovite altered
158942	Greywacke	Greywacke	sulphidic + carbonate pressure shadows	
158943	Argillite	Argillite		strongly chloritized
158944	Siltite	Siltite		
158945	Silty Argillite	Siltite		muscovite altered
158946	Siltite	Siltite		chlorite altered
158947	Siltite	Siltite		
158948	Greywacke	Greywacke		
158949	Siltite	Siltite	with semi-massive sulphide	
158950	Siltite	Siltite		chloritic
158951	Greywacke	Greywacke		muscovite altered
158952	Greywacke	Greywacke		
158953	Siltite	Siltite		
158954	Siltite	Argillite		
158955	Felsic Tuff	Felsic Tuff		muscovite altered
158956	Argillite	Argillite		chlorite-altered with carbonate
158957	Felsic Tuff	Felsic Tuff	with disseminated semi-massive sulphide	muscovite altered
158958	QTZ-eye Tuff	QTZ-eye Tuff		chloritic
158959	Siltite	Siltite		
158960	Siltite	Siltite	argillaceous	
158961	Siltite	Siltite		
158962	Sandy Siltite	Siltite	argillaceous with bedded pyrite	

Table B.2 - Field-Based Sample Descriptions (continued)

Sample Number	Interval Rock Type	Sample Rock Type	Field Modifier	Alteration
158963	Felsic Dyke	Felsic Dyke		
158964	Argillite	Argillite	with quartz veins	chloritic
158965	Argillite	Silty Argillite		chloritic
158966	QTZ-eye Tuff	QTZ-eye Tuff		
158967	QTZ-eye Tuff	QTZ-eye Tuff	bleached	
158968	Siltite	Siltite		
158969	Cherty Tuff	Cherty Tuff		
158970	QFP	QFP		
158971	Silty Argillite	Silty Argillite		
158972	QFP	QFP		
158973	Siltite	Siltite		muscovite altered
158974	Siltite	Silty Argillite		chloritic
158975	Siltite	Siltite		with carbonate spots
158976	Silty Argillite	Silty Argillite		chloritic
158977	Siltite	Silty Argillite		
158978	Sandy Siltite	Tuff	quartz-feldspar phyric	
158979	Greywacke	Greywacke		
158980	Sandy Siltite	Siltite	with disseminated pyrrhotite	
158981	Siltite	Siltite	argillaceous	
158982	Greywacke	Siltite	with sulphides	
158983	Siltite	Siltite	with sulphides	
158984	QFP	QFP		
158985	Felsic Tuff	Felsic Tuff		

Table B.2 - Field-Based Sample Descriptions (continued)

Sample Number	Interval Rock Type	Sample Rock Type	Field Modifier	Alteration
158986	Felsic Tuff	Felsic Tuff		muscovite-altered
158987	Argillite	Argillite		chloritic
158988	Siltite	Siltite		
158989	Felsic Dyke	Felsic Dyke		
158990	Siltite	Siltite	interbedded with argillite & bedded sulphide	
158991	Argillite	Argillite		chloritic
158992	Siltite	Siltite		
158993	Siltite	Siltite-Argillite	bedding contact	
158994	Argillaceous Siltite	Argillaceous Siltite		
158995	Purple Siltite	Purple Siltite		
158996	Siltite	Siltite	with sulphide stockwork	
158997	Siltite	Argillite	deformed	
158998	Siltite	Argillite		chloritic
158999	Argillite	Argillite		chloritic
159000	Siltite	Siltite		

Table B.3.1 – Lab-Based Sample Descriptions

Sample Number	Lab Rock Type	Lab Description	Alteration (1- 5)				Mineralization (1-5)					%
			CB	CL	MU	SL	PO	PY	GN	SP	CP	QV
158779	Greywacke		0	0	0	0	0	1	0	0	1	0
158780	Claystone	siltite at top and bottom	0	2	0	0	0	2	0	0	1	0
158781	Mudstone		0	2	1	0	0	0	0	0	0	0
158782	Claystone		0	2	1	4	0	1	0	0	1	0
158783	Siltstone	weakly crenulated (microfolding)	0	1	0	0	0	1	0	0	1	0
158784	Siltstone		0	3	1	1	0	1	0	0	1	0
158785	QTZ-eye Tuff	mild carbonate (calcite/dolomite) occurrence along fracture surface	1	0	2	2	0	0	0	0	0	0
158786	Cherty Tuff	disseminated sulphide parallel to foliation	0	0	2	3	2	3	0	0	1	0
158787	Claystone		0	2	0	1	0	2	0	0	0	0
158788	QTZ-eye Tuff	weakly deformed	0	0	1	0	0	0	0	0	0	0
158789	Siltstone	weakly crenulated (microfolding)	0	1	1	2	0	0	0	0	0	0
158790	Siltstone		1	1	1	1	0	1	0	0	0	0
158791	QTZ-eye Tuff	mild carbonate (calcite/dolomite) occurrence along fracture surface	1	0	1	2	0	1	0	0	0	0
158792	Basalt	minor calcite/dolomite	1	0	0	0	0	0	0	0	0	0
158793	Basalt	minor calcite/dolomite	1	0	0	0	0	1	0	0	0	0
158794	Black Dyke	minor carbonate (calcite/dolomite) veins	1	3	0	2	0	2	0	0	2	1
158795	QFP	fracture @ 42 to-core-axis; pale pinkish	0	1	1	1	0	1	0	0	0	0
158796	QFP		0	0	2	2	0	1	0	0	1	0
158797	QFP		0	0	2	2	0	1	0	0	1	0
158798	Cherty Tuff	cleaved	0	0	1	3	0	0	0	0	0	1
158799	Cherty Tuff	well cleaved and silicified	0	0	2	4	0	0	0	0	0	0
158800	Greywacke		0	0	0	3	0	0	0	0	0	0
158801	Greywacke	looks altered?	0	0	0	2	0	0	0	0	0	0
158802	Greywacke		0	0	0	2	0	1	0	0	1	0
158803	Greywacke		0	2	1	1	0	2	0	0	2	1

Table B.3.1 – Lab-Based Sample Descriptions (continued)

Sample Number	Lab Rock Type	Lab Description	Alteration (1-5)				Mineralization (1-5)					%
			CB	CL	MU	SL	PO	PY	GN	SP	CP	QV
158804	Greywacke		0	1	1	2	0	0	0	0	0	0
158805	Claystone		0	3	1	1	0	1	0	2	1	0
158806	Dyke	pinkish with abundant carbonate (calcite/dolomite)	3	2	1	1	0	0	0	0	0	0
158807	Cherty Tuff	deformed	0	0	2	3	0	0	0	0	0	0
158808	Siltstone		0	0	1	2	0	0	0	0	0	0
158809	Mudstone		0	0	1	3	0	0	0	0	0	0
158810	Cherty Tuff		0	0	2	3	0	1	0	0	0	0
158811	Cherty Tuff	moderately deformed	2	1	2	2	0	1	0	0	1	0
158812	Siltstone	strongly deformed	0	2	1	2	0	2	0	0	1	0
158813	Cherty Tuff	strongly deformed	0	0	2	2	0	2	0	0	1	0
158814	QFP	moderate carbonate (calcite/dolomite) occurrence	1	2	1	1	0	1	0	0	0	0
158815	QFP		0	0	2	2	0	2	0	0	2	0
158816	QFP		0	0	1	2	0	1	0	0	1	0
158817	Mudstone		0	1	1	0	0	0	0	0	0	0
158818	Siltstone	fine grained Py & Cpy	0	0	0	1	0	1	0	0	1	0
158819	Claystone		0	1	0	0	0	0	0	0	0	0
158820	Siltstone		0	0	0	2	0	2	0	0	2	0
158821	Claystone		0	2	0	0	2	2	0	0	2	0
158822	Mudstone	disseminated Py	0	1	0	0	0	1	0	0	1	0
158823	Siltstone	spotted with calcite/dolomite	1	1	1	1	0	1	0	0	1	0
158824	Dyke	Py blebs; no carbonate	0	0	0	0	0	2	0	0	0	0
158825	Claystone		0	2	0	0	0	1	0	0	0	0
158826	Siltstone	minor calcite/dolomite veins	1	0	0	0	0	0	0	0	0	0
158827	Claystone	minor calcite/dolomite veins	1	3	0	0	0	0	0	0	0	0
158828	Siltstone	dissem Sx	0	0	2	2	0	2	0	0	1	0

Table B.3.1 – Lab-Based Sample Descriptions (continued)

Sample Number	Lab Rock Type	Lab Description	Alteration (1- 5)				Mineralization (1-5)					%
			CB	CL	MU	SL	PO	PY	GN	SP	CP	QV
158829	Siltstone	disseminated fine grained Py; minor calcite/dolomite vein	1	0	1	0	0	2	0	0	2	0
158830	Mudstone	disseminated Py; weak cleavage development	0	1	0	0	0	2	0	0	2	0
158831	Felsic Tuff	weakly crenulated (microfolding)	0	0	0	0	0	0	0	0	0	0
158832	QFP	preferred orientation of quartz-feldspar grains	0	0	1	0	0	0	0	0	0	0
158833	QFP	weakly crenulated (microfolding)	0	1	1	2	0	0	0	0	0	0
158834	Siltstone	massive sulphide	0	0	3	2	0	2	2	2	2	0
158835	Claystone		0	1	3	2	0	2	0	0	2	0
158836	Siltstone		0	0	1	2	0	2	0	0	1	0
158837	Cherty Tuff		0	0	3	3	0	0	0	0	0	0
158838	Siltstone		0	0	2	1	0	0	0	0	0	0
158839	Siltstone	disseminated fine grained Py & Cpy	0	0	1	2	0	1	0	0	1	0
158840	Siltstone	abundant sulphide	0	0	1	2	0	5	0	0	1	0
158841	Claystone		0	0	2	0	1	2	1	1	1	0
158842	Cherty Tuff	disseminated sulphide; deformed and sericitized	0	0	3	3	2	2	0	0	0	0
158843	Claystone		0	1	0	0	0	2	0	0	0	0
158844	Cherty Tuff	minor disseminated sulphide	0	0	1	3	0	1	0	0	0	0
158845	Greywacke	weakly deformed; stretched quartz phenocrysts	0	0	0	1	0	0	0	0	0	0
158846	Siltstone	resembles a felsic tuff	1	1	0	2	0	0	0	0	0	0
158847	Claystone		0	3	0	2	0	2	0	0	0	0
158848	Rhyolite	quartz vein parallel to core axis	0	0	1	0	0	0	0	0	0	0
158849	Rhyolite		0	0	1	0	0	0	0	0	0	0
158850	QFP	pale pinkish feldspar and quartz porphyry	1	0	2	0	0	0	0	0	0	0
158851	Mudstone		0	2	1	2	0	2	0	0	2	0
158852	Siltstone	massive sulphide	0	2	1	3	1	4	0	1	3	2
158853	Siltstone		0	1	1	1	0	1	0	0	1	0

Table B.3.1 – Lab-Based Sample Descriptions (continued)

Sample Number	Lab Rock Type	Lab Description	Alteration (1- 5)				Mineralization (1-5)					%
			CB	CL	MU	SL	PO	PY	GN	SP	CP	QV
158854	Mudstone		1	2	1	2	0	2	0	2	2	0
158855	Mudstone		0	3	1	1	0	2	0	0	2	0
158856	Siltstone	moderately deformed	0	0	1	2	0	0	0	0	0	0
158857	Mudstone		0	3	1	1	0	1	0	0	1	0
158858	Felsic Tuff	tuffaceous? unaltered felsic tuff ?	0	0	1	2	0	0	0	0	0	0
158859	Felsic Tuff	strongly sericitized with Py crystals;	0	0	4	2	0	5	0	0	2	0
158860	Mudstone		0	2	1	1	0	0	0	0	0	0
158861	Felsic Tuff	deformed	0	0	2	2	0	3	0	0	0	0
158862	Felsic Tuff	deformed with abundant disseminated Py	0	0	4	2	0	10	0	0	2	0
158863	QFP	fracture @ 46 to-core-axis	1	0	1	1	0	2	0	0	1	0
158864	Cherty Tuff	well cleaved	1	0	2	3	1	2	0	0	2	0
158865	QFP		0	1	1	0	0	1	0	0	0	0
158866	Cherty Tuff	well cleaved; mod disseminated fine grained sulphide	0	0	2	3	2	3	0	0	2	0
158867	Cherty Tuff	strongly deformed	0	2	1	2	0	1	0	0	0	0
158868	Cherty Tuff		1	0	1	2	0	0	0	0	0	0
158869	Cherty Tuff		2	0	3	2	0	2	0	0	1	0
158870	Cherty Tuff	moderately deformed	0	0	3	2	0	2	0	0	2	0
158871	Siltstone	unaltered	0	0	0	1	0	1	0	0	1	0
158872	Siltstone	thin band of argillite present	0	1	1	1	0	2	0	0	0	0
158873	Dyke	Py blebs; calcite/dolomite dissem	2	0	0	0	0	2	0	0	1	0
158874	Dyke	Py blebs; calcite/dolomite dissem	2	0	0	0	0	2	0	0	0	0
158875	Dyke		0	1	0	0	0	1	0	0	0	0
158876	Siltstone		0	0	2	2	0	2	0	0	1	0
158877	Greywacke	coarse grained Py and disseminated Cpy	0	2	0	0	0	2	0	0	1	0
158878	Claystone	microfolding	0	2	1	2	0	0	0	0	0	0

Table B.3.1 – Lab-Based Sample Descriptions (continued)

Sample Number	Lab Rock Type	Lab Description	Alteration (1- 5)				Mineralization (1-5)					%
			CB	CL	MU	SL	PO	PY	GN	SP	CP	QV
158879	Claystone	some sort of pressure solution present	0	2	0	2	0	2	1	1	1	1
158880	Dyke	calcite/dolomite veinlets	2	0	0	1	0	0	0	0	0	0
158881	Mudstone		0	2	0	1	0	2	0	0	2	0
158882	Greywacke		0	1	0	2	0	0	0	0	0	0
158883	Greywacke	crenulated	0	1	0	0	0	1	0	0	0	0
158884	Siltstone		0	0	1	1	2	1	0	1	1	0
158885	Siltstone		0	1	0	2	0	0	0	0	0	1
158886	Dyke	jointing @ 40 to-core-axis; calcite/dolomite veins	2	0	0	1	0	0	0	0	0	0
158887	Greywacke	minor argillite bands	0	0	2	1	0	1	0	0	1	0
158888	Cherty Tuff	minor cleavage development	0	0	2	2	0	3	0	0	2	0
158889	QTZ-eye Tuff	predominantly quartz-phyric	0	0	2	2	0	1	0	0	0	0
158890	Felsic Tuff		0	0	0	0	0	0	0	0	0	0
158891	Siltstone	minor calcite/dolomite filled joints	2	0	1	2	0	0	0	0	0	0
158892	Felsic Tuff	resembles quartz-eye-tuff; carbonate along fracture surface	2	1	1	1	0	1	0	0	0	0
158893	Mudstone		0	2	2	2	0	2	0	0	2	0
158894	Mudstone		0	2	1	1	0	0	0	0	0	0
158895	Greywacke		0	1	1	0	0	0	0	0	0	0
158896	Siltstone	jointing @ 40to-core-axis	0	0	0	0	0	0	0	0	0	0
158897	Mudstone	disseminated sulphide	0	2	1	2	0	2	0	0	2	1
158898	Claystone	weakly deformed	0	1	1	1	0	2	0	0	1	0
158899	Siltstone	moderately deformed with sericitization	0	0	3	2	0	2	0	0	0	1
158900	Siltstone	sericitized; muscovite-altered	0	0	3	2	3	1	0	0	0	0
158901	QFP	weakly deformed	0	1	0	1	0	0	0	0	0	0
158902	Mudstone		0	3	1	2	0	2	0	0	2	0
158903	QFP	mildly deformed	0	0	1	1	0	0	0	0	0	0

Table B.3.1 – Lab-Based Sample Descriptions (continued)

Sample Number	Lab Rock Type	Lab Description	Alteration (1- 5)				Mineralization (1-5)					%
			CB	CL	MU	SL	PO	PY	GN	SP	CP	QV
158904	Siltstone	disseminated sulphide (~10%) and Fe-staining on core	2	0	0	2	0	3	0	0	2	0
158905	Siltstone	moderately deformed	0	0	3	3	0	1	0	0	1	0
158906	Siltstone		0	0	0	2	0	1	0	1	1	0
158907	Siltstone	weakly deformed	0	1	1	2	0	3	0	0	1	0
158908	Dyke	Disseminated sulphide; minor Py phenocrysts	1	0	1	2	0	2	0	0	2	0
158909	Dyke	Py phenocrysts	2	1	1	2	0	2	0	0	1	0
158910	Mudstone	weakly deformed	2	2	2	2	0	2	0	1	0	1
158911	Claystone	fine grained Py present	0	2	1	2	0	1	0	0	0	0
158912	Dyke	moderate calcareous (calcite/dolomite)	2	0	1	2	0	1	0	0	1	0
158913	Mudstone		0	2	1	1	0	1	0	2	0	1
158914	Dyke	looks like quartz-eye tuff	2	0	1	2	0	1	0	0	0	0
158915	Dyke	moderate calcareous (calcite/dolomite)	2	0	1	1	0	0	0	0	0	0
158916	Claystone	massive sulphide ~ 10%	0	3	1	2	6	1	0	0	1	0
158917	Siltstone		0	2	1	2	0	2	0	1	1	1
158918	Cherty Tuff	speckled	2	0	2	2	0	1	0	0	1	0
158919	QTZ-eye Tuff	microfolding/crenulation ~ 20 to-core-axis	0	0	0	1	0	0	0	0	0	0
158920	QTZ-eye Tuff	calcite/dolomite on fracture surface	1	0	1	1	0	1	0	0	1	0
158921	QFP	preferred orientation ~ 40 to-core-axis	0	0	2	2	0	0	0	0	0	0
158922	Dyke	highly deformed; crenulated/cleaved/microfolding	1	2	1	1	0	0	0	0	0	0
158923	QTZ-eye Tuff	quartz-eyes not well developed; mildly deformed	0	0	1	1	0	0	0	0	0	0
158924	QTZ-eye Tuff		0	1	2	1	0	0	0	0	0	0
158925	Mudstone		0	2	1	1	0	0	0	0	0	0
158926	QFP	Dyke	0	0	1	2	0	0	0	0	0	0
158927	Mudstone	moderately deformed	0	2	1	1	0	2	0	0	1	0
158928	Cherty Tuff		0	0	2	4	0	0	0	0	0	0

Table B.3.1 – Lab-Based Sample Descriptions (continued)

Sample Number	Lab Rock Type	Lab Description	Alteration (1- 5)				Mineralization (1-5)					%
			CB	CL	MU	SL	PO	PY	GN	SP	CP	QV
158929	Dyke	resembles quartz-eye tuff	0	0	0	2	0	0	0	0	0	0
158930	Mudstone		0	2	1	1	0	0	0	0	0	0
158931	Mudstone		0	0	3	1	0	0	0	0	0	0
158932	Claystone	variable sulphide stockwork	1	2	2	1	2	2	0	2	1	0
158933	Greywacke		0	1	2	2	0	0	0	0	0	0
158934	Claystone		0	3	0	2	0	1	0	0	1	0
158935	Mudstone	massive sulphide (bedded & disseminated)	0	1	1	2	0	5	0	0	5	0
158936	Siltstone	microfolding of quartz veins probably due to deformation	0	1	1	3	0	1	0	0	1	2
158937	Mudstone	very strongly cleaved	0	0	5	1	0	0	0	0	0	0
158938	QTZ-eye Tuff	gritty with minor argillite inclusions	0	1	1	2	2	1	0	0	1	0
158939	Felsic Tuff	calcite/dolomite on fracture surface; looks like a dyke	2	2	1	2	0	0	0	0	0	0
158940	Dyke	dissem SX	2	0	1	2	0	3	0	0	2	0
158941	Greywacke		0	0	1	3	0	1	1	1	0	0
158942	Greywacke	massive disseminated sulphide	0	2	0	2	0	5	0	0	0	0
158943	Claystone	weakly deformed	2	3	0	1	0	1	0	0	1	1
158944	Siltstone	crenulated, bedded fine grained sulphide stockwork	0	0	2	2	0	2	2	2	0	0
158945	Siltstone	moderately deformed	1	2	2	3	0	2	0	0	0	2
158946	Siltstone		0	1	1	2	0	1	0	0	0	0
158947	Siltstone		0	1	0	2	0	0	2	1	0	0
158948	Greywacke	sulphide -filled vein	0	1	2	3	0	1	2	1	1	0
158949	Siltstone	abundant disseminated stockwork sulphide	0	1	0	2	0	20	0	0	5	1
158950	Siltstone	mildly spotted like a dyke	0	2	0	2	0	1	1	2	0	0
158951	Greywacke	strongly sericitized to grey green	0	0	3	1	0	0	0	0	0	0
158952	Siltstone		0	1	1	2	0	0	1	1	0	0
158953	Siltstone		0	2	1	2	0	0	2	1	0	2

Table B.3.1 – Lab-Based Sample Descriptions (continued)

Sample Number	Lab Rock Type	Lab Description	Alteration (1- 5)				Mineralization (1-5)					%
			CB	CL	MU	SL	PO	PY	GN	SP	CP	QV
158954	Mudstone		0	1	2	2	0	1	0	1	0	1
158955	Felsic Tuff		0	0	1	2	0	2	0	0	1	0
158956	Claystone	strong calcite/dolomite	4	3	0	1	0	0	0	0	0	0
158957	Felsic Tuff		0	0	2	3	0	0	0	0	0	0
158958	QTZ-eye Tuff		0	1	0	0	0	0	0	0	0	1
158959	Siltstone	moderately deformed	0	2	1	1	0	1	0	0	1	1
158960	Siltstone	strongly deformed, crenulated	0	1	2	2	0	0	0	0	0	0
158961	Siltstone	weakly deformed; cleaved	0	1	1	1	1	0	0	0	0	0
158962	Siltstone	bedded sulphide	0	0	1	2	0	3	0	0	0	0
158963	Dyke		2	1	1	2	0	2	0	0	2	0
158964	Claystone		0	2	1	2	0	2	0	1	1	1
158965	Mudstone		1	2	2	2	0	2	0	0	1	0
158966	QTZ-eye Tuff	weakly deformed, crenulated; euhedral Py; calcite/dolomite vein	1	2	1	1	0	2	0	0	0	0
158967	QTZ-eye Tuff	variably moderately deformed, crenulated, minor calcite/dolomite	1	2	0	2	0	0	0	0	0	0
158968	Siltstone		0	1	1	1	0	1	0	0	1	0
158969	Cherty Tuff	moderately deformed and crenulated; calcite/dolomite along fractures	2	0	1	4	0	0	0	0	0	0
158970	QFP	minor calcite/dolomite	1	1	0	1	0	0	0	0	0	0
158971	Claystone		0	3	1	2	0	1	0	0	2	0
158972	QFP		0	1	0	0	0	0	0	0	0	0
158973	Siltstone		0	0	3	2	0	2	0	0	2	0
158974	Siltstone	strongly crenulated; cleavage probably related to deformation	0	0	3	1	0	0	0	0	0	0
158975	Siltstone	resemble poorly development quartz-eye-tuff	0	1	1	3	0	0	0	0	0	0
158976	Mudstone	moderately deformed	0	3	1	2	0	1	0	1	1	0
158977	Claystone		0	2	1	2	0	2	2	2	0	0
158978	Felsic Tuff		2	0	1	2	0	0	0	0	0	0

Table B.3.1 – Lab-Based Sample Descriptions (continued)

Sample Number	Lab Rock Type	Lab Description	Alteration (1- 5)				Mineralization (1-5)					%
			CB	CL	MU	SL	PO	PY	GN	SP	CP	QV
158979	Greywacke		0	1	1	2	0	1	0	0	0	0
158980	Cherty Tuff	distinct bluish mineral; may be bornite	0	1	1	3	0	2	0	1	2	0
158981	Siltstone		0	3	0	1	0	1	0	1	0	0
158982	Siltstone	massive to bedded sulphide	1	2	1	1	4	2	0	0	1	0
158983	Siltstone	quartz veins 42 to-core-axis; weakly crenulated	0	2	0	2	0	2	0	2	0	2
158984	QFP		0	0	1	1	0	0	0	0	0	0
158985	Felsic Tuff	cleaved, deformed	1	1	1	2	0	2	0	0	0	0
158986	Felsic Tuff		1	0	2	2	0	0	0	0	0	0
158987	Mudstone	not significantly deformed	0	0	2	0	0	0	0	0	0	0
158988	Siltstone		0	0	0	0	0	0	0	0	0	0
158989	Dyke	minor calcite/dolomite	3	1	1	1	0	0	0	0	0	0
158990	Siltstone	patchy bedded sulphide	0	0	1	1	0	2	0	0	1	0
158991	Claystone	microfolding	0	2	0	0	0	1	0	0	0	0
158992	Siltstone		0	0	0	0	0	0	0	0	0	0
158993	Siltstone		0	0	0	1	0	1	0	0	1	0
158994	Siltstone		0	0	0	0	0	0	0	0	0	0
158995	Siltstone	akin to a dyke	0	1	0	1	0	0	0	0	0	0
158996	Siltstone	bedded sulphide	1	2	1	2	0	4	0	0	4	1
158997	Claystone	moderately deformed	0	2	1	3	0	1	0	2	0	0
158998	Claystone		1	2	1	2	0	1	0	0	1	0
158999	Claystone		0	2	1	2	0	1	0	0	1	1
159000	Siltstone	variably moderately deformed	0	1	1	1	0	1	0	0	1	1

Table B.3.2 – Density and Magnetic Susceptibility Measurements

Sample Number	Thin Section	Hand Sample Mass (g)	Hand Sample Volume (ml)	Hand Sample Density (g/ml)	Hand Sample Magnetic Susceptibility	Off-Cut Magnetic Susceptibility
158779		347.30	124.41	2.79	0.05	
158780		334.90	115.93	2.89	0.05	
158781		325.00	113.10	2.87	0.05	
158782		249.10	87.65	2.84	0.03	
158783		349.00	121.58	2.87	0.06	
158784	YES	369.30	127.23	2.90		0.45
158785	YES	241.50	87.65	2.76	?	?
158786		292.40	98.96	2.95	0.02	
158787		303.70	106.03	2.86	0.05	
158788	YES	371.30	132.89	2.79		0.37
158789		358.10	127.23	2.81	0.04	
158790		295.00	104.62	2.82	0.03	
158791		298.20	110.27	2.70	0.04	
158792	YES	208.60	73.51	2.84		0.15
158793	YES	305.80	110.27	2.77		0.13
158794	YES	279.60	96.13	2.91		0.39
158795		339.20	124.41	2.73	0.03	
158796		318.00	115.93	2.74	0.03	
158797		298.20	110.27	2.70	0.02	
158798	YES	290.30	101.79	2.85		0.31
158799	YES	230.50	84.82	2.72		0.41
158800		233.70	84.82	2.76	0.03	
158801	YES	364.40	132.89	2.74		0.27
158802		257.20	93.31	2.76	0.03	
158803		294.70	101.79	2.90	0.06	
158804		270.00	96.13	2.81	0.03	
158805		300.30	93.31	3.22	0.19	
158806		279.50	96.13	2.91	0.08	
158807		278.20	101.79	2.73	0.03	
158808		286.60	101.79	2.82	0.03	
158809		287.30	104.62	2.75	0.03	
158810		283.80	104.62	2.71	0.03	
158811	YES	309.40	110.27	2.81		0.44
158812	YES	319.40	113.10	2.82		0.37
158813	YES	284.70	101.79	2.80		0.26
158814		237.40	84.82	2.80	0.04	
158815		289.40	106.03	2.73	0.02	

Table B.3.2 – Density and Magnetic Susceptibility Measurements (continued)

Sample Number	Thin Section	Hand Sample Mass (g)	Hand Sample Volume (ml)	Hand Sample Density (g/ml)	Hand Sample Magnetic Susceptibility	Off-Cut Magnetic Susceptibility
158816		307.20	113.10	2.72	0.02	
158817		240.90	84.82	2.84	0.15	
158818		290.10	98.96	2.93	0.08	
158819		256.80	87.65	2.93	0.07	
158820		229.50	59.38	3.87	0.12	
158821		258.50	82.00	3.15	0.13	
158822		218.80	73.51	2.98	0.08	
158823		250.80	87.65	2.86	0.02	
158824		236.30	82.00	2.88	0.03	
158825		356.20	124.41	2.86	0.03	
158826	YES	349.40	124.41	2.81		0.3
158827		234.80	84.82	2.77	0.03	
158828		352.10	121.58	2.90	0.02	
158829		344.40	115.93	2.97	0.02	
158830		299.70	104.62	2.86	0.06	
158831		241.00	84.82	2.84	0.03	
158832		212.10	79.17	2.68	0.01	
158833		252.40	90.48	2.79	0.02	
158834	YES	234.90	76.34	3.08		0.41
158835	YES	396.10	134.30	2.95		0.51
158836	YES	310.50	107.44	2.89		0.47
158837	YES	289.20	104.62	2.76		0.38
158838		293.20	101.79	2.88	0.02	
158839		236.80	83.41	2.84	0.01	
158840		255.00	87.65	2.91	0.02	
158841		212.80	73.51	2.89	0.06	
158842	YES	333.10	113.10	2.95		0.62
158843		299.70	104.62	2.86	0.04	
158844		257.70	93.31	2.76	0.02	
158845		276.20	101.79	2.71	0.02	
158846		281.90	101.79	2.77	0.02	
158847		382.20	135.72	2.82	0.04	
158848	YES	239.60	87.65	2.73		0.41
158849	YES	246.00	93.31	2.64		0.49
158850	YES	348.60	124.41	2.80		0.4
158851		408.50	138.54	2.95	0.09	
158852		361.50	124.41	2.91	0.05	

Table B.3.2 – Density and Magnetic Susceptibility Measurements (continued)

Sample Number	Thin Section	Hand Sample Mass (g)	Hand Sample Volume (ml)	Hand Sample Density (g/ml)	Hand Sample Magnetic Susceptibility	Off-Cut Magnetic Susceptibility
158853		227.80	79.17	2.88	0.04	
158854	YES	315.10	110.27	2.86		0.46
158855		258.20	87.65	2.95	0.04	
158856		328.70	113.10	2.91	0.04	
158857	YES	319.10	107.44	2.97		0.38
158858		350.40	121.58	2.88	0.02	
158859		314.30	110.27	2.85	0.02	
158860		256.90	90.48	2.84	0.04	
158861		211.90	73.51	2.88	0.02	
158862	YES	331.50	115.93	2.86		0.59
158863		231.70	84.82	2.73	0.02	
158864	YES	228.20	82.00	2.78		0.46
158865		298.50	110.27	2.71	0.02	
158866	YES	262.50	96.13	2.73		0.5
158867	YES	295.40	104.62	2.82		0.54
158868		279.30	101.79	2.74	0.03	
158869	YES	238.90	82.00	2.91		0.58
158870		322.00	110.27	2.92	0.07	
158871		242.70	90.48	2.68	0.02	
158872		249.20	84.82	2.94	0.04	
158873		241.70	90.48	2.67	0.02	
158874		212.40	73.51	2.89	0.03	
158875		211.50	73.51	2.88	0.04	
158876		302.30	110.27	2.74	0.03	
158877		262.10	93.31	2.81	0.06	
158878		321.40	110.27	2.91	0.06	
158879	YES	311.30	107.44	2.90		0.22
158880		274.30	93.31	2.94	0.06	
158881		248.00	84.82	2.92	0.03	
158882		299.00	101.79	2.94	0.05	
158883		241.80	82.00	2.95	0.03	
158884		229.40	79.17	2.90	0.02	
158885		285.80	98.96	2.89	0.03	
158886		269.80	96.13	2.81	0.03	
158887		340.10	118.75	2.86	0.03	
158888	YES	221.40	76.34	2.90		0.18
158889		243.00	86.24	2.82	0.02	

Table B.3.2 – Density and Magnetic Susceptibility Measurements (continued)

Sample Number	Thin Section	Hand Sample Mass (g)	Hand Sample Volume (ml)	Hand Sample Density (g/ml)	Hand Sample Magnetic Susceptibility	Off-Cut Magnetic Susceptibility
158890	YES	329.50	118.75	2.77		0.42
158891		244.10	87.65	2.78	0.02	
158892	YES	249.70	87.65	2.85		0.58
158893		264.50	93.31	2.83	0.03	
158894		287.60	101.79	2.83	0.03	
158895		188.20	62.20	3.03	0.03	
158896		255.60	91.89	2.78	0.03	
158897		199.90	67.86	2.95	0.04	
158898		349.80	121.58	2.88	0.05	
158899	YES	349.90	121.58	2.88		0.52
158900	YES	228.20	79.17	2.88		0.51
158901		210.00	76.34	2.75	0.02	
158902		212.90	73.51	2.90	0.03	
158903	YES	226.80	82.00	2.77		0.44
158904		268.80	90.48	2.97	0.03	
158905		237.50	82.00	2.90	0.02	
158906		343.90	120.17	2.86	0.04	
158907		276.50	98.96	2.79	0.03	
158908		284.10	101.79	2.79	0.03	
158909	YES	233.40	83.41	2.80		0.58
158910	YES	261.80	90.48	2.89		0.59
158911		187.90	65.03	2.89	0.04	
158912		320.80	113.10	2.84	0.03	
158913		244.90	84.82	2.89	0.06	
158914	YES	246.70	87.65	2.81		0.47
158915		258.60	93.31	2.77	0.03	
158916		295.80	98.96	2.99	0.13	
158917		351.00	122.99	2.85	0.05	
158918		314.50	114.51	2.75	0.02	
158919		171.10	62.20	2.75	0.03	
158920		135.70	48.07	2.82	0.04	
158921		162.90	56.55	2.88	0.05	
158922		159.60	56.55	2.82	0.05	
158923		166.80	59.38	2.81	0.03	
158924		174.70	62.20	2.81	0.03	
158925		119.60	42.41	2.82	0.04	
158926		174.70	65.03	2.69	0.04	

Table B.3.2 – Density and Magnetic Susceptibility Measurements (continued)

Sample Number	Thin Section	Hand Sample Mass (g)	Hand Sample Volume (ml)	Hand Sample Density (g/ml)	Hand Sample Magnetic Susceptibility	Off-Cut Magnetic Susceptibility
158927		160.00	53.72	2.98	0.05	
158928		159.90	59.38	2.69	0.03	
158929		205.20	73.51	2.79	0.05	
158930		155.40	53.72	2.89	0.04	
158931	YES	240.90	83.41	2.89		0.49
158932	YES	367.90	115.93	3.17		0.61
158933	YES	268.90	93.31	2.88		0.59
158934	YES	436.40	147.03	2.97		0.64
158935		259.10	87.65	2.96	0.06	
158936		275.80	96.13	2.87	0.03	
158937	YES	312.10	110.27	2.83		0.54
158938	YES	276.00	96.13	2.87		0.45
158939	YES	243.40	82.00	2.97		0.59
158940		257.30	90.48	2.84	0.04	
158941	YES	256.30	93.31	2.75		0.47
158942	YES	248.30	84.82	2.93		0.51
158943	YES	217.60	73.51	2.96		0.39
158944	YES	260.00	90.48	2.87		0.41
158945	YES	235.10	80.58	2.92		0.42
158946	YES	338.90	118.75	2.85		0.37
158947	YES	299.50	104.62	2.86		0.44
158948	YES	337.20	118.75	2.84		0.39
158949	YES	336.00	111.68	3.01		0.42
158950	YES	322.70	113.10	2.85		0.55
158951	YES	244.70	93.31	2.62		0.41
158952	YES	307.10	107.44	2.86		0.48
158953	YES	296.50	101.79	2.91		0.44
158954	YES	347.10	117.34	2.96		0.48
158955	YES	240.30	76.34	3.15		0.4
158956	YES	206.10	84.82	2.43		0.57
158957	YES	277.40	70.69	3.92		0.38
158958	YES	370.90	96.13	3.86		0.5
158959		303.60	127.23	2.39	0.04	
158960	YES	338.60	104.62	3.24		0.45
158961	YES	240.90	115.93	2.08	?	?
158962		255.40	80.58	3.17	0.03	
158963		281.60	87.65	3.21	0.03	

Table B.3.2 – Density and Magnetic Susceptibility Measurements (continued)

Sample Number	Thin Section	Hand Sample Mass (g)	Hand Sample Volume (ml)	Hand Sample Density (g/ml)	Hand Sample Magnetic Susceptibility	Off-Cut Magnetic Susceptibility
158964		330.90	93.31	3.55	0.04	
158965	YES	330.40	113.10	2.92		0.29
158966	YES	297.40	115.93	2.57		0.46
158967	YES	313.50	107.44	2.92		0.41
158968		289.10	110.27	2.62	0.03	
158969	YES	367.50	107.44	3.42		0.38
158970		345.60	135.72	2.55	0.02	
158971		243.90	115.93	2.10	0.03	
158972		299.90	87.65	3.42	0.02	
158973	YES	368.50	98.96	3.72		0.34
158974	YES	296.60	124.41	2.38		0.44
158975	YES	276.30	101.79	2.71		0.49
158976	YES	211.70	96.13	2.20		0.5
158977	YES	302.90	73.51	4.12		0.44
158978	YES	252.40	107.44	2.35		0.45
158979	YES	325.40	89.06	3.65		0.64
158980		284.30	115.93	2.45	0.02	
158981		256.10	96.13	2.66	0.04	
158982	YES	268.20	82.00	3.27		0.68
158983		296.70	93.31	3.18	0.03	
158984		238.80	108.86	2.19	0.02	
158985	YES	313.90	84.82	3.70		0.46
158986	YES	212.90	110.27	1.93		0.43
158987		280.00	76.34	3.67	0.04	
158988		302.70	101.79	2.97	0.04	
158989		247.30	106.03	2.33	0.05	
158990		375.80	84.82	4.43	0.04	
158991		421.50	127.23	3.31	0.04	
158992	YES	316.60	147.03	2.15		0.42
158993		277.40	107.44	2.58	0.07	
158994		219.30	98.96	2.22	0.04	
158995		495.90	172.47	2.88	0.07	
158996		240.30	82.00	2.93	0.07	
158997	YES	428.20	148.44	2.88		0.41
158998		442.20	148.44	2.98	0.08	
158999		277.90	93.31	2.98	0.05	
159000		209.70	70.69	2.97	0.04	

Table C.1 - Thin Section Petrology

Sample Number	Lithology (Thin Section)	Texture	QZ-Phen Size (μm)	Abund (%)	QZ-Matx Size (μm)	Abund (%)	White Mica Size (μm)	Abund (%)
158784	Mudstone	fine-grained and tuffaceous	100-150	5	< 30	63	v.f.g.	30
158785	QTZ-FS porphyry	fine-grained; isogranular	600-1000	5	20	69	v.f.g.	18
158788	QTZ-FS porphyry	fine-grained	800-2500	5	35	73	v.f.g.	12
158792	Dacitic flow	fine-grained			30	63	v.f.g.	6
158793	Felsic Tuff	fine-grained; isogranular			50	73	v.f.g.	8
158794	Andesitic Flow	fine-grained			30	57		
158798	QTZ-FS porphyry	fine-grained; isogranular	100	3	40	63	v.f.g.	25
158799	QTZ-Phyric Tuff	fine-grained; isogranular	250	2	40	78	v.f.g.	15
158801	Greywacke	coarse-grained			80-100	79	v.f.g.	11
158811	Altered Sediment (?)	fine-grained; highly altered to tell rock type; dacitic			50	75	v.f.g.	19
158812	Mudstone	fine-grained; tuffaceous			20	73	v.f.g.	20
158813	Claystone	fine-grained; isogranular			30	76	v.f.g.	19
158826	Tuff	fine-grained; isogranular			15	73		
158834	Altered Sediment	highly altered					v.f.g.	37
158835	Altered Sediment	very altered			30	45	v.f.g.	19
158836	Mudstone	fine-grained			30	69	v.f.g.	15
158837	Flow	rhyolite; medium-grained; isogranular	300	1	40	59	v.f.g.	32
158842	Siltstone	fine-grained			15	50	v.f.g.	30
158848	QTZ-FS phyric tuff	fine-grained	50	25	35	47	v.f.g.	10
158849	QTZ-FS phyric tuff	fine-grained	70	20	25	30	v.f.g.	10
158850	QTZ-FS porphyry	fine-grained, porphyritic and quartz-dominant	300-1200	10	20	59	v.f.g.	25
158854	Greywacke	fine-grained; porphyritic			80	75		
158857	Greywacke	medium-grained			100	70	v.f.g.	1
158862	Altered Sediment	very altered re-worked			15	10	v.f.g.	40
158864	Cherty Tuff	fine-grained, isogranular	300	3	15	73	v.f.g.	20
158866	QTZ-FS Phyric Tuff	fine-grained; isogranular	200	5	20	82	v.f.g.	8
158867	Claystone	fine-grained; isogranular			20	54	v.f.g.	40

Table C.1 - Thin Section Petrology (continued)

Sample Number	Chlorite Size (μm)	Abund (%)	Opaque Size (μm)	Abund (%)	Titanite Size (μm)	Abund (%)	FS Pheno Size (μm)	Abund (%)	Association
158784			10	2					
158785	v.f.g.	2	6	2			80-120	3	Chlorite-Feldspar
158788	v.f.g.	2	8	1			80 -300	7	Chlorite-Feldspar
158792	v.f.g.	12		2					Clinopyroxene-Carbonate-Epidote
158793	v.f.g.	18	10	2					
158794			8	10					
158798			100	1			40-100	12	Quartz-Sericte-Feldspar
158799			90	5					
158801	NV		60	3					
158811	v.f.g.	2	45	4			110	2	
158812	v.f.g.	3	15	3	8	1			
158813			40	5					
158826	v.f.g.	13	38	4			80	8	
158834	v.f.g.	8	200	4					Opaque mineral-Feldspar
158835			350	8	v.f.g.	1			
158836	v.f.g.	20	120	15					
158837	v.f.g.	2	90	4			60	1	
158842	v.f.g.	15	60	5					Quartz-Chlorite
158848	v.f.g.	8	200	2			100	5	
158849			45	2			800	3	
158850	v.f.g.	3	70	2			800	2	Sericite-Chlorite intergrowth
158854	v.f.g.	15							
158857	v.f.g.	15	50	10					
158862			10	25					
158864			2000	2			50	2	
158866			70	2			120	2	
158867			40	5					

Table C.1 - Thin Section Petrology (continued)

Sample Number	Comments
158784	S1/S2 with weakly developed discrete spaced crenulation cleavage
158785	chlorite is massive, patchy and brownish-violet
158788	Prussian-blue massive chlorite occurring as isolated or 'inclusions' in altered feldspar grains
158792	~ 10% epidote; 10% carbonate; 12% relict clinopyroxene
158793	chlorite is olive-green with minor brownish tints; one grain of 130 by 110 pyrite
158794	~ 35% biotite
158798	FS phenocrysts > QTZ; Sulphide intergrown FS & QTZ; 'augen' FS enveloped by SER; S1/S2 crenulation cleavage; FS grains are fragmented
158799	recrystallized quartz with minor stockwork and isolated anhedral Sulphide grains
158801	
158811	strong discrete spaced crenulation cleavage development; Sulphide disseminated and concentrated along bedding planes
158812	evidence for pressure solution marked by a plane of insoluble material; possible dissolution sites
158813	S1/S2 discrete spaced crenulation cleavage development showing distinct M (mica) and Q (quartz-rich microlithon) domains;
158826	5% carbonate and strong fibrous grains of Prussian-blue chlorite
158834	stockwork sulphides; classic S1/S2 fabric development
158835	recrystallized quartz
158836	
158837	isogranular and recrystallized; exhibit crenulation cleavage
158842	trails of insoluble material probably indicate pressure solution; variably bands of probably insoluble material or Sx
158848	
158849	
158850	isogranular and recrystallized;
158854	
158857	
158862	incidents of subhedral sulphide grains embedded in recrystallized quartz is not uncommon
158864	
158866	crystal-rich tuff predominantly quartz -rich with subordinate FS
158867	well developed S1/S2 distinct mica-rich (M) -quartz-rich (Q) domainal spaced cleavage development

Table C.1 - Thin Section Petrology (continued)

Sample Number	Lithology (Thin Section)	Texture	QZ-Phen Size (μm)	Abund (%)	QZ-Matx Size (μm)	Abund (%)	White Mica Size (μm)	Abund (%)
158869	Altered Sediment (?)	isogranular and cherty			35	55	v.f.g.	35
158879	Mudstone	fine-grained			30	65	v.f.g.	20
158888	Siltstone	medium-grained; isogranular to polygonal			40-100	60	v.f.g.	20
158890	FS-phyric Tuff	dacitic; fine-grained; isogranular to polygonal mosaic	100	2	30	70	v.f.g.	2
158892	FS-Phyric Tuff	isogranular to polygonal			25-30	77	v.f.g.	5
158899	Claystone	medium-grained			20	45	v.f.g.	38
158900	Mudstone	medium-grained	70	6	30	50	v.f.g.	34
158903	QTZ-FS porphyry	fine-grained	1200-2000	3	20	84	v.f.g.	5
158909	Dyke	fine-grained			20	50	v.f.g.	10
158910	Mudstone	very altered					v.g.f.	35
158914	FS-phyric Tuff	porphyritic			25	65	v.f.g.	1
158931	Greywacke	coarse-grained			120-160	40		
158932	Claystone	IF						
158933	Greywacke	coarse-grained			60-120	78	v.f.g.	4
158934	Claystone	fine-grained			20	20	v.f.g.	35
158937	Tuff	very fine-grained and isogranular			15	40	v.f.g.	55
158938	Tuff	fine-grained						
158939	Dyke	very fine-grained						
158941	Greywacke	coarse-grained			200-400	70	v.f.g.	15
158942	QTZ-phyric Tuff	fine-grained	200-350	15	20	55		
158943	very altered	rhyolite						
158944	Siltstone	medium-coarse grained					v.f.g.	20
158945	Flow	aphyric rhyolite			15	80	v.f.g.	2
158946	Mudstone	medium grained			50	60	v.f.g.	5
158947	Mudstone	medium grained			35-55	65	v.f.g.	6
158948	Greywacke	coarse-grained			30-70	72	v.f.g.	5
158949	Siltstone	medium grained			30-65	71	v.f.g.	3

Table C.1 - Thin Section Petrology (continued)

Sample Number	Chlorite Size (μm)	Abund (%)	Opaque Size (μm)	Abund (%)	Titanite Size (μm)	Abund (%)	FS Pheno Size (μm)	Abund (%)	Association
158869			300	5					
158879			30	5					
158888			200	15					
158890	v.f.g.	15					600-1600	15	Chlorite-Feldspar
158892	v.f.g.	8	90	3			700-1800	10	Chlorite-Feldspar
158899	v.f.g.	2	30	15					
158900			60	10			1400	1	
158903	v.f.g.	3	60	1	<10	1	1200-2400	2	Chlorite-Feldspar
158909	v.f.g.	7	70	3					
158910									
158914	v.f.g.	15	110	2			500	17	Feldspar-Chlorite
158931	v.f.g.	30	40	2					
158932	v.f.g.	>50							
158933									
158934			10	25					
158937			90	5					
158938	v.f.g.	8							
158939									
158941									
158942	v.f.g.	35							
158943	v.f.g.	40							
158944			40-100						
158945	v.f.g.	45							
158946	v.f.g.	10							
158947			40-100	8					
158948	v.f.g.	1	110	4			60	2	Quartz-Opaque minerals
158949	v.f.g.	6	80-200	18					

Table C.1 - Thin Section Petrology (continued)

Sample Number	Comments
158869	strong fabric development; dark bands of insoluble material probably related to pressure solution; strongly SER with recrystallized quartz
158879	Diffused crenulation cleavage development
158888	S1/S2 crenulation cleavage with abundant opaque minerals
158890	FS grains are dominant over quartz; chlorite grains are olive-greenish brown
158892	FS grains are dominant over quartz; chlorite grains are olive-greenish brown
158899	Distinct discrete spaced crenulation cleavage with definite mica-rich (M) and quartz (Q) domains
158900	mica-rich (M) and quartz (Q) domains; probably FS-phyric tuff with relict FS partly altered to Prussian-blue chlorite
158903	FS grains are intensely altered and subordinate to quartz grains; chlorite is brownish-purple
158909	carbonate (20%) occurs as aggregates; chlorite is Prussian-blue
158910	titanite-grains with inclusion trails parallel to S1
158914	aggregates of Prussian-blue chlorite
158931	matrix is strongly chloritized
158932	very strongly chlorite altered to Prussian-blue colour
158933	
158934	strongly SER; minor crenulation
158937	strong recrystallization; distinct spaced mica-rich (M) and quartz-rich (Q)
158938	fibrous bands of Prussian-blue chlorite
158939	matrix altered to greenish (probably) chlorite
158941	
158942	
158943	very altered
158944	weakly developed diffused crenulation cleavage
158945	
158946	trails of insoluble material (probably dissolution sites)
158947	
158948	mildly recrystallized and variably sorted; minor STK-WK and isolated anhedral grains recrystallized quartz along margins of STK-WK Sx
158949	

Table C.1 - Thin Section Petrology (continued)

Sample Number	Lithology (Thin Section)	Texture	QZ-Phen Size (μm)	Abund (%)	QZ-Matx Size (μm)	Abund (%)	White Mica Size (μm)	Abund (%)
158950	Mudstone	medium-grained			80	76	v.f.g.	2
158951	Dyke	fine-grained					v.f.g.	15
158952	Mudstone	medium-grained			70-100	73	v.f.g.	4
158953	Claystone	fine-grained						
158954	Mudstone	fine-grained			25	68	v.f.g.	7
158955	Siltstone	fine-grained			20	75		
158956	Very altered	rhyolitic; very fine-grained			v.f.g.	5	v.f.g.	5
158957	Siltstone	medium-grained			40	45	v.f.g.	30
158958	QTZ-phyric Tuff	fine-grained	100-200	3	20	73	v.f.g.	5
158960	Mudstone	fine-grained			60	78	v.fg	6
158961	Mudstone	fine-grained and tuffaceous			25	55	v.fg	18
158965	Mudstone	fine-grained and tuffaceous			20	51	v.fg	35
158966	FS-Phyric Tuff	fine-grained and tuffaceous			10	65		
158967	FS-Phyric Flow	fine-grained			10	65	v.f.g.	18
158969	Cherty Tuff	very fine-grained			10	79	f.g.	< 1
158973	Siltstone	medium-grained			60	35	v.f.g.	45
158974	Mudstone	fine-grained			30	67	v.f.g.	
158975	Andesite Flow	fine-grained		8	20	42	v.f.g.	12
158976	Siltstone	medium-grained			35	50	v.f.g.	40
158977	Claystone	fine-grained			20	60	v.f.g.	13
158978	Mudstone	fine-grained			30	64	v.f.g.	10
158979	Greywacke	coarse-grained			80-200	79	v.f.g.	10
158982	Mudstone	fine-grained			60-100	64	v.f.g.	18
158985	Siltstone	fine-grained			35	68	v.f.g.	10
158986	Siltstone	fine-grained; isogranular	80	3	30	52	v.f.g.	30
158992	Mudstone	medium-grained			40	65	v.f.g.	15
158997	Siltstone	fine-grained			30	55	v.f.g.	25

Table C.1 - Thin Section Petrology (continued)

Sample Number	Chlorite Size (μm)	Abund (%)	Opaque Size (μm)	Abund (%)	Titanite Size (μm)	Abund (%)	FS Pheno Size (μm)	Abund (%)	Association
158950			200	2					
158951	v.f.g.	8							
158952									
158953									
158954	v.f.g.	8							
158955									
158956	v.f.g.								
158957			40	25					
158958	v.f.g.								
158960			40	3					
158961									
158965	v.f.g.	10	60	3		1			Chlorite-Quartz-Sulphide minerals
158966	v.f.g.	18	100				160-1200	25	
158967	v.f.g.	10					500-900	15	
158969									
158973			70	20					
158974									
158975	v.f.g.	19	f.g.	9					
158976			30	10					
158977			40	6					
158978	v.f.g.	8							
158979			30	2					
158982			40-90	20					Carbonate-Sulphide minerals
158985			30	12					
158986			25	20					
158992	v.f.g.	5	100	10					
158997			25	20					

Table C.1 - Thin Section Petrology (continued)

Sample Number	Comments
158950	
158951	
158952	
158953	highly birefirengent mineral in a quartz vein
158954	
158955	minor concentration of coarser-grained quartz minerals is a small segment of the slide
158956	abundant carbonate ~ 30%
158957	
158958	greenish chlorite
158960	
158961	diffused crenulation cleavage
158965	Chlorite occurrence predominantly in quartz -rich domains
158966	one cubic Py grain is 2000 μm; quartz - sulphide -chlorite
158967	pale Prussian-blue chlorite
158969	weakly developed preferred orientation
158973	sulphides concentrated along somewhat dissolution planes probably associated with pressure solution
158974	
158975	
158976	weakly developed diffused crenulation cleavage
158977	
158978	Prussian-blue fibrous chlorite
158979	
158982	
158985	minor but significant carbonate present
158986	disseminated stockwork sulphides
158992	
158997	

Table D.1.1 - Muscovite and Phengite Wt. % Oxide Electron Microprobe Compositions

Samp. ID	MG	*SiO2*	*TiO2*	*Al2O3*	*FeO*	*MnO*	*MgO*	*CaO*	*Na2O*	*K2O*	*Cr2O3*	*Cl*	*P2O5*	*BaO*	*TOTAL*
HML-859	A1	49.17	0.27	33.20	1.26	0.00	1.63	0.00	0.14	8.35	0.07	0.00	0.04	0.05	94.19
HML-870	A1	47.67	1.18	31.25	4.18	0.11	2.58	0.00	0.13	7.69	0.01	0.02	0.06	0.06	94.94
HML-870	A2	49.81	0.23	32.16	1.98	0.00	1.79	0.00	0.12	8.00	0.09	0.00	0.09	0.08	94.36
HML-870	B1	49.59	0.31	32.53	1.76	0.02	1.75	0.00	0.15	7.96	0.00	0.00	0.00	0.20	94.26
HML-870	B2	49.09	0.39	32.14	2.03	0.00	1.73	0.00	0.11	8.15	0.07	0.03	0.04	0.14	93.91
HML-870	C1	48.74	0.32	31.83	3.42	0.18	2.12	0.00	0.08	8.28	0.00	0.01	0.06	0.07	95.10
HML-870	C3	48.78	0.92	32.50	1.77	0.00	1.62	0.04	0.12	8.77	0.07	0.00	0.02	0.16	94.79
HML-870	C2	48.46	0.92	31.26	2.08	0.00	2.05	0.00	0.17	9.00	0.07	0.00	0.00	0.02	94.02
HML-937	B1	51.56	0.04	33.62	1.29	0.02	1.96	0.03	0.18	7.36	0.00	0.00	0.14	0.38	96.57
HML-937	A3	51.22	0.08	31.58	1.63	0.00	2.34	0.02	0.09	7.83	0.07	0.00	0.08	0.38	95.32
HML-937	C2	49.50	0.21	32.32	1.48	0.00	2.02	0.07	0.19	8.80	0.00	0.06	0.01	0.07	94.74
HML-973	B2	50.26	0.37	31.87	2.90	0.00	1.72	0.01	0.18	8.24	0.10	0.00	0.17	0.20	96.01
HML-973	A1	50.72	0.53	31.52	2.49	0.00	2.05	0.00	0.15	8.73	0.04	0.00	0.08	0.05	96.38
HML-973	B1	48.81	0.57	31.88	2.40	0.06	1.60	0.06	0.21	8.94	0.00	0.00	0.08	0.15	94.76
HML-985	A3	49.27	0.31	33.33	2.02	0.00	1.35	0.00	0.11	7.62	0.09	0.00	0.08	0.17	94.35
HML-985	A3	49.95	0.26	33.75	1.88	0.02	1.41	0.05	0.20	7.62	0.01	0.05	0.04	0.15	95.39
HML-985	C2	50.62	0.32	33.50	2.15	0.00	1.58	0.00	0.16	8.20	0.00	0.01	0.06	0.10	96.71
HML-985	B2	46.19	0.33	29.95	6.53	0.05	2.96	0.00	0.24	7.79	0.00	0.00	0.00	0.07	94.12
HML-985	C1	49.75	0.76	34.34	1.98	0.05	1.28	0.00	0.17	8.67	0.00	0.00	0.00	0.00	97.00
HML-985	B1	48.70	0.47	32.64	2.22	0.00	1.35	0.00	0.21	8.36	0.03	0.01	0.08	0.05	94.12
HML-985	A4	48.93	0.17	32.57	1.75	0.08	1.59	0.04	0.53	8.41	0.00	0.08	0.10	0.14	94.39

Table D.1.1 - Muscovite and Phengite Wt. % Oxide Electron Microprobe Compositions (continued)

Samp. ID	MG	*SiO2*	*TiO2*	*Al2O3*	*FeO*	*MnO*	*MgO*	*CaO*	*Na2O*	*K2O*	*Cr2O3*	*Cl*	*P2O5*	*BaO*	*TOTAL*
HML-859	C2	46.71	2.19	32.96	1.46	0.00	1.50	0.10	0.24	9.83	0.00	0.01	0.11	0.11	95.23
HML-859	B1	48.36	0.47	32.19	1.68	0.06	2.16	0.00	0.22	10.08	0.09	0.00	0.05	0.19	95.55
HML-859	A3	47.56	0.37	32.75	1.20	0.00	1.42	0.05	0.24	10.06	0.00	0.02	0.06	0.00	93.73
HML-859	C1	47.77	0.58	33.21	1.17	0.00	1.37	0.00	0.34	10.10	0.11	0.00	0.04	0.36	95.05
HML-859	B2	48.54	0.40	31.28	1.18	0.00	1.89	0.00	0.40	10.09	0.03	0.04	0.00	0.04	93.90
HML-859	A2	47.48	0.11	32.09	1.21	0.06	1.74	0.00	0.29	10.40	0.00	0.00	0.00	0.41	93.79
HML-869	C1	48.68	0.34	29.76	2.54	0.05	2.33	0.00	0.10	10.78	0.17	0.02	0.29	0.39	95.45
HML-869	A3	47.90	0.41	29.59	2.55	0.00	2.14	0.00	0.10	10.89	0.11	0.00	0.18	0.19	94.05
HML-869	A2	48.34	0.38	29.50	2.43	0.08	2.24	0.00	0.09	10.95	0.00	0.03	0.00	0.28	94.30
HML-869	B1	48.32	0.70	29.64	2.26	0.07	2.36	0.00	0.19	10.93	0.03	0.00	0.02	0.14	94.66
HML-869	B2	48.30	0.35	28.99	2.51	0.00	2.31	0.02	0.22	10.83	0.11	0.01	0.05	0.29	93.99
HML-869	A1	49.54	0.29	27.75	2.92	0.03	2.63	0.01	0.10	11.28	0.04	0.00	0.05	0.23	94.87
HML-870	A1	46.75	0.36	31.11	3.93	0.01	2.63	0.00	0.22	10.06	0.09	0.00	0.00	0.00	95.15
HML-870	A2	48.54	0.53	30.22	2.64	0.00	2.18	0.00	0.20	10.56	0.09	0.00	0.13	0.23	95.32
HML-924	C2	50.91	0.35	28.08	1.98	0.00	3.08	0.03	0.26	10.72	0.00	0.02	0.16	0.28	95.86
HML-924	C3	50.89	0.37	27.91	2.36	0.00	3.13	0.02	0.30	10.81	0.00	0.00	0.09	0.22	96.10
HML-924	A2	50.63	0.43	28.11	2.63	0.00	3.21	0.04	0.33	10.89	0.00	0.13	0.07	0.27	96.74
HML-924	B2	49.84	0.47	27.18	2.17	0.07	2.99	0.09	0.38	10.55	0.02	0.00	0.09	0.08	93.91
HML-924	B1	50.05	0.57	27.75	2.34	0.03	3.05	0.01	0.24	10.94	0.07	0.02	0.00	0.19	95.24
HML-924	C1	49.86	0.33	27.75	2.24	0.11	3.16	0.04	0.28	10.83	0.04	0.08	0.00	0.24	94.95
HML-924	A3	50.28	0.49	28.06	2.40	0.06	3.04	0.00	0.33	10.90	0.00	0.07	0.00	0.10	95.73

Table D.1.1 - Muscovite and Phengite Wt. % Oxide Electron Microprobe Compositions (continued)

Samp. ID	MG	*SiO2*	*TiO2*	*Al2O3*	*FeO*	*MnO*	*MgO*	*CaO*	*Na2O*	*K2O*	*Cr2O3*	*Cl*	*P2O5*	*BaO*	*TOTAL*
HML-924	A1	50.00	0.33	28.18	2.53	0.02	2.90	0.09	0.41	11.17	0.00	0.19	0.08	0.33	96.24
HML-937	C3	48.85	0.08	32.36	1.45	0.08	1.81	0.00	0.18	10.33	0.04	0.07	0.00	0.19	95.46
HML-937	B2	49.51	0.12	32.05	1.49	0.06	2.07	0.01	0.20	10.67	0.00	0.03	0.01	0.30	96.50
HML-937	C1	48.80	0.23	32.51	1.35	0.02	2.03	0.00	0.21	10.65	0.08	0.00	0.09	0.14	96.11
HML-937	A1	48.84	0.16	32.01	1.24	0.00	1.99	0.09	0.29	10.66	0.00	0.00	0.03	0.30	95.62
HML-937	A2	48.51	0.30	31.32	1.62	0.05	2.08	0.00	0.17	10.90	0.08	0.02	0.11	0.21	95.36
HML-973	C1	47.94	0.44	31.50	2.40	0.01	1.55	0.00	0.29	10.57	0.00	0.06	0.05	0.18	94.99
HML-973	C2	47.54	0.49	31.60	2.11	0.06	1.57	0.04	0.25	10.59	0.00	0.03	0.03	0.06	94.36
HML-973	C3	48.25	0.48	31.62	2.14	0.00	1.50	0.01	0.26	10.75	0.05	0.00	0.02	0.00	95.09
HML-973	A2	48.56	0.36	31.08	2.29	0.01	1.72	0.00	0.20	10.92	0.02	0.00	0.01	0.18	95.35
HML-985	A1	47.34	0.18	32.02	3.91	0.06	1.82	0.06	0.30	10.17	0.05	0.04	0.14	0.19	96.27
HML-985	A2	44.29	0.26	30.03	1.97	0.00	1.39	0.00	0.30	9.72	0.66	0.03	0.06	0.10	88.80
HML-985	A3	42.47	0.34	28.43	2.75	0.07	1.48	0.03	0.24	9.14	0.68	0.04	0.00	0.07	85.72
HML-985	A3	45.62	0.19	30.88	1.68	0.09	1.44	0.00	0.23	9.73	0.38	0.03	0.00	0.20	90.48
HML-985	B1	46.33	0.33	30.82	2.56	0.00	1.60	0.00	0.15	7.59	0.00	0.00	0.14	0.00	89.52

Table D.1.2 – Molar Composition of Muscovite/Phengite (based on 22 O)

Samp. ID	MG	*Si*	*Ti*	*Al*	*Fe*	*Mn*	*Mg*	*Ca*	*Na*	*K*	*Cr*	*Cl*	*P*	*Ba*
HML-859	A1	6.4940	0.0268	5.1675	0.1388	0.0000	0.3212	0.0004	0.0365	1.4061	0.0070	0.0000	0.0050	0.0026
HML-870	A1	6.3554	0.1187	4.9107	0.4655	0.0124	0.5121	0.0000	0.0345	1.3074	0.0016	0.0034	0.0071	0.0030
HML-870	A2	6.5736	0.0233	5.0012	0.2183	0.0000	0.3528	0.0000	0.0309	1.3462	0.0095	0.0006	0.0105	0.0039
HML-870	B1	6.5512	0.0306	5.0640	0.1939	0.0028	0.3438	0.0000	0.0378	1.3415	0.0000	0.0000	0.0000	0.0103
HML-870	B2	6.5296	0.0389	5.0383	0.2260	0.0000	0.3426	0.0000	0.0275	1.3835	0.0069	0.0072	0.0040	0.0075
HML-870	C1	6.4630	0.0318	4.9735	0.3786	0.0197	0.4190	0.0000	0.0195	1.4003	0.0000	0.0022	0.0072	0.0038
HML-870	C3	6.4549	0.0915	5.0688	0.1962	0.0000	0.3198	0.0063	0.0313	1.4809	0.0073	0.0000	0.0026	0.0082
HML-870	C2	6.4870	0.0929	4.9316	0.2326	0.0000	0.4084	0.0000	0.0433	1.5367	0.0071	0.0000	0.0001	0.0010
HML-937	B1	6.5962	0.0035	5.0689	0.1379	0.0019	0.3732	0.0047	0.0452	1.2016	0.0000	0.0000	0.0148	0.0191
HML-937	A3	6.6776	0.0083	4.8529	0.1774	0.0000	0.4553	0.0027	0.0225	1.3028	0.0069	0.0000	0.0084	0.0194
HML-937	C2	6.5333	0.0209	5.0278	0.1637	0.0000	0.3969	0.0097	0.0491	1.4815	0.0002	0.0136	0.0015	0.0037
HML-973	B2	6.5665	0.0361	4.9064	0.3172	0.0000	0.3342	0.0016	0.0463	1.3731	0.0102	0.0000	0.0188	0.0101
HML-973	A1	6.6002	0.0519	4.8343	0.2708	0.0000	0.3983	0.0000	0.0382	1.4498	0.0046	0.0004	0.0087	0.0025
HML-973	B1	6.4897	0.0573	4.9954	0.2670	0.0067	0.3168	0.0080	0.0541	1.5162	0.0000	0.0000	0.0086	0.0078
HML-985	A3	6.4934	0.0303	5.1771	0.2228	0.0000	0.2646	0.0000	0.0290	1.2811	0.0090	0.0000	0.0088	0.0088
HML-985	A3	6.5046	0.0258	5.1786	0.2050	0.0025	0.2728	0.0068	0.0494	1.2665	0.0013	0.0106	0.0046	0.0075
HML-985	C2	6.5247	0.0313	5.0897	0.2322	0.0000	0.3043	0.0000	0.0407	1.3479	0.0003	0.0018	0.0066	0.0050
HML-985	B2	6.3127	0.0342	4.8236	0.7468	0.0063	0.6021	0.0000	0.0648	1.3579	0.0000	0.0003	0.0000	0.0040
HML-985	C1	6.4140	0.0736	5.2175	0.2137	0.0051	0.2459	0.0000	0.0426	1.4250	0.0000	0.0000	0.0000	0.0000
HML-985	B1	6.4757	0.0465	5.1158	0.2471	0.0000	0.2681	0.0000	0.0553	1.4174	0.0030	0.0018	0.0089	0.0028
HML-985	A4	6.4908	0.0169	5.0913	0.1942	0.0090	0.3144	0.0050	0.1374	1.4238	0.0000	0.0185	0.0111	0.0075

Table D.1.2 - Molar Composition of Muscovite/Phengite (based on 22 O); continued

Samp. ID	MG	*Si*	*Ti*	*Al*	*Fe*	*Mn*	*Mg*	*Ca*	*Na*	*K*	*Cr*	*Cl*	*P*	*Ba*
HML-859	C2	6.2149	0.2187	5.1687	0.1628	0.0000	0.2973	0.0148	0.0620	1.6686	0.0000	0.0028	0.0129	0.0058
HML-859	B1	6.4126	0.0465	5.0291	0.1857	0.0072	0.4268	0.0000	0.0564	1.7049	0.0095	0.0000	0.0054	0.0100
HML-859	A3	6.3980	0.0375	5.1931	0.1345	0.0000	0.2839	0.0074	0.0627	1.7266	0.0000	0.0048	0.0067	0.0000
HML-859	C1	6.3586	0.0582	5.2099	0.1300	0.0001	0.2713	0.0006	0.0880	1.7152	0.0119	0.0000	0.0046	0.0187
HML-859	B2	6.5238	0.0403	4.9540	0.1328	0.0000	0.3789	0.0000	0.1042	1.7304	0.0036	0.0088	0.0000	0.0021
HML-859	A2	6.4250	0.0108	5.1171	0.1374	0.0067	0.3515	0.0000	0.0750	1.7955	0.0000	0.0000	0.0000	0.0219
HML-869	C1	6.5274	0.0347	4.7027	0.2843	0.0055	0.4664	0.0000	0.0270	1.8440	0.0175	0.0036	0.0326	0.0204
HML-869	A3	6.5177	0.0419	4.7461	0.2899	0.0000	0.4345	0.0000	0.0254	1.8898	0.0117	0.0000	0.0209	0.0100
HML-869	A2	6.5631	0.0385	4.7201	0.2757	0.0095	0.4534	0.0000	0.0246	1.8958	0.0000	0.0058	0.0001	0.0147
HML-869	B1	6.5282	0.0710	4.7198	0.2550	0.0082	0.4747	0.0000	0.0499	1.8831	0.0035	0.0000	0.0020	0.0074
HML-869	B2	6.5827	0.0360	4.6571	0.2858	0.0000	0.4700	0.0027	0.0592	1.8826	0.0116	0.0013	0.0055	0.0156
HML-869	A1	6.7066	0.0291	4.4270	0.3305	0.0038	0.5301	0.0021	0.0275	1.9472	0.0046	0.0001	0.0059	0.0124
HML-870	A1	6.3106	0.0362	4.9492	0.4436	0.0012	0.5285	0.0000	0.0583	1.7323	0.0093	0.0000	0.0000	0.0000
HML-870	A2	6.5053	0.0530	4.7733	0.2955	0.0000	0.4344	0.0000	0.0513	1.8060	0.0093	0.0011	0.0153	0.0120
HML-924	C2	6.7543	0.0352	4.3910	0.2196	0.0000	0.6090	0.0039	0.0660	1.8137	0.0000	0.0035	0.0183	0.0146
HML-924	C3	6.7531	0.0367	4.3650	0.2618	0.0000	0.6184	0.0028	0.0759	1.8303	0.0000	0.0000	0.0102	0.0116
HML-924	A2	6.7001	0.0423	4.3835	0.2914	0.0000	0.6328	0.0050	0.0843	1.8374	0.0000	0.0297	0.0084	0.0141
HML-924	B2	6.7616	0.0476	4.3447	0.2459	0.0079	0.6039	0.0129	0.0991	1.8250	0.0018	0.0000	0.0100	0.0042
HML-924	B1	6.7175	0.0571	4.3894	0.2622	0.0029	0.6099	0.0010	0.0613	1.8729	0.0072	0.0052	0.0000	0.0101
HML-924	C1	6.7144	0.0336	4.4036	0.2526	0.0124	0.6342	0.0051	0.0733	1.8610	0.0038	0.0174	0.0000	0.0127
HML-924	A3	6.7104	0.0489	4.4124	0.2679	0.0071	0.6045	0.0000	0.0846	1.8561	0.0000	0.0157	0.0000	0.0052

Table D.1.2 - Molar Composition of Muscovite/Phengite (based on 22 O); continued

Samp. ID	MG	*Si*	*Ti*	*Al*	*Fe*	*Mn*	*Mg*	*Ca*	*Na*	*K*	*Cr*	*Cl*	*P*	*Ba*
HML-924	A1	6.6728	0.0334	4.4312	0.2818	0.0021	0.5769	0.0134	0.1071	1.9006	0.0000	0.0438	0.0094	0.0172
HML-937	C3	6.4756	0.0078	5.0555	0.1605	0.0092	0.3578	0.0000	0.0472	1.7468	0.0045	0.0153	0.0004	0.0100
HML-937	B2	6.5068	0.0114	4.9641	0.1642	0.0063	0.4045	0.0009	0.0504	1.7890	0.0000	0.0060	0.0013	0.0156
HML-937	C1	6.4318	0.0229	5.0499	0.1485	0.0027	0.3985	0.0000	0.0537	1.7900	0.0083	0.0000	0.0097	0.0074
HML-937	A1	6.4782	0.0162	5.0040	0.1379	0.0000	0.3926	0.0132	0.0745	1.8031	0.0000	0.0000	0.0028	0.0158
HML-937	A2	6.4736	0.0304	4.9253	0.1807	0.0055	0.4130	0.0000	0.0445	1.8557	0.0082	0.0035	0.0119	0.0108
HML-973	C1	6.4388	0.0444	4.9857	0.2699	0.0012	0.3100	0.0000	0.0746	1.8100	0.0000	0.0136	0.0062	0.0093
HML-973	C2	6.4181	0.0493	5.0263	0.2378	0.0070	0.3153	0.0063	0.0661	1.8228	0.0003	0.0079	0.0030	0.0030
HML-973	C3	6.4580	0.0486	4.9869	0.2399	0.0000	0.2993	0.0018	0.0681	1.8360	0.0053	0.0000	0.0022	0.0000
HML-973	A2	6.4994	0.0364	4.9021	0.2559	0.0016	0.3438	0.0000	0.0515	1.8638	0.0021	0.0000	0.0016	0.0093
HML-985	A1	6.3164	0.0177	5.0355	0.4358	0.0065	0.3623	0.0083	0.0777	1.7315	0.0054	0.0087	0.0155	0.0098
HML-985	A2	6.3589	0.0276	5.0815	0.2368	0.0000	0.2982	0.0000	0.0825	1.7796	0.0751	0.0065	0.0071	0.0053
HML-985	A3	6.3464	0.0386	5.0064	0.3431	0.0082	0.3288	0.0048	0.0685	1.7419	0.0806	0.0107	0.0000	0.0040
HML-985	A3	6.4037	0.0200	5.1088	0.1966	0.0108	0.3011	0.0000	0.0623	1.7422	0.0426	0.0071	0.0000	0.0111
HML-985	B1	6.4731	0.0348	5.0758	0.2993	0.0000	0.3327	0.0000	0.0393	1.3526	0.0000	0.0000	0.0170	0.0000

Table D.2.1 – Feldspar Wt. % Oxide Electron Microprobe Compositions

Samp. ID	MG	*SiO2*	*TiO2*	*Al2O3*	*FeO*	*MnO*	*MgO*	*CaO*	*Na2O*	*K2O*	*Cr2O3*	*NiO*	*P2O5*	*Cl*	*SrO*	*ZrO*	*La2O3*	*BaO*	*SO4*	*TOTAL*
HML-892	A1-core	67.87	0.07	20.10	0.07	0.00	0.24	0.10	10.15	0.81	0.02	0.00	0.00	0.00	0.00	0.00	0.00	0.00	0.08	99.50
HML-892	A1-rim	69.45	0.00	19.77	0.27	0.00	0.07	0.00	12.08	0.05	0.00	0.03	0.00	0.00	0.00	0.00	0.02	0.00	0.04	101.77
HML-892	A2-core	67.80	0.01	19.49	0.49	0.08	0.43	0.01	9.67	0.12	0.00	0.02	0.00	0.00	0.00	0.00	0.00	0.00	0.00	98.13
HML-892	A2-rim	69.08	0.00	19.67	0.09	0.02	0.07	0.14	9.66	0.17	0.00	0.00	0.00	0.00	0.00	0.21	0.05	0.11	0.02	99.29
HML-892	B1-core	65.05	0.13	22.53	0.62	0.04	0.96	0.08	6.39	3.14	0.02	0.00	0.00	0.00	0.00	0.00	0.05	0.20	0.13	99.34
HML-892	B2-core	69.35	0.00	19.54	0.08	0.00	0.08	0.02	9.34	0.06	0.09	0.00	0.00	0.00	0.00	0.00	0.00	0.00	0.06	98.62
HML-892	B3-rim	66.74	0.05	19.81	0.20	0.00	0.23	0.11	9.19	0.54	0.00	0.03	0.00	0.00	0.00	0.00	0.00	0.00	0.00	96.89
HML-844	B2-rim	69.49	0.12	19.74	0.08	0.02	0.00	0.07	9.44	0.04	0.00	0.08	0.00	0.00	0.00	0.04	0.10	0.00	0.03	99.26
HML-844	A1-core	70.19	0.10	20.03	0.10	0.00	0.19	0.02	9.43	0.30	0.03	0.00	0.00	0.00	0.00	0.00	0.00	0.00	0.00	100.38
HML-844	A2-rim	65.17	0.01	18.96	0.00	0.00	0.01	0.00	0.21	14.57	0.08	0.00	0.00	0.00	0.00	0.00	0.00	1.34	0.11	100.47
HML-892	C-core	69.96	0.00	20.65	0.14	0.00	0.10	0.15	8.52	0.58	0.00	0.00	0.00	0.02	0.00	0.00	0.27	0.16	0.07	100.62
HML-892	C-rim	70.12	0.00	19.58	0.11	0.00	0.00	0.12	9.66	0.05	0.07	0.05	0.00	0.00	0.00	0.00	0.00	0.00	0.03	99.79
HML-892	B-core	69.80	0.11	19.74	0.07	0.02	0.07	0.08	10.09	0.03	0.00	0.00	0.00	0.00	0.00	0.00	0.13	0.00	0.00	100.14
HML-892	B-rim	69.79	0.00	19.77	0.19	0.06	0.08	0.01	9.72	0.07	0.00	0.09	0.00	0.00	0.00	0.00	0.00	0.00	0.00	99.78
HML-892	B1-rim	70.15	0.08	19.88	0.18	0.00	0.10	0.04	9.96	0.06	0.03	0.00	0.00	0.00	0.00	0.00	0.00	0.00	0.00	100.48
HML-892	B2-rim	70.88	0.00	20.00	0.02	0.00	0.09	0.00	9.31	0.02	0.06	0.00	0.00	0.05	0.00	0.08	0.00	0.04	0.00	100.54
HML-892	A2-rim	69.56	0.00	19.76	0.01	0.00	0.13	0.13	9.86	0.08	0.02	0.23	0.00	0.03	0.00	0.00	0.03	0.05	0.12	100.04
HML-832	C-core	65.43	0.05	18.28	0.00	0.02	0.00	0.02	0.77	13.39	0.10	0.04	0.00	0.00	0.00	0.16	0.00	0.19	0.09	98.53
HML-832	C- core	68.63	0.02	19.40	0.00	0.00	0.05	0.13	9.38	0.06	0.00	0.20	0.00	0.03	0.00	0.00	0.00	0.00	0.00	97.90
HML-832	C-rim	69.27	0.00	19.39	0.11	0.00	0.00	0.01	9.36	0.00	0.03	0.16	0.00	0.10	0.00	0.00	0.08	0.02	0.12	98.67

Table D.2.2 - Molar Composition of Feldspar (based on 8 O)

Samp. ID	MG	*Si*	*Ti*	*Al*	*Fe*	*Mn*	*Mg*	*Ca*	*Na*	*K*	*Cr*	*Ni*	*P*	*Cl*	*Sr*	*Zr*	*La*	*Ba*	*S*
HML-892	A1-core	2.976	0.002	1.038	0.002	0.000	0.016	0.005	0.863	0.046	0.001	0.000	0.000	0.000	0.000	0.000	0.000	0.000	0.002
HML-892	A1-rim	2.986	0.000	1.002	0.010	0.000	0.004	0.000	1.007	0.003	0.000	0.001	0.000	0.000	0.000	0.000	0.000	0.000	0.001
HML-892	A2-core	3.002	0.000	1.017	0.018	0.003	0.028	0.000	0.830	0.007	0.000	0.001	0.000	0.000	0.000	0.000	0.000	0.000	0.000
HML-892	A2-rim	3.018	0.000	1.013	0.003	0.001	0.005	0.006	0.818	0.009	0.000	0.000	0.000	0.000	0.000	0.005	0.001	0.008	0.000
HML-892	B1-core	2.873	0.004	1.173	0.023	0.001	0.063	0.004	0.547	0.177	0.001	0.000	0.000	0.000	0.000	0.000	0.001	0.015	0.004
HML-892	B2-core	3.035	0.000	1.008	0.003	0.000	0.005	0.001	0.793	0.003	0.003	0.000	0.000	0.000	0.000	0.000	0.000	0.000	0.002
HML-892	B3-rim	2.992	0.002	1.047	0.007	0.000	0.015	0.005	0.798	0.031	0.000	0.001	0.000	0.000	0.000	0.000	0.000	0.000	0.000
HML-844	B2-rim	3.027	0.004	1.014	0.003	0.001	0.000	0.003	0.798	0.002	0.000	0.003	0.000	0.000	0.000	0.001	0.002	0.000	0.001
HML-844	A1-core	3.024	0.003	1.017	0.004	0.000	0.012	0.001	0.787	0.016	0.001	0.000	0.000	0.000	0.000	0.000	0.000	0.000	0.000
HML-844	A2-rim	2.962	0.000	1.016	0.000	0.000	0.000	0.000	0.019	0.845	0.003	0.000	0.000	0.000	0.000	0.000	0.000	0.104	0.003
HML-892	C-core	3.007	0.000	1.046	0.005	0.000	0.007	0.007	0.710	0.032	0.000	0.000	0.000	0.001	0.000	0.000	0.004	0.012	0.002
HML-892	C-rim	3.038	0.000	0.999	0.004	0.000	0.000	0.006	0.811	0.003	0.002	0.002	0.000	0.000	0.000	0.000	0.000	0.000	0.001
HML-892	B-core	3.022	0.004	1.007	0.002	0.001	0.005	0.004	0.847	0.002	0.000	0.000	0.000	0.000	0.000	0.000	0.002	0.000	0.000
HML-892	B-rim	3.028	0.000	1.011	0.007	0.002	0.005	0.000	0.817	0.004	0.000	0.003	0.000	0.000	0.000	0.000	0.000	0.000	0.000
HML-892	B1-rim	3.023	0.003	1.009	0.007	0.000	0.006	0.002	0.832	0.004	0.001	0.000	0.000	0.000	0.000	0.000	0.000	0.000	0.000
HML-892	B2-rim	3.040	0.000	1.011	0.001	0.000	0.005	0.000	0.774	0.001	0.002	0.000	0.000	0.004	0.000	0.002	0.000	0.003	0.000
HML-892	A2-rim	3.013	0.000	1.009	0.000	0.000	0.009	0.006	0.828	0.005	0.001	0.008	0.000	0.002	0.000	0.000	0.001	0.004	0.003
HML-832	C-core	3.019	0.002	0.994	0.000	0.001	0.000	0.001	0.069	0.789	0.003	0.002	0.000	0.000	0.000	0.004	0.000	0.015	0.003
HML-832	C- core	3.032	0.001	1.010	0.000	0.000	0.003	0.006	0.803	0.003	0.000	0.007	0.000	0.002	0.000	0.000	0.000	0.000	0.000
HML-832	C-rim	3.034	0.000	1.001	0.004	0.000	0.000	0.001	0.795	0.000	0.001	0.006	0.000	0.007	0.000	0.000	0.001	0.002	0.003

Table D.3.1 - Chlorite Wt. % Oxide Electron Microprobe Compositions

Samp. ID	MG	SiO2	TiO2	Al2O3	FeO	MnO	MgO	CaO	Na2O	K2O	Cr2O3	NiO	P2O5	Cl	SrO	ZrO	La2O3	BaO	SO4	TOTAL
HML-805	A1	22.85	0.10	21.36	35.84	0.16	6.20	0.00	0.16	0.06	0.14	0.00	0.00	0.04	0.00	0.00	0.29	0.17	0.00	87.36
HML-942	A1	24.15	0.17	21.74	28.21	0.42	12.02	0.01	0.09	0.00	0.00	0.00	0.00	0.00	0.00	0.04	0.05	0.00	0.08	86.98
HML-945	A1	22.60	0.00	21.80	37.35	0.21	5.50	0.02	0.14	0.01	0.00	0.00	0.00	0.01	0.00	0.00	0.03	0.19	0.01	87.88
HML-868	A1	24.20	0.16	18.15	27.35	0.17	13.21	0.01	0.12	0.00	0.00	0.13	0.00	0.00	0.00	0.00	0.00	0.00	0.00	83.51
HML-805	A2	22.41	0.11	21.24	35.62	0.34	6.28	0.01	0.09	0.00	0.01	0.00	0.00	0.01	0.00	0.00	0.10	0.00	0.00	86.24
HML-942	A2	23.82	0.05	21.67	28.34	0.61	12.24	0.02	0.21	0.03	0.06	0.00	0.00	0.03	0.00	0.04	0.18	0.10	0.11	87.52
HML-945	A2	22.89	0.01	22.16	37.32	0.28	5.53	0.00	0.13	0.01	0.00	0.00	0.00	0.01	0.00	0.11	0.07	0.16	0.00	88.68
HML-868	A2	28.56	0.08	20.97	24.09	0.11	11.37	0.00	0.12	1.08	0.01	0.00	0.18	0.03	0.00	0.00	0.00	0.00	0.11	86.70
HML-805	A3	22.31	0.09	21.56	36.26	0.35	6.30	0.00	0.15	0.00	0.11	0.04	0.00	0.00	0.00	0.09	0.00	0.01	0.07	87.34
HML-942	A3	24.08	0.07	21.43	28.09	0.45	12.11	0.00	0.12	0.03	0.00	0.16	0.00	0.02	0.11	0.08	0.15	0.16	0.04	87.10
HML-945	A3	22.15	0.07	21.22	36.97	0.18	5.20	0.00	0.11	0.00	0.06	0.00	0.00	0.04	0.00	0.00	0.16	0.24	0.00	86.38
HML-868	A3	25.47	0.04	19.25	28.86	0.18	13.19	0.00	0.11	0.00	0.00	0.07	0.02	0.01	0.00	0.00	0.05	0.07	0.05	87.37
HML-945	A4	22.78	0.12	21.88	37.24	0.31	5.48	0.02	0.14	0.06	0.00	0.00	0.00	0.00	0.00	0.00	0.00	0.00	0.17	88.22
HML-868	A4	25.28	0.13	20.23	27.56	0.14	13.97	0.07	0.07	0.00	0.02	0.00	0.00	0.00	0.00	0.00	0.19	0.00	0.00	87.67
HML-805	B1	22.63	0.09	21.38	35.78	0.14	6.18	0.02	0.17	0.01	0.00	0.04	0.00	0.00	0.00	0.00	0.18	0.09	0.01	86.72
HML-942	B1	22.75	0.08	20.28	27.41	0.40	11.38	0.02	0.28	0.03	0.00	0.01	0.00	0.04	0.00	0.13	0.00	0.00	0.17	83.00
HML-945	B1	22.42	0.00	21.85	37.22	0.24	5.39	0.00	0.10	0.00	0.02	0.00	0.00	0.00	0.00	0.00	0.00	0.00	0.09	87.34
HML-868	B1	24.70	0.10	19.53	27.82	0.25	13.06	0.00	0.15	0.00	0.00	0.04	0.00	0.01	0.00	0.00	0.13	0.00	0.19	85.97
HML-805	B2	22.98	0.00	20.56	35.66	0.22	6.54	0.01	0.16	0.02	0.00	0.00	0.00	0.01	0.00	0.00	0.00	0.00	0.00	86.16
HML-942	B2	25.22	0.00	22.84	27.81	0.38	13.30	0.02	0.08	0.00	0.00	0.18	0.01	0.04	0.00	0.01	0.18	0.25	0.05	90.37
HML-945	B2	22.27	0.11	21.87	37.57	0.17	5.11	0.03	0.08	0.03	0.06	0.02	0.00	0.06	0.00	0.01	0.03	0.05	0.04	87.51
HML-868	B2	25.37	0.04	20.18	27.17	0.29	13.87	0.02	0.20	0.02	0.00	0.00	0.00	0.01	0.00	0.00	0.00	0.02	0.02	87.22
HML-805	B3	22.31	0.14	21.05	35.93	0.31	6.44	0.09	0.20	0.00	0.00	0.02	0.00	0.02	0.00	0.17	0.00	0.00	0.04	86.71
HML-945	B3	22.69	0.15	21.71	37.29	0.24	5.58	0.02	0.15	0.00	0.00	0.00	0.00	0.02	0.00	0.00	0.05	0.00	0.00	87.90
HML-868	B3	24.68	0.05	19.75	26.83	0.23	13.43	0.03	0.07	0.04	0.00	0.00	0.00	0.02	0.00	0.05	0.01	0.06	0.18	85.43

Table D.3.1 – Chlorite Wt. % Oxide Electron Microprobe Compositions (continued)

Samp. ID	MG	SiO2	TiO2	Al2O3	FeO	MnO	MgO	CaO	Na2O	K2O	Cr2O3	NiO	P2O5	Cl	SrO	ZrO	La2O3	BaO	SO4	TOTAL
HML-805	C*	22.91	0.01	21.81	38.39	0.26	6.07	0.06	0.02	0.33	0.00	0.11	0.00	0.03	0.00	0.00	0.19	0.01	0.00	90.20
HML-805	C*	39.11	0.00	22.08	24.10	0.45	11.44	4.55	0.24	0.00	0.00	0.00	0.00	0.00	0.00	0.00	0.00	0.12	0.00	102.08
HML-805	C*	38.63	0.11	21.71	21.94	0.50	11.23	4.58	0.09	0.00	0.02	0.01	0.00	0.04	0.00	0.00	0.00	0.00	0.10	98.95
HML-805	C1	22.70	0.05	21.66	36.52	0.29	6.09	0.00	0.20	0.00	0.00	0.00	0.00	0.00	0.00	0.00	0.05	0.05	0.07	87.68
HML-942	C1	39.95	0.00	16.66	22.78	0.34	9.62	0.01	0.10	0.02	0.00	0.00	0.00	0.01	0.00	0.00	0.01	0.00	0.17	89.66
HML-945	C1	22.61	0.08	21.59	37.44	0.23	5.39	0.00	0.02	0.05	0.01	0.00	0.00	0.00	0.00	0.07	0.00	0.00	0.00	87.50
HML-909	C1	26.19	0.05	19.82	27.48	0.31	13.37	0.05	0.01	0.07	0.00	0.18	0.00	0.01	0.00	0.05	0.00	0.00	0.03	87.62
HML-868	C1	25.10	0.00	20.30	27.78	0.18	13.44	0.05	0.17	0.04	0.00	0.00	0.00	0.01	0.00	0.06	0.01	0.00	0.00	87.15
HML-805	C2	22.20	0.16	21.60	35.67	0.31	6.30	0.05	0.22	0.00	0.00	0.08	0.10	0.04	0.00	0.00	0.10	0.09	0.03	86.96
HML-945	C2	22.69	0.02	21.94	37.39	0.15	5.32	0.06	0.11	0.04	0.00	0.00	0.00	0.06	0.00	1.06	0.03	0.11	0.14	89.11
HML-909	C2	24.85	0.15	20.10	27.76	0.32	12.80	0.02	0.17	0.00	0.00	0.00	0.00	0.00	0.00	0.10	0.04	0.00	0.02	86.33
HML-868	C2	27.14	0.13	21.40	27.00	0.04	13.72	0.03	0.10	0.54	0.00	0.06	0.00	0.06	0.00	0.15	0.05	0.00	0.06	90.47
HML-805	C3	22.66	0.00	21.51	35.59	0.26	6.28	0.00	0.16	0.06	0.00	0.00	0.00	0.01	0.00	0.17	0.01	0.19	0.06	86.95
HML-942	C3	24.05	0.04	21.35	27.84	0.48	11.93	0.02	0.10	0.01	0.00	0.00	0.00	0.02	0.00	0.00	0.06	0.00	0.00	85.89
HML-942	C3	24.67	0.09	21.55	27.96	0.55	12.28	0.05	0.16	0.02	0.03	0.00	0.01	0.02	0.00	0.00	0.03	0.00	0.00	87.42
HML-942	C3	24.31	0.00	21.67	28.15	0.56	12.27	0.00	0.13	0.00	0.01	0.00	0.00	0.01	0.00	0.02	0.11	0.11	0.22	87.55
HML-945	C3	22.95	0.07	21.60	37.31	0.32	5.48	0.06	0.00	0.00	0.00	0.00	0.00	0.00	0.00	0.04	0.05	0.03	0.01	87.92
HML-909	C3	24.79	0.14	20.40	28.36	0.42	12.65	0.10	0.10	0.01	0.00	0.00	0.00	0.01	0.00	0.00	0.00	0.01	0.00	86.98
HML-868	C3	24.63	0.10	19.72	26.60	0.13	13.58	0.00	0.00	0.00	0.03	0.03	0.00	0.00	0.00	0.03	0.05	0.00	0.07	84.96
HML-945	C4	22.77	0.05	21.70	37.30	0.37	5.50	0.00	0.00	0.04	0.00	0.00	0.00	0.00	0.00	0.00	0.01	0.17	0.14	88.04
HML-909	C4	24.90	0.01	19.94	27.84	0.25	12.84	0.15	0.07	0.03	0.04	0.00	0.00	0.01	0.00	0.00	0.00	0.00	0.00	86.05
HML-868	C4	25.10	0.00	19.76	26.97	0.17	13.92	0.07	0.10	0.03	0.06	0.00	0.00	0.04	0.00	0.01	0.11	0.08	0.00	86.44
HML-909	D1	23.93	0.02	20.54	28.71	0.19	11.92	0.00	0.15	0.04	0.01	0.19	0.00	0.00	0.00	0.26	0.00	0.00	0.16	86.13
HML-909	D2	24.75	0.09	21.10	28.73	0.31	12.39	0.06	0.05	0.04	0.00	0.00	0.00	0.03	0.00	0.11	0.04	0.03	0.05	87.78

Table D.3.2 – Molar Composition of Chlorite (based on 28 O)

Samp. ID	MG	*Si*	*Ti*	*Al*	*Fe*	*Mn*	*Mg*	*Ca*	*Na*	*K*	*Cr*	*Ni*	*P*	*Cl*	*Sr*	*Zr*	*La*	*Ba*	*S*
HML-805	A1	5.168	0.017	5.693	6.779	0.031	2.088	0.000	0.070	0.018	0.025	0.000	0.000	0.015	0.000	0.000	0.024	0.066	0.000
HML-942	A1	5.233	0.028	5.554	5.113	0.077	3.883	0.002	0.037	0.000	0.000	0.000	0.000	0.000	0.000	0.005	0.004	0.000	0.011
HML-945	A1	5.108	0.000	5.807	7.058	0.041	1.853	0.004	0.059	0.003	0.000	0.000	0.000	0.005	0.000	0.000	0.003	0.075	0.002
HML-868	A1	5.480	0.026	4.844	5.179	0.033	4.457	0.002	0.053	0.000	0.000	0.024	0.000	0.000	0.000	0.000	0.000	0.000	0.000
HML-805	A2	5.138	0.018	5.738	6.828	0.066	2.145	0.003	0.041	0.000	0.001	0.000	0.000	0.004	0.000	0.000	0.009	0.000	0.000
HML-942	A2	5.154	0.009	5.527	5.128	0.112	3.946	0.004	0.087	0.009	0.011	0.000	0.000	0.009	0.000	0.005	0.014	0.036	0.015
HML-945	A2	5.120	0.002	5.843	6.982	0.054	1.843	0.000	0.055	0.003	0.000	0.000	0.000	0.005	0.000	0.014	0.006	0.059	0.000
HML-868	A2	6.013	0.013	5.204	4.241	0.019	3.567	0.000	0.048	0.290	0.002	0.000	0.032	0.012	0.000	0.000	0.000	0.000	0.015
HML-805	A3	5.060	0.016	5.763	6.879	0.066	2.131	0.000	0.064	0.000	0.020	0.006	0.000	0.000	0.000	0.011	0.000	0.006	0.010
HML-942	A3	5.230	0.011	5.486	5.103	0.083	3.918	0.000	0.049	0.008	0.000	0.028	0.000	0.006	0.014	0.010	0.012	0.060	0.006
HML-945	A3	5.108	0.012	5.766	7.130	0.035	1.785	0.000	0.047	0.000	0.010	0.000	0.000	0.014	0.000	0.000	0.013	0.094	0.000
HML-868	A3	5.509	0.007	4.908	5.219	0.033	4.251	0.000	0.048	0.000	0.000	0.012	0.004	0.003	0.000	0.000	0.004	0.026	0.006
HML-945	A4	5.117	0.021	5.793	6.996	0.060	1.835	0.006	0.060	0.018	0.000	0.000	0.001	0.000	0.000	0.000	0.000	0.000	0.024
HML-868	A4	5.413	0.021	5.105	4.933	0.025	4.457	0.017	0.031	0.001	0.003	0.000	0.000	0.000	0.000	0.000	0.015	0.000	0.000
HML-805	B1	5.154	0.016	5.740	6.814	0.028	2.099	0.004	0.074	0.003	0.000	0.007	0.000	0.000	0.000	0.000	0.015	0.034	0.001
HML-942	B1	5.198	0.014	5.461	5.235	0.078	3.874	0.006	0.123	0.010	0.000	0.002	0.000	0.016	0.000	0.016	0.000	0.000	0.025
HML-945	B1	5.096	0.000	5.853	7.075	0.047	1.826	0.000	0.045	0.000	0.004	0.000	0.000	0.000	0.000	0.000	0.000	0.000	0.013
HML-868	B1	5.415	0.016	5.045	5.101	0.046	4.265	0.000	0.063	0.001	0.000	0.007	0.000	0.003	0.000	0.000	0.011	0.000	0.025
HML-805	B2	5.265	0.000	5.549	6.831	0.043	2.233	0.002	0.070	0.004	0.000	0.000	0.000	0.004	0.000	0.000	0.000	0.000	0.000
HML-942	B2	5.225	0.000	5.577	4.818	0.067	4.106	0.005	0.031	0.000	0.000	0.029	0.002	0.014	0.000	0.001	0.014	0.086	0.006
HML-945	B2	5.069	0.019	5.867	7.151	0.034	1.732	0.008	0.035	0.010	0.011	0.003	0.000	0.022	0.000	0.001	0.003	0.017	0.005
HML-868	B2	5.446	0.007	5.106	4.877	0.053	4.436	0.005	0.084	0.004	0.000	0.000	0.000	0.005	0.000	0.000	0.000	0.007	0.003
HML-805	B3	5.100	0.024	5.673	6.868	0.059	2.193	0.021	0.088	0.000	0.000	0.004	0.000	0.008	0.000	0.021	0.000	0.000	0.006
HML-945	B3	5.128	0.025	5.781	7.048	0.045	1.880	0.006	0.065	0.000	0.000	0.000	0.000	0.007	0.000	0.000	0.004	0.000	0.000
HML-868	B3	5.411	0.008	5.104	4.919	0.044	4.388	0.008	0.031	0.011	0.000	0.000	0.000	0.008	0.000	0.006	0.000	0.021	0.024

Table D.3.2 - Composition of chlorite (based on 28 O); continued

Samp. ID	MG	*Si*	*Ti*	*Al*	*Fe*	*Mn*	*Mg*	*Ca*	*Na*	*K*	*Cr*	*Ni*	*P*	*Cl*	*Sr*	*Zr*	*La*	*Ba*	*S*
HML-805	C*	5.079	0.002	5.700	7.117	0.049	2.005	0.014	0.008	0.092	0.000	0.019	0.000	0.012	0.000	0.000	0.015	0.004	0.000
HML-805	C*	6.838	0.000	4.550	3.524	0.066	2.980	0.852	0.081	0.000	0.000	0.000	0.000	0.000	0.000	0.000	0.000	0.035	0.000
HML-805	C*	6.907	0.015	4.575	3.279	0.075	2.990	0.877	0.030	0.000	0.003	0.001	0.000	0.012	0.000	0.000	0.000	0.000	0.012
HML-805	C1	5.121	0.008	5.758	6.890	0.055	2.048	0.000	0.089	0.000	0.000	0.000	0.000	0.000	0.000	0.000	0.004	0.019	0.010
HML-942	C1	7.792	0.000	3.828	3.715	0.056	2.795	0.002	0.039	0.006	0.000	0.000	0.000	0.004	0.000	0.000	0.001	0.000	0.020
HML-945	C1	5.140	0.014	5.784	7.118	0.044	1.828	0.000	0.010	0.016	0.002	0.000	0.000	0.000	0.000	0.008	0.000	0.000	0.000
HML-909	C1	5.597	0.008	4.991	4.910	0.057	4.258	0.011	0.003	0.018	0.000	0.031	0.000	0.003	0.000	0.005	0.000	0.000	0.005
HML-868	C1	5.415	0.000	5.161	5.011	0.033	4.320	0.011	0.072	0.011	0.000	0.000	0.000	0.005	0.000	0.007	0.001	0.000	0.000
HML-805	C2	5.047	0.027	5.786	6.780	0.059	2.134	0.012	0.099	0.000	0.000	0.015	0.020	0.015	0.000	0.000	0.008	0.034	0.005
HML-945	C2	5.088	0.004	5.796	7.010	0.028	1.776	0.015	0.046	0.011	0.000	0.000	0.000	0.022	0.000	0.133	0.002	0.043	0.019
HML-909	C2	5.422	0.024	5.169	5.064	0.059	4.161	0.005	0.073	0.000	0.000	0.000	0.000	0.000	0.000	0.012	0.003	0.000	0.003
HML-868	C2	5.579	0.021	5.186	4.641	0.007	4.203	0.006	0.038	0.142	0.000	0.010	0.000	0.020	0.000	0.017	0.004	0.000	0.008
HML-805	C3	5.140	0.000	5.750	6.749	0.050	2.122	0.001	0.069	0.017	0.000	0.000	0.000	0.002	0.000	0.021	0.001	0.074	0.008
HML-942	C3	5.281	0.007	5.523	5.110	0.089	3.902	0.004	0.041	0.003	0.000	0.000	0.000	0.006	0.000	0.000	0.005	0.000	0.000
HML-942	C3	5.312	0.014	5.469	5.035	0.100	3.940	0.012	0.067	0.007	0.005	0.000	0.002	0.009	0.000	0.000	0.003	0.000	0.000
HML-942	C3	5.230	0.000	5.494	5.065	0.102	3.932	0.000	0.056	0.000	0.001	0.000	0.000	0.002	0.000	0.002	0.008	0.038	0.029
HML-945	C3	5.182	0.012	5.747	7.043	0.060	1.845	0.015	0.001	0.000	0.000	0.000	0.000	0.000	0.000	0.005	0.004	0.011	0.002
HML-909	C3	5.381	0.023	5.218	5.148	0.078	4.090	0.023	0.041	0.002	0.000	0.000	0.000	0.003	0.000	0.000	0.000	0.004	0.000
HML-868	C3	5.425	0.016	5.119	4.898	0.024	4.457	0.000	0.000	0.000	0.005	0.006	0.000	0.000	0.000	0.004	0.004	0.000	0.009
HML-945	C4	5.127	0.008	5.759	7.025	0.070	1.845	0.000	0.001	0.012	0.000	0.000	0.000	0.000	0.000	0.000	0.000	0.064	0.020
HML-909	C4	5.448	0.001	5.142	5.094	0.046	4.185	0.034	0.028	0.007	0.006	0.000	0.000	0.004	0.000	0.000	0.000	0.000	0.000
HML-868	C4	5.443	0.000	5.052	4.892	0.031	4.498	0.017	0.044	0.010	0.011	0.000	0.000	0.015	0.000	0.002	0.009	0.031	0.000
HML-909	D1	5.275	0.004	5.336	5.293	0.035	3.916	0.000	0.066	0.011	0.001	0.034	0.000	0.000	0.000	0.032	0.000	0.000	0.022
HML-909	D2	5.327	0.014	5.351	5.170	0.057	3.974	0.014	0.022	0.011	0.000	0.000	0.000	0.010	0.000	0.013	0.004	0.011	0.006

Table D.4.1 - Carbonate Wt. % Oxide Electron Microprobe Compositions

Samp. ID	MG	*FeO*	*MnO*	*MgO*	*CaO*	*BaO*	*SrO*	*K2O*	*Na2O*	*SO4*	*SiO2*	*TiO2*	*Al2O3*	*P2O5*	*Cl*	*TOTAL*
HML-826	A1	0.338	1.159	0.153	52.903	0.056	0.206	0.037	0.000	0.054	0.129	0.000	0.000	0.046	0.009	55.090
HML-821	A1	1.170	0.781	0.194	54.150	0.202	0.028	0.040	0.060	0.033	0.134	0.000	0.000	0.000	0.042	56.833
HML-914	A1	0.926	0.985	0.322	52.263	0.121	0.125	0.020	0.147	0.110	0.200	0.000	0.022	0.000	0.019	55.259
HML-909	A1	0.507	0.493	0.230	56.139	0.161	0.208	0.042	0.065	0.037	0.169	0.000	0.004	0.016	0.000	58.070
HML-826	A2	0.602	1.574	0.183	53.417	0.074	0.173	0.006	0.129	0.000	0.106	0.040	0.051	0.068	0.000	56.421
HML-821	A2	1.023	0.726	0.132	54.620	0.128	0.102	0.000	0.000	0.066	0.158	0.000	0.000	0.058	0.000	57.012
HML-914	A2	0.579	0.906	0.298	52.949	0.107	0.196	0.021	0.123	0.000	0.127	0.000	0.000	0.023	0.000	55.328
HML-909	A2	0.607	0.552	0.157	54.321	0.321	0.140	0.000	0.039	0.000	0.140	0.000	0.000	0.027	0.000	56.306
HML-826	A3	0.274	1.283	0.195	53.681	0.034	0.099	0.000	0.000	0.000	0.108	0.000	0.000	0.000	0.000	55.675
HML-821	A3	1.016	0.691	0.130	54.964	0.029	0.124	0.000	0.066	0.000	0.071	0.000	0.000	0.145	0.010	57.246
HML-914	A3	0.467	0.862	0.187	55.271	0.000	0.322	0.022	0.075	0.052	0.111	0.060	0.000	0.016	0.034	57.478
HML-909	A3	0.509	0.672	0.186	55.038	0.128	0.088	0.063	0.027	0.000	0.165	0.000	0.000	0.000	0.009	56.884
HML-821	A4	1.012	0.700	0.081	54.464	0.125	0.063	0.000	0.000	0.000	0.175	0.071	0.000	0.000	0.017	56.709
HML-914	A4	0.442	0.665	0.191	55.604	0.229	0.243	0.029	0.022	0.026	0.125	0.000	0.000	0.068	0.000	57.644
HML-821	A5	0.987	0.777	0.097	54.566	0.024	0.114	0.039	0.059	0.050	0.150	0.000	0.000	0.100	0.000	56.964
HML-826	B1	0.910	1.378	0.389	54.438	0.172	0.036	0.012	0.101	0.000	0.134	0.000	0.000	0.029	0.000	57.600
HML-821	B1	0.962	0.697	0.111	53.487	0.000	0.199	0.043	0.090	0.000	0.205	0.000	0.066	0.059	0.000	55.917
HML-914	B1	0.605	0.719	0.170	53.248	0.000	0.280	0.008	0.019	0.000	0.151	0.075	0.000	0.057	0.031	55.362
HML-792	B1	0.325	0.583	0.161	55.154	0.054	0.240	0.032	0.037	0.000	0.198	0.000	0.000	0.073	0.000	56.858
HML-909	B1	0.532	0.460	0.206	54.433	0.000	0.183	0.022	0.000	0.086	0.165	0.048	0.048	0.012	0.027	56.221
HML-826	B2	1.528	1.587	0.479	53.677	0.000	0.132	0.000	0.025	0.053	0.204	0.065	0.000	0.000	0.035	57.784
HML-821	B2	0.778	0.943	0.076	52.378	0.142	0.118	0.015	0.000	0.086	0.091	0.016	0.000	0.000	0.013	54.656
HML-914	B2	0.628	0.684	0.308	54.630	0.015	0.271	0.012	0.138	0.000	0.115	0.000	0.015	0.019	0.035	56.868
HML-792	B2	0.182	0.491	0.084	54.845	0.190	0.068	0.000	0.090	0.158	0.179	0.000	0.000	0.076	0.000	56.363
HML-909	B2	0.429	0.461	0.103	55.579	0.107	0.224	0.000	0.000	0.000	0.122	0.000	0.000	0.141	0.000	57.166
HML-826	B3	0.992	0.906	0.281	54.132	0.127	0.073	0.008	0.009	0.000	0.221	0.000	0.000	0.000	0.030	56.778
HML-821	B3	0.941	0.611	0.160	53.584	0.065	0.168	0.009	0.002	0.056	0.115	0.000	0.012	0.082	0.013	55.817

Table D.4.1 - Carbonate Wt. % Oxide Electron Microprobe Compositions (continued)

Samp. ID	MG	*FeO*	*MnO*	*MgO*	*CaO*	*BaO*	*SrO*	*K2O*	*Na2O*	*SO4*	*SiO2*	*TiO2*	*Al2O3*	*P2O5*	*Cl*	*TOTAL*
HML-914	B3	0.636	0.784	0.197	54.380	0.072	0.236	0.000	0.073	0.037	0.120	0.000	0.000	0.060	0.000	56.595
HML-792	B3	0.256	0.411	0.165	54.993	0.000	0.155	0.050	0.008	0.031	0.129	0.038	0.000	0.043	0.000	56.280
HML-909	B3	0.628	0.665	0.321	54.614	0.000	0.072	0.000	0.000	0.030	0.079	0.068	0.000	0.000	0.008	56.485
HML-792	B4	0.196	0.514	0.095	54.935	0.157	0.086	0.000	0.062	0.003	0.101	0.000	0.011	0.013	0.000	56.171
HML-909	B4	0.615	0.668	0.242	55.571	0.183	0.099	0.006	0.099	0.026	0.156	0.000	0.007	0.000	0.006	57.679
HML-826	C1	0.393	1.137	0.095	55.209	0.051	0.214	0.000	0.000	0.000	0.119	0.000	0.000	0.000	0.000	57.217
HML-821	C1	0.101	1.667	0.021	56.856	0.000	0.000	0.000	0.120	0.000	0.144	0.082	0.000	0.064	0.001	59.055
HML-914	C1	0.622	0.793	0.335	54.837	0.269	0.327	0.014	0.086	0.101	0.145	0.000	0.000	0.121	0.009	57.659
HML-826	C2	0.393	1.219	0.262	55.674	0.005	0.325	0.000	0.066	0.066	0.059	0.000	0.002	0.100	0.026	58.196
HML-821	C2	0.146	1.675	0.038	56.380	0.000	0.003	0.005	0.103	0.086	0.211	0.000	0.024	0.040	0.016	58.727
HML-914	C2	0.604	0.795	0.194	54.066	0.000	0.336	0.033	0.061	0.052	0.204	0.000	0.000	0.099	0.003	56.447
HML-826	C3	0.556	1.321	0.202	55.741	0.200	0.102	0.000	0.064	0.074	0.181	0.000	0.051	0.043	0.020	58.555
HML-821	C3	0.056	1.469	0.000	54.237	0.252	0.009	0.016	0.116	0.000	0.134	0.000	0.000	0.000	0.030	56.320
HML-914	C3	0.615	0.852	0.215	54.326	0.039	0.145	0.042	0.126	0.024	0.175	0.000	0.000	0.000	0.005	56.563
HML-821	C4	0.162	2.007	0.004	55.120	0.030	0.031	0.033	0.028	0.000	0.193	0.110	0.020	0.067	0.005	57.810
HML-821	D1	0.957	0.606	0.115	55.165	0.042	0.095	0.006	0.035	0.049	0.158	0.000	0.000	0.050	0.021	57.299
HML-792	D1	0.239	0.654	0.112	54.468	0.003	0.143	0.015	0.056	0.050	0.228	0.003	0.000	0.085	0.027	56.082
HML-821	D2	0.938	0.831	0.098	54.996	0.000	0.035	0.007	0.103	0.102	0.105	0.000	0.000	0.013	0.000	57.228
HML-792	D2	0.233	0.646	0.088	54.984	0.000	0.116	0.015	0.041	0.021	0.186	0.020	0.000	0.000	0.000	56.349
HML-821	D3	0.870	0.804	0.139	54.660	0.000	0.086	0.007	0.006	0.000	0.173	0.047	0.040	0.030	0.000	56.861
HML-792	D3	0.358	0.756	0.154	54.074	0.223	0.250	0.002	0.032	0.118	0.130	0.000	0.000	0.000	0.011	56.106
HML-821	D4	0.990	0.745	0.137	54.611	0.149	0.228	0.000	0.101	0.071	0.179	0.000	0.036	0.143	0.000	57.391
HML-821	D5	0.967	0.541	0.197	54.691	0.000	0.161	0.000	0.079	0.009	0.066	0.021	0.011	0.010	0.000	56.754
HML-909	F1	0.293	0.398	0.091	55.185	0.041	0.075	0.000	0.058	0.030	0.080	0.086	0.000	0.017	0.027	56.381
HML-909	F2	0.512	0.549	0.183	55.345	0.275	0.160	0.034	0.064	0.000	0.112	0.000	0.000	0.063	0.005	57.302

Table D.4.2 - Molar Composition of Carbonate (based on 3 O)

Samp. ID	MG	*Fe*	*Mn*	*Mg*	*Ca*	*Ba*	*Sr*	*K*	*Na*	*S*	*Si*	*Ti*	*Al*	*P*	*Cl*
HML-826	A1	0.014	0.050	0.012	2.886	0.005	0.006	0.002	0.000	0.002	0.007	0.000	0.000	0.002	0.001
HML-821	A1	0.048	0.033	0.014	2.864	0.017	0.001	0.003	0.006	0.001	0.007	0.000	0.000	0.000	0.003
HML-914	A1	0.039	0.042	0.024	2.835	0.010	0.004	0.001	0.014	0.003	0.010	0.000	0.001	0.000	0.002
HML-909	A1	0.020	0.020	0.017	2.897	0.013	0.006	0.003	0.006	0.001	0.008	0.000	0.000	0.001	0.000
HML-826	A2	0.025	0.066	0.014	2.852	0.006	0.005	0.000	0.012	0.000	0.005	0.002	0.003	0.003	0.000
HML-821	A2	0.042	0.030	0.010	2.875	0.011	0.003	0.000	0.000	0.002	0.008	0.000	0.000	0.002	0.000
HML-914	A2	0.025	0.039	0.023	2.877	0.009	0.006	0.001	0.012	0.000	0.006	0.000	0.000	0.001	0.000
HML-909	A2	0.025	0.023	0.012	2.890	0.027	0.004	0.000	0.004	0.000	0.007	0.000	0.000	0.001	0.000
HML-826	A3	0.012	0.055	0.015	2.902	0.003	0.003	0.000	0.000	0.000	0.005	0.000	0.000	0.000	0.000
HML-821	A3	0.042	0.029	0.010	2.889	0.002	0.004	0.000	0.006	0.000	0.003	0.000	0.000	0.006	0.001
HML-914	A3	0.019	0.036	0.014	2.894	0.000	0.009	0.001	0.007	0.002	0.005	0.002	0.000	0.001	0.003
HML-909	A3	0.021	0.028	0.014	2.904	0.011	0.003	0.004	0.003	0.000	0.008	0.000	0.000	0.000	0.001
HML-821	A4	0.042	0.029	0.006	2.887	0.010	0.002	0.000	0.000	0.000	0.009	0.003	0.000	0.000	0.001
HML-914	A4	0.018	0.027	0.014	2.891	0.019	0.007	0.002	0.002	0.001	0.006	0.000	0.000	0.003	0.000
HML-821	A5	0.041	0.032	0.007	2.879	0.002	0.003	0.002	0.006	0.002	0.007	0.000	0.000	0.004	0.000
HML-826	B1	0.037	0.057	0.028	2.841	0.014	0.001	0.001	0.010	0.000	0.007	0.000	0.000	0.001	0.000
HML-821	B1	0.040	0.030	0.008	2.877	0.000	0.006	0.003	0.009	0.000	0.010	0.000	0.004	0.003	0.000
HML-914	B1	0.026	0.031	0.013	2.893	0.000	0.008	0.001	0.002	0.000	0.008	0.003	0.000	0.002	0.003
HML-792	B1	0.013	0.024	0.012	2.909	0.005	0.007	0.002	0.004	0.000	0.010	0.000	0.000	0.003	0.000
HML-909	B1	0.022	0.019	0.015	2.900	0.000	0.005	0.001	0.000	0.003	0.008	0.002	0.003	0.001	0.002
HML-826	B2	0.062	0.065	0.035	2.800	0.000	0.004	0.000	0.002	0.002	0.010	0.002	0.000	0.000	0.003
HML-821	B2	0.033	0.041	0.006	2.881	0.012	0.004	0.001	0.000	0.003	0.005	0.001	0.000	0.000	0.001
HML-914	B2	0.026	0.029	0.023	2.891	0.001	0.008	0.001	0.013	0.000	0.006	0.000	0.001	0.001	0.003
HML-792	B2	0.008	0.021	0.006	2.899	0.016	0.002	0.000	0.009	0.005	0.009	0.000	0.000	0.003	0.000
HML-909	B2	0.018	0.019	0.008	2.914	0.009	0.006	0.000	0.000	0.000	0.006	0.000	0.000	0.006	0.000
HML-826	B3	0.041	0.038	0.021	2.864	0.011	0.002	0.000	0.001	0.000	0.011	0.000	0.000	0.000	0.003
HML-821	B3	0.039	0.026	0.012	2.883	0.006	0.005	0.001	0.000	0.002	0.006	0.000	0.001	0.003	0.001

Table D.4.2 - Molar Composition of Carbonate (based on 3 O); continued

Samp. ID	MG	*Fe*	*Mn*	*Mg*	*Ca*	*Ba*	*Sr*	*K*	*Na*	*S*	*Si*	*Ti*	*Al*	*P*	*Cl*
HML-914	B3	0.026	0.033	0.015	2.887	0.006	0.007	0.000	0.007	0.001	0.006	0.000	0.000	0.003	0.000
HML-792	B3	0.011	0.017	0.012	2.929	0.000	0.004	0.003	0.001	0.001	0.006	0.001	0.000	0.002	0.000
HML-909	B3	0.026	0.028	0.024	2.903	0.000	0.002	0.000	0.000	0.001	0.004	0.003	0.000	0.000	0.001
HML-792	B4	0.008	0.022	0.007	2.932	0.013	0.002	0.000	0.006	0.000	0.005	0.000	0.001	0.001	0.000
HML-909	B4	0.025	0.027	0.018	2.888	0.015	0.003	0.000	0.009	0.001	0.008	0.000	0.000	0.000	0.001
HML-826	C1	0.016	0.047	0.007	2.908	0.004	0.006	0.000	0.000	0.000	0.006	0.000	0.000	0.000	0.000
HML-821	C1	0.004	0.067	0.001	2.896	0.000	0.000	0.000	0.011	0.000	0.007	0.003	0.000	0.003	0.000
HML-914	C1	0.025	0.032	0.024	2.843	0.022	0.009	0.001	0.008	0.003	0.007	0.000	0.000	0.005	0.001
HML-826	C2	0.016	0.050	0.019	2.878	0.000	0.009	0.000	0.006	0.002	0.003	0.000	0.000	0.004	0.002
HML-821	C2	0.006	0.068	0.003	2.882	0.000	0.000	0.000	0.010	0.003	0.010	0.000	0.001	0.002	0.001
HML-914	C2	0.025	0.033	0.014	2.876	0.000	0.010	0.002	0.006	0.002	0.010	0.000	0.000	0.004	0.000
HML-826	C3	0.022	0.053	0.014	2.852	0.016	0.003	0.000	0.006	0.002	0.009	0.000	0.003	0.002	0.002
HML-821	C3	0.002	0.062	0.000	2.893	0.021	0.000	0.001	0.011	0.000	0.007	0.000	0.000	0.000	0.003
HML-914	C3	0.026	0.036	0.016	2.887	0.003	0.004	0.003	0.012	0.001	0.009	0.000	0.000	0.000	0.000
HML-821	C4	0.007	0.083	0.000	2.869	0.002	0.001	0.002	0.003	0.000	0.009	0.004	0.001	0.003	0.000
HML-821	D1	0.039	0.025	0.008	2.892	0.003	0.003	0.000	0.003	0.001	0.008	0.000	0.000	0.002	0.002
HML-792	D1	0.010	0.028	0.008	2.907	0.000	0.004	0.001	0.005	0.002	0.011	0.000	0.000	0.004	0.002
HML-821	D2	0.038	0.035	0.007	2.890	0.000	0.001	0.000	0.010	0.003	0.005	0.000	0.000	0.001	0.000
HML-792	D2	0.010	0.027	0.006	2.928	0.000	0.003	0.001	0.004	0.001	0.009	0.001	0.000	0.000	0.000
HML-821	D3	0.036	0.034	0.010	2.890	0.000	0.002	0.000	0.001	0.000	0.009	0.002	0.002	0.001	0.000
HML-792	D3	0.015	0.032	0.011	2.886	0.019	0.007	0.000	0.003	0.004	0.006	0.000	0.000	0.000	0.001
HML-821	D4	0.040	0.031	0.010	2.851	0.012	0.006	0.000	0.010	0.002	0.009	0.000	0.002	0.006	0.000
HML-821	D5	0.040	0.023	0.015	2.903	0.000	0.005	0.000	0.008	0.000	0.003	0.001	0.001	0.000	0.000
HML-909	F1	0.012	0.017	0.007	2.935	0.003	0.002	0.000	0.006	0.001	0.004	0.003	0.000	0.001	0.002
HML-909	F2	0.021	0.023	0.013	2.894	0.023	0.005	0.002	0.006	0.000	0.005	0.000	0.000	0.003	0.000

Table D.5.1 - Biotite Wt. % Oxide Electron Microprobe Compositions

Samp. ID	MG	*SiO2*	*TiO2*	*Al2O3*	*FeO*	*MnO*	*MgO*	*CaO*	*Na2O*	*K2O*	*Cr2O3*	*Cl*	*P2O5*	*BaO*	*TOTAL*
HML-794	A1	39.88	2.43	14.62	17.50	0.17	11.61	0.06	0.10	9.47	0.00	0.00	0.04	0.00	95.89
HML-794	B1	38.48	1.76	15.65	17.56	0.15	11.39	0.07	0.16	9.87	0.00	0.02	0.00	0.15	95.27
HML-794	B2	38.64	2.17	15.59	18.17	0.16	11.05	0.03	0.19	9.86	0.09	0.00	0.00	0.00	95.95
HML-794	B3	38.58	2.21	15.53	17.87	0.25	11.31	0.00	0.20	9.61	0.00	0.02	0.07	0.00	95.66
HML-794	B4	42.06	2.11	14.29	17.78	0.10	11.16	0.00	0.21	9.24	0.00	0.00	0.12	0.04	97.10
HML-794	B5	37.83	2.80	14.48	18.39	0.14	11.02	0.04	0.30	9.66	0.06	0.01	0.06	0.00	94.79
HML-794	B6	38.06	2.56	15.22	18.13	0.14	11.05	0.04	0.26	9.95	0.01	0.01	0.01	0.00	95.43
HML-794	B7	39.39	2.45	14.76	17.24	0.10	11.50	0.00	0.23	9.71	0.07	0.00	0.00	0.00	95.45
HML-794	B8	38.55	2.32	15.21	17.87	0.15	11.11	0.01	0.23	9.82	0.06	0.01	0.04	0.04	95.42

Table D.5.2 - Molar Composition of Biotite (based on 22 O)

Samp. ID	MG	*Si*	*Ti*	*Al*	*Fe*	*Mn*	*Mg*	*Ca*	*Na*	*K*	*Cr*	*Cl*	*P*	*Ba*
HML-794	A1	5.9426	0.2727	2.5677	2.1802	0.0218	2.5777	0.0093	0.0294	1.8007	0.0000	0.0000	0.0053	0.0000
HML-794	B1	5.8041	0.1996	2.7820	2.2142	0.0195	2.5602	0.0119	0.0455	1.8995	0.0000	0.0000	0.0000	0.0000
HML-794	B2	5.8020	0.2445	2.7591	2.2820	0.0200	2.4725	0.0040	0.0557	1.8891	0.0107	0.0000	0.0005	0.0000
HML-794	B3	5.7961	0.2496	2.7492	2.2451	0.0323	2.5326	0.0000	0.0569	1.8419	0.0000	0.0000	0.0091	0.0000
HML-794	B4	6.1470	0.2317	2.4611	2.1721	0.0125	2.4296	0.0000	0.0588	1.7228	0.0000	0.0000	0.0145	0.0000
HML-794	B5	5.7764	0.3218	2.6056	2.3476	0.0176	2.5073	0.0063	0.0881	1.8821	0.0077	0.0000	0.0073	0.0000
HML-794	B6	5.7628	0.2913	2.7161	2.2959	0.0176	2.4938	0.0058	0.0750	1.9214	0.0017	0.0000	0.0012	0.0000
HML-794	B7	5.9082	0.2761	2.6087	2.1623	0.0128	2.5690	0.0000	0.0657	1.8580	0.0077	0.0000	0.0004	0.0000
HML-794	B8	5.8157	0.2628	2.7041	2.2544	0.0189	2.4984	0.0009	0.0666	1.8894	0.0071	0.0000	0.0055	0.0000

Table D.6.1 - Epidote Wt. % Oxide Electron Microprobe Compositions

Samp. ID	MG	SiO2	TiO2	Al2O3	FeO	MnO	MgO	CaO	Na2O	K2O	Cr2O3	Cl	P2O5	BaO	TOTAL
HML-792	E1	38.71	0.00	25.03	10.68	0.26	0.17	23.09	0.12	0.00	0.00	0.00	0.05	0.02	98.13
HML-792	E2	38.67	0.00	24.35	10.49	0.33	0.27	22.81	0.16	0.13	0.08	0.04	0.00	0.00	97.34
HML-792	C1	39.35	0.06	25.37	10.22	0.05	0.20	24.14	0.09	0.06	0.00	0.06	0.05	0.10	99.74
HML-792	C2	39.08	0.22	25.11	10.05	0.08	0.15	23.35	0.04	0.06	0.04	0.00	0.01	0.12	98.31
HML-792	C3	39.40	0.10	25.01	10.33	0.10	0.26	23.92	0.16	0.00	0.04	0.03	0.05	0.00	99.39

Table D.6.2 - Molar Composition of Epidote (based on 12.5 O)

Samp. ID	MG	Si	Ti	Al	Fe	Mn	Mg	Ca	Na	K	Cr	Cl	P	Ba
HML-792	E1	3.1007	0.0000	2.3633	0.7151	0.0178	0.0203	1.9819	0.0191	0.0000	0.0000	0.0000	0.0033	0.0007
HML-792	E2	3.1257	0.0000	2.3194	0.7090	0.0229	0.0328	1.9755	0.0252	0.0138	0.0049	0.0050	0.0000	0.0000
HML-792	C1	3.0993	0.0035	2.3553	0.6734	0.0034	0.0231	2.0370	0.0143	0.0056	0.0000	0.0075	0.0030	0.0032
HML-792	C2	3.1155	0.0133	2.3591	0.6698	0.0052	0.0180	1.9948	0.0063	0.0059	0.0028	0.0000	0.0007	0.0039
HML-792	C3	3.1127	0.0061	2.3284	0.6824	0.0067	0.0306	2.0243	0.0246	0.0000	0.0026	0.0042	0.0030	0.0000

Table E.1 – Lithogeochemical Analysis

Samp Num	A.M. A.U. D.L	SiO2 XRF % 0.01	Al2O3 XRF % 0.01	CaO XRF % 0.01	MgO XRF % 0.01	Na2O XRF % 0.01	K2O XRF % 0.01	Fe2O3 XRF % 0.01	MnO XRF % 0.01	TiO2 XRF % 0.001	P2O5 XRF % 0.01	Cr2O3 XRF % 0.01	LOI XRF % 0.01	Sum XRF % 0.01	Rb XRF ppm 2	Sr XRF ppm 2	Y XRF ppm 2	Zr XRF ppm 2	Nb XRF ppm 2
158779		79.000	8.360	0.120	1.420	0.070	1.400	7.160	0.070	0.633	0.070	0.020	1.75	100.1	65	8	31	264	11
158780		63.900	16.900	0.160	1.650	0.140	3.860	8.290	0.070	1.026	0.100	0.020	3.75	100.0	180	17	61	243	19
158781		51.700	23.800	0.180	2.010	0.200	5.730	9.810	0.090	1.346	0.120	0.020	4.10	99.3	234	24	72	221	22
158782		71.100	12.000	0.100	1.750	0.050	2.240	9.350	0.080	0.663	0.070	0.005	2.60	100.1	96	12	47	193	12
158783		64.000	15.300	0.120	1.960	0.100	3.720	9.320	0.060	0.823	0.100	0.010	3.80	99.4	164	14	52	243	17
158784		62.900	16.600	0.300	2.100	0.790	4.010	8.100	0.370	1.011	0.200	0.010	2.95	99.5	165	16	57	233	18
158785		78.800	11.500	0.240	1.240	0.260	3.370	2.080	0.040	0.257	0.090	0.010	2.25	100.2	151	11	35	139	10
158786		64.500	15.200	0.090	0.810	0.090	4.760	8.060	0.020	0.977	0.050	0.020	5.60	100.3	197	22	47	246	17
158787		63.200	16.200	0.320	2.210	0.630	3.790	8.880	0.260	0.988	0.210	0.020	3.10	99.9	147	21	53	233	20
158788		73.800	13.700	0.300	1.350	3.470	2.350	2.920	0.030	0.299	0.100	0.010	1.65	100.1	97	36	45	158	11
158789		65.800	13.200	0.520	3.930	4.730	0.280	7.040	0.050	0.738	0.210	0.005	2.20	98.7	10	49	50	241	14
158790		64.600	15.800	0.220	2.240	0.670	4.380	7.030	0.080	0.981	0.120	0.010	3.05	99.3	170	18	52	250	17
158791		63.600	14.700	0.290	4.590	5.680	0.260	6.610	0.100	0.765	0.140	0.010	2.25	99.1	10	60	44	239	14
158792		64.500	14.400	2.110	3.630	3.820	2.120	5.560	0.100	0.720	0.140	0.005	3.05	100.2	65	93	43	221	12
158793		65.100	14.500	0.510	4.280	2.940	2.360	6.080	0.070	0.715	0.160	0.010	2.75	99.6	81	42	49	244	14
158794		56.500	15.300	1.010	4.720	3.370	4.420	9.400	0.160	1.464	0.340	0.005	2.00	98.9	132	61	54	183	14
158795		73.600	13.100	0.520	0.930	2.890	4.780	2.190	0.020	0.300	0.110	0.010	1.45	100.0	133	52	45	155	12
158796		74.000	12.200	0.270	1.360	1.970	5.640	2.650	0.030	0.259	0.100	0.030	1.50	100.2	128	60	38	141	9
158797		74.400	12.500	0.210	0.970	2.040	5.840	1.850	0.030	0.265	0.100	0.020	1.90	100.2	143	57	40	137	10
158798		75.600	12.900	0.600	1.320	2.600	2.700	1.740	0.030	0.189	0.130	0.020	2.20	100.2	127	50	40	104	10
158799		77.500	12.800	0.280	0.750	2.960	2.710	0.970	0.005	0.281	0.160	0.010	1.50	100.0	130	43	47	151	10
158800		71.900	13.300	0.820	2.010	3.700	1.830	3.680	0.040	0.524	0.150	0.005	2.05	100.2	77	61	59	327	15

Table E.1 – Lithogeochemical Analysis (continued)

	Ba XRF ppm 20	Be ICP ppm 0.5	Na ICP % 0.01	Mg ICP % 0.01	Al ICP % 0.01	P ICP % 0.01	K ICP % 0.01	Ca ICP % 0.01	Sc ICP ppm 0.5	Ti ICP % 0.01	V ICP ppm 2	Cr ICP ppm 1	Mn ICP ppm 2	Fe ICP % 0.01	Co ICP ppm 1	Ni ICP ppm 1	Cu ICP ppm 0.5	Zn ICP ppm 0.5
158779	222	0.25	0.005	0.6	1.73	0.03	0.11	0.07	1.3	0.005	21	81	383	4.17	12	33	8.1	36.4
158780	599	0.25	0.01	0.69	1.82	0.04	0.13	0.09	1	0.005	18	58	335	4.5	13	34	35.3	142
158781	722	0.6	0.01	0.9	2.37	0.05	0.18	0.11	1.5	0.005	26	42	356	5.1	15	40	2.3	71
158782	357	0.25	0.005	0.76	2.19	0.02	0.09	0.06	1.4	0.005	18	49	440	5.32	25	24	19.4	65.9
158783	454	0.25	0.01	0.83	1.69	0.03	0.15	0.07	0.7	0.005	15	38	379	5.28	22	27	102	70.3
158784	443	0.25	0.01	0.82	1.65	0.08	0.18	0.17	0.8	0.01	17	52	1240	4.01	16	37	31.8	124
158785	342	0.25	0.005	0.3	0.47	0.04	0.13	0.15	0.25	0.005	1	37	205	0.77	3	5	1.1	22.1
158786	504	0.25	0.005	0.02	0.21	0.02	0.18	0.06	0.25	0.005	6	53	32	4.62	16	52	35	516
158787	478	0.25	0.01	0.9	1.92	0.08	0.25	0.18	1.2	0.005	23	43	977	4.49	15	39	42.8	100
158788	236	0.25	0.02	0.4	0.71	0.04	0.17	0.16	0.25	0.005	5	73	167	1.4	4	26	2	13.2
158789	34	0.25	0.04	1.74	2.22	0.08	0.03	0.2	9.2	0.02	36	40	325	4.13	0.5	11	1.3	17.8
158790	536	0.25	0.01	0.82	1.52	0.04	0.27	0.12	0.8	0.005	15	50	302	3.33	13	31	21.2	28.9
158791	25	0.25	0.04	1.98	2.19	0.06	0.03	0.15	9.6	0.005	74	72	639	3.79	11	18	1.4	64
158792	467	0.5	0.03	1.56	1.7	0.06	0.18	0.78	5	0.06	37	57	606	2.83	9	20	17.4	63.1
158793	361	0.6	0.02	1.82	1.99	0.06	0.2	0.28	3.1	0.005	26	64	430	3.24	9	8	3.3	25.8
158794	447	1	0.02	2.34	2.7	0.13	1.32	0.53	18.5	0.19	209	30	648	5.04	18	9	3.3	159
158795	398	0.25	0.02	0.28	0.51	0.04	0.32	0.3	1.1	0.03	6	56	124	0.95	3	3	1.7	14
158796	1130	0.5	0.02	0.6	0.69	0.04	0.18	0.16	1.1	0.01	8	89	182	1.53	3	32	2.3	15.6
158797	1090	0.25	0.02	0.29	0.26	0.04	0.18	0.12	0.6	0.005	2	62	147	0.85	2	4	1.5	11.2
158798	504	0.25	0.02	0.3	0.48	0.05	0.16	0.35	0.25	0.005	3	70	179	0.74	2	25	1.6	10.6
158799	512	0.25	0.02	0.06	0.22	0.06	0.18	0.16	0.25	0.005	1	73	29	0.24	0.5	4	1.6	1.4
158800	528	0.25	0.02	0.7	1	0.06	0.13	0.39	0.8	0.02	9	45	233	1.86	5	16	1.6	30.1

Table E.1 – Lithogeochemical Analysis (continued)

	As ICP ppm 3	Sr ICP ppm 0.5	Y ICP ppm 0.5	Zr ICP ppm 0.5	Mo ICP ppm 1	Ag ICP ppm 0.2	Cd ICP ppm 1	Sn ICP ppm 10	Sb ICP ppm 5	Ba ICP ppm 1	La ICP ppm 0.5	W ICP ppm 10	Pb ICP ppm 2	Bi ICP ppm 5	H2O+ CHM % 0.1	C CHM % 0.01	S CHM % 0.01
158779	4	2.1	6.1	10.9	0.5	0.4	0.5	5	2.5	17	22.9	5	4	2.5	2.5	0.03	0.12
158780	1.5	2	6.1	15.8	0.5	0.1	0.5	5	2.5	19	34.6	5	1	2.5	3.7	0.03	0.33
158781	8	3.4	10.7	25.8	0.5	0.3	0.5	5	2.5	27	49.8	5	1	2.5	4.9	0.07	0.02
158782	12	1.4	4.9	12.6	0.5	0.4	0.5	5	2.5	15	24	5	1	5	3.5	0.1	0.14
158783	13	2.5	6.3	13.5	0.5	0.2	0.5	5	2.5	17	20.5	5	7	8	3.6	0.01	1.63
158784	46	4.5	10.7	4.5	0.5	0.3	0.5	5	2.5	21	28.3	5	6	2.5	3.4	0.1	0.37
158785	88	3.3	5.6	5.3	0.5	0.1	0.5	5	2.5	15	21.2	5	9	2.5	2	0.09	0.02
158786	113	2.2	7.6	11.5	2	1.1	0.5	5	6	18	28.8	5	403	2.5	2.3	0.02	5.63
158787	67	7.1	12.8	4.3	0.5	0.4	0.5	5	2.5	32	26.3	5	23	2.5	3.6	0.09	0.32
158788	1.5	5.1	8.8	12.1	2	0.1	0.5	5	2.5	18	26.7	5	4	2.5	1.7	0.09	0.03
158789	1.5	6.4	8.8	6.8	0.5	0.2	0.5	5	2.5	3	27.4	5	1	2.5	2.9	0.02	0.04
158790	8	4.8	9.7	7	0.5	0.1	0.5	5	2.5	37	33.4	5	1	2.5	3	0.05	0.16
158791	1.5	5.6	7.6	10.6	0.5	0.4	0.5	5	2.5	6	27.7	5	1	2.5	3.1	0.1	0.005
158792	1.5	28.3	11.8	4.4	0.5	0.1	0.5	5	2.5	31	20	5	1	2.5	2.6	0.26	0.02
158793	1.5	9.5	10.2	5.6	0.5	0.4	0.5	5	2.5	29	30.2	5	3	2.5	3.4	0.07	0.05
158794	12	22.9	4.5	10.4	0.5	0.3	0.5	5	2.5	59	15.1	5	9	2.5	2.8	0.19	0.02
158795	1.5	11.9	8.9	27.3	0.5	0.3	0.5	5	2.5	23	20.1	5	7	2.5	1.1	0.18	0.005
158796	1.5	8	5.5	13.5	0.5	0.2	0.5	5	2.5	33	11.9	5	5	2.5	1.2	0.12	0.16
158797	1.5	6.5	7.5	18.7	0.5	0.1	0.5	5	2.5	33	19.6	5	16	2.5	0.9	0.27	0.04
158798	1.5	12.7	9.1	15.6	1	0.1	0.5	5	2.5	32	13.4	5	39	2.5	1.6	0.25	0.01
158799	1.5	6	12.4	24.3	2	0.1	0.5	5	2.5	40	19.5	5	3	2.5	1.2	0.05	0.04
158800	1.5	18	8.4	26.7	0.5	0.2	0.5	5	2.5	39	18.4	5	3	2.5	1.9	0.1	0.05

Table E.1 – Lithogeochemical Analysis (continued)

Samp Num	A.M. A.U. D.L	SiO2 XRF % 0.01	Al2O3 XRF % 0.01	CaO XRF % 0.01	MgO XRF % 0.01	Na2O XRF % 0.01	K2O XRF % 0.01	Fe2O3 XRF % 0.01	MnO XRF % 0.01	TiO2 XRF % 0.001	P2O5 XRF % 0.01	Cr2O3 XRF % 0.01	LOI XRF % 0.01	Sum XRF % 0.01	Rb XRF ppm 2	Sr XRF ppm 2	Y XRF ppm 2	Zr XRF ppm 2	Nb XRF ppm 2
158801		80.000	7.740	0.090	1.590	0.050	1.250	6.690	0.040	0.545	0.060	0.020	2.05	100.2	61	6	29	241	11
158802		80.200	8.150	0.110	1.380	0.060	1.640	5.910	0.040	0.645	0.070	0.020	1.75	100.1	69	7	34	296	13
158803		58.300	17.700	0.180	2.020	0.140	3.850	12.200	0.090	1.087	0.100	0.020	3.65	99.5	161	21	62	268	21
158804		76.100	9.130	0.600	3.640	0.020	1.500	5.590	0.100	0.709	0.060	0.020	2.70	100.2	69	7	37	276	12
158805		23.400	21.700	0.270	5.320	0.040	0.350	40.200	0.270	1.176	0.080	0.005	6.50	99.4	16	9	79	287	17
158806		44.400	12.900	9.830	5.830	0.590	1.250	12.600	0.200	2.087	0.180	0.020	9.35	99.2	46	156	42	132	9
158807		75.600	11.800	0.400	1.960	3.260	1.620	2.640	0.040	0.237	0.140	0.005	1.65	99.4	82	37	50	124	10
158808		72.100	11.500	0.760	2.230	1.330	2.040	5.820	0.060	0.795	0.080	0.010	2.30	99.2	91	21	44	236	15
158809		70.900	14.300	0.450	1.690	1.290	3.180	5.120	0.050	0.894	0.080	0.010	2.30	100.4	154	27	52	293	17
158810		80.000	10.100	0.370	0.890	4.260	0.630	2.150	0.020	0.318	0.110	0.010	0.95	99.8	33	44	32	121	11
158811		74.500	11.300	0.410	1.690	1.010	2.140	5.580	0.050	0.823	0.240	0.020	2.30	100.3	102	25	60	312	15
158812		61.300	18.800	0.180	2.010	1.360	4.310	6.890	0.060	1.112	0.120	0.010	3.30	99.6	199	29	64	237	21
158813		68.600	14.800	0.200	2.200	1.190	3.400	5.730	0.070	0.896	0.140	0.020	2.75	100.1	173	23	47	215	17
158814		73.400	13.400	0.110	1.850	0.870	4.860	3.120	0.030	0.291	0.040	0.010	2.00	100.1	203	20	56	161	12
158815		76.000	11.800	0.260	1.570	3.560	3.780	1.690	0.020	0.242	0.100	0.020	1.05	100.2	91	55	31	132	8
158816		74.800	12.800	0.200	1.180	3.300	4.500	1.850	0.020	0.271	0.100	0.020	1.00	100.2	102	54	40	146	9
158817		65.200	16.500	0.140	1.580	0.110	3.730	8.090	0.070	1.107	0.100	0.020	3.35	100.1	164	17	57	297	20
158818		65.100	15.600	0.150	2.150	0.070	3.210	9.480	0.070	1.012	0.110	0.020	3.10	100.1	142	13	55	271	17
158819		57.900	20.900	0.150	1.970	0.130	4.760	9.020	0.070	1.141	0.110	0.010	3.80	100.1	211	20	60	191	22
158820		67.700	12.700	0.090	1.780	0.060	2.420	11.400	0.070	0.781	0.080	0.020	2.90	100.1	110	13	49	216	14
158821		48.100	15.000	0.960	3.330	0.005	1.070	24.600	0.200	0.898	0.480	0.010	4.40	99.2	48	13	55	227	13
158822		58.800	15.900	0.100	2.430	0.080	3.460	14.000	0.130	1.058	0.090	0.020	3.80	100.1	141	8	59	242	18

Table E.1 – Lithogeochemical Analysis (continued)

	Ba XRF ppm 20	Be ICP ppm 0.5	Na ICP % 0.01	Mg ICP % 0.01	Al ICP % 0.01	P ICP % 0.01	K ICP % 0.01	Ca ICP % 0.01	Sc ICP ppm 0.5	Ti ICP % 0.01	V ICP ppm 2	Cr ICP ppm 1	Mn ICP ppm 2	Fe ICP % 0.01	Co ICP ppm 1	Ni ICP ppm 1	Cu ICP ppm 0.5	Zn ICP ppm 0.5
158801	188	0.25	0.005	0.71	1.72	0.03	0.07	0.06	1.1	0.005	19	66	264	4	12	20	4.7	40.1
158802	221	0.25	0.005	0.6	1.5	0.03	0.08	0.07	0.9	0.005	17	66	247	3.5	8	34	4.2	31.1
158803	546	0.6	0.01	0.93	2.62	0.04	0.12	0.1	1.6	0.005	29	67	385	6.61	20	40	19.2	59.9
158804	260	0.25	0.005	1.5	1.81	0.03	0.05	0.12	1.2	0.04	20	53	558	2.84	11	30	1.4	61.3
158805	10	1.4	0.01	2.65	8.23	0.02	0.005	0.13	9.4	0.02	113	68	1400	>15	48	53	14.5	268
158806	101	0.6	0.01	2.84	3.7	0.07	0.06	5.26	9.8	0.15	156	104	1240	6.6	33	33	31.5	109
158807	416	0.25	0.02	0.73	0.83	0.06	0.07	0.16	0.25	0.01	3	53	221	1.37	2	4	32.2	286
158808	276	0.25	0.01	0.91	1.52	0.03	0.12	0.16	1.3	0.06	21	60	378	3.15	13	35	39.5	37.3
158809	410	0.25	0.01	0.64	1.27	0.04	0.18	0.14	0.8	0.04	13	59	257	2.8	12	29	19.6	59.4
158810	104	0.25	0.03	0.36	0.62	0.04	0.06	0.12	0.25	0.02	8	61	131	1.32	3	26	4.8	11.3
158811	317	0.25	0.01	0.69	1.45	0.12	0.14	0.29	0.9	0.005	16	87	255	3.15	13	25	9.8	72.7
158812	601	0.5	0.01	0.77	1.59	0.04	0.2	0.1	1	0.01	18	32	219	3.39	17	37	12.6	85.7
158813	420	0.25	0.01	0.85	1.39	0.06	0.17	0.13	0.7	0.005	16	61	364	3.13	14	29	37.9	73.8
158814	673	0.6	0.01	0.41	0.67	0.02	0.53	0.07	0.25	0.03	4	58	116	1.15	4	21	1.7	13.1
158815	798	0.25	0.03	0.73	0.67	0.04	0.32	0.15	1.5	0.02	8	112	133	1.02	2	5	4.9	12.1
158816	772	0.6	0.03	0.46	0.61	0.04	0.22	0.11	1.2	0.01	8	91	164	0.98	2	29	1.8	12.1
158817	546	0.25	0.01	0.66	1.95	0.04	0.16	0.09	1.1	0.005	20	58	335	4.52	12	29	2.8	43.6
158818	491	0.5	0.01	0.94	2.44	0.04	0.23	0.09	1.6	0.005	27	63	354	5.2	15	37	2.4	34
158819	591	0.6	0.01	0.88	2.27	0.04	0.19	0.1	1.3	0.005	23	43	333	4.91	16	39	1.4	40.1
158820	378	0.6	0.005	0.81	2.22	0.03	0.12	0.06	1.3	0.005	26	67	376	6.46	21	44	33.7	34.7
158821	254	0.9	0.005	1.75	5.31	0.17	0.07	0.5	4.2	0.01	63	58	1080	13	128	32	2450	552
158822	645	0.5	0.005	1.05	2.43	0.03	0.16	0.06	1.1	0.005	27	47	515	7.15	272	46	565	63.3

Table E.1 – Lithogeochemical Analysis (continued)

	As	Sr	Y	Zr	Mo	Ag	Cd	Sn	Sb	Ba	La	W	Pb	Bi	H2O+	C	S
	ICP	ICP	ICP	ICP	ICP	ICP	ICP	ICP	ICP	ICP	ICP	ICP	ICP	ICP	CHM	CHM	CHM
	ppm	ppm	ppm	ppm	ppm	ppm	ppm	ppm	ppm	ppm	ppm	ppm	ppm	ppm	%	%	%
	3	0.5	0.5	0.5	1	0.2	1	10	5	1	0.5	10	2	5	0.1	0.01	0.01
158801	1.5	1.3	5.3	10.9	0.5	0.1	0.5	5	2.5	10	21.4	5	1	2.5	2.5	0.02	0.11
158802	1.5	1.6	5.2	11.5	0.5	0.1	0.5	5	2.5	12	23.1	5	1	2.5	2.3	0.08	0.02
158803	1.5	3.9	13.4	16.2	0.5	0.3	0.5	5	2.5	18	40.9	5	5	2.5	4.4	0.08	0.34
158804	5	2.1	4.3	4.8	0.5	0.5	0.5	5	2.5	10	9.4	5	1	2.5	3.1	0.03	0.005
158805	22	5.3	8.3	10.2	0.5	2.6	8	5	8	2	*INF	5	185	11	10.2	0.14	0.17
158806	24	142	11.3	4.7	0.5	0.4	1	5	2.5	9	8.9	5	30	2.5	5	1.89	0.02
158807	4	5.2	11.2	27.3	0.5	0.8	0.5	5	2.5	184	9.2	5	239	6	1.8	0.04	0.23
158808	4	2.6	6.8	13.7	0.5	0.3	0.5	5	2.5	17	22.2	5	1	2.5	2.6	0.11	0.16
158809	8	5.1	10.2	21.1	0.5	0.2	0.5	5	2.5	26	27.8	5	3	2.5	2.7	0.09	0.17
158810	1.5	2.9	8.9	12.9	0.5	0.1	0.5	5	2.5	9	8.1	5	1	2.5	1	0.01	0.08
158811	10	10.7	6.7	15.2	0.5	0.4	0.5	5	2.5	21	20.1	5	4	2.5	2.5	0.04	0.08
158812	18	6.4	11.4	18.8	0.5	0.1	0.5	5	2.5	32	32.3	5	6	2.5	3.5	0.1	0.09
158813	6	7.5	5.4	22.8	0.5	0.1	0.5	5	2.5	25	14.1	5	3	2.5	3	0.09	0.34
158814	1.5	7.7	10.5	29.2	2	0.4	0.5	5	2.5	49	16.2	5	9	2.5	2.2	0.17	0.18
158815	1.5	8.1	6.9	17.6	2	0.1	0.5	5	2.5	33	11.7	5	5	2.5	0.8	0.14	0.15
158816	1.5	6.2	11.3	16.7	0.5	0.3	0.5	5	2.5	29	22.2	5	3	2.5	1.2	0.03	0.04
158817	4	2.8	10.3	26.1	0.5	0.2	0.5	5	2.5	25	27.3	5	2	2.5	3.8	0.12	0.1
158818	1.5	3	7	24.5	0.5	0.3	0.5	5	2.5	38	33.3	5	1	2.5	3.9	0.09	0.27
158819	7	2.9	10.2	28.4	0.5	0.1	0.5	5	2.5	26	46.4	5	1	2.5	4.3	0.02	0.09
158820	9	2	4.5	10	1	0.2	0.5	5	2.5	17	21	5	3	2.5	3.5	0.02	1.02
158821	134	8.7	11	9	8	3.6	5	5	2.5	14	*INF	5	22	*INF	6.4	0.29	0.71
158822	334	1.8	8.5	8.4	0.5	0.9	0.5	5	2.5	29	31.6	5	83	2.5	4.2	0.005	1.42

Table E.1 – Lithogeochemical Analysis (continued)

Samp Num	A.M. A.U. D.L	SiO2 XRF % 0.01	Al2O3 XRF % 0.01	CaO XRF % 0.01	MgO XRF % 0.01	Na2O XRF % 0.01	K2O XRF % 0.01	Fe2O3 XRF % 0.01	MnO XRF % 0.01	TiO2 XRF % 0.001	P2O5 XRF % 0.01	Cr2O3 XRF % 0.01	LOI XRF % 0.01	Sum XRF % 0.01	Rb XRF ppm 2	Sr XRF ppm 2	Y XRF ppm 2	Zr XRF ppm 2	Nb XRF ppm 2
158823		65.500	14.500	0.940	2.850	0.270	3.970	6.190	0.100	0.742	0.150	0.005	3.55	98.9	161	21	53	224	13
158824		66.700	13.900	0.750	2.750	1.250	2.830	7.720	0.090	0.682	0.150	0.005	3.15	100.2	121	27	45	225	13
158825		65.700	15.200	0.120	1.920	0.090	4.300	8.070	0.130	1.003	0.070	0.010	3.00	99.8	157	9	41	270	17
158826		64.900	14.600	1.490	2.920	5.300	0.500	6.560	0.090	0.720	0.160	0.010	2.90	100.3	24	68	44	238	12
158827		67.500	15.100	0.450	1.670	0.760	3.400	7.180	0.200	0.955	0.130	0.020	2.70	100.1	155	20	50	240	18
158828		65.300	15.200	0.200	0.960	0.110	4.790	6.940	0.020	0.950	0.090	0.020	5.50	100.2	221	14	49	241	17
158829		67.400	15.600	0.550	1.070	0.080	4.690	5.640	0.060	0.972	0.110	0.020	3.90	100.2	224	19	43	256	18
158830		65.200	15.700	0.550	2.100	0.180	3.850	8.050	0.360	0.931	0.150	0.010	3.30	100.5	179	19	53	209	17
158831		59.200	14.700	1.540	5.040	3.620	1.110	9.810	0.120	1.462	0.340	0.005	3.35	100.3	36	59	49	220	15
158832		76.600	12.200	0.370	0.650	3.200	4.590	1.290	0.010	0.267	0.100	0.020	0.80	100.1	99	61	30	140	10
158833		77.200	12.100	0.210	0.850	0.730	4.180	1.990	0.020	0.267	0.090	0.010	2.15	99.9	159	19	42	144	11
158834		49.000	21.600	0.130	1.390	0.180	5.530	15.400	0.050	1.125	0.080	0.020	5.35	100.1	225	25	105	353	22
158835		63.500	17.700	0.230	0.930	0.190	5.260	6.500	0.030	0.955	0.160	0.020	4.55	100.1	219	20	55	195	17
158836		61.500	16.800	0.860	3.530	0.120	4.170	6.620	0.080	1.049	0.100	0.030	4.85	99.9	174	16	52	259	18
158837		77.700	12.600	0.200	0.980	0.130	3.820	1.590	0.010	0.221	0.140	0.010	2.70	100.1	175	14	56	135	11
158838		66.300	16.400	0.130	2.450	0.100	4.170	5.250	0.050	0.964	0.080	0.020	4.15	100.2	189	18	55	264	19
158839		68.100	13.400	0.790	1.620	0.780	3.710	5.580	0.030	0.765	0.100	0.020	4.40	99.4	159	26	44	203	14
158840		59.400	13.000	0.140	2.300	0.080	3.520	13.000	0.040	0.795	0.090	0.030	7.70	100.3	146	12	52	208	12
158841		57.700	20.300	0.150	2.050	0.080	5.670	7.690	0.080	1.158	0.110	0.020	4.00	99.2	229	18	55	208	22
158842		60.900	17.800	0.120	1.960	0.090	5.480	7.210	0.040	0.984	0.100	0.020	4.25	99.1	219	16	57	177	18
158843		67.900	13.000	0.200	3.150	0.050	3.080	7.080	0.090	0.763	0.150	0.020	3.15	98.7	128	9	51	265	15
158844		73.800	13.000	0.410	1.370	3.730	2.480	2.850	0.030	0.397	0.110	0.010	1.80	100.1	92	50	53	286	14

XRF = x-ray fluorescence spectrometry; ICP = inductively-coupled plasma spectrometry

Table E.1 – Lithogeochemical Analysis (continued)

	Ba XRF ppm 20	Be ICP ppm 0.5	Na ICP % 0.01	Mg ICP % 0.01	Al ICP % 0.01	P ICP % 0.01	K ICP % 0.01	Ca ICP % 0.01	Sc ICP ppm 0.5	Ti ICP % 0.01	V ICP ppm 2	Cr ICP ppm 1	Mn ICP ppm 2	Fe ICP % 0.01	Co ICP ppm 1	Ni ICP ppm 1	Cu ICP ppm 0.5	Zn ICP ppm 0.5
158823	1040	0.25	0.01	1.17	1.74	0.06	0.23	0.44	1.7	0.03	16	49	568	3.14	12	7	16.4	150
158824	908	0.25	0.01	1.21	2	0.06	0.14	0.4	1.8	0.005	20	25	500	4.1	12	13	11.4	124
158825	886	0.25	0.01	0.74	1.72	0.03	0.29	0.06	1	0.005	16	38	467	3.81	11	22	28.7	103
158826	143	0.25	0.04	1.31	2	0.06	0.05	0.83	6.7	0.005	50	63	582	3.83	11	12	23.7	67.7
158827	400	0.25	0.02	0.64	1.62	0.04	0.26	0.26	1	0.01	19	70	783	3.62	14	43	22.3	70.9
158828	589	0.25	0.01	0.06	0.39	0.04	0.33	0.11	0.25	0.005	8	55	60	3.74	17	47	19.6	59
158829	570	0.25	0.01	0.15	0.48	0.04	0.27	0.32	0.5	0.005	7	44	264	2.73	11	35	29.8	442
158830	516	0.25	0.01	0.91	1.79	0.06	0.28	0.33	1.2	0.02	18	39	1520	4.26	12	35	31.8	146
158831	243	0.6	0.02	2.19	2.75	0.12	0.17	0.68	9.6	0.07	114	31	556	5.14	29	2	1.4	58.6
158832	900	0.25	0.04	0.2	0.36	0.04	0.24	0.21	1.1	0.005	7	109	81	0.68	3	33	5.5	6.5
158833	540	0.25	0.02	0.05	0.36	0.04	0.47	0.12	0.25	0.005	3	74	35	0.3	2	20	4.8	2.8
158834	559	0.7	0.01	0.49	1.26	0.04	0.15	0.08	0.25	0.005	13	43	262	7.71	22	29	555	108
158835	557	0.6	0.02	0.21	0.71	0.06	0.26	0.12	0.9	0.005	10	65	96	3.62	19	51	26.2	195
158836	502	0.25	0.01	1.57	1.68	0.04	0.12	0.18	0.8	0.06	16	74	488	3.68	16	34	24.8	117
158837	296	0.25	0.01	0.19	0.38	0.06	0.17	0.12	0.25	0.005	1	73	73	0.75	2	9	4.7	11.8
158838	487	0.25	0.01	0.98	1.2	0.03	0.17	0.07	0.7	0.005	11	69	302	2.91	12	37	12.4	69.2
158839	573	0.25	0.01	0.47	0.59	0.04	0.17	0.47	0.25	0.005	7	75	177	3.14	12	26	18.9	20.5
158840	484	0.5	0.01	0.93	1.12	0.03	0.13	0.07	0.25	0.005	14	80	219	6.49	19	27	16	39.2
158841	903	0.6	0.01	0.82	1.67	0.04	0.27	0.09	1.1	0.005	18	43	465	4.15	14	45	39.2	552
158842	908	0.25	0.01	0.64	1	0.04	0.21	0.08	0.6	0.005	11	49	250	3.97	17	45	109	95.7
158843	411	0.6	0.005	1.44	2.12	0.06	0.21	0.12	0.9	0.005	16	80	574	3.85	7	26	21.2	58.8
158844	466	0.25	0.03	0.39	0.72	0.04	0.23	0.23	1.1	0.005	6	64	161	1.27	4	13	1.5	14.8

Table E.1 – Lithogeochemical Analysis (continued)

	As ICP ppm 3	Sr ICP ppm 0.5	Y ICP ppm 0.5	Zr ICP ppm 0.5	Mo ICP ppm 1	Ag ICP ppm 0.2	Cd ICP ppm 1	Sn ICP ppm 10	Sb ICP ppm 5	Ba ICP ppm 1	La ICP ppm 0.5	W ICP ppm 10	Pb ICP ppm 2	Bi ICP ppm 5	H2O+ CHM % 0.1	C CHM % 0.01	S CHM % 0.01
158823	3	11.3	13.2	12	0.5	0.2	0.5	5	2.5	72	29.1	5	114	2.5	3.2	0.18	0.16
158824	1.5	10.4	8.5	9.5	0.5	0.6	0.5	5	2.5	46	26	5	124	6	3.2	0.15	0.07
158825	1.5	2.7	11.1	12.2	0.5	0.3	0.5	5	2.5	66	32.1	5	4	2.5	3.4	0.03	0.005
158826	1.5	18.3	6	11.1	0.5	0.3	0.5	5	2.5	17	29.4	5	7	2.5	2.6	0.29	0.03
158827	44	7.1	6.8	7.8	0.5	0.5	0.5	5	2.5	33	33.1	5	24	2.5	3	0.08	0.17
158828	162	3.7	4.9	9.3	2	0.5	0.5	5	6	48	29.8	5	44	2.5	2.4	0.03	4.36
158829	24	7.7	5.2	11.9	0.5	1.9	0.5	5	2.5	32	30.3	5	519	2.5	2.5	0.15	2.22
158830	1.5	8.4	6.3	6.9	0.5	0.5	0.5	5	2.5	35	25.9	5	10	2.5	3.4	0.09	0.57
158831	21	29.5	4.7	5.8	0.5	0.4	0.5	5	2.5	27	16.5	5	6	2.5	3.7	0.18	0.01
158832	4	16.2	6	14.9	0.5	0.1	0.5	5	2.5	32	17.2	5	5	2.5	0.8	0.08	0.08
158833	5	6.7	9.2	17.5	0.5	0.1	0.5	5	2.5	63	20.4	5	5	2.5	1.5	0.03	0.05
158834	283	2.8	10.7	47.1	0.5	0.8	1	5	2.5	15	32	5	52	2.5	4.1	0.08	4.3
158835	8	4.4	8	37	0.5	0.4	0.5	5	2.5	30	30.3	5	116	2.5	3.1	0.02	2.94
158836	11	2.8	8	23.9	4	0.1	0.5	5	2.5	15	32.2	5	27	2.5	4	0.1	1.87
158837	3	3	9.2	27.7	0.5	0.2	0.5	5	2.5	17	16.5	5	18	2.5	2.2	0.01	0.52
158838	14	2.6	9.7	24.5	0.5	0.1	0.5	5	2.5	20	31.1	5	11	2.5	3.5	0.21	1.82
158839	15	9.5	6.8	20.8	0.5	0.1	0.5	5	2.5	28	11.8	5	15	2.5	2.4	0.24	3.51
158840	43	2.3	2.8	16.3	0.5	0.4	0.5	5	2.5	18	8.2	5	23	2.5	2.8	0.02	6.58
158841	1.5	3.2	9.4	26.6	0.5	0.2	0.5	5	2.5	47	42.4	5	2	2.5	4	0.02	0.9
158842	1.5	3.1	6	23.3	0.5	0.2	0.5	5	2.5	37	26.1	5	10	2.5	3.3	0.07	1.8
158843	1.5	3.2	11	13.5	2	0.1	0.5	5	2.5	31	39.2	5	1	2.5	3.6	0.05	0.05
158844	1.5	11.5	11.4	53.6	2	0.2	0.5	5	2.5	46	27.9	5	1	2.5	1.7	0.12	0.02

Table E.1 – Lithogeochemical Analysis (continued)

Samp Num	A.M. A.U. D.L	SiO2 XRF % 0.01	Al2O3 XRF % 0.01	CaO XRF % 0.01	MgO XRF % 0.01	Na2O XRF % 0.01	K2O XRF % 0.01	Fe2O3 XRF % 0.01	MnO XRF % 0.01	TiO2 XRF % 0.001	P2O5 XRF % 0.01	Cr2O3 XRF % 0.01	LOI XRF % 0.01	Sum XRF % 0.01	Rb XRF ppm 2	Sr XRF ppm 2	Y XRF ppm 2	Zr XRF ppm 2	Nb XRF ppm 2
158845		75.600	12.100	0.300	1.100	1.870	4.990	2.250	0.020	0.358	0.090	0.010	1.05	100.0	137	65	49	237	12
158846		74.000	12.800	0.390	1.780	3.100	3.830	2.160	0.020	0.379	0.100	0.010	1.30	100.1	134	65	56	258	17
158847		67.600	15.600	0.250	2.200	0.170	5.220	4.770	0.130	0.631	0.130	0.020	3.05	99.9	216	19	53	187	16
158848		75.000	12.300	0.330	0.830	2.030	5.860	2.330	0.020	0.351	0.100	0.020	0.80	100.1	135	59	55	241	13
158849		75.600	11.700	0.250	0.960	0.240	7.290	2.570	0.030	0.337	0.100	0.020	0.90	100.2	163	61	48	223	13
158850		75.300	12.500	0.370	1.080	0.420	5.540	2.510	0.030	0.267	0.100	0.020	1.90	100.1	175	27	41	140	12
158851		47.100	24.400	0.150	2.540	0.170	5.840	12.300	0.100	1.416	0.120	0.020	4.75	99.1	220	23	82	240	25
158852		74.000	7.000	0.100	1.640	0.010	0.940	12.300	0.060	0.511	0.080	0.020	3.35	100.1	43	3	19	177	8
158853		81.900	6.810	0.090	1.480	0.030	0.980	6.680	0.050	0.488	0.060	0.020	1.45	100.1	46	6	30	197	8
158854		65.700	9.930	0.220	3.170	0.005	0.640	16.100	0.140	0.657	0.080	0.010	3.45	100.1	30	5	41	224	12
158855		60.900	16.900	0.240	1.860	0.110	3.460	11.800	0.090	1.062	0.160	0.020	3.25	99.9	154	19	59	241	18
158856		64.700	17.300	0.130	1.640	0.120	4.170	7.690	0.050	1.037	0.100	0.020	2.95	100.0	167	18	53	238	20
158857		51.100	15.800	0.100	3.450	0.040	1.010	22.900	0.150	1.034	0.090	0.010	4.40	100.1	44	9	35	199	17
158858		68.400	12.900	0.110	1.740	0.070	3.480	6.960	0.010	0.934	0.080	0.020	5.10	100.0	131	12	47	305	15
158859		62.100	18.700	0.410	1.720	0.160	5.200	5.560	0.010	1.161	0.060	0.020	4.95	100.2	199	18	54	291	22
158860		78.000	9.620	0.070	1.210	0.060	1.930	6.440	0.030	0.664	0.050	0.020	2.10	100.3	80	8	37	212	12
158861		69.300	12.400	0.080	3.060	0.050	3.080	6.210	0.020	0.895	0.070	0.010	4.80	100.1	114	12	39	279	15
158862		59.500	16.900	0.110	2.100	0.100	4.800	8.470	0.020	1.045	0.080	0.020	5.75	99.1	171	16	58	309	20
158863		75.500	12.500	0.270	0.730	2.460	5.070	2.110	0.020	0.270	0.100	0.020	1.00	100.2	132	51	43	141	11
158864		74.700	13.200	0.310	1.300	2.340	3.230	2.330	0.020	0.318	0.150	0.020	2.25	100.2	160	30	50	148	11
158865		74.600	12.500	0.280	1.030	1.700	5.990	2.270	0.020	0.271	0.100	0.010	1.25	100.2	159	53	41	142	9
158866		78.200	11.400	0.260	1.510	3.250	2.010	1.580	0.020	0.193	0.140	0.010	1.55	100.2	94	31	36	114	8

Table E.1 – Lithogeochemical Analysis (continued)

	Ba XRF ppm 20	Be ICP ppm 0.5	Na ICP % 0.01	Mg ICP % 0.01	Al ICP % 0.01	P ICP % 0.01	K ICP % 0.01	Ca ICP % 0.01	Sc ICP ppm 0.5	Ti ICP % 0.01	V ICP ppm 2	Cr ICP ppm 1	Mn ICP ppm 2	Fe ICP % 0.01	Co ICP ppm 1	Ni ICP ppm 1	Cu ICP ppm 0.5	Zn ICP ppm 0.5
158845	957	0.6	0.02	0.34	0.61	0.04	0.32	0.18	1.3	0.02	6	73	115	0.99	2	4	4.6	12.8
158846	900	0.6	0.03	0.64	0.8	0.04	0.52	0.22	1.4	0.04	7	85	136	1.06	1	4	1.3	15.7
158847	725	0.25	0.01	0.68	1.13	0.05	0.33	0.15	0.5	0.005	8	72	812	2.1	7	17	2.6	53.6
158848	895	0.25	0.02	0.31	0.58	0.04	0.19	0.19	1.2	0.005	7	81	143	1.23	2	4	13.6	11.1
158849	1200	0.25	0.01	0.34	0.72	0.04	0.26	0.09	1.2	0.005	6	88	185	1.32	1	4	2.3	10.8
158850	705	0.25	0.01	0.15	0.48	0.04	0.34	0.22	0.25	0.005	1	49	128	0.68	3	3	1	6.9
158851	760	0.6	0.01	1.26	3.07	0.04	0.17	0.09	1.7	0.005	33	49	493	6.6	19	33	11.6	72.8
158852	152	0.25	0.005	0.79	1.94	0.03	0.06	0.06	1.1	0.005	24	86	362	7.12	22	23	131	223
158853	153	0.25	0.005	0.7	1.8	0.03	0.07	0.06	1.1	0.005	19	80	303	4.14	8	17	11.1	62.9
158854	119	0.6	0.005	1.65	3.69	0.03	0.05	0.1	3.3	0.01	48	61	843	9.41	20	28	99.6	221
158855	516	0.6	0.01	0.85	2.6	0.06	0.18	0.13	1.5	0.01	29	53	403	6.47	21	41	29	63.7
158856	507	0.25	0.01	0.71	2	0.04	0.15	0.08	1.2	0.005	20	40	326	4.37	13	33	2.6	39.2
158857	149	0.9	0.005	1.83	5.7	0.03	0.03	0.06	5.1	0.01	78	69	912	12.5	42	30	49.9	101
158858	432	0.25	0.005	0.65	0.86	0.03	0.14	0.07	0.25	0.005	9	42	83	4.15	20	36	9.4	26.9
158859	632	0.25	0.005	0.36	0.54	0.02	0.18	0.05	0.25	0.005	6	39	43	2.95	17	38	12.4	25.1
158860	280	0.25	0.01	0.52	1.63	0.02	0.1	0.04	1.1	0.005	16	66	217	3.79	21	17	3.3	21.6
158861	380	0.25	0.005	1.28	1.22	0.02	0.11	0.05	0.25	0.005	12	35	86	3.54	18	28	8.2	35.6
158862	542	0.25	0.01	0.81	1.01	0.03	0.12	0.07	0.25	0.005	10	30	103	4.8	20	38	32.3	32
158863	901	0.25	0.02	0.21	0.44	0.04	0.21	0.15	0.6	0.005	4	62	95	0.97	3	5	5.4	12.3
158864	539	0.25	0.02	0.22	0.38	0.06	0.2	0.18	0.25	0.005	1	64	73	1.04	3	8	13.1	5.6
158865	1000	0.25	0.02	0.41	0.65	0.04	0.31	0.17	1.1	0.02	7	56	140	1.2	3	5	2.4	14
158866	320	0.7	0.02	0.43	0.5	0.05	0.14	0.14	0.7	0.005	2	60	96	0.76	2	4	4.4	10.8

Table E.1 – Lithogeochemical Analysis (continued)

	As ICP ppm 3	Sr ICP ppm 0.5	Y ICP ppm 0.5	Zr ICP ppm 0.5	Mo ICP ppm 1	Ag ICP ppm 0.2	Cd ICP ppm 1	Sn ICP ppm 10	Sb ICP ppm 5	Ba ICP ppm 1	La ICP ppm 0.5	W ICP ppm 10	Pb ICP ppm 2	Bi ICP ppm 5	H2O+ CHM % 0.1	C CHM % 0.01	S CHM % 0.01
158845	1.5	13.6	11.3	63.5	2	0.3	0.5	5	2.5	50	27.6	5	5	2.5	1.4	0.11	0.03
158846	1.5	15.6	13.2	72	1	0.1	0.5	5	2.5	82	25.5	5	11	2.5	1.3	0.09	0.02
158847	5	9.8	8.8	19.7	1	0.4	0.5	5	2.5	51	23.4	5	10	2.5	3.1	0.09	0.08
158848	1.5	9.2	9.6	40.4	1	0.3	0.5	5	2.5	32	20.4	5	2	2.5	1.2	0.27	0.12
158849	1.5	8.9	9.2	39.6	2	0.1	0.5	5	2.5	44	26.8	5	6	2.5	1.5	0.02	0.12
158850	1.5	9.2	8.5	16.5	1	0.1	0.5	5	2.5	46	27.3	5	8	2.5	1.8	0.06	0.06
158851	4	3.4	8.3	47.3	0.5	0.4	0.5	5	2.5	29	45.4	5	1	2.5	5.4	0.09	0.15
158852	148	1.6	2.5	13	0.5	1.2	2	5	2.5	8	6.7	5	247	5	2.6	0.22	3.41
158853	1.5	1.6	4.5	10.8	1	0.1	0.5	5	2.5	10	17.7	5	14	2.5	2.3	0.01	0.09
158854	1.5	1.8	6.5	9	0.5	0.6	2	5	2.5	8	*INF	5	28	2.5	4.3	0.1	1.26
158855	1.5	3.1	15.5	19.4	0.5	0.3	0.5	5	2.5	27	39.1	5	5	2.5	4.1	0.12	0.49
158856	1.5	3.2	9.2	16.6	1	0.3	0.5	5	2.5	26	38.4	5	1	2.5	3.7	0.06	0.005
158857	48	1.3	7.8	11.8	0.5	0.4	3	5	2.5	8	*INF	5	3	7	6.4	0.01	0.08
158858	82	2.2	2.3	11.8	0.5	0.1	0.5	5	2.5	17	7.5	5	13	2.5	2.6	0.02	4.17
158859	136	1.9	3	15.4	1	0.1	0.5	5	2.5	19	7.9	5	7	2.5	3.2	0.09	3.12
158860	19	1.5	3.8	9.2	2	0.1	0.5	5	2.5	16	29.6	5	1	5	2.6	0.03	0.02
158861	127	1.7	2.4	13.3	0.5	0.4	0.5	5	2.5	13	6.4	5	6	2.5	2.9	0.005	3.19
158862	1660	2.2	2.6	13.6	0.5	0.3	0.5	5	2.5	14	7	5	10	2.5	3.2	0.02	4.8
158863	1.5	6.9	9	17.2	2	0.1	0.5	5	2.5	34	25.1	5	7	2.5	1.1	0.13	0.15
158864	5	8.9	9.9	21.7	2	0.1	0.5	5	2.5	38	10.9	5	6	2.5	1.6	0.2	0.58
158865	1.5	8.8	8.4	18.8	0.5	0.1	0.5	5	2.5	31	17.1	5	5	2.5	1.2	0.11	0.06
158866	1.5	7.5	8.1	22.5	3	0.3	0.5	5	2.5	23	9.5	5	3	2.5	1.4	0.14	0.14

Table E.1 – Lithogeochemical Analysis (continued)

Samp Num	A.M. A.U. D.L	SiO2 XRF % 0.01	Al2O3 XRF % 0.01	CaO XRF % 0.01	MgO XRF % 0.01	Na2O XRF % 0.01	K2O XRF % 0.01	Fe2O3 XRF % 0.01	MnO XRF % 0.01	TiO2 XRF % 0.001	P2O5 XRF % 0.01	Cr2O3 XRF % 0.01	LOI XRF % 0.01	Sum XRF % 0.01	Rb XRF ppm 2	Sr XRF ppm 2	Y XRF ppm 2	Zr XRF ppm 2	Nb XRF ppm 2
158867		74.300	11.200	0.100	1.580	1.800	1.820	5.960	0.050	0.795	0.060	0.005	1.90	99.7	85	24	33	260	14
158868		71.300	14.000	0.420	1.690	3.920	2.280	3.580	0.030	0.601	0.160	0.005	2.00	100.1	84	66	58	350	16
158869		61.200	18.700	0.190	1.770	0.080	6.420	6.690	0.020	1.039	0.080	0.020	3.85	100.3	253	15	55	191	18
158870		57.800	21.100	0.110	2.070	0.790	5.620	7.460	0.050	1.158	0.090	0.020	3.95	100.3	240	26	61	211	21
158871		72.900	13.300	0.500	1.410	4.670	1.600	3.310	0.050	0.534	0.150	0.010	1.50	100.1	60	69	67	340	15
158872		66.800	15.400	0.140	2.370	0.060	3.970	6.610	0.060	0.841	0.090	0.020	3.65	100.1	154	14	44	283	17
158873		74.100	12.600	0.580	0.980	5.050	0.940	3.610	0.040	0.386	0.140	0.005	1.55	100.1	42	62	72	346	19
158874		43.900	12.900	9.990	6.580	2.380	0.070	12.400	0.230	1.995	0.190	0.020	9.50	100.1	4	171	32	129	7
158875		80.200	8.780	0.080	1.390	0.040	1.890	5.440	0.040	0.573	0.060	0.010	1.75	100.3	82	6	31	174	11
158876		71.600	12.900	0.170	1.340	0.090	3.170	6.640	0.040	0.847	0.060	0.010	2.65	99.7	135	16	44	247	14
158877		73.900	10.800	0.170	1.350	0.070	2.350	7.450	0.050	0.801	0.080	0.010	2.60	99.7	104	9	31	286	15
158878		52.500	22.800	0.180	2.010	0.140	5.740	10.500	0.080	1.303	0.120	0.020	4.30	99.9	232	25	70	220	24
158879		52.000	18.200	0.120	2.680	0.090	3.170	18.500	0.120	1.061	0.100	0.020	4.40	100.5	132	12	54	182	19
158880		45.100	16.300	1.340	15.100	0.005	0.450	12.600	0.170	1.304	0.130	0.050	7.80	100.3	21	9	20	80	5
158881		63.300	16.300	0.280	2.240	0.100	3.660	9.360	0.090	1.001	0.140	0.010	3.25	99.9	152	15	46	240	18
158882		72.700	9.730	0.080	1.810	0.020	1.150	11.300	0.070	0.686	0.070	0.020	2.30	99.9	50	6	38	223	12
158883		67.100	15.400	0.120	1.780	0.110	3.430	8.060	0.070	1.006	0.080	0.010	2.90	100.2	139	12	50	271	17
158884		59.700	19.200	0.100	2.070	0.150	4.760	8.270	0.070	1.129	0.070	0.020	3.80	99.4	221	17	63	224	21
158885		68.500	13.300	0.290	2.500	0.500	2.780	7.770	0.160	0.890	0.110	0.010	3.20	100.1	133	16	47	250	15
158886		44.700	15.400	7.640	8.890	2.630	0.600	9.840	0.280	1.107	0.100	0.040	9.10	100.4	23	103	21	71	4
158887		61.500	17.600	0.140	1.800	0.100	4.730	7.500	0.060	1.057	0.110	0.020	5.40	100.2	208	19	53	209	18
158888		67.800	14.600	0.110	0.780	0.110	4.500	6.720	0.020	0.953	0.060	0.020	4.40	100.2	179	19	45	263	17

Table E.1 – Lithogeochemical Analysis (continued)

	Ba XRF ppm 20	Be ICP ppm 0.5	Na ICP % 0.01	Mg ICP % 0.01	Al ICP % 0.01	P ICP % 0.01	K ICP % 0.01	Ca ICP % 0.01	Sc ICP ppm 0.5	Ti ICP % 0.01	V ICP ppm 2	Cr ICP ppm 1	Mn ICP ppm 2	Fe ICP % 0.01	Co ICP ppm 1	Ni ICP ppm 1	Cu ICP ppm 0.5	Zn ICP ppm 0.5
158867	246	0.25	0.01	0.63	1.36	0.02	0.09	0.05	1	0.01	18	45	212	3.24	13	25	29.6	92.7
158868	612	0.25	0.03	0.53	0.86	0.07	0.21	0.21	1.1	0.02	9	49	122	1.66	5	4	10.9	10.3
158869	1470	0.6	0.01	0.27	0.59	0.03	0.33	0.11	0.6	0.005	7	34	84	3.1	16	36	35	23.5
158870	659	0.25	0.01	0.69	1.22	0.03	0.23	0.06	0.7	0.005	14	51	280	3.84	18	44	38.9	81.7
158871	519	0.25	0.03	0.44	0.7	0.06	0.15	0.27	0.9	0.01	7	60	183	1.53	5	4	19.1	24.3
158872	560	0.25	0.005	0.94	1.4	0.04	0.17	0.08	0.8	0.005	12	59	366	3.53	14	23	83.3	86.4
158873	252	0.25	0.02	0.36	0.73	0.06	0.08	0.32	1.4	0.005	4	39	227	2.02	3	2	41.8	54.3
158874	10	0.5	0.01	2.81	3.39	0.07	0.005	5.04	25.5	0.1	198	103	1260	5.84	34	27	42.6	80.6
158875	256	0.25	0.005	0.59	1.41	0.02	0.12	0.05	0.9	0.005	14	55	279	3.18	9	17	13.3	105
158876	499	0.25	0.005	0.54	1.49	0.03	0.08	0.09	1	0.005	15	50	238	3.73	10	22	11.4	25.3
158877	401	0.25	0.005	0.55	1.59	0.03	0.07	0.06	0.9	0.005	17	44	247	4.2	10	22	13.1	26.7
158878	823	0.7	0.005	0.92	2.44	0.04	0.19	0.11	1.6	0.005	26	51	326	5.38	20	48	17	39.7
158879	414	0.7	0.005	1.36	3.84	0.03	0.11	0.07	2.4	0.005	46	67	593	9.95	36	43	29.2	83.3
158880	65	0.7	0.005	5.22	4.5	0.04	0.005	0.36	12.2	0.05	130	195	710	4.65	42	31	6.2	193
158881	530	0.25	0.005	1.07	2.32	0.06	0.13	0.15	1.3	0.005	24	45	563	5.27	21	50	136	168
158882	176	0.25	0.005	0.86	2.8	0.02	0.08	0.05	2.2	0.005	34	84	455	6.53	17	21	9.4	57.5
158883	462	0.25	0.01	0.75	2.13	0.03	0.19	0.07	1.3	0.005	23	46	327	4.52	14	30	4.3	39.2
158884	618	0.25	0.01	0.82	1.5	0.03	0.17	0.05	0.8	0.005	16	35	372	4.39	7	33	53	46.8
158885	384	0.25	0.005	0.99	1.59	0.04	0.09	0.16	0.9	0.005	17	43	662	3.99	14	29	34.5	136
158886	46	0.25	0.01	3.47	3.31	0.03	0.02	4	9.7	0.07	98	193	1410	4.21	33	59	29	86.1
158887	623	0.25	0.005	0.54	0.75	0.04	0.16	0.09	0.25	0.005	9	29	305	4.05	15	36	16.6	165
158888	399	0.25	0.005	0.03	0.2	0.03	0.17	0.07	0.25	0.005	5	38	29	3.79	16	33	31.3	111

Table E.1 – Lithogeochemical Analysis (continued)

	As	Sr	Y	Zr	Mo	Ag	Cd	Sn	Sb	Ba	La	W	Pb	Bi	H2O+	C	S
	ICP	ICP	ICP	ICP	ICP	ICP	ICP	ICP	ICP	ICP	ICP	ICP	ICP	ICP	CHM	CHM	CHM
	ppm	ppm	ppm	ppm	ppm	ppm	ppm	ppm	ppm	ppm	ppm	ppm	ppm	ppm	%	%	%
	3	0.5	0.5	0.5	1	0.2	1	10	5	1	0.5	10	2	5	0.1	0.01	0.01
158867	9	3.4	5.5	10.5	0.5	0.7	0.5	5	2.5	15	26.9	5	198	2.5	2.3	0.02	0.18
158868	1.5	14.6	11.4	45.4	2	0.1	0.5	5	2.5	63	39.8	5	1	2.5	1.9	0.04	0.12
158869	1.5	6.1	5.2	20.5	0.5	0.2	0.5	5	2.5	86	20.3	5	6	2.5	3	0.06	1.69
158870	1.5	4.8	6.9	34	0.5	0.3	0.5	5	2.5	29	13.1	5	1	2.5	3.7	0.09	1.25
158871	1.5	19.2	16.3	39.7	1	0.1	0.5	5	2.5	54	36.7	5	4	2.5	1.5	0.08	0.18
158872	1.5	2.9	4.5	19.4	1	0.1	0.5	5	2.5	25	21.8	5	11	2.5	3.3	0.01	0.86
158873	1.5	4.1	16.7	37	1	0.1	0.5	5	2.5	23	42.6	5	12	2.5	1.3	0.1	0.41
158874	28	131	8.2	2.9	0.5	0.1	0.5	5	2.5	0.5	6.9	5	14	2.5	4.8	1.81	0.29
158875	4	1.6	3	12.3	0.5	0.3	0.5	5	2.5	18	20.5	5	3	2.5	2.3	0.03	0.14
158876	1.5	3.6	7.5	21.5	0.5	0.2	0.5	5	2.5	33	25.2	5	3	2.5	2.9	0.09	0.3
158877	4	1.6	5.1	16.5	0.5	0.3	0.5	5	2.5	11	23.6	5	3	2.5	2.7	0.03	0.49
158878	1.5	5	13.2	31.8	0.5	0.1	0.5	5	2.5	32	53.1	5	3	2.5	4.7	0.02	0.13
158879	7	2.2	6.1	18.8	0.5	0.7	2	5	2.5	18	*INF	5	2	2.5	5.5	0.06	1.09
158880	35	6.4	3.6	1.5	0.5	0.4	0.5	5	2.5	0.5	4.2	5	49	2.5	8.4	0.13	0.005
158881	9	2.7	11.8	12.6	0.5	0.4	0.5	5	2.5	22	44.3	5	1	2.5	3.9	0.03	0.45
158882	4	1.7	4.2	8.5	0.5	0.2	0.5	5	2.5	13	23.9	5	2	2.5	3.5	0.02	0.04
158883	8	2	4.9	18.7	0.5	0.2	0.5	5	2.5	28	38.8	5	1	2.5	3.6	0.04	0.02
158884	12	2.1	7	14.7	0.5	0.4	0.5	5	2.5	21	33.7	5	3	2.5	3.8	0.02	1.15
158885	22	5.4	3.4	6.7	0.5	0.4	0.5	5	2.5	11	27.1	5	15	2.5	3.1	0.04	1.01
158886	43	73.1	5.4	2.5	0.5	0.6	0.5	5	2.5	1	4.7	5	6	2.5	5.3	1.5	0.01
158887	168	2.6	5.9	12.6	0.5	0.5	0.5	5	2.5	18	25.7	5	83	2.5	3.1	0.04	4.33
158888	26	2.4	6.7	11.5	1	0.6	0.5	5	2.5	14	29.5	5	78	2.5	2.1	0.02	3.97

Table E.1 – Lithogeochemical Analysis (continued)

Samp Num	A.M. A.U. D.L	SiO2 XRF % 0.01	Al2O3 XRF % 0.01	CaO XRF % 0.01	MgO XRF % 0.01	Na2O XRF % 0.01	K2O XRF % 0.01	Fe2O3 XRF % 0.01	MnO XRF % 0.01	TiO2 XRF % 0.001	P2O5 XRF % 0.01	Cr2O3 XRF % 0.01	LOI XRF % 0.01	Sum XRF % 0.01	Rb XRF ppm 2	Sr XRF ppm 2	Y XRF ppm 2	Zr XRF ppm 2	Nb XRF ppm 2
158889		75.800	12.700	0.660	1.460	0.930	3.900	2.130	0.020	0.272	0.100	0.010	2.35	100.4	162	22	47	144	10
158890		65.700	14.400	0.690	4.210	5.380	0.440	5.890	0.050	0.687	0.140	0.005	2.25	99.9	17	58	46	243	12
158891		76.800	12.400	0.520	0.820	4.650	1.460	1.760	0.020	0.203	0.140	0.010	1.05	99.9	61	55	50	142	9
158892		65.900	14.600	0.580	3.810	5.020	0.830	6.320	0.060	0.721	0.160	0.010	2.15	100.2	27	56	41	247	14
158893		57.800	19.700	0.300	1.870	0.180	5.030	8.280	0.080	1.302	0.090	0.020	3.75	98.6	204	16	70	332	23
158894		53.800	22.500	0.180	2.270	0.170	5.970	8.300	0.090	1.234	0.120	0.020	4.00	98.9	254	22	57	212	25
158895		57.700	20.500	0.140	1.680	0.180	5.350	8.560	0.060	1.113	0.110	0.020	3.55	99.0	223	17	59	188	22
158896		78.600	8.090	0.090	1.470	0.030	1.260	7.810	0.040	0.606	0.060	0.020	2.00	100.1	65	7	33	243	10
158897		57.900	17.500	0.200	2.360	0.100	3.670	12.400	0.120	1.097	0.090	0.020	3.60	99.1	149	14	51	267	20
158898		56.500	20.900	0.510	1.990	0.130	6.200	7.090	0.050	1.190	0.110	0.020	3.95	98.9	250	19	55	211	21
158899		54.000	24.200	0.160	1.990	0.130	6.100	7.760	0.070	1.361	0.130	0.020	4.10	100.2	251	21	69	237	24
158900		61.500	18.300	0.110	2.130	0.100	4.820	7.660	0.050	1.124	0.070	0.020	3.65	99.7	192	13	56	245	20
158901		74.400	13.400	0.220	1.210	4.470	2.500	2.560	0.030	0.289	0.110	0.010	0.90	100.1	114	55	47	160	9
158902		68.100	14.500	0.210	1.820	0.130	4.440	7.020	0.130	0.916	0.110	0.010	2.60	100.1	166	16	49	232	17
158903		77.500	11.500	0.340	1.420	4.090	1.180	2.550	0.030	0.259	0.090	0.020	1.05	100.1	45	46	41	140	9
158904		60.100	14.800	1.470	4.440	0.770	2.920	7.950	0.250	1.573	0.360	0.005	4.20	99.0	98	32	52	214	15
158905		64.900	16.500	0.090	2.370	0.090	5.100	5.140	0.060	0.994	0.070	0.020	4.85	100.3	195	16	31	240	18
158906		67.200	9.420	0.120	7.980	0.005	0.290	8.920	0.230	0.705	0.090	0.020	4.75	99.7	12	2	21	257	12
158907		61.300	13.200	0.140	4.370	0.050	2.810	10.400	0.090	0.943	0.100	0.020	5.65	99.1	108	11	49	309	17
158908		65.200	15.100	0.780	3.110	3.530	1.580	7.170	0.080	0.755	0.160	0.005	2.70	100.2	75	40	49	243	13
158909		64.900	14.200	1.720	2.740	4.440	1.100	6.350	0.070	0.728	0.150	0.005	2.70	99.1	47	70	44	232	13
158910		57.700	18.100	0.900	2.520	0.080	4.610	9.790	0.080	1.113	0.100	0.020	3.70	98.9	179	13	59	251	19

Table E.1 – Lithogeochemical Analysis (continued)

	Ba XRF ppm 20	Be ICP ppm 0.5	Na ICP % 0.01	Mg ICP % 0.01	Al ICP % 0.01	P ICP % 0.01	K ICP % 0.01	Ca ICP % 0.01	Sc ICP ppm 0.5	Ti ICP % 0.01	V ICP ppm 2	Cr ICP ppm 1	Mn ICP ppm 2	Fe ICP % 0.01	Co ICP ppm 1	Ni ICP ppm 1	Cu ICP ppm 0.5	Zn ICP ppm 0.5
158889	474	0.25	0.01	0.26	0.46	0.04	0.2	0.38	0.25	0.005	1	58	145	0.75	3	5	1.9	6.5
158890	104	1.2	0.03	1.8	1.93	0.06	0.05	0.29	7.5	0.04	51	47	294	3.16	8	7	2.1	15.9
158891	203	0.25	0.04	0.23	0.53	0.06	0.17	0.31	0.25	0.005	2	69	100	0.9	2	5	2.9	6.1
158892	271	0.25	0.03	1.71	2.05	0.07	0.08	0.22	4.9	0.03	45	59	362	3.78	10	8	1.6	22.6
158893	601	0.25	0.01	0.78	2.03	0.04	0.16	0.1	1.2	0.005	21	58	328	4.57	15	32	5.1	52.4
158894	823	0.25	0.01	1.11	2.32	0.05	0.17	0.12	1.3	0.005	22	34	408	4.73	16	46	2.3	50
158895	637	0.25	0.02	0.74	2.13	0.04	0.17	0.09	1.1	0.005	22	40	274	4.83	15	42	0.9	35.4
158896	165	0.25	0.01	0.72	2.09	0.02	0.1	0.06	1.3	0.005	22	98	290	5.18	20	29	7.7	37.6
158897	473	0.25	0.01	1.2	3.09	0.04	0.15	0.12	2	0.005	34	75	569	7.19	22	39	13.5	86.7
158898	747	0.25	0.02	0.8	1.3	0.05	0.15	0.14	0.7	0.005	13	37	279	4.32	20	43	89.8	66.3
158899	995	0.25	0.01	0.85	1.86	0.05	0.13	0.11	1	0.005	19	38	308	4.39	22	47	73.3	61.6
158900	677	0.25	0.005	0.87	1.49	0.03	0.13	0.07	0.7	0.005	16	40	316	4.58	18	40	82.5	74.6
158901	470	0.25	0.03	0.4	0.69	0.05	0.59	0.12	0.8	0.06	6	66	123	1.3	3	6	2.2	10
158902	615	0.25	0.01	0.6	1.35	0.04	0.38	0.13	0.9	0.01	14	35	446	3.2	17	30	25	29.2
158903	300	0.25	0.03	0.53	0.75	0.04	0.12	0.15	0.5	0.01	5	85	194	1.41	4	6	2.4	11.5
158904	261	0.25	0.01	2.13	2.41	0.15	0.13	0.85	2.6	0.01	56	29	1630	4.68	13	5	60.7	76.6
158905	459	0.25	0.005	0.71	0.72	0.03	0.13	0.07	0.25	0.005	7	42	312	3.05	14	29	17.7	20.2
158906	20	0.25	0.005	4.03	3.83	0.04	0.02	0.08	2.9	0.005	44	83	1450	5.26	17	25	7.5	176
158907	308	0.25	0.01	2.18	2.35	0.04	0.11	0.08	1	0.005	24	69	560	6.28	28	34	7.5	133
158908	530	0.25	0.03	1.43	2.12	0.07	0.13	0.47	3	0.005	29	52	549	4.23	14	8	9.3	73.2
158909	342	0.25	0.03	1.23	1.92	0.06	0.08	0.88	4.3	0.03	37	47	451	3.87	15	8	6.4	37.1
158910	792	0.25	0.01	1.19	2.35	0.04	0.19	0.15	1.1	0.02	23	48	494	5.68	17	38	13.3	158

Table E.1 – Lithogeochemical Analysis (continued)

	As ICP ppm 3	Sr ICP ppm 0.5	Y ICP ppm 0.5	Zr ICP ppm 0.5	Mo ICP ppm 1	Ag ICP ppm 0.2	Cd ICP ppm 1	Sn ICP ppm 10	Sb ICP ppm 5	Ba ICP ppm 1	La ICP ppm 0.5	W ICP ppm 10	Pb ICP ppm 2	Bi ICP ppm 5	H2O+ CHM % 0.1	C CHM % 0.01	S CHM % 0.01
158889	1.5	11.3	6.3	14	1	0.1	0.5	5	2.5	28	21.5	5	1	2.5	2	0.19	0.01
158890	1.5	11.5	14.7	7.6	2	0.1	0.5	5	2.5	13	27.6	5	1	2.5	2.7	0.08	0.01
158891	1.5	12.7	10	20.3	2	0.1	0.5	5	2.5	29	20.6	5	3	2.5	1.1	0.1	0.03
158892	1.5	8.3	8.8	8.1	1	0.1	0.5	5	2.5	24	31.5	5	1	2.5	2.7	0.03	0.01
158893	1.5	2.9	8.3	17.8	0.5	0.1	0.5	5	2.5	20	43	5	9	2.5	4	0.02	0.07
158894	1.5	3.2	9	23.8	0.5	0.1	0.5	5	2.5	26	49.4	5	1	2.5	4.5	0.03	0.02
158895	8	2.6	8.1	24.5	0.5	0.1	0.5	5	2.5	24	40	5	1	2.5	4.1	0.05	0.01
158896	10	1.5	4	11.5	0.5	0.1	0.5	5	2.5	12	21.5	5	3	2.5	2.6	0.07	0.12
158897	8	3.8	9.1	15.3	0.5	0.1	0.5	5	2.5	21	34.4	5	1	2.5	4.5	0.06	0.2
158898	1.5	4	5.9	28	0.5	0.1	0.5	5	2.5	21	39.8	5	1	2.5	3.7	0.08	1.31
158899	14	3.3	6.7	27.4	1	0.1	0.5	5	2.5	23	14.2	5	9	2.5	4.3	0.05	0.25
158900	1.5	2.2	5.5	15.9	2	0.1	0.5	5	2.5	19	25.4	5	12	2.5	3.6	0.01	1.08
158901	1.5	6.8	8.5	14.4	2	0.1	0.5	5	2.5	50	25.3	5	3	2.5	1.1	0.02	0.01
158902	71	8.8	5.8	7	0.5	0.1	0.5	5	2.5	49	30.6	5	1	2.5	2.9	0.03	0.15
158903	1.5	6.8	11.8	13.4	2	0.1	0.5	5	2.5	30	20.1	5	7	2.5	1.3	0.06	0.005
158904	24	17.6	4.9	5.8	0.5	0.1	0.5	5	2.5	11	13.4	5	4	2.5	3.9	0.2	1.31
158905	43	2.6	3	7.7	0.5	0.1	0.5	5	2.5	12	17.5	5	11	2.5	2.9	0.01	2.66
158906	11	2.4	2.9	3.9	0.5	0.1	0.5	5	2.5	2	18	5	1	2.5	4.9	0.02	0.51
158907	53	2.7	3.5	6.8	0.5	0.1	0.5	5	2.5	11	21.5	5	7	6	3.9	0.02	3.7
158908	11	9.6	5.2	10.5	1	0.1	0.5	5	2.5	38	28.1	5	1	2.5	3	0.16	0.12
158909	5	22.8	12.3	8.3	1	0.1	0.5	5	2.5	25	31.4	5	8	2.5	2.4	0.28	0.05
158910	7	3.5	7.5	8.2	0.5	0.1	0.5	5	2.5	33	33.1	5	2	2.5	4.2	0.02	0.53

Table E.1 – Lithogeochemical Analysis (continued)

Samp Num	A.M. A.U. D.L	SiO2 XRF % 0.01	Al2O3 XRF % 0.01	CaO XRF % 0.01	MgO XRF % 0.01	Na2O XRF % 0.01	K2O XRF % 0.01	Fe2O3 XRF % 0.01	MnO XRF % 0.01	TiO2 XRF % 0.001	P2O5 XRF % 0.01	Cr2O3 XRF % 0.01	LOI XRF % 0.01	Sum XRF % 0.01	Rb XRF ppm 2	Sr XRF ppm 2	Y XRF ppm 2	Zr XRF ppm 2	Nb XRF ppm 2
158911		67.400	14.200	0.140	1.620	0.060	3.450	8.980	0.070	0.721	0.060	0.010	2.80	99.7	136	10	62	182	16
158912		64.200	14.100	2.580	2.010	4.190	1.520	5.910	0.090	0.697	0.140	0.020	3.20	98.7	60	85	44	228	13
158913		56.600	16.500	0.130	2.470	0.050	3.030	15.200	0.140	1.035	0.070	0.020	3.70	99.0	115	10	61	230	18
158914		65.100	14.500	2.040	2.670	4.160	1.360	5.790	0.080	0.692	0.140	0.005	2.85	99.6	62	107	52	243	14
158915		64.700	14.700	2.620	2.230	5.010	1.040	5.930	0.090	0.726	0.150	0.005	3.20	100.6	45	113	43	228	12
158916		50.200	13.500	0.160	2.450	0.070	1.820	24.600	0.140	0.899	0.120	0.010	4.55	98.6	78	12	35	294	15
158917		76.600	8.200	0.110	1.630	0.070	1.020	9.870	0.080	0.604	0.060	0.020	2.00	100.3	48	7	28	244	10
158918		73.000	13.200	1.470	0.900	5.500	0.890	3.050	0.050	0.425	0.120	0.010	1.70	100.4	39	78	53	271	14
158919		67.500	14.100	0.870	3.490	3.520	1.740	5.360	0.060	0.684	0.150	0.005	2.70	100.3	59	51	46	223	11
158920		65.600	14.400	0.540	3.910	4.130	1.200	6.870	0.060	0.683	0.150	0.005	2.55	100.2	39	57	49	241	12
158921		62.800	14.100	0.400	6.280	2.140	1.330	8.230	0.060	0.690	0.150	0.005	3.90	100.2	57	35	43	231	12
158922		52.700	18.400	0.450	6.450	4.230	1.480	10.400	0.080	1.071	0.290	0.005	3.80	99.5	56	46	64	341	21
158923		67.100	14.400	0.340	3.290	4.020	1.490	5.800	0.030	0.668	0.150	0.005	2.25	99.6	61	41	47	242	14
158924		77.000	11.700	0.270	1.700	2.940	2.150	2.100	0.020	0.248	0.090	0.020	1.45	99.7	83	28	39	139	10
158925		64.700	16.200	0.260	1.830	0.950	4.460	6.950	0.060	1.006	0.150	0.010	2.60	99.3	169	20	91	241	17
158926		66.200	14.000	0.710	3.180	4.900	0.880	6.070	0.040	0.665	0.150	0.005	1.95	98.9	33	51	50	231	14
158927		64.400	14.900	0.630	2.400	0.790	3.010	9.450	0.150	0.900	0.270	0.010	3.00	100.0	126	26	52	215	16
158928		75.700	13.000	0.320	2.570	0.100	3.600	1.810	0.030	0.288	0.150	0.010	2.50	100.2	141	14	51	144	11
158929		65.600	14.800	0.720	3.140	5.420	0.450	6.760	0.060	0.720	0.150	0.005	2.10	99.9	19	66	45	244	13
158930		60.600	17.300	0.840	4.070	0.100	3.830	7.580	0.100	1.031	0.090	0.020	3.90	99.6	160	18	54	238	19
158931		62.600	17.500	0.150	4.520	0.110	3.350	6.670	0.110	1.075	0.100	0.010	3.95	100.2	147	16	55	271	19
158932		23.700	21.900	0.200	9.590	0.020	0.320	34.700	0.380	1.392	0.150	0.010	7.75	100.1	16	7	56	302	21

Table E.1 – Lithogeochemical Analysis (continued)

	Ba XRF ppm 20	Be ICP ppm 0.5	Na ICP % 0.01	Mg ICP % 0.01	Al ICP % 0.01	P ICP % 0.01	K ICP % 0.01	Ca ICP % 0.01	Sc ICP ppm 0.5	Ti ICP % 0.01	V ICP ppm 2	Cr ICP ppm 1	Mn ICP ppm 2	Fe ICP % 0.01	Co ICP ppm 1	Ni ICP ppm 1	Cu ICP ppm 0.5	Zn ICP ppm 0.5
158911	594	0.25	0.01	0.74	2.14	0.03	0.17	0.09	1.1	0.005	16	49	384	5.42	13	20	26	53.1
158912	591	0.25	0.03	0.88	1.6	0.06	0.12	1.49	3.2	0.02	27	51	613	3.49	10	7	16.8	85
158913	424	0.25	0.01	1.33	3.72	0.03	0.13	0.08	2.1	0.005	45	71	675	9.11	29	38	21.3	122
158914	480	0.25	0.03	1.16	1.68	0.07	0.11	1.11	3	0.03	23	49	541	3.35	9	7	10.1	53.3
158915	351	0.25	0.03	0.98	1.64	0.06	0.1	1.59	4.1	0.01	33	49	620	3.52	11	9	16.8	72.1
158916	276	0.25	0.005	1.37	4	0.05	0.1	0.1	2.8	0.005	53	67	800	14.7	70	62	508	115
158917	151	0.25	0.005	0.84	2.63	0.02	0.07	0.06	1.8	0.005	30	79	479	6.56	15	24	7.1	41.2
158918	195	0.25	0.03	0.37	0.77	0.05	0.1	0.91	1.2	0.005	10	58	357	1.8	3	5	4.4	47.5
158919	376	0.25	0.02	1.53	1.85	0.06	0.15	0.52	3.2	0.005	26	43	380	3.14	7	7	1.4	29.8
158920	343	0.25	0.03	1.78	2.23	0.06	0.12	0.3	3.8	0.01	36	55	398	4.12	10	8	3	23.6
158921	141	0.25	0.02	3.15	3.04	0.06	0.1	0.24	6.4	0.005	41	59	393	4.93	15	9	1.7	25.2
158922	130	0.25	0.02	3.13	3.52	0.12	0.1	0.27	8.8	0.005	40	20	477	6.19	15	2	1.5	30.6
158923	236	0.25	0.03	1.51	1.92	0.06	0.14	0.18	3.3	0.005	26	44	216	3.55	8	6	1.3	13.6
158924	374	0.25	0.02	0.54	0.69	0.04	0.17	0.17	0.25	0.005	4	72	111	1.06	3	5	2.2	7.1
158925	592	0.25	0.01	0.7	1.54	0.07	0.27	0.15	1	0.005	16	37	220	3.37	11	29	1.9	14.5
158926	276	0.25	0.03	1.42	1.86	0.06	0.09	0.27	4.6	0.04	42	40	210	3.59	9	6	2	14
158927	385	0.25	0.01	1.16	2.52	0.11	0.21	0.38	1.5	0.005	29	46	945	5.69	17	48	113	131
158928	346	0.25	0.005	0.81	0.8	0.07	0.13	0.16	0.25	0.005	1	62	152	0.77	1	6	2.6	15.9
158929	120	0.25	0.04	1.5	2.21	0.07	0.04	0.33	6.6	0.03	56	52	401	4.3	11	7	1.7	25.9
158930	645	0.25	0.01	2.1	2.8	0.04	0.15	0.16	1.4	0.06	27	55	628	4.45	13	37	1.3	57.8
158931	392	0.25	0.005	2.27	2.7	0.04	0.09	0.1	1.3	0.005	25	42	669	3.86	17	34	1	65.4
158932	22	0.25	0.005	5.13	8.9	0.05	0.02	0.11	10.2	0.01	120	78	2270	>15	57	44	115	177

Table E.1 – Lithogeochemical Analysis (continued)

	As ICP ppm 3	Sr ICP ppm 0.5	Y ICP ppm 0.5	Zr ICP ppm 0.5	Mo ICP ppm 1	Ag ICP ppm 0.2	Cd ICP ppm 1	Sn ICP ppm 10	Sb ICP ppm 5	Ba ICP ppm 1	La ICP ppm 0.5	W ICP ppm 10	Pb ICP ppm 2	Bi ICP ppm 5	H2O+ CHM % 0.1	C CHM % 0.01	S CHM % 0.01
158911	1.5	2.5	5.7	9.5	2	0.1	0.5	5	2.5	30	26.3	5	1	2.5	3.3	0.03	0.14
158912	1.5	37.5	13.4	10.8	0.5	0.1	0.5	5	2.5	46	31.1	5	5	2.5	2.4	0.51	0.02
158913	1.5	2.2	7.3	10.2	0.5	0.1	0.5	5	2.5	19	*INF	5	1	2.5	4.9	0.06	0.25
158914	1.5	45.5	10.7	14.2	2	0.1	0.5	5	2.5	35	33.3	5	20	2.5	2.5	0.38	0.1
158915	1.5	47.9	7.6	9.2	1	0.1	0.5	5	2.5	30	30.2	5	4	2.5	2.4	0.52	0.07
158916	1.5	3.7	4.6	10.5	0.5	0.8	5	5	2.5	12	*INF	5	32	8	4.7	0.02	4.1
158917	5	1.6	3.5	6	0.5	0.1	0.5	5	2.5	9	16.6	5	1	2.5	3	0.03	0.06
158918	1.5	28.3	5.7	13.7	2	0.1	0.5	5	2.5	22	30.9	5	14	2.5	1.1	0.33	0.04
158919	1.5	14.4	5.9	6.1	0.5	0.1	0.5	5	2.5	31	30	5	1	2.5	2.7	0.16	0.005
158920	1.5	16.2	12.4	6.9	0.5	0.1	0.5	5	2.5	29	33.2	5	3	2.5	3	0.07	0.03
158921	1.5	20.9	5.6	5.4	0.5	0.1	0.5	5	2.5	12	23.8	5	3	2.5	4.4	0.05	0.06
158922	1.5	19	5.3	7.9	0.5	0.1	0.5	5	2.5	9	32.6	5	2	2.5	4.8	0.03	0.03
158923	1.5	8.7	5.7	6.3	1	0.1	0.5	5	2.5	22	30.3	5	2	2.5	2.8	0.04	0.01
158924	1.5	6.7	6.6	7.1	2	0.1	0.5	5	2.5	31	30	5	1	2.5	1.6	0.07	0.005
158925	3	5.9	11.3	8.3	0.5	0.1	0.5	5	2.5	41	32.8	5	1	2.5	2.9	0.04	0.03
158926	1.5	9.5	7.8	5.3	0.5	0.1	0.5	5	2.5	25	27.6	5	1	2.5	2.5	0.09	0.03
158927	3	10.4	8.3	6	1	0.1	0.5	5	2.5	25	34.3	5	145	2.5	3.5	0.06	0.16
158928	1.5	3.6	10	23.4	2	0.1	0.5	5	2.5	14	18.1	5	1	2.5	2.5	0.02	0.04
158929	1.5	6.7	15.2	9.9	1	0.1	0.5	5	2.5	11	31.3	5	1	2.5	2.5	0.09	0.02
158930	1.5	2.9	7.2	6.3	0.5	0.1	0.5	5	2.5	27	36.8	5	1	2.5	4.5	0.05	0.005
158931	11	2.4	4.9	9.3	0.5	0.1	0.5	5	2.5	10	38.7	5	1	2.5	4.6	0.02	0.04
158932	1050	7.9	3.4	9.1	0.5	0.5	7	5	6	0.5	*INF	5	235	498	10.5	0.03	1.31

Table E.1 – Lithogeochemical Analysis (continued)

Samp Num	A.M. A.U. D.L	SiO2 XRF % 0.01	Al2O3 XRF % 0.01	CaO XRF % 0.01	MgO XRF % 0.01	Na2O XRF % 0.01	K2O XRF % 0.01	Fe2O3 XRF % 0.01	MnO XRF % 0.01	TiO2 XRF % 0.001	P2O5 XRF % 0.01	Cr2O3 XRF % 0.01	LOI XRF % 0.01	Sum XRF % 0.01	Rb XRF ppm 2	Sr XRF ppm 2	Y XRF ppm 2	Zr XRF ppm 2	Nb XRF ppm 2
158933		82.300	7.030	0.100	1.230	0.030	1.150	6.160	0.040	0.515	0.080	0.020	1.75	100.5	56	7	33	199	9
158934		67.100	16.000	0.100	1.560	0.110	3.720	7.700	0.070	0.885	0.100	0.020	2.85	100.3	168	15	35	159	15
158935		56.600	17.600	0.140	1.750	0.130	3.980	13.400	0.070	1.048	0.100	0.020	5.15	100.2	184	15	75	259	17
158936		73.500	10.800	0.140	1.770	0.050	1.950	8.710	0.070	0.772	0.090	0.030	2.40	100.3	90	7	46	255	14
158937		73.600	15.000	0.240	1.030	0.090	4.700	2.040	0.005	0.230	0.170	0.005	2.95	100.2	200	11	54	133	10
158938		65.400	14.300	0.810	3.190	4.880	0.610	7.140	0.060	0.701	0.160	0.005	2.20	99.5	24	62	51	235	12
158939		44.600	16.400	1.130	12.800	0.520	0.310	15.700	0.170	1.159	0.160	0.030	6.90	100.0	15	14	37	156	7
158940		67.000	13.500	0.560	3.220	4.670	0.360	7.790	0.070	0.688	0.150	0.010	2.10	100.2	15	57	42	227	14
158941		74.100	11.700	0.300	1.880	0.005	2.300	6.290	0.070	0.721	0.070	0.020	2.75	100.1	101	9	36	254	13
158942		55.800	12.000	0.380	6.330	0.005	0.100	19.200	0.270	0.386	0.110	0.005	5.45	100.1	8	4	49	158	11
158943		28.100	20.400	0.580	21.700	0.005	0.040	18.000	0.320	0.600	0.250	0.005	10.30	100.3	4	7	75	257	16
158944		65.300	13.300	0.680	2.780	0.060	2.310	10.600	0.120	0.861	0.070	0.010	3.60	99.8	100	10	43	275	14
158945		73.300	7.680	0.040	1.980	0.010	0.170	13.800	0.090	0.236	0.030	0.005	2.45	99.9	10	2	18	140	9
158946		79.000	8.590	0.170	1.370	0.050	1.550	6.800	0.040	0.572	0.110	0.010	1.85	100.2	72	10	28	189	10
158947		77.800	8.280	0.100	1.380	0.050	1.460	8.210	0.050	0.614	0.070	0.020	2.05	100.1	66	6	33	209	11
158948		78.100	8.190	0.090	1.280	0.050	1.440	7.900	0.050	0.613	0.060	0.020	2.35	100.2	69	7	30	189	11
158949		64.700	11.800	0.140	1.720	0.080	2.480	12.600	0.060	0.921	0.080	0.020	4.90	99.6	116	9	45	362	16
158950		76.600	7.080	0.110	1.770	0.005	0.470	11.200	0.080	0.533	0.080	0.020	2.15	100.2	24	4	26	217	8
158951		53.000	15.400	0.210	9.760	0.040	1.380	11.400	0.170	1.617	0.150	0.030	5.80	99.0	61	14	30	107	7
158952		77.000	9.220	0.100	1.710	0.040	1.520	7.480	0.060	0.640	0.070	0.020	2.25	100.2	73	5	33	232	11
158953		68.100	11.900	0.080	2.330	0.050	1.820	11.400	0.100	0.895	0.040	0.010	3.30	100.1	84	5	39	221	14
158954		52.400	21.000	0.230	2.450	0.120	4.210	13.700	0.090	1.468	0.140	0.020	4.10	100.1	180	19	80	348	24

Table E.1 – Lithogeochemical Analysis (continued)

	Ba XRF ppm 20	Be ICP ppm 0.5	Na ICP % 0.01	Mg ICP % 0.01	Al ICP % 0.01	P ICP % 0.01	K ICP % 0.01	Ca ICP % 0.01	Sc ICP ppm 0.5	Ti ICP % 0.01	V ICP ppm 2	Cr ICP ppm 1	Mn ICP ppm 2	Fe ICP % 0.01	Co ICP ppm 1	Ni ICP ppm 1	Cu ICP ppm 0.5	Zn ICP ppm 0.5
158933	162	0.25	0.005	0.6	1.74	0.03	0.08	0.07	1.1	0.005	19	107	311	4.19	8	21	15	49.2
158934	460	0.25	0.01	0.73	2.04	0.03	0.14	0.07	1	0.005	21	55	287	4.64	10	29	4	36.5
158935	630	0.25	0.01	0.78	2.11	0.04	0.12	0.09	1	0.005	19	48	358	7.84	36	47	105	112
158936	247	0.25	0.005	0.86	2.28	0.04	0.11	0.09	1.3	0.005	25	114	404	5.44	12	29	10.8	57.6
158937	643	0.25	0.005	0.07	0.18	0.07	0.11	0.16	0.25	0.005	1	27	22	0.91	3	5	5	7.2
158938	195	0.25	0.03	1.46	2.13	0.07	0.05	0.25	5.6	0.03	45	28	396	4.35	11	6	10.8	19.4
158939	83	0.25	0.005	5.65	5.61	0.06	0.02	0.42	15.4	0.1	148	166	905	7.59	31	36	2	57.3
158940	84	0.25	0.03	1.45	2.19	0.06	0.03	0.29	5.9	0.01	54	64	407	4.77	18	9	27.6	26.3
158941	275	0.25	0.005	0.88	1.63	0.03	0.12	0.1	0.8	0.005	15	62	445	3.95	17	28	61.3	3230
158942	10	0.25	0.005	3.33	5.19	0.04	0.005	0.1	2.5	0.03	26	33	1690	10.8	28	13	8.7	258
158943	10	0.25	0.02	9.21	7.32	0.1	0.005	0.26	3.8	0.02	26	11	1520	7.93	29	9	990	357
158944	417	0.25	0.005	1.39	2.67	0.03	0.11	0.11	1.6	0.03	29	55	767	6.32	31	26	2180	297
158945	37	0.25	0.005	1.01	3.3	0.01	0.01	0.03	3	0.005	19	37	629	8.49	40	17	35.3	78.6
158946	199	0.25	0.005	0.63	1.79	0.05	0.06	0.11	1	0.005	18	67	275	4.27	10	26	6.6	49.6
158947	192	0.25	0.005	0.62	1.75	0.03	0.09	0.06	1.2	0.005	20	76	285	5.08	21	32	18.8	36.7
158948	199	0.25	0.005	0.58	1.69	0.03	0.09	0.06	1.2	0.005	20	67	279	4.88	16	19	21.9	35.7
158949	331	0.25	0.005	0.81	2.05	0.04	0.12	0.09	1	0.005	23	66	359	7.84	80	30	43.3	83.9
158950	74	0.25	0.005	0.92	2.77	0.03	0.04	0.07	2.1	0.005	35	73	505	7.26	19	27	16.8	109
158951	154	0.25	0.02	3.93	4.11	0.06	0.03	0.14	8.8	0.005	135	235	836	5.47	40	36	52.6	141
158952	270	0.25	0.005	0.82	2.06	0.03	0.09	0.07	1.3	0.005	20	76	380	4.81	13	22	7.2	52.1
158953	271	0.25	0.005	1.09	2.72	0.02	0.08	0.05	1.5	0.005	30	61	479	6.7	17	31	13.9	75.2
158954	764	0.25	0.01	1.23	3.35	0.06	0.12	0.14	1.9	0.005	36	56	531	8.06	20	43	28.9	63

Table E.1 – Lithogeochemical Analysis (continued)

	As ICP ppm 3	Sr ICP ppm 0.5	Y ICP ppm 0.5	Zr ICP ppm 0.5	Mo ICP ppm 1	Ag ICP ppm 0.2	Cd ICP ppm 1	Sn ICP ppm 10	Sb ICP ppm 5	Ba ICP ppm 1	La ICP ppm 0.5	W ICP ppm 10	Pb ICP ppm 2	Bi ICP ppm 5	H2O+ CHM % 0.1	C CHM % 0.01	S CHM % 0.01
158933	5	1.6	3.1	5.8	2	0.1	0.5	5	7	11	28.1	5	1	2.5	2.3	0.02	0.03
158934	1.5	2	6.1	11.7	2	0.1	0.5	5	2.5	18	34.1	5	1	2.5	3.6	0.04	0.02
158935	55	2.2	7.5	18.1	0.5	0.6	0.5	5	2.5	15	33.5	5	140	6	3.9	0.04	3.82
158936	1.5	2.2	4.8	8.9	1	0.1	0.5	5	2.5	13	22.2	5	1	2.5	3.2	0.04	0.08
158937	10	3.5	9	30	2	0.1	0.5	5	2.5	15	12.6	5	10	2.5	2.3	0.02	0.77
158938	1.5	5.7	10.2	5.7	3	0.1	0.5	5	2.5	15	20.1	5	1	2.5	2.8	0.03	0.16
158939	1.5	6.1	10.7	4.9	3	0.2	0.5	5	6	4	14.9	5	1	2.5	8.2	0.09	0.02
158940	1.5	3.8	14.5	9.4	3	0.1	0.5	5	2.5	7	31.9	5	1	2.5	2.8	0.09	0.36
158941	1.5	1.9	7	11.3	0.5	1.2	6	5	2.5	13	28.2	5	927	2.5	2.9	0.02	0.74
158942	87	1.8	8.5	18.6	0.5	0.5	2	5	2.5	0.5	*INF	5	40	51	6.1	0.05	1.59
158943	1.5	8.1	17.6	21.4	0.5	0.8	0.5	5	2.5	0.5	39.1	5	204	2.5	11.7	0.03	0.21
158944	25	1.6	6	7	1	1.3	1	5	2.5	18	21.9	5	85	*INF	4	0.05	0.98
158945	46	0.7	3	7.1	1	0.1	0.5	5	2.5	0.5	*INF	5	6	2.5	3.8	0.03	0.25
158946	3	2.4	4.3	6.9	1	0.1	0.5	5	2.5	6	24.2	5	1	2.5	2.5	0.02	0.03
158947	1.5	1.4	5.3	4.7	2	0.1	0.5	5	2.5	9	22.9	5	2	2.5	2.5	0.02	0.6
158948	1.5	1.6	4.7	4.8	0.5	0.1	0.5	5	2.5	9	20.4	5	3	2.5	2.5	0.02	0.7
158949	39	2	6.6	9	0.5	0.1	0.5	5	2.5	13	32	5	5	2.5	3.1	0.04	4.32
158950	1.5	1.4	3.7	5.1	0.5	0.1	0.5	5	2.5	3	14.8	5	7	2.5	3.2	0.05	0.3
158951	36	3.5	2.5	2.1	0.5	0.1	0.5	5	2.5	5	5.5	5	6	2.5	6.1	0.05	0.02
158952	4	1.5	4.7	9.9	1	0.2	0.5	5	2.5	14	24.8	5	23	2.5	2.8	0.02	0.06
158953	1.5	1.4	4.5	9.4	0.5	0.2	0.5	5	2.5	10	24.7	5	5	2.5	3.8	0.02	0.23
158954	1.5	4.4	11.4	14	0.5	0.2	0.5	5	2.5	20	*INF	5	15	2.5	5.2	0.02	0.28

Table E.1 – Lithogeochemical Analysis (continued)

Samp Num	A.M. A.U. D.L	SiO2 XRF % 0.01	Al2O3 XRF % 0.01	CaO XRF % 0.01	MgO XRF % 0.01	Na2O XRF % 0.01	K2O XRF % 0.01	Fe2O3 XRF % 0.01	MnO XRF % 0.01	TiO2 XRF % 0.001	P2O5 XRF % 0.01	Cr2O3 XRF % 0.01	LOI XRF % 0.01	Sum XRF % 0.01	Rb XRF ppm 2	Sr XRF ppm 2	Y XRF ppm 2	Zr XRF ppm 2	Nb XRF ppm 2
158955		70.700	12.700	0.700	2.070	0.040	3.170	7.030	0.120	0.754	0.140	0.020	2.65	100.1	123	13	42	228	14
158956		25.500	20.100	6.560	22.500	0.005	0.270	8.670	1.560	0.347	0.280	0.005	14.50	100.2	13	72	72	171	12
158957		63.800	15.500	0.530	2.850	0.080	4.390	6.550	0.050	1.006	0.080	0.020	5.15	100.2	175	16	50	271	17
158958		66.600	12.800	0.980	4.370	1.420	1.640	8.070	0.090	0.860	0.190	0.020	3.05	100.1	69	23	40	179	11
158959		70.800	13.000	0.100	1.590	0.060	2.690	8.340	0.060	0.898	0.070	0.010	2.45	100.1	111	11	42	267	15
158960		72.800	11.900	0.090	1.360	0.080	2.390	8.120	0.050	0.711	0.060	0.020	2.45	100.2	106	12	42	219	14
158961		67.500	15.000	0.120	1.590	0.080	3.280	8.690	0.080	0.850	0.080	0.005	2.75	100.2	142	12	41	200	14
158962		66.800	14.600	0.400	2.840	1.660	2.750	7.090	0.080	0.722	0.150	0.010	3.30	100.5	132	27	46	227	13
158963		64.200	14.400	3.160	2.070	3.310	2.070	5.850	0.120	0.709	0.150	0.005	3.25	99.4	91	90	47	232	13
158964		47.900	25.500	0.190	2.130	0.130	6.520	11.100	0.110	1.425	0.140	0.020	4.20	99.5	263	18	70	234	25
158965		66.100	13.500	0.660	3.780	0.970	2.410	8.190	0.120	0.835	0.110	0.020	3.10	99.8	104	16	43	224	13
158966		64.900	15.100	1.000	2.600	4.350	1.380	7.530	0.120	0.742	0.160	0.005	2.25	100.3	58	73	46	242	14
158967		75.200	12.700	0.440	1.210	2.780	2.590	3.170	0.040	0.390	0.110	0.020	1.35	100.2	107	40	55	268	14
158968		79.900	7.720	0.100	1.300	0.030	1.490	7.040	0.050	0.572	0.070	0.020	1.75	100.1	60	6	27	231	10
158969		79.200	12.000	0.270	0.460	5.160	1.220	0.930	0.010	0.161	0.110	0.005	0.55	100.1	54	69	33	109	8
158970		72.800	12.600	0.540	1.770	4.370	2.720	2.880	0.030	0.276	0.090	0.010	1.00	99.2	114	58	40	154	10
158971		63.100	17.100	0.640	2.120	0.100	5.070	7.200	0.190	1.003	0.170	0.010	3.45	100.3	186	27	59	199	19
158972		68.700	15.600	0.900	2.220	4.540	3.190	2.980	0.050	0.352	0.130	0.010	1.45	100.3	143	86	61	189	14
158973		57.900	17.200	0.100	0.920	0.110	5.560	10.500	0.040	1.137	0.070	0.020	6.55	100.2	199	17	56	314	21
158974		64.700	17.100	0.150	1.900	0.120	3.980	7.330	0.060	1.036	0.100	0.020	3.75	100.4	157	21	48	242	18
158975		54.500	17.700	0.610	4.860	0.060	3.000	12.400	0.170	1.886	0.450	0.005	4.20	100.0	109	15	71	270	18
158976		66.700	16.300	0.100	1.710	0.110	4.110	7.120	0.070	0.979	0.070	0.010	2.90	100.3	152	14	44	218	18

Table E.1 – Lithogeochemical Analysis (continued)

	Ba XRF ppm 20	Be ICP ppm 0.5	Na ICP % 0.01	Mg ICP % 0.01	Al ICP % 0.01	P ICP % 0.01	K ICP % 0.01	Ca ICP % 0.01	Sc ICP ppm 0.5	Ti ICP % 0.01	V ICP ppm 2	Cr ICP ppm 1	Mn ICP ppm 2	Fe ICP % 0.01	Co ICP ppm 1	Ni ICP ppm 1	Cu ICP ppm 0.5	Zn ICP ppm 0.5
158955	367	0.25	0.005	0.86	1.46	0.06	0.2	0.19	1	0.03	15	54	719	4.03	21	29	25.3	144
158956	38	0.25	0.005	8.08	5.71	0.11	0.005	4.2	1.9	0.02	12	5	6860	3.09	3	15	2.7	411
158957	473	0.25	0.005	0.85	0.84	0.04	0.11	0.14	0.25	0.03	8	41	230	3.77	17	33	12.2	23.1
158958	321	0.25	0.01	1.98	2.54	0.07	0.11	0.27	3.9	0.05	40	86	572	4.49	15	19	6.9	69.5
158959	339	0.25	0.005	0.68	1.99	0.03	0.12	0.06	1	0.005	20	54	288	4.68	16	26	1.3	39.1
158960	440	0.25	0.005	0.59	1.93	0.02	0.11	0.06	1.1	0.005	17	77	256	4.78	14	27	7	27.3
158961	508	0.25	0.005	0.71	2.1	0.03	0.1	0.08	1.3	0.005	21	37	421	5.06	14	24	7.7	130
158962	647	0.25	0.01	1.17	1.73	0.06	0.14	0.2	1.7	0.005	20	44	499	4.03	11	8	8.9	321
158963	430	0.25	0.02	0.88	1.5	0.07	0.13	1.89	2	0.02	20	40	753	3.32	10	8	22.1	62.6
158964	862	0.25	0.01	0.9	2.27	0.05	0.2	0.12	1.1	0.005	23	37	375	5.45	16	40	15.7	50
158965	717	0.25	0.01	1.74	2.4	0.05	0.15	0.24	2.7	0.03	32	60	690	4.57	13	19	6	180
158966	693	0.25	0.03	1.13	1.91	0.06	0.14	0.48	4.3	0.03	35	38	604	4.29	13	7	98	97.5
158967	897	0.25	0.02	0.34	0.69	0.05	0.2	0.18	0.8	0.02	4	69	193	1.37	5	6	17.9	20.3
158968	283	0.25	0.005	0.61	1.76	0.03	0.12	0.07	1.1	0.005	20	97	273	4.46	12	20	8.8	27.1
158969	224	0.25	0.03	0.09	0.24	0.04	0.16	0.14	0.25	0.005	1	53	47	0.36	0.5	3	1.8	5.7
158970	415	0.25	0.02	0.74	0.92	0.04	0.8	0.33	1.4	0.08	9	59	201	1.67	8	6	2.1	18
158971	867	0.25	0.005	0.7	1.45	0.06	0.38	0.38	0.8	0.005	14	33	759	3.09	14	32	16.3	50.1
158972	623	0.25	0.02	0.81	0.99	0.06	0.9	0.54	1	0.08	7	47	308	1.5	2	8	1.9	57.9
158973	797	0.25	0.03	0.005	0.18	0.03	0.23	0.06	0.25	0.005	6	34	23	5.93	18	37	97.2	17
158974	532	0.25	0.01	0.87	1.89	0.04	0.15	0.1	1.1	0.005	19	52	406	4.43	12	36	5.4	59.5
158975	321	0.25	0.005	2.64	4.24	0.19	0.1	0.4	5.3	0.005	92	18	1140	7.72	22	5	1.4	219
158976	500	0.25	0.01	0.8	1.95	0.03	0.16	0.07	1	0.005	19	44	325	4.24	13	29	1.4	49.2

Table E.1 – Lithogeochemical Analysis (continued)

	As ICP ppm 3	Sr ICP ppm 0.5	Y ICP ppm 0.5	Zr ICP ppm 0.5	Mo ICP ppm 1	Ag ICP ppm 0.2	Cd ICP ppm 1	Sn ICP ppm 10	Sb ICP ppm 5	Ba ICP ppm 1	La ICP ppm 0.5	W ICP ppm 10	Pb ICP ppm 2	Bi ICP ppm 5	H2O+ CHM % 0.1	C CHM % 0.01	S CHM % 0.01
158955	801	4.8	5.9	4.5	2	1	0.5	5	2.5	23	27	5	218	2.5	2.9	0.04	0.73
158956	1.5	72.9	15.6	12	1	0.3	0.5	5	2.5	0.5	12.2	5	63	2.5	10.5	1.49	0.005
158957	76	3	6.2	2.9	0.5	0.1	0.5	5	2.5	11	23.5	5	17	2.5	3.2	0.03	3.09
158958	7	5.3	4.6	4.5	2	0.1	0.5	5	2.5	18	15.8	5	3	2.5	3.7	0.03	0.04
158959	11	1.6	4.5	7.4	0.5	0.1	0.5	5	2.5	15	28	5	1	2.5	3.3	0.03	0.02
158960	10	2.2	7.8	8.6	1	0.1	0.5	5	2.5	18	25.1	5	1	2.5	3	0.04	0.03
158961	29	2.2	6.3	7	5	0.1	0.5	5	2.5	15	25	5	1	2.5	3.6	0.02	0.06
158962	29	5.8	4.9	9.6	2	0.1	0.5	5	2.5	32	20	5	266	2.5	3.1	0.03	0.74
158963	1.5	54.5	8	18.3	1	0.1	0.5	5	2.5	28	27.7	5	1	2.5	2.2	0.63	0.27
158964	1.5	4.5	10.1	17.2	1	0.1	0.5	5	2.5	27	49	5	3	2.5	4.8	0.01	0.18
158965	1.5	6.4	6.7	7.7	0.5	0.1	0.5	5	2.5	47	20.1	5	117	2.5	3.7	0.04	0.1
158966	1.5	14.9	9	12	0.5	0.1	0.5	5	2.5	66	27	5	5	2.5	2.6	0.13	0.16
158967	1.5	7.4	15.4	30.7	3	0.1	0.5	5	2.5	77	27.7	5	14	2.5	1.8	0.04	0.01
158968	1.5	2	4.6	6.2	1	0.1	0.5	5	2.5	21	11.4	5	1	2.5	2.4	0.05	0.04
158969	1.5	6.9	8.1	17.9	2	0.1	0.5	5	2.5	26	9.9	5	1	2.5	0.7	0.05	0.005
158970	4	13.3	5.8	13.2	1	0.1	0.5	5	2.5	49	12.4	5	1	2.5	1.1	0.09	0.07
158971	32	15	5.1	4.9	0.5	0.1	0.5	5	2.5	69	26.6	5	1	2.5	3.2	0.09	0.15
158972	1.5	27	10.2	19.4	2	0.1	0.5	5	2.5	80	24.7	5	24	2.5	1.5	0.18	0.02
158973	206	2.3	7.4	8.6	0.5	0.5	0.5	5	2.5	31	31.4	5	39	2.5	2.5	0.03	6.18
158974	49	5	4.5	9.8	2	0.1	0.5	5	12	48	35	5	1	2.5	3.7	0.17	0.14
158975	1.5	6.6	6.1	10.9	0.5	0.6	0.5	5	2.5	12	34	5	206	2.5	5.3	0.02	0.02
158976	13	2.7	4.9	8	0.5	0.1	0.5	5	2.5	23	30.5	5	2	2.5	3.4	0.01	0.06

Table E.1 – Lithogeochemical Analysis (continued)

Samp Num	A.M. A.U. D.L	SiO2 XRF % 0.01	Al2O3 XRF % 0.01	CaO XRF % 0.01	MgO XRF % 0.01	Na2O XRF % 0.01	K2O XRF % 0.01	Fe2O3 XRF % 0.01	MnO XRF % 0.01	TiO2 XRF % 0.001	P2O5 XRF % 0.01	Cr2O3 XRF % 0.01	LOI XRF % 0.01	Sum XRF % 0.01	Rb XRF ppm 2	Sr XRF ppm 2	Y XRF ppm 2	Zr XRF ppm 2	Nb XRF ppm 2
158977		65.400	16.300	0.130	2.000	0.100	3.950	7.680	0.090	1.017	0.100	0.010	3.25	100.1	162	13	49	235	19
158978		65.400	14.800	0.980	3.120	2.430	2.200	7.330	0.090	0.878	0.240	0.005	2.75	100.3	98	34	58	254	16
158979		78.000	7.680	0.090	1.750	0.030	0.940	9.070	0.080	0.494	0.060	0.020	1.90	100.1	39	5	27	205	10
158980		80.000	7.820	0.110	1.220	0.040	1.710	6.630	0.050	0.597	0.060	0.020	1.85	100.2	78	8	21	242	10
158981		65.500	16.100	0.140	1.750	0.090	3.630	8.880	0.070	1.015	0.090	0.010	2.90	100.3	145	16	53	257	19
158982		66.200	9.040	0.980	1.690	0.030	1.650	16.300	0.080	0.592	0.070	0.020	3.40	100.2	84	18	41	204	10
158983		77.700	8.540	0.130	2.330	0.020	1.380	7.370	0.060	0.650	0.070	0.020	2.20	100.5	62	8	28	283	12
158984		74.800	13.500	0.390	0.900	5.270	1.450	2.280	0.030	0.296	0.110	0.020	1.05	100.2	68	69	48	164	10
158985		66.000	16.100	0.630	1.790	0.830	3.850	6.230	0.100	0.878	0.120	0.010	2.75	99.4	161	30	50	242	17
158986		63.500	15.700	0.120	1.690	0.140	4.250	7.260	0.030	1.014	0.090	0.020	5.75	99.7	173	22	39	261	18
158987		56.800	19.900	0.160	7.450	0.130	3.090	6.150	0.080	1.246	0.120	0.010	5.05	100.4	141	22	58	327	22
158988		69.900	11.400	0.140	4.330	0.040	1.460	8.880	0.080	0.717	0.070	0.010	3.15	100.2	62	10	37	223	13
158989		41.900	15.800	8.390	8.680	1.090	1.330	10.100	0.200	1.178	0.090	0.050	11.20	100.2	54	93	26	72	4
158990		62.000	15.400	0.120	4.220	0.090	2.830	9.770	0.090	0.936	0.090	0.010	4.40	100.0	117	11	52	255	18
158991		66.100	16.000	0.170	1.770	0.140	3.740	7.720	0.060	0.985	0.100	0.010	3.00	100.0	157	15	55	228	17
158992		79.200	8.570	0.120	1.380	0.050	1.650	6.660	0.040	0.599	0.050	0.020	2.00	100.4	73	7	34	251	10
158993		67.800	14.100	0.120	1.600	0.090	2.980	9.370	0.070	0.843	0.080	0.020	2.60	99.8	127	14	51	224	15
158994		78.700	8.840	0.090	1.450	0.040	1.700	6.600	0.040	0.617	0.060	0.020	1.90	100.1	75	6	27	232	12
158995		43.500	16.500	1.270	15.400	0.005	0.190	13.500	0.250	1.401	0.120	0.080	7.60	99.8	11	4	23	75	3
158996		70.200	7.210	0.490	2.790	0.005	0.140	14.900	0.120	0.500	0.070	0.020	3.75	100.3	10	2	28	177	9
158997		58.000	18.900	0.210	2.040	0.130	4.390	10.600	0.090	1.161	0.150	0.020	3.70	99.6	185	16	67	267	20
158998		28.200	20.700	1.360	17.500	0.005	0.230	19.700	0.430	1.677	0.140	0.150	9.15	99.3	12	5	36	87	6
158999		60.900	18.300	0.140	2.040	0.120	4.190	9.050	0.070	1.066	0.090	0.010	3.50	99.5	184	18	76	197	19
159000		77.700	8.450	0.140	1.700	0.030	1.320	7.780	0.050	0.615	0.090	0.010	2.15	100.1	62	6	40	232	10

Table E.1 – Lithogeochemical Analysis (continued)

	Ba XRF ppm 20	Be ICP ppm 0.5	Na ICP % 0.01	Mg ICP % 0.01	Al ICP % 0.01	P ICP % 0.01	K ICP % 0.01	Ca ICP % 0.01	Sc ICP ppm 0.5	Ti ICP % 0.01	V ICP ppm 2	Cr ICP ppm 1	Mn ICP ppm 2	Fe ICP % 0.01	Co ICP ppm 1	Ni ICP ppm 1	Cu ICP ppm 0.5	Zn ICP ppm 0.5
158977	497	0.25	0.005	0.87	1.79	0.04	0.15	0.08	0.8	0.005	17	38	494	4.41	14	34	2.3	75.9
158978	525	0.25	0.02	1.42	2.2	0.1	0.14	0.44	3.1	0.04	21	48	632	4.38	9	5	4.4	113
158979	194	0.25	0.005	0.9	2.43	0.03	0.06	0.06	1.7	0.005	28	80	475	5.88	13	20	8	117
158980	282	0.25	0.005	0.53	1.26	0.03	0.09	0.07	0.7	0.005	13	75	266	4.15	35	23	9.9	49.7
158981	484	0.25	0.005	0.82	2.27	0.04	0.12	0.09	1.3	0.005	25	52	351	5.29	11	30	7.3	133
158982	390	0.25	0.005	0.75	1.76	0.03	0.11	0.56	0.5	0.01	22	58	452	9.61	62	28	430	36.3
158983	195	0.25	0.005	1.16	2.19	0.03	0.07	0.09	1.5	0.005	23	74	437	4.71	11	24	5.8	55
158984	311	0.25	0.03	0.29	0.6	0.05	0.16	0.25	0.7	0.01	5	68	234	1.3	3	7	2.8	14
158985	455	0.25	0.01	0.77	1.61	0.06	0.16	0.37	0.9	0.005	14	36	596	3.61	15	31	29.3	82.9
158986	480	0.25	0.005	0.49	0.58	0.04	0.11	0.09	0.25	0.005	8	34	172	4.77	20	34	16	105
158987	337	0.25	0.01	3.6	3.4	0.05	0.09	0.11	1.6	0.005	29	45	485	3.34	10	32	0.8	68
158988	186	0.25	0.01	2.37	3.31	0.03	0.06	0.07	1.9	0.005	31	67	565	5.43	15	28	3.2	62.1
158989	100	0.25	0.01	4.2	4.17	0.04	0.04	5.27	11.2	0.05	109	210	1180	5.21	34	63	37.4	101
158990	360	0.25	0.01	2.24	3	0.04	0.1	0.09	1.4	0.005	29	56	607	6.06	15	40	25	102
158991	653	0.25	0.01	0.85	2.13	0.04	0.12	0.12	1.4	0.005	21	46	301	4.73	13	32	2.2	61.4
158992	257	0.25	0.01	0.67	1.76	0.03	0.09	0.06	1	0.005	18	83	279	4.48	14	30	9.9	81.6
158993	377	0.25	0.01	0.77	2.36	0.03	0.11	0.07	1.4	0.005	25	59	396	5.81	16	30	8	87.5
158994	222	0.25	0.005	0.64	1.71	0.03	0.08	0.06	1	0.005	17	70	257	4.02	9	23	2.4	37.9
158995	20	0.25	0.005	6.18	5.47	0.04	0.005	0.25	13.4	0.1	147	352	1170	5.92	39	127	20.2	349
158996	34	0.25	0.005	1.48	3.26	0.03	0.01	0.12	3.3	0.03	45	83	774	9.45	57	43	448	115
158997	660	0.25	0.01	0.98	2.6	0.06	0.12	0.13	1.4	0.005	28	47	398	6.18	18	39	15.6	53.5
158998	28	0.25	0.01	7.4	7.11	0.05	0.005	0.25	15.5	0.09	175	687	2040	8.61	54	276	1.8	538
158999	508	0.25	0.01	0.92	2.31	0.04	0.12	0.09	1.3	0.005	25	40	319	5.17	13	37	6.6	58.1
159000	185	0.25	0.01	0.83	2.11	0.04	0.08	0.09	1.1	0.005	22	65	330	5.12	10	24	22.1	55.7

Table E.1 – Lithogeochemical Analysis (continued)

	As ICP ppm 3	Sr ICP ppm 0.5	Y ICP ppm 0.5	Zr ICP ppm 0.5	Mo ICP ppm 1	Ag ICP ppm 0.2	Cd ICP ppm 1	Sn ICP ppm 10	Sb ICP ppm 5	Ba ICP ppm 1	La ICP ppm 0.5	W ICP ppm 10	Pb ICP ppm 2	Bi ICP ppm 5	H2O+ CHM % 0.1	C CHM % 0.01	S CHM % 0.01
158977	1.5	2.7	4.7	8.8	0.5	0.1	0.5	5	2.5	19	32.9	5	1	2.5	3.5	0.02	0.4
158978	1.5	10.1	10.5	7.7	0.5	0.1	0.5	5	2.5	32	30.1	5	8	2.5	3.3	0.12	0.05
158979	4	1.4	3.2	4.6	0.5	0.1	0.5	5	2.5	10	15.1	5	3	2.5	2.9	0.03	0.06
158980	6	2	4	5.6	1	0.1	0.5	5	2.5	12	24	5	3	2.5	2	0.03	0.92
158981	1.5	2.9	7.5	9.7	0.5	0.1	0.5	5	2.5	16	32.7	5	1	2.5	3.7	0.02	0.09
158982	1.5	12.6	3.7	9	0.5	0.4	2	5	2.5	20	*INF	5	30	2.5	2.7	0.19	4.78
158983	1.5	2	4.6	8.1	3	0.1	0.5	5	2.5	10	23	5	8	2.5	2.9	0.03	0.1
158984	1.5	12.6	10	11.6	1	0.1	0.5	5	2.5	31	28.9	5	4	2.5	1.2	0.07	0.03
158985	8	10	11.3	6.1	0.5	0.1	0.5	5	2.5	20	37	5	34	2.5	3.1	0.1	0.25
158986	62	2.3	5.8	11.4	0.5	0.1	0.5	5	2.5	10	23.2	5	37	2.5	2.8	0.02	4.82
158987	1.5	5.8	3.2	10.4	0.5	0.1	0.5	5	2.5	11	47.6	5	1	2.5	4.6	0.03	0.04
158988	12	2.3	2.3	7.6	0.5	0.1	0.5	5	2.5	7	28.1	5	4	2.5	4.1	0.03	0.04
158989	31	64.1	8.7	2.9	0.5	0.1	0.5	5	2.5	5	4.4	5	11	2.5	5.9	1.78	0.005
158990	11	1.8	6.3	13.5	0.5	0.1	0.5	5	2.5	13	33.8	5	32	2.5	4.4	0.02	1.28
158991	49	2.2	9.6	7.4	2	0.1	0.5	5	2.5	22	38.4	5	3	2.5	3.4	0.04	0.22
158992	1.5	1.4	6.2	7	1	0.1	0.5	5	2.5	13	21.9	5	2	2.5	2.3	0.01	0.32
158993	7	2.2	8.8	8.8	0.5	0.1	0.5	5	2.5	14	32.9	5	1	2.5	3.3	0.01	0.15
158994	1.5	1.4	3.5	6.7	1	0.1	0.5	5	2.5	11	21.7	5	1	2.5	2.5	0.03	0.03
158995	8	2.7	4.5	2.9	0.5	0.1	0.5	5	7	0.5	4.2	5	259	2.5	7.9	0.08	0.02
158996	46	1.7	5.6	6.2	0.5	3.3	1	5	2.5	1	*INF	5	291	10	3.4	0.05	2.77
158997	4	3.1	7.9	14.9	1	0.1	0.5	5	2.5	20	42.9	5	4	2.5	3.3	0.04	0.23
158998	34	4.1	6.5	2.9	0.5	0.2	1	5	9	1	*INF	5	55	2.5	10.9	0.02	0.04
158999	5	3.5	8	18.9	0.5	0.1	0.5	5	2.5	16	41	5	6	2.5	3.7	0.02	0.05
159000	1.5	2.4	4.8	11.1	0.5	0.1	0.5	5	2.5	10	19.3	5	3	2.5	2.3	0.03	0.25